

The Infrared Universe

Jonathan Holland

January 13, 2026

*Near: far.
Ineluctable modality of the visible.*

— James Joyce, *Ulysses* [42]

Abstract

We develop a mesoscopic framework for semiclassical gravity in which the cosmological exterior is treated as an open quantum subsystem coupled to a horizon reservoir and described by a non-Riemannian Carnot–Carathéodory (CC) tangent geometry. In this setting, conservation laws hold locally as expectation-value identities, $\nabla_\mu \langle J^\mu \rangle = 0$, while the global charge content of the exterior evolves through irreversible horizon fluxes. When matter degrees of freedom cross a causal horizon, their conserved quantum numbers are sequestered into inaccessible modes, producing an apparent depletion in the exterior sector. Global unitarity then requires compensating source terms in the exterior continuity equations. This repopulation is not baryogenesis but a generic open-system effect arising from tracing over horizon and ultrasoft infrared degrees of freedom.

Black holes act as irreversible entropy converters, while the cosmological horizon functions as an effectively infinite entropy sink. The resulting entropy throughput drives an increase in exterior free energy that must be dissipated through accessible channels. Causality strongly constrains these channels: ultraviolet excitations propagate within the same light cones as the infalling matter and cannot enforce the required causal separation. Entropy and conserved charges must therefore return predominantly through long-wavelength geometric modes. The infrared geometric sector emerges as the dominant entropy-acceptance channel in any horizon-coupled nonequilibrium steady state, with matter and radiation production appearing as secondary, thermodynamically constrained processes.

The CC tangent geometry provides the complementary kinematical structure. Its intrinsic mesoscopic scale σ governs both particle kinematics and the excitation of infrared geometric modes. In the photon sector, CC mixing acts as an effective cavity whose stationary state is Planckian, with the photon temperature determined dynamically by the entropy-acceptance capacity of the infrared sector rather than imposed as an external boundary condition. In the matter sector, the same geometric

structure yields asymptotically flat or rising rotation curves through horizontal CC geodesics. These phenomena arise from a single dynamically selected mesoscopic scale rather than independent assumptions.

Horizon thermodynamics, mesoscopic continuity, and infrared geometry together lock this scale to the cosmological expansion rate, $H \sim \sigma$, yielding a steady-state Universe in which expansion, entropy export, photon equilibration, and large-scale kinematics are controlled by a single underlying frequency. Throughout, the emphasis is on structural consistency between open-system thermodynamics, causal geometry, and conservation laws; observational agreements are presented as necessary consistency conditions rather than phenomenological inputs.

Contents

1	Introduction	7
1.1	MOND as an Implicit Sub-Riemannian Theory	9
1.2	The Λ CDM framework and its conceptual fragmentation	10
1.3	Roadmap	12
2	Heisenberg Kinematics and Radial Potentials	12
2.1	Canonical one-form and horizontal momenta	13
2.2	Free Hamiltonian in polar coordinates	13
2.3	Adding a radial potential	14
2.4	Circular orbits and rotational velocity	14
2.5	Virial theorem	15
2.6	Causal implications and a cartoon view of the model	16
3	Bulk Carnot Geometry and the Origin of σ	17
3.1	A $(3, 3)$ nilpotent model	17
3.2	Planar motions and the Heisenberg limit	18
3.3	Embedding in a sub-Lorentzian bulk	18
3.4	Geometric interpretation of the mesoscopic scale	19
4	Mesoscopic Continuity Equations	20
4.1	Observer-Dependence and Causal Partitioning	21
4.2	Coarse-grained currents and null boundaries	21
4.3	Entropy biases and compensating source terms	22
4.4	Baryon continuity equation	22
4.5	Scaling, dimensional analysis, and the role of σ	23
5	The Cosmic Microwave Background as a Steady-State Radiative Equilibrium	24
5.1	Why a stationary 2.7 K bath is thermodynamically natural	24
5.2	Why the photon bath does not cool under expansion	25
5.3	Conceptual summary	26

6 Horizon–Coupled Thermodynamics	26
6.1 Entropy production and horizon export	31
6.2 IR entropy from cosmic expansion	31
6.3 Grand-canonical constraints for the reduced exterior state	32
6.4 Stationarity and coupled balance laws	32
6.5 Entropy Balance, Horizon Charges, and the Necessity of Baryon Creation	33
6.6 Baryon number continuity	34
6.7 A GKSL realization of exterior baryon repopulation	36
6.8 Why Entropy Returns in the Infrared	38
6.9 Free Energy and Internal Dissipation	40
6.10 Feedback and Selection of σ_*	40
6.11 Infrared Universality	41
6.12 Summary	41
6.13 High- σ Regime: Dynamical Self-Limitation and Inefficient Black-Hole Sequestration	41
6.14 Why Free Energy Is Not Exhaustively Dissipated into Infrared Gravitational Modes	43
7 Entropy–Acceptance Temperature and the Horizon as a Cold Sink	44
7.1 Entropy–Acceptance Temperature	44
7.2 Black Holes as Cold Entropy Amplifiers	44
7.3 The Cosmological Horizon as an Effective Zero–Temperature Sink	45
7.4 Entropy Cascade	45
8 Minimal Thermodynamic Structure: Cold Entropy Export and Free–Energy Balance	45
8.1 Cold Entropy Export	45
8.2 Fixed Radiative Temperature of the Exterior	46
8.3 Free–Energy Increase	46
8.4 Chemical–Potential Imbalance	46
8.5 Restoration of Equilibrium	47
8.6 Summary	47
9 Minimum Exterior Temperature and Entropy–Sink Selection	47
9.1 Free-energy balance and minimum temperature	47
9.2 Why photons are <i>not</i> the dominant entropy sink	48
10 Stationary Solutions and Cosmological Implications	50
10.1 The stationary system	50
10.2 Determination of the expansion rate	51
10.3 Baryon equilibrium	51
10.4 Stationary radiation density	51
10.5 Rotation curves and macroscopic geometry	52
10.6 Global consistency and observational tests	53

11 Photon Confinement, Carnot Mixing, and Blackbody Equilibrium	54
11.1 Effective confinement in Carnot–Carathéodory geometry	54
11.2 Sub-Laplacian mixing and ergodicity	55
11.3 Photon Heating, Geometric Thermalization, and the Absence of Radiative Runaway	55
11.4 Structural relation between entropy–acceptance and radiative temperatures	56
12 Entropy Throughput and the Origin of Apparent Expansion	58
12.1 The exterior as an open thermodynamic system	58
12.2 Free energy stored in resolved degrees of freedom	58
12.3 Steady-state entropy balance	59
12.4 Stationary CC geometry and timescale separation	59
12.5 Resolved degrees of freedom, “tiles,” and apparent expansion	59
12.6 Free–Energy Throughput and Entropy Export: Quantitative Closure	60
12.7 Sanity check on the entropy–export engine: required T_{ext}	63
13 Emergent Carnot–Carathéodory Geometry and the Horizon Fixed Point	65
13.1 The horizon as a thermodynamic boundary condition	65
13.2 Cold entropy, collapse timescales, and geometric response	66
13.3 Why purely Riemannian tangent geometries are disfavored	66
13.4 CC geometry as a thermodynamic fixed point	67
13.5 Fixed-point interpretation	67
13.6 Relaxation of the Control Parameter σ	68
14 A Geometric Viewpoint on Luminosity Decay	69
14.1 Wavefronts and angular accessibility	69
14.2 The Heisenberg group as a geometric toy model	69
14.3 Distance and effective luminosity	70
14.4 Interpretation	71
14.5 Local Phase Inheritance and Coarse–Grained Continuity	71
14.6 Single–packet CC phase drift and effective luminosity decay	72
14.7 Vertical Mixing, Fat–Tailed Phase Occupation, and the Stability of the Photon Bath	75
14.8 Radiation and detection in the (3, 3) Carnot geometry	76
15 Late-Time Cosmology, Chemical Steady State, and the Origin of Quasars	77
15.1 Quasars as Terminal Galactic Attractors	77
15.2 Nucleosynthesis Beyond the Primordial Paradigm	78
15.3 Preferential Metal Sequestration	78
15.4 Chemical Equilibrium and the Helium Fixed Point	78
15.5 Summary	79

16 The Cosmic Helium Budget	79
16.1 Helium as a Mesoscopic Observable	80
16.2 Equilibrium Condition	80
16.3 Microphysical Origin of the Helium Fixed Point	80
16.4 Role of Metal Sequestration	81
16.5 Thermodynamic consumption of metals as an exterior principle .	81
16.6 Interpretation	82
17 The Heisenberg Angular Spectrum: Geometry, Dispersion, and Thermodynamic Phase Normalization	83
17.1 Motivation	84
17.2 Heisenberg Geometry and the Sublaplacian	85
17.3 Angular Dispersion and $\sqrt{\ell}$ Scaling	85
17.4 Oscillatory Angular Spectrum	86
17.5 Thermodynamic Determination of β	87
17.6 Phenomenological Implications	87
17.7 Robustness and Parameter–Independence	89
17.8 Future Directions	89
18 Anisotropic Tracing, Heisenberg Relaxation, and the Ledger Variable	90
18.1 Operational meaning of coarse–graining	90
18.2 Open systems and anisotropic coarse–graining	91
18.3 Semiclassical reduction and degenerate diffusion	92
18.4 Nilpotentization and Carnot–group tangent structure	92
18.5 The 2+1 Heisenberg prototype and its stochastic lift	93
18.6 Markovian closure, coarse–graining, and the necessity of a ledger	94
18.7 The Effective Algebra as a Central Extension	95
18.8 From infinitesimal commutators to macroscopic ledgers	96
18.9 Thermodynamic interpretation and free–energy accounting	98
18.10 Equality of reduced states and inequivalence of lost microstates .	100
18.11 Ledger variables, accessibility, and path–dependent observables .	102
18.12 Uniqueness of the Lévy area and implications for the ledger . .	103
18.13 Emergence of Lévy Area from Directional Coarse Graining . .	104
18.14 Summary	110
19 A Minimal Reaction–Diffusion Model for the Mesoscopic Scale σ	111
19.1 Thermodynamic status of the mesoscopic scale σ	112
19.2 What is being modeled, and why a self–limiting feedback is expected	113
19.3 A minimal reaction–diffusion closure	115
19.4 Radial variation of the mesoscopic scale and kinematic admissibility	117
19.5 Fast response, slow mesoscopic relaxation, and hysteresis	120
19.6 Observational diagnostics and falsifiability	121

20 Baryon acoustic oscillations, redshift and polarization	123
20.1 What BAO Observations Measure	123
20.2 Condition for a Constant Physical BAO Ruler	125
20.3 Non-uniqueness of the Redshift–Distance Mapping	128
20.4 Redshift as a Stochastic Accumulation Process	129
20.5 Observational Calibration and Consistency	131
20.6 Stochastic Redshift Accumulation on Ledger Space	132
20.7 Optical Effects from Redshift Fluctuations	134
20.8 Observability, Ledger Drift, and the Apparent Reionization Window	136
20.9 Observational Status and Falsifiability	138
20.10A Resonant Hazard Profile and Emergent Cosmic Noon	140
21 The glass universe	143
21.1 Ontological postulates	144
21.2 Jacobson–Clausius transport on $\Omega \times S^1$	145
21.3 Directional memory and constitutive trace–out	147
21.4 Open–system coupling, expansion, and forced return	150
21.5 Interpretation of the BAO–like correlation scale	152
21.6 Feasibility of galaxy replacement on the BAO scale	156
22 Mesoscopic σ Seeding, Amplification, and Relaxation in Hierarchical Structure Formation	158
22.1 Elevated σ as a Mesoscopic Seed	159
22.2 Dwarf Galaxies as Environmental σ Amplifiers	159
22.3 Coherent Assembly of Larger Galaxies from σ –Seeded Regions	160
22.4 Self–Limitation and Relaxation of σ	160
22.5 Late–Time IGM and Observable Consequences	160
22.6 Summary of the Mesoscopic Feedback Loop	161
22.7 Timing of Dwarf Formation and the Persistence of Satellite Populations	161
22.8 Temperature–Polarization Correlations: Interpretation of EE and TE	162
23 Ledger Area, Parity, and the Forced Form of the σ Dynamics	165
23.1 Lévy Area as the Unique Surviving Orientation Invariant	167
23.2 The Ledger Variable and Parity	167
23.3 Worldline Memory Versus Mesoscopic Representation of σ	168
23.4 Onsager Forcing and the Forced Landau Form	169
23.5 Why All Nontrivial Constitutive Control Resides in the Lévy Channel	171
23.6 The Coarse Pseudoscalar Flux as a Projection Operator	173
23.7 Continuum Interpretation: Vorticity and Shear	174
23.8 System–Level Versus Observer–Level Coarse Graining	175
23.9 Resolved Motion, Unresolved Circulation, and the Definition of J	176
23.10 Coherent Rotation and the Relaxation of σ	177

23.11	Ontological Status of σ , A , and J	178
23.12	Pseudoscalar Neutrality as Predictability Neutrality	179
23.13	Projected Generator for the Neutral Memory Process	182
24	General Relativity as UV Kernel and Emergent IR Geometry	183
24.1	Local dynamics versus emergent kinematics	184
24.2	GR as collision kernel in the open exterior	184
24.3	Mesoscopic thermodynamics and emergent cosmological scales .	185
24.4	General covariance and CC constitutive laws	186
24.5	Einstein Gravity as an Equation of State, and the Mesoscopic Universe as a Bigger Box	187
24.6	Cosmological interpretation	188
A	Curved model geometries	194
A.1	$SU(2)$	194
A.2	$SL_2(\mathbb{R})$	200
A.3	$Sp(2)$	205
A.4	$Sp(1, 1)$	206

1 Introduction

Cosmological observations reveal a striking conjunction of late-time regularities: galaxies exhibit flattened or rising rotation curves, the cosmic radiation field maintains an almost perfect blackbody spectrum, and the cosmic baryon density remains nearly constant despite ongoing expansion [57, 62, 28, 1]. In the standard Λ CDM interpretation these features arise from distinct physical mechanisms—dark matter, primordial radiation, and a tuned early-universe baryogenesis episode—linked only indirectly through a shared Friedmann background. In this work we explore a different possibility: that *all three phenomena reflect a single mesoscopic structure of spacetime*, governed by a distinguished infrared frequency scale.

Our starting point is the observation that the coarse-grained, late-time Universe does not behave as a closed system. Any comoving worldtube loses degrees of freedom across its cosmological horizon at a steady rate, while black holes act as powerful localized sinks that absorb entropy and sequester conserved charges into exponentially redshifted interior states [31, 5, 37, 22]. The exterior region is therefore an *open thermodynamic subsystem*, and its macroscopic evolution must be described by balance laws that include horizon exchange [15, 69, 39]. These laws take a simple and universal form: for any conserved or effectively conserved quantity, one obtains continuity equations of the type

$$\partial_t n_X + 3Hn_X = -\Phi_X + \Gamma_X,$$

where the flux term Φ_X encodes loss to horizon degrees of freedom and the source term Γ_X arises from the horizon-induced chemical potential in the reduced exterior density matrix.

A consistent late-time cosmology must therefore supplement local conservation with a global entropy budget. Matter accreting into black holes produces an enormous entropy increase in their horizons, while cosmological expansion continuously exports entropy to the cosmological horizon. To maintain stationarity, this outward flow must be compensated by an entropy-production channel in the exterior region.

The principal result of this paper is that entropy export from the exterior region proceeds through a hierarchy of channels in which long-wavelength geometric (gravitational) modes constitute the dominant carrier. These infrared modes transport entropy efficiently and causally to the horizon and thereby define the primary entropy-acceptance channel of the exterior. The energy needed to sustain this geometric throughput is supplied indirectly by a much smaller but structurally essential fraction of the free-energy budget that cycles through baryonic matter. In the exterior sector, baryons are continually regenerated to compensate for horizon sequestration of their conserved charges; over cosmological timescales they remain dynamically stable, accumulate into deep gravitational potentials, and are ultimately accreted into black holes, releasing large amounts of horizon entropy. In this sense, the baryon-accretion cycle provides the work-producing component of a cosmic Carnot engine [54, 8, 19], while the infrared geometric modes represent the principal entropy-transport channel that maintains the stationary nonequilibrium state.

The second structural ingredient is geometric. We show that the appropriate tangent geometry for large-scale cosmic dynamics is not Riemannian but *Carnot–Carathéodory*, modeled locally by a Heisenberg or more general step-two Carnot group [33, 7, 48]. Such geometries contain an intrinsic infrared frequency σ , arising from the noncommutativity of their horizontal and vertical directions.

A central role in this framework is played not by a new fundamental constant, but by an emergent infrared rate that characterizes the steady-state coarse-graining of the exterior system. In Carnot–Carathéodory geometry this rate appears as a mesoscopic spectral scale σ , reflecting the timescale on which horizontal and vertical degrees of freedom mix under irreversible entropy flow. Crucially, σ is not imposed a priori: it is selected dynamically by the requirement that entropy export to the horizon be balanced by entropy-acceptance channels in the exterior. In the resulting steady state, σ adjusts to the cosmological expansion rate, yielding $\sigma \sim H$ as a consistency condition rather than a postulate [47, 50]. Once this identification is made, a number of apparently independent cosmic phenomena become different expressions of the same mesoscopic scale: rotation curves, baryon equilibrium, and the equilibrium temperature of the photon bath all follow directly from σ .

Crucially, the parameter σ should not be interpreted as an exactly conserved microscopic quantity. Rather, it is a thermodynamic state variable characterizing the stationary mesoscopic exterior, analogous to temperature or chemical potential in ordinary nonequilibrium systems. Local gravitational excitations and horizon fluxes generically induce fluctuations in σ , but coarse-grained entropy production drives relaxation toward a stable stationary value σ_* determined by

global entropy throughput. Thus constancy of σ should thus be understood as an adiabatic or stationary approximation: σ is an intensive control variable that equilibrates under global entropy throughput, and in Sections 2–18 we work in the regime where its relaxation time is long compared to orbital, radiative, and mixing timescales. Local deviations and slow spatial variation of σ are introduced explicitly only in Section 19, where σ is promoted to a dynamical field.

The framework that emerges is a *horizon-coupled steady-state cosmology* in which baryons, radiation, and infrared geometric modes continuously circulate entropy and conserved charge between the exterior and its horizons. Rather than invoking phenomenologically distinct components—dark matter, dark energy, primordial baryogenesis, and a relic radiation field—the model derives their observational signatures from a single mesoscopic mechanism. Galactic rotation curves arise from sub-Riemannian kinematics; the cosmic radiation field is a thermodynamic equilibrium sustained by geometric confinement and ordinary astrophysical heating; and the baryon density is maintained by the compensating source required by horizon thermodynamics. All of these features are controlled by the same mesoscopic rate selected by the horizon-coupled steady state.

The remainder of the introduction situates this framework in relation to MOND and Λ CDM and prepares the ground for the detailed continuity, geometry, and thermodynamic analysis that follows.

1.1 MOND as an Implicit Sub-Riemannian Theory

In its original Bekenstein–Milgrom formulation [4, 47, 25], MOND is defined by a nonlinear Lagrangian for the gravitational potential,

$$\mathcal{L}_{\text{MOND}} = -\frac{a_0^2}{8\pi G} F\left(\frac{|\nabla\Phi|^2}{a_0^2}\right) + \rho\Phi,$$

which yields a modified Poisson equation

$$\nabla \cdot \left[\mu\left(\frac{|\nabla\Phi|}{a_0}\right) \nabla\Phi \right] = 4\pi G\rho.$$

Because the operator acting on Φ is no longer the Euclidean Laplacian but a *directionally weighted* one, MOND dynamics are governed by an anisotropic diffusion operator resembling a horizontal sub-Laplacian on a Carnot manifold. The system propagates information preferentially along a distinguished set of directions (those where $|\nabla\Phi|$ is small), in close analogy with the Heisenberg horizontal distribution.

This formal similarity is striking: the MOND kinetic operator is not far from the quadratic form obtained from a Heisenberg or general Carnot–Carathéodory tangent geometry, in which the Laplacian is replaced by a horizontal sum of squares. In both cases the resulting dynamics are effectively sub-Riemannian, and the corresponding spectral scale plays the role of an emergent acceleration or frequency.

What MOND lacks, however, is a *mechanism* for the scale a_0 . It is inserted by hand and remains unexplained. In the present framework, by contrast, the mesoscopic spectral scale σ arises from the geometry itself and is dynamically locked to the Hubble rate through horizon thermodynamics. Thus

$$a_0 \sim \sigma \sim H_0,$$

giving a natural origin for the empirical MOND scale.

From this viewpoint MOND may be interpreted as a phenomenological glimpse of a deeper geometric structure—a nonlinear diffusion equation that partially encodes sub-Riemannian kinematics, but without identifying the underlying noncommutative tangent geometry or its thermodynamic origin.

A common first question is whether the present framework supplies a new gravitational field equation. It does not, and this is not a shortcoming. The horizon-coupled exterior is not a field in the sense of general relativity but an open, mesoscopic ensemble governed by transport, relaxation, and irreversible tracing-out of degrees of freedom. Asking for a field equation here is akin to asking for a single dynamical equation governing all fluid turbulence or all gas dynamics: the request presupposes a microscopic determinism that the coarse-grained system does not possess. The correct objects are extensive variables and their continuity equations, together with the geometric structure imposed by anisotropic relaxation to a Carnot–Carathéodory fixed point. In this setting, geometry and transport emerge from the ensemble itself; they are not obtained by solving a variational field theory on a differentiable manifold. General relativity enters only as the ultraviolet interaction kernel governing local collapse, lensing, and compact objects—not as an infrared cosmological geometry. In short, there is nothing for a field equation to govern: the large-scale cosmological state is not a solution to a differential equation on a metric manifold, but the statistical steady state of an open, horizon-coupled ensemble.

Much of what MOND captures phenomenologically can be interpreted, in this light, as an early glimpse of the correct infrared variational structure: a geometry in which the effective kinematics are governed not by the scaling of a Riemannian manifold but by the sub-Riemannian relaxation of a Carnot tangent cone. What MOND records empirically, the present framework supplies geometrically and thermodynamically.

1.2 The Λ CDM framework and its conceptual fragmentation

Modern cosmology rests on the empirical success of the Λ CDM model in fitting a wide range of observations: the Hubble–Lemaître law, the angular power spectrum of the cosmic microwave background (CMB), the large-scale distribution of galaxies, and the statistics of gravitational lensing, among others [1, 75, 53]. At the same time, the theoretical underpinnings of this framework remain conceptually fragmented. The standard model requires, as independent ingredients, a cold dark matter component to explain galactic and cluster dynamics, a dark

energy component to drive late-time acceleration, an inflationary phase introduced to address horizon and flatness problems, and a hot primordial radiation era to account for the CMB. Each ingredient is phenomenologically successful in its own domain, but their mutual relations are largely kinematic rather than dynamical or thermodynamic.

From the standpoint of entropy flow and charge conservation, this fragmentation is significant. None of the components of Λ CDM communicate thermodynamically (in a unified, ongoing balance-law sense): the entropy generated by structure formation, the entropy sequestered behind horizons, and the observed radiation density are not linked by a common continuity principle. The model provides no mechanism by which the cosmic baryon density, radiation density, and expansion rate should be related to one another in a stationary universe. Instead, each is set by separate initial conditions or phenomenological parameters.

The mesoscopic framework developed here replaces this modular structure with a set of coupled balance laws governing charge flow, entropy flow, and horizon thermodynamics. In this view, the observed cosmic densities and kinematics arise from ongoing equilibrium conditions rather than primordial initial states. The question is therefore not whether Λ CDM fits current observations—it does—but whether its component parts reflect a unified physical process or a set of independent empirical patches. The present work explores the possibility that a single mesoscopic scale σ , arising from the Carnot–Carathéodory tangent geometry, underlies both local kinematics and global thermodynamic balance. Throughout this work, σ should be understood not as a fundamental parameter but as an emergent bookkeeping rate characterizing the steady-state coarse-graining of an open, horizon-coupled system.

Scope and status of the present work. The aim of this paper is *structural*, not phenomenological in the usual data-fitting sense. We do not attempt a calibrated replacement for Λ CDM, nor do we perform systematic likelihood fits to observational datasets. Instead, our goal is to establish that a single, horizon-coupled, open-system framework with mesoscopic Carnot–Carathéodory geometry admits *self-consistent entry points* for all major cosmological observables. Specifically, we show that nothing in the proposed architecture is *a priori* incompatible with the observed cosmic microwave background temperature and angular power spectrum, baryon acoustic oscillations and physical ruler constraints, galactic rotation curves, late-time expansion, cosmic mass fractions (including helium abundance), or the observed “cosmic noon” peak in luminosity density. Where concrete calculations are presented, they are deliberately formulated as *toy models* or kinematic existence proofs, intended to demonstrate qualitative plausibility and internal consistency rather than to reproduce precision data. Throughout, observational quantities are used to fix scales, normalize dimensionless parameters, or illustrate consistency, not to claim definitive explanatory closure. The results should therefore be read as establishing a calibratable theoretical architecture—one capable, in principle, of hosting quantitative models

of cosmological phenomena—rather than as a finished phenomenological model.

1.3 Roadmap

The structure of the paper reflects this logic. Section 2 develops the kinematical consequences of a Heisenberg tangent geometry, showing how horizontal geodesics generate flat or rising rotation curves without additional matter components. Section 3 embeds this geometry in a broader Carnot–Carathéodory framework and identifies the mesoscopic spectral rate σ as an emergent infrared scale. Section 4 derives the open-system continuity equations appropriate to a horizon-coupled exterior and identifies the compensating source terms required by conserved charges. Sections 5–8 build the thermodynamic core of the framework: the photon bath is shown to be a stationary radiative equilibrium of a geometric cavity; black holes and horizons drive irreversible entropy export; and the resulting free-energy imbalance selects σ dynamically. Section 9 explains why photons are not the dominant entropy sink and why infrared geometric modes must carry the bulk of entropy throughput. Section 10 assembles the stationary cosmological solution — expansion rate, baryon density, radiation density, and rotation curves — as corollaries of the same mesoscopic scale. Sections 11–12 analyze photon confinement and apparent expansion in more detail, connecting sub-Riemannian mixing to radiative equilibrium and to the free-energy scale associated with expansion. Sections 13–14 reinterpret CC geometry as a thermodynamic fixed point and explore observational consequences for luminosity distance and late-time cosmology. Sections 15–16 develop the chemical and nucleosynthetic implications of a steady-state exterior, including quasars as terminal attractors and the origin of the helium fraction. Section 17 examines the angular power spectrum of the photon bath and the thermodynamic selection of the $\sqrt{\ell}$ scaling in the toy CMB model. Section 18 connects the mesoscopic framework to open-system coarse-graining and the algebraic structure of the ledger variable. Section 19 models local deviations from equilibrium σ . Section 24 situates general relativity as the ultraviolet interaction kernel within this framework and clarifies the relation between emergent geometry and local gravitation. An appendix provides concrete curved model geometries that illuminate the Carnot–Carathéodory tangent structure. Taken together, these components present a unified steady-state cosmology in which rotation curves, baryon balance, the 2.7 K radiation field, and the cosmological expansion rate arise from a single horizon-locked mesoscopic scale.

2 Heisenberg Kinematics and Radial Potentials

The galactic disc is modeled, to leading mesoscopic order, by the Heisenberg group

$$\mathcal{H} = \mathbb{R} \times \mathbb{C}, \quad (s, z)(s', z') = (s + s' + \Im(\bar{z}z'), z + z'),$$

whose tangent symplectic geometry naturally produces the mesoscopic frequency scale σ that governs large-radius rotation curves. This section develops the ex-

plastic Hamiltonian mechanics of this system.

2.1 Canonical one-form and horizontal momenta

The canonical one-form on $T^*\mathcal{H}$ is

$$\psi = \sigma ds + \zeta dz + \bar{\zeta} d\bar{z},$$

with corresponding symplectic form $\omega = d\psi$ and Poisson bracket defined by ω^{-1} .

Define the horizontal momenta

$$P = \zeta - \frac{i}{2} \bar{z} \sigma, \quad \bar{P} = \bar{\zeta} + \frac{i}{2} z \sigma,$$

which satisfy the central relation

$$\{P, \bar{P}\} = i\sigma.$$

The Hamiltonian vector fields $\hat{P}, \hat{\bar{P}}$ descend to the standard Heisenberg horizontal frame on \mathcal{H} .

2.2 Free Hamiltonian in polar coordinates

Take the free Hamiltonian to be

$$K = 2P\bar{P}.$$

In the abelian limit $\sigma \rightarrow 0$, this reduces to the usual free particle Hamiltonian $K = \frac{1}{2}(p_x^2 + p_y^2)$.

Introduce polar coordinates $z = re^{i\theta}$ and conjugate momenta R, L via

$$\psi = R dr + L d\theta + \sigma ds.$$

A standard computation yields

$$P = -\frac{ie^{-i\theta}}{2} \left(\frac{L}{r} + iR + r\sigma \right),$$

and hence

$$K = 2P\bar{P} = \frac{1}{2} \left(R^2 + \frac{(L + r^2\sigma)^2}{r^2} \right). \quad (1)$$

With canonical Poisson brackets

$$\{r, R\} = 1, \quad \{\theta, L\} = 1, \quad \{s, \sigma\} = 1,$$

Hamilton's equations for the free motion are

$$\dot{r} = \{r, K\} = R, \quad (2)$$

$$\dot{\theta} = \{\theta, K\} = \frac{L + r^2\sigma}{r^2}, \quad (3)$$

$$\dot{s} = \{s, K\} = L + r^2\sigma, \quad (4)$$

$$\dot{R} = \{R, K\} = \frac{L^2}{r^3} - \sigma^2 r, \quad (5)$$

$$\dot{L} = \dot{\sigma} = 0. \quad (6)$$

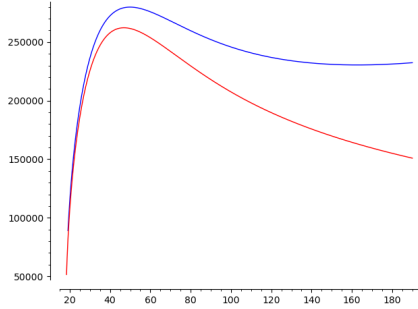


Figure 1: Rotation curve, with a naive exponential (Freeman) decay matter model, for M31 galaxy. Top curve: nonzero σ ; bottom curve: $\sigma = 0$. This uses the following parameters: $G = 2.26954 \times 10^{-69} \text{ kpc}^3/\text{kg} \cdot \text{s}^2$, $M = 2 \times 10^{42} \text{ kg}$ (mass of a typical galaxy like M31), $\sigma = 10^{-17} \text{ s}^{-1} \approx 5H_0$, $r_0 = 10 \text{ kpc}$ (scale parameter).

Thus even in the absence of a potential, generic trajectories in the (r, θ) -plane are curved, with a characteristic mesoscopic frequency σ .

2.3 Adding a radial potential

Add a central potential $V(r)$ and consider the full Hamiltonian

$$H = K + V(r) = \frac{1}{2} \left(R^2 + \frac{(L + r^2\sigma)^2}{r^2} \right) + V(r).$$

Hamilton's equations become

$$\dot{r} = R, \tag{7}$$

$$\dot{\theta} = \frac{L + r^2\sigma}{r^2}, \tag{8}$$

$$\dot{s} = L + r^2\sigma, \tag{9}$$

$$\dot{R} = \frac{L^2}{r^3} - \sigma^2 r - V'(r), \tag{10}$$

$$\dot{L} = \dot{\sigma} = 0. \tag{11}$$

For radial infall with $\dot{\theta} = 0$ we have $L = -r^2\sigma$, and hence

$$\ddot{r} = -V'(r).$$

Thus $V(r) = -m/r$ yields the inverse-square law.

2.4 Circular orbits and rotational velocity

For circular orbits of constant radius $r = r_0$ we have $R = \dot{R} = 0$, so

$$\frac{L^2}{r^3} - \sigma^2 r - V'(r) = 0, \tag{12}$$

i.e.

$$L^2 = \sigma^2 r^4 + r^3 V'(r). \quad (13)$$

In the limit $\sigma \rightarrow 0$, this becomes the Newtonian condition $L^2 = r^3 V'(r)$.

The tangential velocity is

$$v(r) = r\dot{\theta} = \frac{L + r^2\sigma}{r}.$$

Using (13), we obtain

$$v(r) = \sigma r \pm \sqrt{\sigma^2 r^2 + v_N^2(r)}, \quad (14)$$

where $v_N^2(r) = rV'(r)$ is the Newtonian circular velocity.

Equation (14) is the basic phenomenological prediction of the Heisenberg tangent geometry: the Newtonian velocity is modified by a geometric term σr , with the two contributions combining nonlinearly.

2.5 Virial theorem

Let $G = Rr$. Then

$$\dot{G} = \{G, H\}.$$

A short calculation yields

$$\{G, H\} = R^2 + \frac{L^2}{r^2} - \sigma^2 r^2 - rV'(r). \quad (15)$$

For orbits that remain confined to the galactic disc, G is bounded and the usual virial theorem implies

$$\left\langle R^2 + \frac{L^2}{r^2} - \sigma^2 r^2 - rV'(r) \right\rangle = 0,$$

where $\langle - \rangle$ denotes the long-time average along the flow. Under an ergodic hypothesis, this extends to the spatial average over the disc. In particular, for circular orbits ($R = 0$) the virial identity is equivalent to the circular-balance condition (13).

In the present framework the virial relation acquires an additional term because the horizontal momenta on the Heisenberg group are not canonically conjugate to the radial coordinate in the Euclidean sense. The effective Hamiltonian for circular motion contains a contribution $\frac{1}{2}\sigma^2 r^2$ arising from the noncommutative structure of the horizontal bundle, and this term survives the time average that produces the virial theorem. The result is a modified virial balance

$$\langle v^2 \rangle = \frac{GM(r)}{r} + \sigma^2 r^2,$$

so that the flat (or slowly rising) rotation curve follows naturally when the mesoscopic scale σ equals the Hubble rate H . In this sense the virial equilibrium of a galaxy is tied directly to the same mesoscopic scale that controls the horizon-exterior entropy balance.

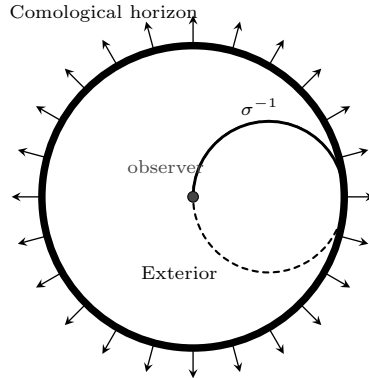


Figure 2: Basic 2-dimensional Heisenberg model. A projected geodesic is shown, from an observer to the cosmological horizon. The observer's causal access is limited by the radius of curvature. The “Exterior” is the universe that the observer may observe.

2.6 Causal implications and a cartoon view of the model

Figure 2.6 summarizes the basic causal structure of the Heisenberg model developed in this section. The observer occupies the center of the inner circle, while the cosmological horizon is depicted as the outer boundary. Projected geodesics emanating from the observer bend along Heisenberg curves of radius σ^{-1} rather than extending radially, and therefore remain confined to a causal wedge that intersects the horizon only along admissible directions. This geometry captures the essential point: in a mesoscopic Carnot–Carathéodory setting, the observer's past light cone is intrinsically curved, and signals reaching the observer must originate from within this curved causal region. No assumptions about energy loss, dissipation, or luminosity are required at this stage; the figure reflects only the underlying causal limitation imposed by the geometry itself. In later sections, this causal wedge will provide the geometric foundation for the transport, tracing, and thermodynamic phenomena that follow. The outward arrows represent the continuous flux generated by cosmological expansion across a horizon whose geometric radius remains fixed, emphasizing that expansion changes the global state of the exterior without altering the causal boundary itself: the horizon does not recede, but expansion drives flux through it.

3 Bulk Carnot Geometry and the Origin of σ

The Heisenberg model of Section 2 captures the *tangent* Carnot–Carathéodory (CC) geometry experienced by test particles moving in a two-dimensional galactic disc. In this section we indicate, at a schematic level, how such a tangent model arises from a higher-dimensional bulk geometry, and how the distinguished mesoscopic scale σ appears as the unique frequency associated with that bulk structure.

3.1 A (3,3) nilpotent model

Consider a six-dimensional step-two nilpotent Lie algebra

$$\mathfrak{n} = \mathfrak{g}_- \oplus \mathfrak{g}_+,$$

where $\mathfrak{g}_- \cong \mathbb{R}^3$ is “horizontal” and $\mathfrak{g}_+ \cong \mathbb{R}^3$ is central. Physically, \mathfrak{g}_- represents ordinary spatial directions and \mathfrak{g}_+ encodes noncommutative “phase” directions associated with angular structure. Let (x^i) be linear coordinates on \mathfrak{g}_- and (h_i) coordinates on \mathfrak{g}_+ , with conjugate momenta (p_i) and (ω_i) , $i = 1, 2, 3$. We equip the phase space

$$(x^i, h_i, p_i, \omega_i)$$

with the standard symplectic form

$$\sum_i dp_i \wedge dx^i + \sum_i d\omega_i \wedge dh_i.$$

Define the *horizontal momenta*

$$P_i = p_i + (\omega \times x)_i, \quad i = 1, 2, 3, \tag{16}$$

where $(\omega \times x)_i = \epsilon_{ijk} \omega_j x_k$ is the usual Euclidean cross product. A short computation gives the Poisson brackets

$$\{P_i, P_j\} = \epsilon_{ijk} \omega_k, \quad \{\omega_i, \cdot\} = 0, \tag{17}$$

so the ω_k are central and the P_i generate a two-step nilpotent algebra with three-dimensional center. In particular, for fixed ω this is a (3,3) Carnot group: the horizontal layer \mathfrak{g}_- is spanned by the P_i , while the central layer \mathfrak{g}_+ is spanned by the ω_k .

The free (kinetic) Hamiltonian is

$$K = \frac{1}{2} \delta^{ij} P_i P_j = \frac{1}{2} (P_x^2 + P_y^2 + P_z^2), \tag{18}$$

so that the corresponding Hamiltonian vector fields reproduce the horizontal frame of the (3,3) Carnot group. The key point is that for fixed ω the only invariant quantity carried by the central layer is its Euclidean norm $|\omega|$. This norm sets a distinguished frequency scale in the free dynamics: the generic free

trajectories are curved with curvature proportional to $|\omega|$, in close analogy with cyclotron orbits in a magnetic field.

Radial potentials $V(r)$, with $r^2 = x \cdot x$, can be added without disturbing this structure by taking

$$H = K + V(r).$$

The horizontal geometry remains Carnot, and the noncommutativity of the momenta continues to enforce a characteristic mesoscopic scale $|\omega|$ in the motion.

3.2 Planar motions and the Heisenberg limit

The Heisenberg model used for galactic discs appears as a planar subgeometry of the $(3, 3)$ system. Suppose the free trajectory remains confined to a plane—for example, $z = \text{constant}$ —and does not degenerate to motion along a straight line. The equations of motion then imply

$$p_z = 0, \quad \omega_x = \omega_y = 0,$$

so that only the central parameter ω_z survives. In this regime the horizontal momenta reduce to

$$P_x = p_x + \omega_z y, \tag{19}$$

$$P_y = p_y - \omega_z x, \tag{20}$$

with bracket

$$\{P_x, P_y\} = \omega_z,$$

and the Hamiltonian

$$K = \frac{1}{2}(P_x^2 + P_y^2)$$

is exactly the Heisenberg kinetic energy studied in Section 2 after the identification $\sigma \equiv \omega_z$. Thus the two-dimensional Heisenberg geometry governing disc kinematics is the natural planar reduction of a three-dimensional $(3, 3)$ Carnot geometry.

In particular, the mesoscopic frequency σ that appears in the radial Hamiltonian

$$K = \frac{1}{2}(R^2 + (L + \sigma r^2)^2/r^2)$$

is nothing more than the modulus of the central element ω in the underlying $(3, 3)$ Carnot group. At the purely geometric level, σ is the unique invariant scale associated with the noncommutative horizontal structure.

3.3 Embedding in a sub-Lorentzian bulk

The nilpotent model described above should be regarded as the *tangent* geometry of a more global, curved spacetime. One convenient way to organize such bulk models is via an involutive decomposition of a semisimple Lie algebra. Let

\mathfrak{g} be a real semisimple Lie algebra equipped with an involution $\theta : \mathfrak{g} \rightarrow \mathfrak{g}$, and write

$$\mathfrak{g} = \mathfrak{g}_+ \oplus \mathfrak{g}_-$$

for the ± 1 eigenspaces. The subspace \mathfrak{g}_- carries an indefinite quadratic form Q (the restriction of the Killing form), and the bracket satisfies

$$[\mathfrak{g}_-, \mathfrak{g}_-] \subset \mathfrak{g}_+.$$

In this setting \mathfrak{g}_- plays the role of a horizontal subspace and \mathfrak{g}_+ the “vertical” directions generated by their commutators. A *sub-Lorentzian* CC metric is obtained by declaring \mathfrak{g}_- to be the horizontal bundle and Q its metric.

Explicit examples include:

- $\mathfrak{g} = \mathfrak{sp}(4, \mathbb{R}) \cong \mathfrak{so}(2, 3)$, whose symmetric space models a noncommutative de Sitter-like bulk;
- $\mathfrak{g} = \mathfrak{sp}(1, 1) \cong \mathfrak{so}(1, 4)$, giving an anti-de Sitter-like bulk.

In each case, an appropriate choice of involution θ yields a four-dimensional horizontal subspace \mathfrak{g}_- with Lorentzian signature $(1, 3)$ and a compatible Hamiltonian

$$K = \frac{1}{2} Q^{ab} P_a P_b$$

constructed from the corresponding momenta P_a .

To recover the Carnot limit relevant for mesoscopic kinematics, one introduces a small parameter ε that rescales the Lie algebra as

$$\mathfrak{g}_- \mapsto \mathfrak{g}_-, \quad \mathfrak{g}_+ \mapsto \varepsilon^2 \mathfrak{g}_+,$$

and truncates the Lie bracket modulo $O(\varepsilon^3)$. In the limit $\varepsilon \rightarrow 0$ the bulk geometry degenerates to a step-two Carnot group whose horizontal layer is \mathfrak{g}_- and whose center is \mathfrak{g}_+ . At this level the only surviving invariant scale is the norm of the central element $\omega \in \mathfrak{g}_+$, which we identify with the mesoscopic frequency σ .

3.4 Geometric interpretation of the mesoscopic scale

From the bulk standpoint, the frequency σ appearing in Heisenberg kinematics and in the mesoscopic balance laws has a simple interpretation: it is the unique infrared scale associated with the curvature and noncommutativity of the CC tangent geometry. In the semisimple bulk model it is proportional to the inverse curvature radius of the corresponding de Sitter or anti-de Sitter space; in the nilpotent limit it appears as the norm $|\omega|$ of the central element defining the Carnot structure.

Horizon thermodynamics then ties this geometric scale to the cosmic expansion rate through the entropy-balance and continuity relations: stationarity of the mesoscopic medium selects

$$\sigma \sim H,$$

so that the same scale governs

- the curvature of horizontal geodesics in the Heisenberg limit (flattened rotation curves),
- the mixing and effective confinement of photons in the CC geometry (thermal radiation),
- and the excitation of long-wavelength geometric modes that balance horizon entropy production.

In this way the bulk CC geometry provides a concrete origin for the mesoscopic spectral scale σ that underlies the kinematic and thermodynamic phenomena analyzed in the rest of the paper.

4 Mesoscopic Continuity Equations

The microscopic conservation laws of quantum field theory must be translated into a coarse-grained, horizon-coupled framework appropriate to expanding spacetimes with nontrivial tangent geometry. At mesoscopic scales—intermediate between local particle interactions and global cosmological averages—the relevant observables satisfy continuity equations modified by irreversible exchange with causally inaccessible sectors.

We work in comoving coordinates on a spatially expanding background with scale factor $a(t)$ and Hubble parameter $H = \dot{a}/a$. Let $n_X(t)$ denote the *physical* (proper) number density of any conserved or effectively conserved charge X . Integrating the associated current J_X^μ over a comoving control volume whose boundary becomes null at the cosmological horizon, and allowing degrees of freedom to exit the exterior Hilbert space through causal decoupling, yields the general balance law [76, 21, 60]

$$\partial_t n_X + 3Hn_X = -\Phi_X + \Gamma_X. \quad (21)$$

Here Φ_X is the physical loss rate (per unit volume) of X -carrying degrees of freedom from the observer-accessible sector, while Γ_X is the corresponding source term for mesoscopic charge conservation. Since conserved quantities are defined only on the reduced, observer-accessible Hilbert space, there is no meaningful notion of a conserved charge across the full spacetime Hilbert space. The balance law therefore pertains solely to the exterior sector: loss through the causal boundary must be matched, in the reduced description, by a compensating source term if mesoscopic stationarity is to be maintained. This matching is not imposed by microscopic conservation, but arises from the open-system dynamics of the exterior Hilbert space.

The two additional terms Φ_X and Γ_X encode the essential mesoscopic physics:

- **Exterior loss flux Φ_X :** the rate at which charge-carrying excitations are transported into causally inaccessible sectors—such as cosmological horizons or, on sufficiently long timescales, compact objects—and cease to contribute to the reduced exterior density operator.

- **Compensating source Γ_X :** the effective creation rate required to maintain mesoscopic charge balance in the exterior description when X –carrying degrees of freedom are irreversibly exported. This term reflects the open–system thermodynamics of the exterior and may be parameterized in terms of an *exterior entropy–exchange scale* T_{ext} , which governs the energetic cost of processing entropy through the open channel. It should not be confused with the radiative temperature of the photon bath ($T_\gamma \simeq 2.7 \text{ K}$), which acts as a passive buffer and need not control Γ_X .

In this section we make these objects precise for the physically relevant charge $X = B$ (baryon number). The same open–system formalism applies to any conserved quantum number whose irreversible export from the exterior can alter its effective density; this includes lepton number and other global or weakly gauged charges. Electric charge is excluded from this class, since its long–range gauge field imprints the total charge on the exterior region and prevents horizon–mediated depletion.

4.1 Observer–Dependence and Causal Partitioning

An important note is that the causal horizon invoked throughout this work should not be interpreted as an observer–independent physical boundary [69, 73]. Horizons in semiclassical gravity are inherently observer–relative: an observer freely crossing another’s horizon does not encounter any local singularity, and each observer traces over degrees of freedom inaccessible to the other.

The role of the horizon in the present framework is therefore not ontological but operational. For any semiclassical observer, the causal structure induces a natural partition of the global Hilbert space into accessible and inaccessible sectors. Tracing over the latter renders the exterior an open quantum system, with irreversible entropy fluxes governed by modular dynamics [15, 18, 69, 9].

All thermodynamic statements in this work refer to this observer–relative exterior system. Physical predictions depend only on the universality of causal partitioning, not on the existence of a preferred or absolute horizon.

4.2 Coarse-grained currents and null boundaries

Let $V(t)$ be a comoving volume whose boundary is everywhere timelike except at the cosmological horizon, where the causal structure degenerates. Formally,

$$\frac{d}{dt} \int_{V(t)} J_X^0 d^3x = - \int_{\partial V(t)} J_X^i dS_i + \int_{\partial V_{\text{hor}}} J_X^\mu k_\mu dA,$$

where k^μ is the null generator of the horizon [72]. The first term gives the usual bulk flux; the second term represents loss of charge into the interior degrees of freedom. After dividing by the comoving volume and taking $V \rightarrow \infty$, one obtains the averaged flux Φ_X that appears in (21).

Crucially, Φ_X depends only on the *asymptotic* charge content of matter streams approaching the horizon and not on the microscopic details of local

interactions. This reflects the fact that horizon absorption is a kinematic process governed by the causal structure of spacetime.

4.3 Entropy biases and compensating source terms

Tracing over causally inaccessible degrees of freedom induces an information-theoretic bias in the reduced exterior state. In an open quantum system, this bias need not correspond to thermal equilibrium with a bath; rather, it reflects the fact that the reduced density operator maximizes entropy subject to the constraints imposed by the coarse-grained exterior observables [15, 65].

In the present context, the irreversible export of charge-carrying degrees of freedom across a causal horizon alters the entropy of the inaccessible sector in a charge-dependent manner. The exterior state therefore acquires an effective bias proportional to the entropy gradient

$$\frac{\partial S_{\text{inacc}}}{\partial Q_X},$$

evaluated on the traced-over sector. This quantity plays the role of a generalized thermodynamic force, biasing exterior fluctuations without introducing a physical horizon temperature or an equilibrium ensemble.

For baryon number, this entropy bias favors configurations in which the exterior charge deficit induced by horizon export is statistically compensated. In an irreversible nonequilibrium steady state, such a bias generically produces a compensating source term whose rate is set by the mesoscopic coarse-graining timescale rather than by a thermal bath [65, 23].

Accordingly, we parameterize the baryon creation rate as

$$\Gamma_B \sim \sigma \mathcal{F}_B,$$

where σ is the mesoscopic spectral scale introduced by the Carnot–Carathéodory tangent geometry, and \mathcal{F}_B is a functional encoding the entropy bias induced by baryon transport into inaccessible sectors. This term appears as the source Γ_B in the mesoscopic continuity equation (21).

4.4 Baryon continuity equation

Specializing to $X = B$, and writing the physical baryon density as n_B , we obtain

$$\partial_t n_B + 3Hn_B = -\Phi_B + \Gamma_B. \quad (22)$$

The interpretation is as follows:

- The expansion term $3Hn_B$ represents the dilution of baryon density in physical volumes due to cosmological expansion.
- The flux Φ_B accounts for the loss of baryon-carrying degrees of freedom from the observer-accessible sector, through transport into causally inaccessible regions such as cosmological horizons and, on sufficiently long timescales, compact objects.

- The source Γ_B represents a compensating baryon production term in the exterior description, induced by irreversible export of baryon number and required to maintain mesoscopic charge balance in a steady-state regime.

In a statistically stationary cosmological medium—understood as a coarse-grained steady state averaged over timescales long compared to the mesoscopic scale—one may set $\partial_t n_B = 0$, yielding the balance condition

$$3Hn_B = -\Phi_B + \Gamma_B.$$

This relation determines the steady-state baryon density once the cosmic expansion rate H and the exterior entropy-exchange and transport properties governing Φ_B and Γ_B are fixed.

Conservation on distinct Hilbert spaces

Baryon number is conserved globally on Cauchy hypersurfaces and statistically conserved in the exterior subsystem, but these two conservation statements refer to distinct operators on distinct Hilbert spaces. Horizons prevent the global Hilbert space from factorizing into an exterior tensor an inaccessible interior component, so the global baryon charge is not the sum of an exterior and interior charge. The baryon created in the exterior and the baryon sequestered behind the horizon are not counted by a common additive operator, so there is no possibility of double-counting or violation of conservation. In this sense baryon number is conserved in the exterior subsystem and also conserved globally, because the two operators live in different operator algebras that cannot be embedded into a single tensor decomposition.

4.5 Scaling, dimensional analysis, and the role of σ

The mesoscopic spectral scale σ arising from the Heisenberg (or more general Carnot–Carathéodory) tangent geometry enters the baryon continuity equation as the characteristic *rate* governing irreversible coarse-graining and long-wavelength mode mixing in the exterior system. It does not represent a temperature or equilibrium scale, but rather the inverse timescale over which exterior observables are reorganized by mesoscopic kinematics.

In the present framework, the compensating source term Γ_B is controlled by two ingredients: an entropy bias induced by the irreversible export of baryon number from the exterior sector, and the mesoscopic rate at which this bias is dynamically realized. Dimensional analysis therefore implies

$$\Gamma_B \sim \mathcal{F}_B \sigma,$$

where \mathcal{F}_B is a dimensionful coefficient. This coefficient encodes the efficiency with which entropy bias is converted into baryon-carrying exterior degrees of freedom, and depends on the structure of the available exterior channels rather than on any thermal properties of a radiation bath.

Observational analyses of galactic rotation curves [46, 25] indicate that the same mesoscopic scale satisfies $\sigma \sim H_0$. This identification should be understood as a nonequilibrium steady-state offset: the intrinsic relaxation of the Carnot geometry favors $\sigma \rightarrow 0$, but irreversible horizon coupling arrests this decay and selects a mesoscopic rate that clusters at H_0 . In a statistically stationary cosmological medium, the baryon continuity equation then implies that the physical baryon density is set parametrically by the cosmic expansion rate,

$$n_B \sim \frac{\Phi_B}{H_0} + O(1),$$

up to dimensionless factors determined by the details of baryon loss and entropy processing.

This closes the mesoscopic system: the same geometric scale σ that governs infrared kinematics and rotational dynamics also controls the long-term baryon balance of the universe in a nonequilibrium steady-state description.

5 The Cosmic Microwave Background as a Steady-State Radiative Equilibrium

The cosmic microwave background (CMB) is traditionally interpreted as relic radiation from a hot early epoch. In the framework developed here, we adopt an alternative but observationally compatible interpretation, in which the CMB is understood as the stationary radiative sector of an open quantum system, whose exterior degrees of freedom equilibrate to a fixed *radiative* temperature with respect to the physical time flow of finite observers [14, 65]. This temperature,

$$T_{\text{CMB}} \simeq 2.7 \text{ K},$$

characterizes the photon bath described by the reduced exterior density matrix and reflects the thermodynamic state of the resolved ultraviolet and mid-infrared field degrees of freedom.

This radiative temperature must be sharply distinguished from the *entropy-acceptance temperature* of the horizon. The cosmological horizon does not act as a radiative heat bath but as an effectively zero-temperature entropy sink, capable of absorbing entropy with negligible energy cost. The observed CMB temperature therefore does not represent a temperature of the horizon itself, nor a relic of a primordial epoch, but is a property of the exterior state-flow pair $(\mathcal{A}_{\text{ext}}, \tau_t)$ governing late-time observers.

5.1 Why a stationary 2.7 K bath is thermodynamically natural

The exterior radiation field interacts rapidly with baryons, dust, plasma, and starlight [52, 58], and it mixes efficiently under the horizon-coupled Carnot–Carathéodory (CC) geometry. These processes ensure that the photon bath

remains close to thermal equilibrium under continuous injection, scattering, absorption, and mode redistribution [52, 58]. The bath thus functions as an effective thermal regulator: any injected power is redistributed across the spectrum, and perturbations away from a thermal form are smoothed by geometric mixing. The bath thus functions as a *fast spectral thermalizer*: any injected power is quickly redistributed, and any perturbation away from a thermal spectrum is smoothed by geometric mixing.¹

Because the photon bath occupies only a tiny fraction of the total free-energy budget of the exterior sector, maintaining its temperature requires only a negligible energy throughput [27, 52]. In particular, the free energy liberated by horizon entropy export is many orders of magnitude larger than the radiative energy needed to sustain a $T_{\text{CMB}} \simeq 2.7 \text{ K}$ bath. As a result, the photon field is maintained at its equilibrium temperature even when ultrasoft gravitational modes “leak” entropy across the horizon. The required replenishment is thermodynamically cheap.

5.2 Why the photon bath does not cool under expansion

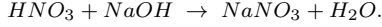
In standard FRW reasoning, radiation redshifts as a^{-4} and cools unless it is continually replenished [77, 21]. In the present framework, redshift represents not a loss of energy to “nothing” but the transfer of energy into the infrared geometric sector, where it contributes to the free-energy account that ultimately drives entropy export across the horizon. The photon bath does not drain away; it is continually reheated by absorbing an exceedingly small fraction of the free

¹The role played here by the photon bath is closely analogous to the use of *free-energy buffers* in chemistry and biophysics. In such systems (for example, the ATP/ADP/ P_i couple in cellular metabolism or standard redox buffers in electrochemistry), a regulated intermediate reservoir maintains an approximately stationary intensive parameter (chemical potential, redox potential, or effective temperature) while large free-energy fluxes pass through it. Entropy production is not minimized locally in the buffer but is exported to the ultimate environment, allowing irreversible processes to proceed without large excursions of the buffered variable.

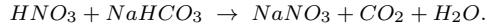
The photon bath in the present framework plays an analogous role: it redistributes free energy while remaining near a stationary state, and it is not the final entropy sink of the system.

As a simple laboratory analogue, consider a buffered acid–base titration in which acid is slowly added to a bicarbonate solution. Over a wide range of added acid, the system irreversibly degrades free energy while the *buffered intensive variable* (the proton chemical potential, or pH) remains nearly constant; once the buffering capacity is exhausted, this regulation fails and the pH rapidly decreases.

By contrast, adding nitric acid directly to a sodium hydroxide solution produces a strongly exothermic neutralization in which temperature and local chemical–potential gradients change rapidly,



Introducing sodium bicarbonate moderates this interaction by providing an intermediate buffered channel in which free energy is absorbed and redistributed with smaller excursions of intensive variables,



In both cases the total entropy production is comparable, but the buffered pathway spreads dissipation over a larger phase space and suppresses violent local responses.

energy liberated by the irreversible sequestration of matter and structure into the horizon.

If the photon temperature were momentarily to fall below its stationary value, the bath would absorb additional free energy until equilibrium was restored. Because the required energy is minuscule compared to the available free-energy flux, this re-equilibration occurs with negligible effect on the global free-energy budget. Thus radiation maintains a stable temperature set by the exterior state, rather than by initial conditions.

5.3 Conceptual summary

These considerations do not, by themselves, determine the numerical value of the photon temperature. Rather, they show that once this temperature is selected by infrared geometric and entropic constraints, it is robustly maintained against expansion and perturbations. Within this framework, a photon bath at the observed temperature is dynamically stable and thermodynamically inexpensive to maintain. In particular, such a bath persists near 2.7 K because:

1. it is a fast thermalizer of injected free energy;
2. maintaining its temperature requires negligible power compared to the free-energy flux associated with horizon entropy export;
3. redshift losses feed the infrared geometric sector rather than depleting the exterior of energy; and
4. any deficit is corrected by tiny adjustments in the absorbed free-energy flux, rather than by bulk photon creation.

This interpretation situates the CMB within the same mesoscopic thermodynamic framework that governs baryon balance and global entropy flow, and it prepares the ground for the horizon-coupled thermodynamics developed in the next section.

We emphasize that this reinterpretation is intended as an effective late-time thermodynamic description. It does not deny the empirical success of early-universe modeling in accounting for the CMB spectrum, isotropy, or anisotropy structure, but rather addresses how a thermal photon bath can remain stable in an open, horizon-coupled universe over cosmological timescales.

6 Horizon-Coupled Thermodynamics

The mesoscopic continuity equations derived in Section 4 describe the balance of conserved charges in an expanding spacetime with horizon exchange. We now incorporate the complementary requirement of *entropy balance*. In a horizon-coupled cosmology, entropy is not conserved as a comoving density, but flows irreversibly through the exterior system and into a causal sink. Stationarity

must therefore be formulated as a balance of entropy *fluxes*, rather than as a closed-system conservation law.

The thermodynamic structure developed in this section is that of an open, nonequilibrium steady state. Entropy is continuously produced, transported, and exported, yet no macroscopic entropy reservoir accumulates entropy secularly. To make this explicit, we distinguish three extensive entropy sectors:

$$S_{\text{obs}}, \quad S_{\text{BH}}, \quad S_{\text{hor}},$$

denoting respectively the entropy of observer-accessible degrees of freedom, the Bekenstein–Hawking entropy of black holes within the cosmological causal wedge, and the entropy of the cosmological horizon.

The exterior entropy is defined as

$$S_{\text{ext}} \equiv S_{\text{obs}} + S_{\text{BH}}, \quad (23)$$

and in the late-time steady state all extensive exterior entropies are stationary:

$$\dot{S}_{\text{obs}} = 0, \quad \dot{S}_{\text{BH}} = 0, \quad \dot{S}_{\text{ext}} = 0. \quad (24)$$

Stationarity here refers to the *total* entropy in each sector, not to the absence of entropy flux. Each sector functions as a throughput reservoir whose inflow and outflow of entropy balance exactly in steady state.

Gravitational collapse, accretion, and structure formation continuously transfer entropy from observer-accessible degrees of freedom into black-hole microstates, while an equal entropy flux transfers black-hole microstates into the cosmological horizon. The black-hole sector therefore acts as an intermediate entropy amplifier: it neither accumulates nor depletes entropy in steady state, but mediates irreversible entropy flow between the exterior medium and the horizon.

The cosmological horizon is the unique entropy sink. Its entropy increases monotonically,

$$\dot{S}_{\text{hor}} > 0, \quad (25)$$

ensuring consistency with the second law for the combined system. The apparent constancy of S_{ext} does not signal reversibility or equilibrium. Rather, it reflects a balance of entropy fluxes in an open system.

Thermodynamically, the exterior operates as an *irreversible Carnot engine*. Free energy is processed within the exterior at an effective temperature T_{ext} , amplified into large amounts of entropy by gravitational collapse, and ultimately dumped into the cosmological horizon, which functions as an effectively zero-temperature reservoir. Because $T_{\text{hor}} \ll T_{\text{ext}}$, the entropy increase of the horizon associated with a given energy flux exceeds the entropy throughput of the exterior sectors, guaranteeing strictly positive net entropy production despite the stationarity of S_{obs} and S_{BH} .

With this bookkeeping fixed,² the remainder of this section formulates the mesoscopic continuity equations governing entropy throughput, identifies the infrared geometric channel responsible for entropy export and return, and shows how these fluxes enforce a self-consistent steady state with stationary exterior entropies.

Entropy export versus horizon entropy. A notational distinction is essential. Throughout this section, \dot{S}_{cos} (and its density \dot{s}_{cos}) denotes an *entropy flux*—the rate at which exterior entropy S_{ext} is transported across the cosmological horizon and removed from the exterior Hilbert space as causal access is lost due to expansion. It is therefore an *outgoing flux of exterior entropy*, not the time derivative of the entropy of the horizon itself.

By contrast, \dot{S}_{hor} denotes the rate of change of the entropy associated with the cosmological horizon as a thermodynamic system. These two quantities are not equal. The second law for the combined exterior–horizon system requires

$$\dot{S}_{\text{hor}} \geq \dot{S}_{\text{cos}}, \quad (26)$$

with strict inequality whenever entropy is produced irreversibly in the transfer of exported degrees of freedom into horizon microstates. In the language of nonequilibrium thermodynamics, \dot{S}_{cos} is an entropy *current*, while \dot{S}_{hor} includes both this current and the additional entropy production associated with coupling to an effectively cold reservoir. Failure to distinguish these quantities would amount to confusing entropy transport with entropy production.

Entropy export and stationarity. In the bookkeeping adopted here, black-hole entropy is included in the exterior entropy $S_{\text{ext}} = S_{\text{obs}} + S_{\text{BH}}$. Although black-hole entropy is continually generated by collapse and accretion, it does not accumulate secularly. In a horizon-coupled steady state, the rate at which entropy is channeled into black-hole microstates is exactly balanced by the rate at which exterior entropy is exported across the cosmological horizon as causal access is lost due to expansion.

Black holes therefore act as entropy amplifiers and staging reservoirs within the exterior system. They neither create nor destroy entropy in the global sense; rather, they mediate an irreversible entropy flux from the exterior medium into the horizon. The cosmological horizon serves as the unique entropy sink, while

²A subtle but important point concerns the role of black-hole entropy in the exterior bookkeeping. Black holes amplify entropy through accretion, but the microscopic degrees of freedom responsible for the Bekenstein–Hawking entropy are causally tied to the same irreversible channel that exports entropy to the cosmological horizon. From a mesoscopic standpoint, it is therefore equally consistent to regard black-hole entropy as (i) part of the instantaneous exterior entropy, or (ii) entropy already irreversibly coupled to a future causal boundary.

These two descriptions differ only by a bookkeeping convention and have no physical consequence for the balance laws. What is invariant is the *entropy export rate* and the associated free-energy release. All subsequent equations depend only on this flux, not on the notional location of the entropy at intermediate times.

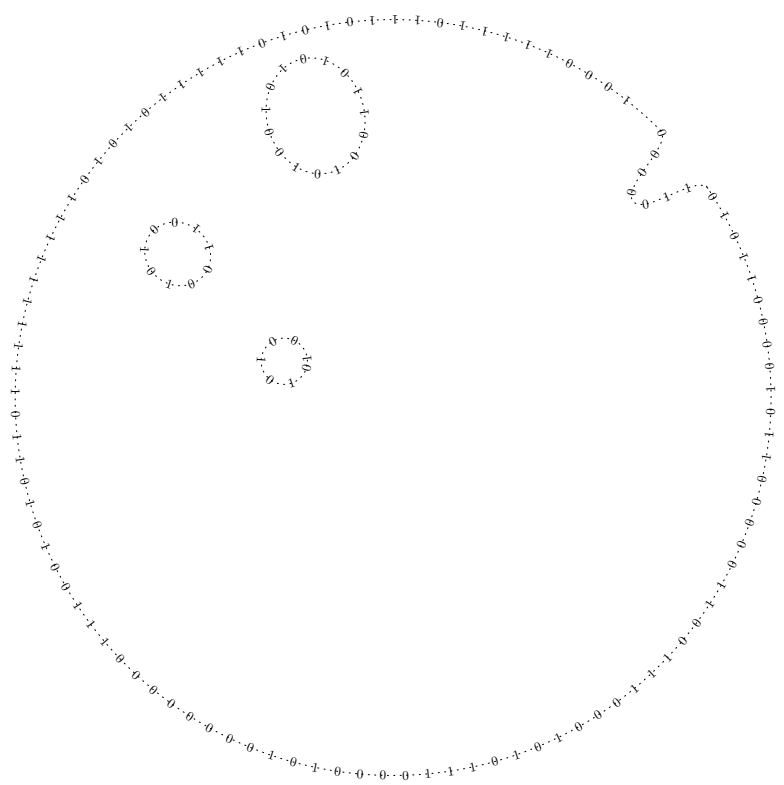


Figure 3: A “holographic” view. Black holes nucleate in the exterior, and their entropy microstates are encoded as qubits on their horizons. As expansion drives them outward, these horizon degrees of freedom are absorbed into the microstates of the cosmological horizon.

the detailed partition of exterior entropy into observer-accessible and black-hole components plays no role in the balance laws.

As a consequence, entropy production within the exterior does not imply secular growth of the total exterior entropy. Stationarity is achieved dynamically through a balance of entropy fluxes. In steady state,

$$\dot{S}_{\text{ext}} \approx 0, \quad (27)$$

even though entropy is continually exported from the exterior and the entropy of the horizon increases monotonically in accordance with the second law.

Entropy continuity equation. Let $s_{\text{ext}}(t)$ denote the coarse-grained physical entropy density of the exterior system. Applying Reynolds transport to a comoving world-tube bounded by the cosmological horizon yields the mesoscopic entropy balance equation [74]

$$\dot{s}_{\text{ext}} + 3H s_{\text{ext}} = -\dot{s}_{\text{cos}} + \dot{s}_{\text{IR}}, \quad (28)$$

where:

- $\dot{s}_{\text{cos}} > 0$ is the entropy *flux density* exported from the exterior across the cosmological horizon, i.e. the rate at which exterior entropy is removed from the exterior Hilbert space by loss of causal access due to expansion; and
- $\dot{s}_{\text{IR}} > 0$ is the rate at which expansion-driven infrared geometric modes inject entropy into the exterior system.

The term $3H s_{\text{ext}}$ represents the kinematic dilution of physical entropy density due to cosmic expansion; it is the advective contribution associated with the time-dependent exterior volume and should not be interpreted as a separate entropy export channel. By contrast, \dot{s}_{cos} represents an irreversible entropy current across the horizon. Black-hole entropy production does not appear as an independent source term: because the total black-hole entropy S_{BH} is stationary in steady state, its production by accretion is exactly balanced by export across the horizon and is therefore contained implicitly in \dot{s}_{cos} .

Stationary exterior entropy density. In a horizon-coupled steady state the physical entropy density of the exterior is approximately stationary,

$$\dot{s}_{\text{ext}} \approx 0. \quad (29)$$

Under this condition, Eq. (28) reduces to the algebraic balance relation

$$3H s_{\text{ext}} = \dot{s}_{\text{IR}} - \dot{s}_{\text{cos}}, \quad (30)$$

which fixes the *volumetric entropy return rate* required for stationarity. The dilution of entropy density by cosmic expansion and the irreversible export of exterior entropy across the horizon must be exactly compensated, in steady state, by entropy supplied through expansion-induced infrared geometric degrees of freedom.

6.1 Entropy production and horizon export

At the semiclassical level, black-hole formation and growth are governed by the Bekenstein–Hawking area law [6, 74]. Matter accretion produces a large amount of entropy per unit accreted energy, amplifying entropy within the exterior system. In the present framework this amplification does not lead to secular growth of exterior entropy. Instead, the entropy generated by black-hole growth is transferred to the cosmological horizon on cosmological timescales, contributing to the irreversible increase of horizon entropy while leaving S_{ext} stationary.

The baryon flux Φ_B introduced in Section 4 contributes directly to this entropy processing. Baryon sequestration into black holes enhances entropy amplification and thereby increases the export rate \dot{s}_{cos} . The resulting thermodynamic imbalance is compensated by the baryon creation term Γ_B in the baryon continuity equation (22), restoring a stationary exterior baryon density.

Photons and neutrinos also cross the cosmological horizon, but they do not control the entropy balance. Although a cold photon bath can carry large entropy per unit energy, routing the free-energy budget primarily into electromagnetic heating does not maximize entropy throughput into the ultimate cold reservoir. The dominant steady-state entropy circuit is instead gravitational and infrared: collapse and accretion amplify entropy, while expansion-driven infrared geometric modes provide the channel that exports this entropy irreversibly to the cosmological horizon. In this sense the photon sector acts as a passive thermometer of the medium, whereas the infrared gravitational sector is the active carrier that closes the entropy budget in Eq. (28).

6.2 IR entropy from cosmic expansion

Cosmic expansion excites long-wavelength gravitational and geometric modes in the mesoscopic Carnot–Carathéodory geometry. These infrared modes carry entropy without being constrained by baryon or lepton charges and can be produced in enormous numbers at small energy cost. Their net contribution to the entropy budget is encoded in \dot{s}_{IR} in (28).

Dimensional considerations and the kinematics of the Carnot tangent geometry imply that the excitation rate of IR modes scales with the distinguished mesoscopic frequency σ . In the horizon-coupled steady state, the mesoscopic rate σ is arrested at a value of order H (while the intrinsic geometric relaxation favors $\sigma \rightarrow 0$ in the absence of horizon coupling). Heuristically, the spectrum of IR modes behaves as a standing-wave system constrained by the global causal structure. The sign of \dot{s}_{IR} is such that expansion *adds* entropy to the exterior sector: on mesoscopic scales the production of long-wavelength geometric modes increases the exterior entropy density and counteracts the loss to horizons, allowing a stationary solution of (28).

From the standpoint of the combined system, \dot{S}_{IR} is the unique large channel through which expansion-driven geometry can return entropy to the mesoscopic medium. It is the entropy analogue of the creation term Γ_B in the baryon

continuity equation: both are horizon-induced, infrared processes that restore stationarity in the presence of continuous accretion.

6.3 Grand-canonical constraints for the reduced exterior state

Tracing over horizon-inaccessible degrees of freedom yields a reduced exterior state that is naturally of grand-canonical type [64, 12]. In particular [10], the reduced density operator takes the schematic form

$$\rho_{\text{ext}} \propto \exp \left[-K_{\text{mod}} - \sum_X \alpha_X Q_X \right], \quad (31)$$

where K_{mod} is the modular generator associated with the horizon-defined factorization and the α_X encode the conjugate biases (chemical potentials) enforcing conditional entropy maximization at fixed exterior charges.

In the present framework, the temperature T_{ext} plays a single, unambiguous physical role. It governs the entropy-processing capacity of the exterior medium and sets the scale for the production of infrared modes and baryons that compensate expansion-driven dilution. The associated mesoscopic source terms are therefore controlled by T_{ext} , which functions as an entropy-return temperature rather than a horizon temperature.

The photon bath acts as a rapidly equilibrating, passive buffer that records this temperature spectrally. Its near-Planckian distribution reflects the stationary value of T_{ext} but does not itself drive entropy return or baryon repopulation, in close analogy with buffered intermediate reservoirs in chemical thermodynamics.

By contrast, the cosmological horizon functions as an effectively zero-temperature entropy sink. Because it absorbs entropy at negligible energetic cost, it does not participate in the entropy-return channel and does not set the scale of infrared production or chemical bias. Its role is purely absorptive, not regulatory.

In particular, the baryon bias may be written schematically as

$$\mu_B \equiv T_{\text{ext}} \alpha_B, \quad (32)$$

so that $\mu_B > 0$ corresponds to a reduced exterior state that favors baryon repopulation when baryon-carrying degrees of freedom are exported across horizons. In steady state the baryon source term adjusts so that $\Gamma_B = \Phi_B - 3Hn_B$, fixing the stationary exterior density.

6.4 Stationarity and coupled balance laws

The entropy continuity equation (28) and the baryon continuity equation (22) together determine the large-scale thermodynamic and kinematic state of an expanding universe whose mesoscopic structure admits a closure in terms of the distinguished spectral scale σ .

Explicitly, the coupled mesoscopic balance laws are

$$\dot{s}_{\text{ext}} + 3Hs_{\text{ext}} = -\dot{s}_{\text{cos}} + \dot{s}_{\text{IR}}, \quad (33)$$

$$\dot{n}_B + 3Hn_B = -\Phi_B + \Gamma_B. \quad (34)$$

In a steady-state cosmological medium one has $\dot{s}_{\text{ext}} = 0$ and $\dot{n}_B = 0$, and (33)–(34) reduce to the algebraic relations

$$\dot{s}_{\text{IR}} = 3Hs_{\text{ext}} + \dot{s}_{\text{cos}}, \quad 3Hn_B = -\Phi_B + \Gamma_B. \quad (35)$$

The first equation expresses the global second law for the combined horizon–exterior system; the second fixes the equilibrium baryon density once the horizon-induced fluxes Φ_B and Γ_B are specified.

Because both \dot{s}_{IR} and Γ_B scale with the mesoscopic frequency σ , the expansion rate H , the cosmic baryon density, and the horizon thermodynamics are all governed by the same infrared scale.

The next subsection analyzes in more detail how horizon-induced entropy flow enforces mesoscopic baryon creation in such a steady state.

6.5 Entropy Balance, Horizon Charges, and the Necessity of Baryon Creation

The mesoscopic exterior universe is not a closed thermodynamic system. Cosmological expansion continually removes degrees of freedom from the causal wedge of late-time observers, exporting both entropy and conserved charges into horizon–inaccessible sectors. Any steady-state description must therefore account not only for conserved currents but for the irreversible *loss of access* to those currents.

From the standpoint of the full quantum field theory, baryon number is exactly conserved. From the standpoint of the reduced exterior state, however, baryon density decreases as baryon–carrying worldlines are transported across the cosmological horizon. Black–hole accretion provides an additional localized realization of the same mechanism, sequestering baryon number into horizon–adjacent, exponentially redshifted modes. In neither case is baryon number destroyed; what changes is the factorization of the global Hilbert space into accessible and inaccessible sectors.

Coarse–graining over the inaccessible sector therefore produces an exterior density operator with a positive baryon chemical potential $\mu_B > 0$. Restoring steady state does not require the return of the original infalling baryons—a process exponentially suppressed by horizon redshift—but rather the appearance of new baryons in the exterior sector. Baryon creation is thus not an ad hoc assumption but the thermodynamically preferred response of an open system subject to continuous horizon–induced depletion.

The free energy required for baryon realization is supplied by entropy export into horizon microstates. Black–hole Hawking radiation is negligible for astrophysical masses; instead, entropy balance is achieved through the excitation of

ultra-soft infrared modes associated with cosmological expansion. These modes can carry arbitrarily large entropy at negligible energy cost, liberating free energy sufficient to offset the rest-mass cost of baryon materialization by many orders of magnitude. At the mesoscopic level the baryon therefore appears first *in potentia*, as a grand-canonical bias in the reduced exterior state; a localized ultraviolet proton emerges only where local energy conditions permit.

Why lepton number does not impose a thermodynamic constraint.

Although both baryon number B and lepton number L are exactly conserved in the full quantum field theory at the energies relevant here, they play very different roles in the thermodynamics of the mesoscopic exterior. The difference is not microscopic but energetic.

Baryons are heavy, long-lived, and gravitationally bound. Their removal from the exterior through cosmological expansion or black-hole accretion produces a genuine deficit in the reduced exterior density operator. Each lost baryon carries an entropy cost proportional to the inverse horizon temperature, and the exterior therefore develops a nonzero baryon chemical potential. Steady-state balance forces baryon creation.

Leptons, by contrast, are thermodynamically inexpensive. Once sufficient free energy is available to realize baryons, the additional energy required to produce the accompanying leptons needed for charge neutrality is negligible by comparison. Electron production therefore adjusts automatically to whatever baryon population emerges and never limits the equilibrium.

Any residual excess of lepton number is carried almost entirely by neutrinos. Because neutrinos interact only weakly, they decouple from the exterior free-energy recycling loop, redshift with the radiation field, and are gradually transported out of the causal wedge of late-time observers by cosmic expansion. This lepton background has no significant back-reaction on the mesoscopic state and does not influence the baryon chemical potential.

Thus lepton number must be conserved globally, but it does not constrain the steady state. Lepton creation is not an independent thermodynamic requirement; it is a trivial corollary of baryon realization and charge neutrality. The only conserved charge whose loss forces a macroscopic response in a horizon-coupled steady state is baryon number.

6.6 Baryon number continuity

Let $\rho_B(t)$ denote the physical baryonic mass density contained in the exterior region accessible to late-time observers. Although the underlying quantum field theory exactly conserves the baryon current, the exterior is an *open system*: cosmological expansion continually transports baryon-carrying degrees of freedom across the cosmological horizon, removing them from the exterior Hilbert space. Baryon number therefore does not obey a closed comoving conservation law in the reduced description.

At mesoscopic scales the appropriate continuity equation on an expanding

background takes the form

$$\dot{\rho}_B + 3H\rho_B = \dot{\rho}_B^{(\text{create})} - \dot{\rho}_B^{(\text{loss})}, \quad (36)$$

where $\dot{\rho}_B^{(\text{create})}$ denotes the rate at which baryonic mass is injected into the exterior sector, and $\dot{\rho}_B^{(\text{loss})}$ denotes the rate at which baryonic mass is exported from the exterior Hilbert space. The loss term represents a *flux across a causal boundary* rather than local destruction of baryon number.

The dominant contribution to $\dot{\rho}_B^{(\text{loss})}$ arises from transport of baryon-carrying degrees of freedom across the cosmological horizon. Localized black-hole accretion provides an additional, spatially inhomogeneous contribution but does not control the homogeneous baryon balance of the universe. It is therefore convenient to write

$$\dot{\rho}_B^{(\text{loss})} = \dot{\rho}_{\text{cos}} + \dot{\rho}_{\text{acc}}, \quad (37)$$

where $\dot{\rho}_{\text{cos}}$ denotes the horizon-export term and $\dot{\rho}_{\text{acc}}$ the baryonic mass flux captured by black holes.

In a stationary exterior description, $\dot{\rho}_B = 0$, and Eq. (36) reduces to the steady-state balance condition

$$\dot{\rho}_B^{(\text{create})} = 3H\rho_B + \dot{\rho}_{\text{cos}} + \dot{\rho}_{\text{acc}}. \quad (38)$$

The term $3H\rho_B$ reflects the kinematic dilution of physical density in an expanding volume, while $\dot{\rho}_{\text{cos}}$ encodes irreversible export of baryon number from the causal wedge of late-time observers.

The purpose of comparing $\dot{\rho}_B^{(\text{create})}$ with the black-hole accretion rate density $\dot{\rho}_{\text{acc}}$ is not to suggest a causal link between baryon creation and black-hole growth, but to provide an empirical scale against which the required replenishment rate may be judged. The steady-state condition $\dot{\rho}_B^{(\text{create})} \sim 3H\rho_B$ fixes the magnitude of baryon injection required by cosmological expansion and horizon export, independent of any localized collapse phenomena. By contrast, $\dot{\rho}_{\text{acc}}$ is an observationally accessible tracer of baryonic mass processing in the late universe.

Observationally [32], the ratio of baryonic mass density to black-hole mass density lies in the range $\rho_B/\rho_{\text{BH}} \sim 10^2\text{--}10^3$, while the ratio of the cosmic star-formation rate density to the black-hole accretion rate density is also of order 10^3 . The fact that these independently inferred ratios are of similar magnitude indicates that the baryon replenishment required to maintain a stationary exterior medium is not parametrically large compared to known late-time baryonic processing rates. Black-hole growth thus serves as a useful empirical yardstick, while remaining a subleading sink in the global baryon balance.

From this perspective, baryon “creation” in a steady-state universe is not a microscopic violation of baryon number but the open-system response of the exterior sector to continual charge export across the cosmological horizon. Black-hole accretion enters only as a correction to this global balance.

Remark. The same bookkeeping that enforces baryon balance also constrains the lepton budget in the neutrino sector. In steady state, the cosmological electron-type neutrino and antineutrino backgrounds (with local sources such as supernovae, neutron stars, and active galactic nuclei excised) must obey a mesoscopic continuity equation of the schematic form

$$\dot{n}_{\nu_e} + \dot{n}_{\bar{\nu}_e} + 3H(n_{\nu_e} + n_{\bar{\nu}_e}) = S_\nu(\sigma). \quad (39)$$

Here $S_\nu(\sigma)$ encodes both neutrino production from weak processes near compact objects and the antineutrino flux associated with infrared baryon repopulation. As in the baryon case, this source term is not free: it is fixed by the same horizon-coupled balance laws that determine the baryon creation rate and the net rate at which lepton number is transported out of the cosmological causal wedge by expansion.

The large-scale ν_e – $\bar{\nu}_e$ background therefore furnishes a conceptually sharp consistency condition: after subtracting local astrophysical contributions, the relic electron-type neutrino density should match the value implied by the balance equation for the observed expansion rate H .

In practice, however, this test is extremely challenging. Most proposed detection strategies for the cosmic neutrino background are sensitive only to some combination of n_{ν_e} and $n_{\bar{\nu}_e}$, with limited ability to distinguish neutrinos from antineutrinos, while $\nu_e\bar{\nu}_e$ annihilation into e^+e^- can further obscure the relation between the individual number densities and the underlying source terms. The neutrino sector therefore provides the cleanest setting in the model where the frequency scale σ is tied *directly* to the Hubble rate via a continuity equation, with minimal mediation by buffered degrees of freedom, but exploiting this link observationally would require unprecedented control over both the relic neutrino background and its ν_e – $\bar{\nu}_e$ composition.

6.7 A GKSL realization of exterior baryon repopulation

The mesoscopic baryon continuity equation

$$\partial_t n_B + 3Hn_B = -\Phi_B + \Gamma_B \quad (40)$$

expresses the fact that baryon number is conserved neither as a global extensive quantity on the observer-accessible Hilbert space nor as a locally closed current once horizon exchange is taken into account. While Sections 6.5–6.6 motivated the existence of the compensating source term Γ_B on thermodynamic grounds, it is useful to exhibit an explicit open-quantum-system realization in which such a term arises dynamically.

System–environment split. We adopt an effective a horizon-relative system/environment factorization of the global Hilbert space, schematically written as

$$\mathcal{H} = \mathcal{H}_{\text{ext}} \otimes \mathcal{H}_{\text{hor}}, \quad (41)$$

where \mathcal{H}_{ext} contains the degrees of freedom accessible to a given semiclassical observer, and \mathcal{H}_{hor} represents the traced–over horizon and ultrasoft infrared sector. In this simplified model of splitting, the total dynamics is unitary on \mathcal{H} and conserves the global baryon charge

$$N_B^{\text{tot}} = N_B^{\text{ext}} + N_B^{\text{hor}}, \quad [H_{\text{tot}}, N_B^{\text{tot}}] = 0, \quad (42)$$

but the reduced exterior state $\rho_{\text{ext}} = \text{Tr}_{\text{hor}} \rho$ evolves non–unitarily.

Minimal GKSL generator. At mesoscopic scales, and under standard weak–coupling and Markovian assumptions, the reduced exterior dynamics admits a Gorini–Kossakowski–Sudarshan–Lindblad (GKSL) form. Writing $\Psi(x)$ for an effective exterior baryon field operator (for definiteness, a low–energy proton field), the minimal completely positive generator capable of exchanging baryon number with the horizon sector is

$$\frac{d\rho_{\text{ext}}}{dt} = -i[H_{\text{eff}}, \rho_{\text{ext}}] + \int d^3x \left(\gamma_+(x) \mathcal{D}[\Psi^\dagger(x)]\rho_{\text{ext}} + \gamma_-(x) \mathcal{D}[\Psi(x)]\rho_{\text{ext}} \right), \quad (43)$$

where $\mathcal{D}[L]\rho = L\rho L^\dagger - \frac{1}{2}\{L^\dagger L, \rho\}$. The two Lindblad channels have a direct physical interpretation: γ_- encodes irreversible export of exterior baryon number into causally inaccessible sectors (the microscopic origin of Φ_B), while γ_+ encodes compensating repopulation of the exterior algebra (the microscopic origin of Γ_B). Here $\Psi(x)$ should be understood as a coarse–grained (smeared) field operator on the mesoscopic scale of the effective description, so that the local dissipator is well-defined within the EFT cutoff.

Importantly, the appearance of creation–like operators Ψ^\dagger does not signal a violation of global baryon conservation. Rather, it reflects the fact that baryon number is exchanged across the horizon–defined system–environment split. At the pre–trace level one may view this as arising from an interaction Hamiltonian of the schematic form

$$H_{\text{int}} = \int d^3x (\Psi^\dagger(x) \otimes E_-(x) + \Psi(x) \otimes E_+(x)), \quad (44)$$

with environment operators E_\pm that raise or lower N_B^{hor} so that $[H_{\text{int}}, N_B^{\text{tot}}] = 0$. Tracing over \mathcal{H}_{hor} then yields the GKSL structure (43).

Grand–canonical exterior steady state. The irreversible export of baryon–carrying degrees of freedom into the horizon sector induces an entropy bias in the reduced exterior state. In the presence of both Lindblad channels, the GKSL evolution admits a stationary grand–canonical fixed point of the form

$$\rho_* \propto \exp[-\beta_{\text{acc}}(H_{\text{eff}} - \mu_B N_B^{\text{ext}})], \quad (45)$$

where β_{acc} is the entropy–acceptance scale associated with horizon exchange (distinct from the radiative temperature of the photon bath), and μ_B is an

effective exterior baryon chemical potential. Detailed balance may be imposed mode-by-mode (or locally in a Wigner sense) as

$$\frac{\gamma_+(k)}{\gamma_-(k)} = \exp \left[-\beta_{\text{acc}}(\varepsilon_k - \mu_B) \right], \quad (46)$$

which ensures that $\rho_* \propto \exp[-\beta_{\text{acc}}(H_{\text{eff}} - \mu_B N_B^{\text{ext}})]$ is a stationary state. This makes explicit the sense in which baryon repopulation is driven by an entropy bias rather than by a fundamental baryogenesis interaction.

Recovery of the mesoscopic continuity law. Let $n_B(x) = \Psi^\dagger(x)\Psi(x)$ and $N_B^{\text{ext}} = \int d^3x n_B(x)$. From (43) one obtains (for fermionic Ψ)

$$\frac{d}{dt} \langle N_B^{\text{ext}} \rangle = \int d^3x \left(\gamma_+(x) \langle 1 - n_B(x) \rangle - \gamma_-(x) \langle n_B(x) \rangle \right), \quad (47)$$

expressing gain from horizon-to-exterior transfer and loss from exterior export, with Pauli blocking in the gain channel. After coarse-graining over the mesoscopic cell size (on which Ψ is defined) and converting to comoving density in an FRW background, this yields

$$\partial_t n_B + 3Hn_B = -\Phi_B + \Gamma_B, \quad (48)$$

with Φ_B and Γ_B identified as the coarse-grained loss and gain functionals of the reduced state.

The GKSL description above acts on the same enlarged Markovian state space introduced in Section 18 to restore local closure after coarse-graining. In particular, the Lindblad generator is defined on the Heisenberg-type state space that includes the central (Lévy-area) ledger variable, ensuring that baryon exchange, entropy production, and geometric mixing are described within a single consistent open-system framework.

6.8 Why Entropy Returns in the Infrared

The mesoscopic framework developed here posits that the dominant channel by which entropy is returned from horizons to the exterior sector is infrared and geometric rather than ultraviolet and particulate. That is, the entropy flow responsible for restoring stationarity appears primarily as long-wavelength curvature and graviton-like modes, not as a burst of high-energy quanta or an uncontrolled proliferation of cold photons. In this subsection we clarify why this must be the case once relativistic causality and the horizon-defined factorization of the exterior Hilbert space are taken seriously.

The relevant causal partition is set by the *cosmological horizon*. In an expanding FRW spacetime, baryon-carrying degrees of freedom are transported out of the causal wedge of late-time observers at a finite FRW time, even though no local microphysical process “destroys” the baryon along its worldline. From the standpoint of local quantum field theory, a proton that eventually crosses a

black-hole horizon experiences nothing special at the crossing itself: in a freely falling frame the short-distance physics of QCD and the local Hilbert space factorization remain intact. Any description in which the proton is literally annihilated at the horizon is therefore unphysical. What changes is the causal accessibility of that proton to the exterior sector.

From the exterior viewpoint, the loss of causal access produces a mesoscopic depletion of baryon number. The expectation value of the exterior baryon current obeys

$$\nabla_\mu \langle J_B^\mu \rangle_{\text{ext}} = -\Phi_B + \Gamma_B,$$

where $\Phi_B > 0$ encodes the export of baryon number from the exterior Hilbert space and Γ_B is the compensating source term required to maintain a stationary exterior density. At the level of the full Hilbert space no charge is lost, but for the reduced exterior state a “hole” opens in the baryon sector. As discussed in Section 6.5, this depletion drives a thermodynamically favored re-equilibration of the exterior medium.

The crucial consistency condition is not tied to any particular infalling worldline but to the horizon-defined factorization of the quantum state. Compensating baryons produced in the exterior sector must lie outside the cosmological causal wedge associated with the lost degrees of freedom. This requirement follows directly from the open-system interpretation of Γ_B : the compensating charge represents degrees of freedom that were previously inaccessible to the exterior and must remain so with respect to the horizon that defines that exterior.

It is nevertheless useful to phrase this requirement heuristically in terms of local observers. From the viewpoint of an infalling proton, local QFT remains valid and the horizon crossing is innocuous. Any compensating baryons that were causally accessible along the same worldline would therefore appear as a duplication of baryon number within a single connected causal domain. This picture should be understood as an intuition aid rather than the fundamental mechanism enforcing charge balance; the primary causal partition is set by the cosmological horizon itself.

Once this horizon-defined separation is recognized, the infrared character of the entropy return channel follows naturally. Ultraviolet excitations—hard photons, short-wavelength particles, or local scattering processes—populate the same light cones and remain confined to the same local field algebra. They do not alter the causal partition of spacetime and therefore cannot implement the large-scale reorganization of accessible versus inaccessible degrees of freedom required by horizon-coupled equilibration.

Infrared geometric modes, by contrast, are tied directly to horizon-scale physics. Long-wavelength gravitons and curvature perturbations modify the redshift structure, the effective causal wedges, and the entanglement between interior and exterior sectors on mesoscopic scales. Such modes can carry large amounts of entropy at small energy cost and are unconstrained by baryon or lepton number. They therefore provide a natural channel through which the exterior state can re-equilibrate while respecting both local QFT and the global

horizon-defined factorization of the Hilbert space.

From this perspective, graviton production plays a structural rather than a microscopic role in the baryon continuity equation. It is not invoked as a direct source of entropy but as the collective geometric response that enforces consistent causal separation between exterior and inaccessible degrees of freedom. Baryon creation is therefore *necessarily* an infrared phenomenon in this framework: it is encoded in long-wavelength geometric modes that are invisible to any single local inertial frame but manifest in the global causal structure set by the cosmological horizon.

This also clarifies why entropy is returned primarily in the infrared rather than the ultraviolet. UV channels do not modify causal structure and thus cannot mediate horizon-scale equilibration. IR geometric modes alone (i) carry large entropy at minimal energy cost, (ii) remain neutral under all conserved charges, and (iii) implement the horizon-defined separation required by relativistic causality. For these reasons the mesoscopic steady state routes entropy flow into long-wavelength geometry rather than into an unchecked proliferation of UV quanta.

6.9 Free Energy and Internal Dissipation

The exterior system is maintained at a fixed entropy acceptance temperature T_{ext} , while entropy is continuously exported to the horizon at negligible energetic cost. The exterior free energy,

$$F_{\text{ext}} = E_{\text{ext}} - T_{\text{ext}} S_{\text{ext}}, \quad (49)$$

therefore changes according to

$$\dot{F}_{\text{ext}} = -T_{\text{ext}} \dot{S}_{\text{cos}}. \quad (50)$$

High free energy corresponds to abundant internal entropy-production channels (structure formation, collapse, black-hole growth). Low free energy signals that these internal channels are exhausted: chemical potentials are flat, gradients are weak, and further internal rearrangements no longer produce entropy.

6.10 Feedback and Selection of σ_*

In a closed system the Carnot geometry relaxes toward the abelian limit $\sigma \rightarrow 0$; in a horizon-coupled NESS this relaxation is arrested at a nonzero σ_* . This driven selection follows from a feedback between free energy, structure persistence, and geometric dissipation:

Large σ . If σ is too large, directional excitation persists without settling into stable macroscopic order, leading to over-energization, mass loss, and the rapid erosion of structural supports. Entropy production drops, reducing the entropy flux to the horizon. With fewer irreversible processes active, correlations persist longer and the effective decay rate inferred from long-time dynamics decreases. Thus excessively large σ self-quenches.

Small σ . If σ is too small, directional information is rapidly isotropized, but coarse-grained structures persist because entropy export is throttled by the slow relaxation rate. Once internal entropy production is exhausted, the second law requires entropy to be exported geometrically, and correlations lose their structural supports. This shortens correlation lifetimes and increases the effective decay rate, driving σ upward.

Fixed Point. The value σ_* is therefore schematically selected by the condition

$$\left. \frac{d}{d\sigma} \dot{S}_{\text{cos}}(\sigma) \right|_{\sigma=\sigma_*} = 0, \quad (51)$$

corresponding to maximal entropy throughput to the horizon. This fixed point is stable: deviations of σ in either direction reduce entropy export and induce geometric back-reaction that restores σ toward σ_* .

Crucially, σ does not measure the degree of macroscopic order, but the efficiency with which directional information is processed and exported; both over-excited and over-quenched regimes reduce entropy throughput.

6.11 Infrared Universality

Because the feedback operates only on long-wavelength correlations and does not depend on microscopic physics, the selected value σ_* is an infrared quantity. At late times the only available timescale is the horizon crossing time, so

$$\sigma_* \sim H_0, \quad (52)$$

up to order-unity factors. The Carnot–Carathéodory tangent geometry discussed earlier is thus understood as the geometric fixed point associated with entropy-maximizing horizon coupling.

6.12 Summary

The relaxation of σ does not proceed through a dynamical equation for $\sigma(t)$, but through self-consistent selection. Excessively rapid geometric relaxation destroys the structures required for entropy production, while excessively slow relaxation exhausts internal dissipation and forces entropy export. The observed value σ_* maximizes entropy throughput to the horizon and represents the unique stable infrared relaxation rate compatible with a nonequilibrium steady state.

6.13 High- σ Regime: Dynamical Self-Limitation and Inefficient Black-Hole Sequestration

To clarify the physical meaning of large σ , it is important to distinguish between *directionally selective coarse-graining* and ordinary isotropic mixing. The mesoscopic scale σ^{-1} characterizes the timescale on which directional information is

exported into horizon-coupled degrees of freedom. Elevated σ therefore signals a reduced dynamics in which directional correlations survive long enough to influence coarse-grained transport, rather than being immediately erased by angular decorrelation.

However, a regime of uniformly and persistently large σ is not dynamically benign. Directional selectivity in the reduced dynamics necessarily manifests as *directionally biased motion*: coherent streaming, rotation, shear, or sustained nonaxisymmetric flows. At fixed mass and size, such bias implies elevated characteristic velocities and increased kinetic energy per baryon. In shallow galactic potentials, this immediately encounters a binding-energy constraint.

Energetic self-limitation. For a bound structure of mass M and characteristic radius R , long-lived orbits require velocities of order $v^2 \sim GM/R$. If directional coherence drives organized velocities significantly above this scale without a compensating deepening of the gravitational potential, baryons become marginally bound. Gas is then readily lost through fountains, winds, and feedback-assisted escape, and stellar orbits thicken or disperse. This constraint is especially severe in low-mass systems, where escape velocities are small and even modest increases in organized motion lead to substantial mass loss.

As a result, elevated σ cannot be spatially uniform or indefinitely maintained. The same persistent directional excitation that sustains large σ also accelerates the loss of bound baryonic mass, weakening the potential well and shortening the lifetime of coherent structures. This feedback drives the system toward a state in which angular decorrelation once again dominates and σ relaxes toward its cosmological baseline.

Hot, inefficient assembly. In practice, systems approaching this self-limiting regime assemble in a “hot” and impulsive manner. Directional coherence is repeatedly excited by inflows, interactions, or instabilities, but fails to persist long enough to organize deep, stable potential wells. Gas is shock-heated, velocity dispersion is high, and star formation proceeds in bursty, feedback-dominated episodes rather than through long-lived, rotation-supported disks. The resulting structures are dynamically active but weakly bound.

Suppression of black-hole sequestration. Efficient growth of central black holes requires sustained, cold, and coherent inflow over many dynamical times. In the self-limiting high- σ regime, this condition is generically not met. Elevated organized velocities increase angular-momentum barriers, while mass loss and potential shallowing disrupt the long, steady accretion episodes needed for efficient sequestration. Even when inflow is intermittently triggered, it is rapidly reheated or expelled before contributing substantially to black-hole growth.

The net effect is that large σ increases the *rate* at which directional information is processed and exported, but reduces the *efficiency* with which baryonic mass is converted into deep gravitational entropy sinks. Because black holes

dominate entropy amplification per unit energy, this inefficiency directly suppresses long-time entropy throughput to the horizon.

Interpretation. This dynamical constraint provides a concrete reason why very large σ is not self-consistent in a nonequilibrium steady state. Directional selectivity beyond a certain amplitude over-energizes baryons relative to their binding energy, forcing mass loss, rapid relaxation, and eventual isotropization. The universe therefore admits only transient, localized excursions to large σ , while the global exterior relaxes toward an entropy-throughput optimum σ_* that balances directional organization against dynamical stability.

6.14 Why Free Energy Is Not Exhaustively Dissipated into Infrared Gravitational Modes

Although infrared gravitational modes represent the energetically cheapest carriers of entropy, the exterior system does not dissipate all available free energy directly into gravitons. The reason is that populating infrared geometric degrees of freedom is itself a form of irreversible mixing that erases large-scale correlations and directional memory. Excessive geometric relaxation suppresses the formation of coherent gravitational structures—deep potential wells, sustained anisotropies, and long-lived inflows—that are required for efficient entropy amplification through collapse and black-hole growth. While infrared gravitons provide an efficient sink for entropy, they do not by themselves amplify entropy; that role is played by nonlinear gravitational structures whose formation depends on the persistence of correlations over many dynamical times. Free energy therefore cannot be optimally discharged by immediate conversion into infrared modes alone. Instead, the system must retain sufficient free energy to support structure formation, allowing entropy to be processed and amplified before being exported geometrically. The resulting balance between correlation persistence and geometric relaxation selects a finite infrared decay rate and prevents the degenerate limit in which free energy is dissipated directly into gravitons without prior structural processing.

In a spacetime with a positive cosmological constant, the dominant large-scale response to excess free energy may be interpreted, at a coarse-grained level, as the continual injection of infrared geometric degrees of freedom through expansion. While this process need not be described microscopically as graviton emission, it is morally equivalent in thermodynamic terms: free energy is converted directly into long-wavelength geometric structure that dilutes correlations, redshifts resolved modes, and enlarges the available configuration space without prior processing through nonlinear structure formation. In this degenerate limit, free energy is discharged primarily by geometric expansion itself, rather than being routed through entropy-amplifying channels such as collapse and black-hole growth. The present framework instead describes a more general nonequilibrium regime in which expansion is only one outlet among several, and where free energy must be partially retained to sustain the structures that

maximize long-time entropy throughput before entropy is exported to infrared geometric modes.

7 Entropy–Acceptance Temperature and the Horizon as a Cold Sink

In gravitational systems far from equilibrium, multiple notions of “temperature” coexist and must be carefully distinguished. The temperature relevant for entropy bookkeeping is not, in general, the radiative or spectral temperature associated with particle emission, but rather the thermodynamic derivative governing entropy acceptance. Throughout this work we therefore distinguish between *radiative temperatures* and *entropy–acceptance temperatures*.

7.1 Entropy–Acceptance Temperature

For any open subsystem exchanging entropy with its environment, we define the entropy–acceptance temperature by the Clausius relation

$$T_{\text{acc}} \equiv \frac{\delta E_{\text{grav}}}{\delta S_{\text{grav}}}, \quad (53)$$

where δE_{grav} is the change in gravitational energy required to absorb an entropy increment δS_{grav} . This quantity orders subsystems by their ability to accept entropy [74]: entropy flows from larger dE/dS to smaller dE/dS . In this sense, a “colder” subsystem is one that can absorb entropy at lower energetic cost.

This definition is independent of radiative emission and applies equally to non-stationary and non-Killing horizons.

7.2 Black Holes as Cold Entropy Amplifiers

For a stationary black hole, the entropy–acceptance temperature coincides with the Hawking temperature [5, 74],

$$T_{\text{BH}} = \left(\frac{\partial E}{\partial S} \right)_{\text{BH}} = \frac{\hbar c^3}{8\pi k_B GM}. \quad (54)$$

Astrophysical black holes therefore have extremely small T_{BH} . This low temperature does not indicate inefficiency; rather, it reflects the fact that adding a small amount of energy opens an enormous gravitational phase space. Black holes are thus thermodynamically cold while simultaneously acting as highly efficient entropy amplifiers, converting modest input entropy (e.g. from QCD degrees of freedom) into vastly larger gravitational entropy [5, 74].

7.3 The Cosmological Horizon as an Effective Zero-Temperature Sink

The cosmological horizon in the present framework differs qualitatively from a stationary black hole horizon [31, 74]. It does not correspond to a fixed Killing generator and does not radiate in the Hawking sense. Instead, it functions as an infrared sink for gravitational entropy produced elsewhere in the exterior region.

For entropy absorbed by the horizon, the associated energetic cost is negligible compared to that required for black hole entropy growth [31]. Operationally,

$$\delta E_{\text{horizon}} \approx 0 \quad \text{for} \quad \delta S_{\text{grav}} > 0, \quad (55)$$

so that

$$T_{\text{horizon}}^{(\text{acc})} = \frac{\delta E_{\text{horizon}}}{\delta S_{\text{grav}}} \approx 0 \quad (56)$$

to the precision relevant for exterior gravitational bookkeeping. In this entropy-acceptance sense, the cosmological horizon is colder than any black hole and acts as the terminal entropy sink of the universe.

7.4 Entropy Cascade

With these definitions, the thermodynamic ordering of subsystems is unambiguous:

$$\left(\frac{dE}{dS} \right)_{\text{matter}} > \left(\frac{dE}{dS} \right)_{\text{BH}} > \left(\frac{dE}{dS} \right)_{\text{horizon}} \approx 0. \quad (57)$$

Entropy flows from ordinary matter into black holes, where it is greatly amplified into gravitational degrees of freedom, and is ultimately sequestered by the cosmological horizon at negligible energetic cost. This hierarchy underlies the nonequilibrium steady state described in this work.

8 Minimal Thermodynamic Structure: Cold Entropy Export and Free-Energy Balance

The thermodynamic content of the model is deliberately minimal and can be stated independently of any microscopic details. The exterior region is treated as an open system coupled to a cold entropy reservoir, identified with the cosmological horizon. The essential features are as follows.

8.1 Cold Entropy Export

Entropy is continuously removed from the exterior description as degrees of freedom become horizon-coupled and are traced out [49, 11, 66]. This entropy export occurs at effectively zero energetic cost:

$$\delta E_{\text{ext}} \approx 0, \quad \delta S_{\text{ext}} < 0. \quad (58)$$

The reservoir absorbs entropy without returning energy [41, 8], and its state is not altered by this exchange. No heat flow is associated with this process; only information and distinguishability are lost from the exterior algebra.

8.2 Fixed Radiative Temperature of the Exterior

The resolved radiative sector of the exterior system remains locked to a finite temperature [34, 14],

$$T_{\text{rad}} \simeq 2.7 \text{ K}, \quad (59)$$

with respect to the physical time of finite observers [27]. This temperature characterizes the equilibrium state of the photon bath [44] and other rapidly mixing radiative degrees of freedom, and does not govern the effective temperature of infrared geometric modes or horizon-coupled degrees of freedom. The horizon functions as an information-erasing boundary condition rather than as a thermal medium.

8.3 Free-Energy Increase

At fixed exterior temperature, the loss of entropy implies an increase in free energy [16, 55, 23],

$$F_{\text{ext}} = E_{\text{ext}} - T_{\text{ext}} S_{\text{ext}}, \quad (60)$$

so that

$$\delta F_{\text{ext}} = -T_{\text{ext}} \delta S_{\text{ext}} > 0. \quad (61)$$

Removing entropy at zero energetic cost therefore drives the exterior system out of equilibrium by raising its free energy. This increase does not correspond to heating or energy injection; rather, it represents an excess capacity for irreversible reorganization.

8.4 Chemical-Potential Imbalance

The raised free energy manifests as shifts in the chemical potentials associated with resolved degrees of freedom [20]. For any approximately conserved quantity N_i ,

$$\mu_i = \left(\frac{\partial F_{\text{ext}}}{\partial N_i} \right)_T, \quad (62)$$

entropy loss drives the system away from equilibrium values $\mu_i = 0$. In particular, chemical potentials associated with baryon number and with the number of resolved gravitational degrees of freedom (“tiles”) become nonzero when entropy is exported to the horizon.

8.5 Restoration of Equilibrium

At fixed temperature, equilibrium is restored by reducing free energy. The most efficient mechanism is the appearance of new low-energy, high-entropy degrees of freedom, which lowers F_{ext} without requiring external energy input. In the present framework this takes the form of:

- repopulation of resolved gravitational degrees of freedom (tile creation), and
- rebalancing of baryon number within the resolved exterior sector.

This process is not thermal pair production and does not require $kT \sim m$. Rather, it is the open-system response of a finite-temperature exterior whose entropy is continuously exported to a cold reservoir.

8.6 Summary

The thermodynamic cycle may therefore be summarized succinctly:

$$\begin{aligned} \text{cold entropy export} &\Rightarrow \text{free-energy increase} \Rightarrow & (63) \\ \text{chemical-potential imbalance} &\Rightarrow \text{repopulation of degrees of freedom.} \end{aligned}$$

All energetic content remains within the exterior system; only entropy is removed. The horizon functions as a zero-temperature entropy sink, while the exterior maintains a finite equilibrium temperature through continual reorganization.

9 Minimum Exterior Temperature and Entropy-Sink Selection

A recurring concern is whether the horizon-driven entropy export invoked in this framework can supply sufficient free energy to support (i) baryon repopulation of the exterior and (ii) the steady-state expansion implied by tile creation, without assuming a high exterior temperature. Here we show that the *minimum* effective temperature required is extraordinarily low, $T_{\text{min}} \sim 10^{-11}\text{--}10^{-10}$ K, and explain why photon heating to $T_{\gamma} \simeq 2.7$ K remains thermodynamically natural despite this.

9.1 Free-energy balance and minimum temperature

For an open system exchanging entropy with a reservoir, the available free-energy production rate associated with entropy export is

$$\dot{F}_{\text{avail}} \simeq T_{\text{ext}} \dot{S}_{\text{out}}. \quad (64)$$

In a horizon-coupled steady state, black holes are removed from the exterior at a rate set by the Hubble expansion [5, 37, 22], so the entropy export per unit volume is

$$\dot{s}_{\text{out}} \simeq 3H s_{\text{BH}}, \quad (65)$$

where s_{BH} is the comoving black-hole entropy density.

To maintain a constant baryon mass density ρ_b against dilution, a conservative upper bound on the required volumetric power is

$$\dot{u}_b \simeq 3H \rho_b c^2. \quad (66)$$

Additional expansion-support channels (e.g. IR geometric modes) can be included via an effective energy density ρ_{exp} , giving

$$\dot{u}_{\text{req}} \simeq 3H(\rho_b + \rho_{\text{exp}})c^2. \quad (67)$$

Matching free-energy supply to demand,

$$T_{\text{ext}} \dot{s}_{\text{out}} = \dot{u}_{\text{req}}, \quad (68)$$

and noting that the common factor $3H$ cancels, we obtain the minimum required exterior temperature

$$\boxed{T_{\text{min}} \simeq \frac{(\rho_b + \rho_{\text{exp}})c^2}{s_{\text{BH}}}}. \quad (69)$$

The black-hole entropy density may be written as

$$s_{\text{BH}} \simeq \rho_{\text{BH}} \frac{S_{\text{BH}}}{M}, \quad \frac{S_{\text{BH}}}{M} = \frac{4\pi k_B G}{\hbar c} M, \quad (70)$$

where ρ_{BH} is the black-hole mass density and M a characteristic black-hole mass. Substituting,

$$\boxed{T_{\text{min}} \simeq \frac{\hbar c^3}{4\pi k_B G} \frac{\rho_b + \rho_{\text{exp}}}{\rho_{\text{BH}} M}}. \quad (71)$$

Using representative present-day values [61] ($\rho_b \simeq 0.05\rho_c$, $\rho_{\text{BH}} \sim 4 \times 10^5 M_{\odot} \text{Mpc}^{-3}$, $M \sim 10^8 M_{\odot}$), one finds

$$T_{\text{min}} \sim 10^{-11} \text{--} 10^{-10} \text{K}, \quad (72)$$

even if ρ_{exp} is taken comparable to the observed dark-energy density. Thus the entropy export associated with black-hole horizon crossing provides an ample free-energy budget at an extremely low effective exterior temperature.

9.2 Why photons are *not* the dominant entropy sink

The existence of a low T_{min} does not imply that the optimal use of available free energy is to “dump it into photons.” In a horizon-coupled nonequilibrium steady state, the relevant selection rule is not to maximize the instantaneous entropy

increase of the *local* bath, but to maximize the *net entropy throughput* into the ultimate cold reservoir (the horizon), i.e. to maximize the entropy exported per unit free energy expended.

A convenient back-of-the-envelope measure of “entropy yield per joule” for a channel is the effective ratio

$$\frac{dS}{dE} \sim \frac{1}{T_{\text{eff}}}, \quad (73)$$

where T_{eff} is the temperature of the degrees of freedom that actually absorb the entropy in that channel.

Photon bath. For a thermal photon population [16] at temperature T_γ ,

$$\frac{dS}{dE} \Big|_\gamma = \frac{1}{T_\gamma}. \quad (74)$$

At $T_\gamma \simeq 2.7$ K, this ratio is large compared to many *local, nonrelativistic* dissipation channels, which explains why the photon bath can act as a convenient *buffer* for modest excess free energy. However, its low entropy elasticity implies that even small entropy injection rapidly raises T_γ , rendering photon heating an inefficient channel for sustained entropy throughput compared to horizon-mediated or ultrasoft geometric sinks.

Black holes and horizon-coupled storage. However, the dominant entropy sink in the present architecture is the creation and export of *cold entropy* in black-hole/horizon degrees of freedom. For a Schwarzschild black hole [5, 37],

$$S_{\text{BH}} = \frac{4\pi k_B G}{\hbar c} M^2, \quad T_H = \frac{\hbar c^3}{8\pi k_B G} \frac{1}{M}, \quad (75)$$

so

$$\frac{dS_{\text{BH}}}{dE} = \frac{dS_{\text{BH}}}{d(Mc^2)} = \frac{1}{T_H}. \quad (76)$$

Because T_H is extraordinarily small for astrophysical black holes, the entropy yield per joule in the black-hole channel is correspondingly enormous [22]. For example, for $M \sim 10^8 M_\odot$ one has $T_H \sim 10^{-16}$ K, so

$$\frac{(dS/dE)_{\text{BH}}}{(dS/dE)_\gamma} = \frac{T_\gamma}{T_H} \sim 10^{15} - 10^{16}. \quad (77)$$

Thus, per unit energy invested, increasing black-hole (and ultimately horizon) entropy is vastly more effective than heating a 2.7 K photon bath.

Thermodynamic ordering of channels. This establishes the intended hierarchy: available free energy is preferentially routed into processes that *build cold entropy that can be exported*, namely baryon repopulation and subsequent

accretion/sequestration into black holes, followed by horizon depletion. Photon heating is not the optimal entropy sink; rather, the photon bath functions as an intermediary that (i) rapidly equilibrates and (ii) buffers small mismatches between injection and export. The steady-state value $T_\gamma \simeq 2.7$ K should therefore be interpreted not as the temperature of the exterior reservoir, but as a dynamically selected “thermometer” temperature fixed by balance between entropy injection, angular mixing/thermalization, and infrared leakage into geometric and horizon-coupled modes.

10 Stationary Solutions and Cosmological Implications

The coupled continuity and entropy balance equations developed in Sections 4 and 6 determine the large-scale thermodynamic and kinematic state of an expanding universe whose mesoscopic structure is governed by a distinguished spectral scale σ . In this section we analyze the stationary solutions of this system and derive their physical implications for rotation curves, radiation fields, baryon equilibrium, and the linkage between cosmic expansion and horizon thermodynamics.

This section should be read as an analysis of scaling relations and structural consistency rather than as a closed-form solution of the full dynamical system. Numerical coefficients and detailed microphysics are deliberately suppressed in favor of identifying the unique infrared scale governing stationary cosmological behavior.

10.1 The stationary system

Combining the baryon continuity equation

$$\partial_t n_B + 3Hn_B = -\Phi_B + \Gamma_B,$$

with the steady-state entropy balance (coarse-grained over a comoving patch),

$$3H S_{\text{ext}} = -\dot{S}_{\text{cos}} + \dot{S}_{\text{IR}},$$

we obtain the stationary-state system

$$3Hn_B = -\Phi_B + \Gamma_B, \tag{78}$$

$$\dot{S}_{\text{IR}} = 3H S_{\text{ext}} + \dot{S}_{\text{cos}}. \tag{79}$$

The first equation fixes the baryon number density once H , Φ_B , and Γ_B are specified. The second constrains the stationary expansion rate H through a competition between accretion-driven horizon entropy production and IR entropy removal by expansion.

Because both Φ_B and Γ_B depend on horizon-coupled acceptance scales and effective chemical potentials, while their mesoscopic realization is controlled by

the constitutive frequency σ , the stationary system closes on a single mesoscopic rate scale whose NESS expectation satisfies $\langle \sigma \rangle \sim H_0$.

10.2 Determination of the expansion rate

The entropy fluxes admit the schematic scalings [55, 23]

$$\dot{S}_{\text{hor}} \sim + \frac{F_{\text{proc}}}{T_{\text{acc}}}, \quad \dot{S}_{\text{IR}} \sim -\kappa H,$$

where F_{proc} is the net free-energy flux processed through collapse, accretion, and horizon-sequestering channels (with the radiative bath acting as a fast thermalizer but not the dominant reservoir), and T_{acc} is the effective entropy–acceptance temperature of the horizon-coupled sink [41, 31].

Setting $\dot{S}_{\text{hor}} + \dot{S}_{\text{IR}} = 0$ yields

$$H \sim \frac{F_{\text{proc}}}{\kappa T_{\text{acc}}}.$$

In the present framework the acceptance scale is set by the mesoscopic frequency σ (equivalently $k_B T_{\text{acc}} \sim \hbar \sigma$ in units where this identification is meaningful), giving the steady-state scaling relation

$$H \sim \sigma,$$

consistent with the mesoscopic frequency inferred independently from galactic kinematics [46].

10.3 Baryon equilibrium

Given $H \sim \sigma$, the baryon continuity equation in steady state becomes

$$3\sigma n_B = -\Phi_B + \Gamma_B.$$

The horizon-induced creation rate satisfies $\Gamma_B \propto \sigma$, while the flux Φ_B is constrained by the black hole population and the long-term behavior of the radiation field. Thus the equilibrium baryon density satisfies

$$n_B \sim \frac{\Phi_B}{\sigma} + O(1),$$

consistent with the observed near-constancy of cosmic baryon density without appeal to early-universe baryogenesis [52].

10.4 Stationary radiation density

In the present framework, the radiation energy density in the exterior is regulated by thermodynamic balance rather than by direct thermal contact with the horizon. Entropy export across the horizon continually releases free energy into

the exterior subsystem, which must be absorbed by available degrees of freedom. Because the photon bath thermalizes rapidly and possesses a large phase space [27, 14], it provides an efficient channel for absorbing a small fraction of this free energy, thereby maintaining a near-stationary blackbody distribution.

At the level of dimensional analysis, this suggests that the stationary radiation density scales with the selected infrared control parameter σ [16],

$$u_\gamma \sim \sigma^4,$$

up to numerical factors reflecting the efficiency of free-energy transfer into the radiative sector. Identifying σ phenomenologically with a late-time infrared scale of order the Hubble rate, $\sigma \sim H_0$ [56], yields a radiation density of the observed order of magnitude.

The stability of this stationary state does not rely on redshift dilution alone. If the radiation density temporarily exceeds its equilibrium value, excess energy can be transferred into ultrasoft geometric modes [13] and associated entropy-export channels. Conversely, if the radiation density falls slightly below equilibrium, free energy released by ongoing horizon-coupled processes and by nuclear activity in the exterior reheats the photon bath.

Re-equilibration of the photon bath around its stationary temperature therefore carries a negligible energetic cost. The only substantive requirement is that the exterior supply a steady, low-level radiative throughput sufficient to balance the slow leakage of energy into ultrasoft geometric modes.

The observed CMB temperature may thus be viewed as reflecting a dynamic balance between free-energy injection, rapid thermalization within the photon sector, and slow leakage into infrared geometric degrees of freedom.

10.5 Rotation curves and macroscopic geometry

Section 2 established that the large-radius rotation curve satisfies

$$v(r) = \sigma r \pm \sqrt{\sigma^2 r^2 + v_N^2(r)}.$$

For r sufficiently large, the Newtonian contribution becomes subdominant and the velocity approaches the linear asymptote

$$v(r) \sim 2\sigma r.$$

The success of this relation in describing flattened and rising rotation curves [57, 46] across a wide range of galactic systems supports the underlying mesoscopic geometric picture.

(Deviations from this asymptote are expected in systems with strong environmental coupling or incomplete IR equilibration.)

Black holes as local CC generators. If the exterior Carnot–Carathéodory (CC) geometry arises from irreversible tracing-out of degrees of freedom, then every causal horizon acts as a local generator of CC curvature. Black hole

horizons are the most intense localized entropy-export channels in nature, and therefore the strongest sources of ledger drift and IR mode production. In the present framework this implies that supermassive and stellar-mass black holes must imprint a localized CC deformation on exterior geodesic flow, producing an effective enhancement of central binding mass. Observationally, such a deformation is indistinguishable from a local concentration of dark matter; however, no new matter is required. The effect is purely geometric, arising from horizon coupling rather than particle density. This perspective suggests that the exterior geometry in the vicinity of black holes should acquire a localized CC deformation, appearing observationally as an excess of central binding mass that attenuates smoothly with radius. The effect does not require new matter degrees of freedom; rather, it reflects horizon-coupled geometry induced by irreversible tracing-out. In this sense, black holes generate their own localized “dark” mass profiles, not as particulate halos but as CC structure.

It is important to emphasize that the magnitude of the local CC deformation depends not only on the rate of tracing-out but on its anisotropy. A massive black hole horizon traces out correlations at a high rate, but because this process is strongly isotropic in phase space it generates relatively weak directional curvature in the exterior. In this sense, the presence of a large black hole can suppress rather than enhance the local value of σ , anchoring the geometry and reducing the effective dark-matter signature in its immediate environment. This provides a natural explanation for the observed contrast between dynamically chaotic dwarf and low-surface-brightness galaxies, which exhibit large apparent mass discrepancies, and massive bulge systems with supermassive black holes, which are more baryon-dominated and display smoother rotation structure. In the present framework, σ measures anisotropic irreversibility rather than total entropy export, so isotropic horizon coupling produces a small σ even when the entropy flux is large.

10.6 Global consistency and observational tests

The horizon-coupled mesoscopic framework yields a cosmology in which [52, 17]:

- the Hubble rate arises dynamically from thermodynamic balance,
- the cosmic radiation density is set by thermodynamic balance in a horizon-coupled open system,
- the baryon density is maintained by horizon-induced creation,
- galactic rotation curves reflect the same spectral scale σ ,
- and all of these quantities remain stationary without a hot big bang [52].

These predictions can be tested through:

1. detailed comparison of rotation curve slopes with the inferred Hubble parameter in low-redshift systems,

2. measurements of the CMB energy density independent of big bang assumptions,
3. examination of baryon deficits and black hole mass densities as probes of Φ_B ,
4. and potential detection of horizon-driven neutrino or photon excitations corresponding to Γ_B .

The unified appearance of σ across these phenomena suggests that the mesoscopic structure of spacetime—approximated here by a Heisenberg or general Carnot tangent model—provides the missing link between local galactic dynamics and global cosmological equilibrium.

11 Photon Confinement, Carnot Mixing, and Blackbody Equilibrium

A central feature of the mesoscopic framework developed in this work is that, in a Carnot–Carathéodory geometry [48], the propagation and mixing of photon degrees of freedom give rise to an *effectively cavity-like* statistical behavior on cosmological scales. In this setting, the cosmic radiation field is naturally described as a stationary photon bath characterized by a thermal distribution at late times.

The role of cosmological expansion in this framework is not to establish equilibrium through local interactions, but to provide the large-scale kinematic conditions under which horizon coupling and mesoscopic mixing lead to a stable blackbody spectrum. This section formalizes the physical basis for this effective confinement, outlines the mixing properties implied by the sub–Laplacian, and shows how the observed cosmic blackbody spectrum [29] can be understood within an open–system, steady–state description of the cosmological exterior.

11.1 Effective confinement in Carnot–Carathéodory geometry

A distinctive feature of Carnot–Carathéodory (CC) geometries such as the Heisenberg group is that null geodesics are governed by the horizontal distribution rather than by the full tangent bundle. In the Heisenberg case, the Hamiltonian flow is generated by the horizontal momenta (P, \bar{P}) with the central coordinate s playing the role of a gauge parameter. The resulting geodesics are not straight rays but curved horizontal trajectories analogous to cyclotron orbits [30]: they have a characteristic curvature on scales determined by the mesoscopic control parameter σ and possess a finite geometric “return time” even in the absence of any scattering.

Thus photons do not stream radially to infinity along Euclidean null lines. Instead, their horizontal projections undergo recurrent motion, revisiting neighborhoods of their initial position after a time of order σ^{-1} . Motion in the central

(“vertical”) direction corresponds to the noncommutative phase of the Heisenberg group and carries no physical displacement once one projects onto the underlying abelian quotient. The physically relevant dynamics is therefore entirely horizontal, and it is this horizontal cyclotron-like structure that produces effective confinement.

Because the CC geodesic flow forces recurrence, the mesoscopic medium behaves as a *photon cavity* [59] even in the absence of appreciable baryonic opacity. Scattering, absorption, and re-emission merely enhance the mixing that the geometry already enforces. The photon distribution function $f(t, x, \omega)$ therefore evolves primarily under the horizontal Heisenberg generators,

$$\partial_t f + X_1 f + X_2 f = C[f],$$

with $C[f]$ encoding subdominant interactions with the baryonic medium. The geometric confinement supplied by the CC structure ensures that radiation remains trapped and repeatedly reprocessed on timescales long compared to H^{-1} , permitting the establishment of an approximately Planckian stationary state, with relaxation set by the selected geometric mixing scale σ .

11.2 Sub-Laplacian mixing and ergodicity

The geometric mixing mechanism arises from the sub-Laplacian [30, 70]

$$\Delta_{\text{sub}} = X_1^2 + X_2^2,$$

whose heat kernel is well known to satisfy strong regularity, rapid decay away from characteristic directions, and a spectral gap above the ground state [30, 70]. These properties imply that solutions to the kinetic equation are driven toward equilibrium on timescales much shorter than cosmological expansion.

Although angular mixing is not fully isotropic, the sub-Laplacian provides sufficient ergodicity for the photon bath to become well-mixed. Together with continuous emission and absorption in the radiating medium, the radiation field therefore approaches a distribution function of the form [59]

$$f(\omega) = \frac{1}{\exp(\omega/T_{\text{rad}}) - 1},$$

independent of spatial position and angular direction up to mesoscopic corrections, where T_{rad} is the effective temperature of the steady-state radiating medium.

11.3 Photon Heating, Geometric Thermalization, and the Absence of Radiative Runaway

In the horizon-coupled steady state developed in this work, the cosmic photon bath is neither a relic of an early hot phase nor a passive background subject only to adiabatic redshift. Rather, it is a dynamically maintained subsystem,

continuously heated by the absorption of free energy generated by irreversible entropy export into horizons, and continuously cooled through its coupling to the expanding geometric infrared sector.

Continuous photon heating. When matter collapses and accretes across a horizon, a large amount of *cold entropy* is removed from the exterior region. This raises the free energy of the remaining exterior degrees of freedom, which must be dissipated through available channels. Ordinary radiative processes in baryonic matter (stellar emission, bremsstrahlung, line radiation, and reprocessing by dust and gas) provide one such channel, continuously injecting energy into the photon field [59]. Photon heating is therefore ongoing and unavoidable in a stationary horizon-coupled universe: it is the radiative expression of free energy absorption in the exterior sector.

Why photons do not dominate entropy throughput. Despite being energetically inexpensive, photons are *poor entropy sinks* in the present framework. The dominant entropy-recapture channel is instead carried by long-wavelength geometric and curvature modes [13] associated with the infrared sector of the Carnot–Carathéodory (CC) tangent geometry. These modes can absorb large entropy per unit energy and are unconstrained by baryonic or electromagnetic quantum numbers. From a thermodynamic standpoint, exporting entropy into IR geometric degrees of freedom is therefore far more efficient than dumping it into a bath of increasingly cold photons. As a result, the photon field remains a secondary, slaved subsystem: it is heated by free energy absorption but does not control the global entropy balance.

11.4 Structural relation between entropy–acceptance and radiative temperatures

The effectively zero entropy–acceptance temperature associated with the cosmological horizon should not be confused with the $T \simeq 2.7$ K temperature characterizing the exterior radiation field. These two temperatures are linked by the open-system structure of the theory, but not by their magnitudes.

Both quantities arise as thermodynamic derivatives of the same entropy balance, taken with respect to different variables. The exterior temperature T_{ext} characterizes the stationary state of exterior observables with respect to the physical time flow of finite observers and governs entropy processing and particle production in the exterior medium. By contrast, the entropy–acceptance temperature associated with the horizon reflects the energetic cost of absorbing entropy into inaccessible degrees of freedom and is effectively zero. It does not characterize a thermal bath and does not regulate exterior dynamics.

The fact that these two temperatures differ parametrically is not a tension but a structural feature of an open, irreversible cosmological system. The photon bath records the value of T_{ext} spectrally as a passive buffer, while the horizon

functions solely as an entropy sink. No phenomenological relation between their magnitudes is implied or required.

Compatibility with steady-state energy balance. Although the photon temperature is geometrically admitted, the existence of a stationary state requires consistency with the coarse-grained energy balance equation

$$\dot{\rho}_\gamma + 4H\rho_\gamma = \dot{\rho}_\gamma^{(\text{net})}, \quad (80)$$

where $\dot{\rho}_\gamma^{(\text{net})}$ denotes the net radiative heating rate from baryonic processes. In equilibrium, this reduces to

$$4H\rho_\gamma = \dot{\rho}_\gamma^{(\text{net})}, \quad (81)$$

which should be read not as a temperature-setting relation but as a *compatibility condition*: only those steady states in which baryonic emissivity is sufficient to maintain the geometrically imposed photon energy density are dynamically allowed.³

Absence of cold-photon runaway. At first sight, the photon field might appear free to absorb arbitrarily large entropy by producing vast numbers of ultra-soft photons. In the present framework, however, such a runaway is thermodynamically disfavored. Because IR geometric modes dominate entropy transport at far lower free-energy cost [55, 23], the system preferentially routes entropy into the geometric sector rather than into extreme photon occupation numbers. The photon bath therefore relaxes toward a thermalized form admitted by the CC mixing dynamics, with an effective temperature T_{rad} determined by the steady-state routing of free energy among available channels; its total energy density is then slaved to the expansion rate, while excess entropy is exported through geometric degrees of freedom. A microscopic comparison of the relative entropic efficiencies of cold-photon production and IR geometric excitation lies beyond the scope of this mesoscopic treatment, but the hierarchy of channels suffices to exclude radiative overproduction in the steady state.

In this sense, the cosmic radiation field behaves as a blackbody in an effectively confining CC medium [29], whose near-thermal form is stabilized by rapid mesoscopic mixing and whose energy density is maintained by continuous free-energy absorption in the exterior.

³As a purely heuristic consistency check, one may combine the observed Hubble rate with standard FRW-based estimates of the present-day bolometric luminosity density of galaxies [2, 36] in the steady-state relation $4H\rho_\gamma = \dot{\rho}_\gamma^{(\text{net})}$. Doing so yields an equilibrium photon temperature in the kelvin range, typically of order $T_\gamma \sim 1$ K, rather than picokelvin or gigakelvin scales. This estimate should not be interpreted as a prediction of the photon temperature, which in the present framework is fixed by the geometric KMS periodicity of the stationary mesoscopic state, as enforced by the CC modular flow and its compatibility with the horizon-imposed causal structure. Its sole purpose is to demonstrate that known astrophysical heating rates are not grossly inconsistent with maintaining a photon bath at a few kelvin. Because both the luminosity density and the comoving volume element entering this estimate are inferred under an abelian FRW prior, while the present model replaces this by a non-abelian Carnot–Carathéodory geometry on Hubble scales, order-unity deviations are neither unexpected nor significant.

12 Entropy Throughput and the Origin of Apparent Expansion

The late-time cosmological exterior in the present framework is not a closed thermodynamic system but an open nonequilibrium steady state (NESS) [15, 65]. Matter, radiation, and geometric excitations continually enter and exit the resolved exterior description through irreversible coupling to black-hole interiors and horizon-adjacent infrared (IR) degrees of freedom. The purpose of this section is to show how this steady-state entropy throughput gives rise to phenomena normally attributed to cosmological expansion, while the local Carnot–Carathéodory (CC) tangent geometry remains stationary as a mesoscopic constitutive law.

12.1 The exterior as an open thermodynamic system

The cosmological exterior is defined operationally as the subsystem whose degrees of freedom remain resolvable by finite observers. Black-hole interiors and horizon-coupled or ultrasoft IR modes are excluded: they are irreversibly traced over in the reduced description [15]. As a result, the exterior continuously exchanges entropy and degrees of freedom with its environment and cannot be treated as a closed system.

The essential elements of this open-system architecture are [15, 65]:

1. the cosmological horizon, which acts as an effectively infinite entropy sink through irreversible tracing of inaccessible degrees of freedom;
2. black holes, which efficiently destroy correlations and organized structure during collapse and accretion;
3. a working medium consisting of baryons, photons, and long-wavelength geometric excitations governed locally by the CC tangent law; and
4. compensating repopulation of the working medium through horizon-coupled processes.

No finite hot reservoir is required. Entropy production is driven by the irreversible destruction of structure, while entropy removal is enforced by the horizon’s unbounded capacity [13, 78].

12.2 Free energy stored in resolved degrees of freedom

The thermodynamically relevant quantity in this framework is not conserved matter–energy but free energy stored in distinguishable, resolvable degrees of freedom. Let ρ denote the coarse-grained exterior state and let ρ_* be the stationary reference state selected by the horizon-coupled IR sector, assumed to be KMS with respect to the emergent mesoscopic time flow. The available free energy is

$$F_{\text{dof}}(\rho) \equiv F(\rho) - F(\rho_*) = T_{\text{ext}} S(\rho \parallel \rho_*), \quad (82)$$

where $S(\rho\|\rho_*)$ is the relative entropy [71, 24]. This quantity measures free energy stored in correlations, gradients, and organized structure rather [71] than in rest mass. Here T_{ext} is the entropy–acceptance temperature associated with the resolved exterior degrees of freedom. It is not the Hawking temperature of any horizon, nor the temperature of the photon bath, but an effective intensive parameter governing the conversion of entropy removal into available free energy in the reduced description.

Although black holes are radiatively cold in the Hawking sense, they are thermodynamically effective entropy generators because collapse and accretion irreversibly convert structured exterior degrees of freedom into black–hole interior entropy. Since black–hole interiors are excluded from the exterior algebra, this entropy is traced out of the reduced description and constitutes an irreversible entropy flux out of the exterior system.

12.3 Steady-state entropy balance

The coarse-grained entropy of the exterior obeys [65, 23]

$$\dot{S}_{\text{ext}} = \sigma - J_S, \quad (83)$$

where $\sigma \geq 0$ is the entropy production rate and J_S is the entropy flux into the traced-out sector. In the late-time steady state,

$$\langle \dot{S}_{\text{ext}} \rangle = 0 \quad \Rightarrow \quad \langle \sigma \rangle = \langle J_S \rangle. \quad (84)$$

Entropy does not accumulate in the exterior [43]. Instead, free energy is continually generated through structure formation, destroyed by collapse and accretion, and exported from the exterior description through irreversible tracing of black–hole interior and horizon–coupled degrees of freedom at the same average rate.

12.4 Stationary CC geometry and timescale separation

The CC tangent geometry and its associated mixing operator \mathcal{L}_{CC} govern local propagation, causal structure, and spectral mixing. This geometry is not a dynamical state variable. It is the rapidly re-attained fixed point of local equilibration with the horizon-coupled IR sector [81].

On timescales [81] $\tau_{\text{mix}} \ll H^{-1}$, local observables relax back to this stationary CC structure. At the same time, the global exterior state evolves slowly because resolvable degrees of freedom are continually removed from the description. The coexistence of fast local equilibration and slow global drift is the defining signature of the nonequilibrium steady state realized here.

12.5 Resolved degrees of freedom, “tiles,” and apparent expansion

In the present framework, the fundamental bookkeeping object is not matter or energy but the number of resolved degrees–of–freedom units (“tiles”) comprising

ing the exterior description. Each tile carries a finite information and entropy capacity. Tiles are irreversibly removed from the exterior when their degrees of freedom become entangled with horizon-coupled modes or black-hole interior states and are therefore traced over in the reduced description [15, 78].

In a nonequilibrium steady state, the loss of tiles must be exactly balanced by the creation of new tiles in the exterior sector. This effective conservation of tile number is not a dynamical law but a consistency requirement of the steady-state coarse-graining. It forces the resolved domain to grow so that finite densities of matter, radiation, and entropy can be maintained.

This growth produces increasing mean separations, cosmological redshift, and dilution relations without invoking any microscopic pressure, force, or local metric stretching. Apparent expansion is therefore the macroscopic manifestation of tile creation required to maintain a stationary exterior description under continuous entropy sequestration.

Equivalently, “expansion” in this framework is not postulated as a local geometric deformation but emerges as a bookkeeping drift induced by time-dependent coarse-graining [81, 43]. At each epoch t , finite observers access only an exterior algebra of observables,

$$\mathcal{A}_{\text{ext}}(t) = \text{Tr}_{\text{hor+IR}}(\mathcal{A}_{\text{full}}),$$

obtained by tracing over horizon-interior and ultrasoft infrared degrees of freedom. As the horizon continually partitions the quantum state, the effective observable algebra and its resolved phase-space volume drift in time. Stationarity of physical densities in the reduced theory therefore requires a compensating rescaling of the effective spatial measure, which appears observationally as an expansion law with rate H .

The tile picture is a mnemonic for this behavior: the number of resolved degrees-of-freedom units defining the exterior description remains fixed by the coarse-graining scheme, while their effective physical support grows as modes are traced out and replenished.

12.6 Free–Energy Throughput and Entropy Export: Quantitative Closure

In this subsection we collect several independent order-of-magnitude estimates for the free–energy fluxes required to maintain a stationary late–time exterior, and compare them with the free energy made available by entropy export into the traced–out sector (black–hole interiors and horizon–coupled IR modes).. The purpose is not to derive detailed microphysics, but to establish that the steady–state bookkeeping closes at the observed scales.

Throughout, all quantities are evaluated per unit *physical* volume, and we take $H \simeq H_0$.

Photon bath stationarity. A stationary photon bath at temperature T_γ in an expanding background requires continuous replenishment to offset redshift

and dilution. The radiation energy density obeys

$$\dot{\rho}_\gamma + 4H\rho_\gamma = \dot{\rho}_{\text{inj}}.$$

Imposing $\dot{\rho}_\gamma = 0$ gives the required injection rate

$$\dot{\rho}_{\text{inj}}^{(\gamma)} = 4H\rho_\gamma. \quad (85)$$

For a blackbody bath at $T_\gamma \simeq 2.7 \text{ K}$, $\rho_\gamma = a_{\text{rad}} T_\gamma^4 \simeq 4 \times 10^{-14} \text{ J m}^{-3}$, so

$$\dot{\rho}_{\text{inj}}^{(\gamma)} \sim 4 \times 10^{-31} \text{ W m}^{-3}.$$

This is an extremely small free-energy requirement.

Stationarity of baryon density. Maintaining a constant baryon mass density ρ_b against expansion requires

$$\dot{\rho}_b + 3H\rho_b = Q_b, \quad \Rightarrow \quad \dot{\rho}_{\text{inj}}^{(b)} = 3H\rho_b.$$

With $\rho_b \simeq 4 \times 10^{-11} \text{ J m}^{-3}$,

$$\dot{\rho}_{\text{inj}}^{(b)} \sim 2 \times 10^{-28} \text{ W m}^{-3}. \quad (86)$$

This term dominates over the photon requirement by several orders of magnitude, but remains small on absolute scales.

Free-energy scale associated with expansion. If the expansion is interpreted as the continuous creation of long-wavelength gravitational degrees of freedom, the relevant free-energy scale admits a convenient comparison with the dark-energy density ρ_Λ .⁴ For a constant ρ_Λ , the energy contained in a physical volume grows as $E_\Lambda = \rho_\Lambda V$, yielding a power density

$$P_{\text{exp}} = \frac{\dot{E}_\Lambda}{V} = 3H\rho_\Lambda \sim 3 \times 10^{-27} \text{ W m}^{-3}. \quad (87)$$

Here ρ_Λ is used purely as an effective parameter encoding the observational profile of expansion, not as a fundamental vacuum energy density. This scale exceeds the combined photon and baryon stationarity requirements by roughly two orders of magnitude, leaving substantial free-energy throughput available.

Entropy export from black-hole accretion (black holes traced out). In the present bookkeeping, black holes are not part of the exterior algebra: their interior degrees of freedom are irreversibly traced out. Entropy generated by black-hole growth therefore constitutes an entropy flux out of the exterior system.

⁴Our ansatz here is that required throughput scale can be compared after the fact with the effective dark-energy density inferred in Λ CDM fits

For a Schwarzschild black hole of mass M , the first law gives

$$dE = T_{\text{BH}}(M) dS_{\text{BH}}, \quad T_{\text{BH}}(M) = \frac{\hbar c^3}{8\pi G k_B M}.$$

If exterior energy $\dot{E}_{\text{in}} = \dot{M}_{\text{in}} c^2$ crosses the horizon, the associated entropy production rate is

$$\dot{S}_{\text{BH}} = \frac{\dot{E}_{\text{in}}}{T_{\text{BH}}(M)}.$$

Since black holes are excluded from the exterior algebra, this entropy is traced out of the reduced description. Per unit physical volume, the entropy export rate is therefore

$$\dot{s}_{\text{out}}^{(\text{BH})} = \int dM n_{\text{BH}}(M) \frac{\dot{M}_{\text{in}}(M) c^2}{T_{\text{BH}}(M)} \equiv \frac{\dot{u}_{\text{in}}^{(\text{tot})}}{T_{\text{BH}}^{\text{eff}}}, \quad (88)$$

where $\dot{u}_{\text{in}}^{(\text{tot})}$ is the total energy flux into black-hole mass per unit volume and $T_{\text{BH}}^{\text{eff}}$ is the accretion-weighted effective Hawking temperature.

Free energy produced by cold entropy export. If this entropy is traced out into a much colder reservoir (the cosmological horizon), then the maximum free-energy production rate in the exterior is

$$P_{\text{free}}^{(\text{BH})} \approx (T_{\text{ext}} - T_{\text{sink}}) \dot{s}_{\text{out}}^{(\text{BH})} \approx T_{\text{ext}} \frac{\dot{u}_{\text{in}}^{(\text{tot})}}{T_{\text{BH}}^{\text{eff}}}, \quad (89)$$

where T_{ext} is the entropy-acceptance temperature of the exterior degrees of freedom and $T_{\text{sink}} \ll T_{\text{ext}}$ has been assumed.

Using the observed late-time cosmic black-hole accretion rate density, $\dot{u}_{\text{in}}^{(\text{tot})} \sim 10^{-33} - 10^{-34} \text{ W m}^{-3}$, and accretion dominated by supermassive black holes with $T_{\text{BH}}^{\text{eff}} \sim 10^{-17} - 10^{-15} \text{ K}$, one finds

$$P_{\text{free}}^{(\text{BH})} \sim \left(\frac{T_{\text{ext}}}{10^{-9} \text{ K}} \right) \times 10^{-27} \text{ W m}^{-3}.$$

Closure. Taken together, these estimates show that:

- the free energy required to maintain a stationary photon bath and baryon density is extremely small;
- the expansion naturally provides a free-energy throughput at the $3H\rho_{\Lambda}$ scale;
- irreversible entropy export through black-hole growth (with black-hole interiors excluded from the exterior algebra) provides an entropy sink capable of supporting the required free-energy throughput at the observed expansion scale.

This quantitative coincidence supports the interpretation of the late-time Universe as a horizon-coupled nonequilibrium steady state.

12.7 Sanity check on the entropy–export engine: required T_{ext}

We now perform a quantitative sanity check on the entropy–export mechanism, under the explicit assumption that black holes are *not* part of the exterior algebra. Black–hole interiors are traced out, and the growth of black–hole entropy therefore constitutes an irreversible entropy flux *out* of the exterior system. The purpose of this subsection is to determine the range of exterior entropy–acceptance temperatures T_{ext} required for this entropy export to support the free–energy throughput associated with baryon creation and effective “tile creation,” as inferred phenomenologically from the observed expansion scale.

Entropy export from black–hole accretion. For a Schwarzschild black hole of mass M , the first law gives

$$dE = T_{\text{BH}}(M) dS_{\text{BH}}, \quad T_{\text{BH}}(M) = \frac{\hbar c^3}{8\pi G k_B M}. \quad (90)$$

If exterior energy $\dot{E}_{\text{in}} = \dot{M}_{\text{in}} c^2$ crosses the horizon, the associated entropy production rate is

$$\dot{S}_{\text{BH}} = \frac{\dot{E}_{\text{in}}}{T_{\text{BH}}(M)}. \quad (91)$$

Since black holes are excluded from the exterior algebra, this entropy is counted as an entropy flux into the traced–out sector. Per unit physical volume, the total entropy export rate is therefore

$$\dot{s}_{\text{out}}^{(\text{BH})} = \int dM n_{\text{BH}}(M) \frac{\dot{M}_{\text{in}}(M) c^2}{T_{\text{BH}}(M)} \equiv \frac{\dot{u}_{\text{in}}^{(\text{tot})}}{T_{\text{BH}}^{\text{eff}}}, \quad (92)$$

where $\dot{u}_{\text{in}}^{(\text{tot})}$ is the total energy flux into black–hole mass per unit volume, and $T_{\text{BH}}^{\text{eff}}$ denotes the accretion–weighted harmonic mean Hawking temperature.

Free energy liberated by entropy removal. Entropy export into an effectively zero–temperature sink produces available free energy in the exterior bookkeeping at the rate

$$\dot{f}_{\text{avail}}^{(\text{BH})} = (T_{\text{ext}} - T_{\text{sink}}) \dot{s}_{\text{out}}^{(\text{BH})} \approx T_{\text{ext}} \dot{s}_{\text{out}}^{(\text{BH})} = T_{\text{ext}} \frac{\dot{u}_{\text{in}}^{(\text{tot})}}{T_{\text{BH}}^{\text{eff}}}, \quad (93)$$

where T_{ext} is the entropy–acceptance temperature of the resolved exterior degrees of freedom and $T_{\text{sink}} \simeq 0$ has been assumed.

This free–energy production is a statement about the coarse–grained availability of work in the reduced description; it does not represent a radiative luminosity injected into the exterior.

Observed accretion scale. At late times, the cosmic mean black-hole accretion rate density is observationally inferred to be

$$\dot{\rho}_{\text{BH}}(z \simeq 0) \sim (3\text{--}6) \times 10^{-6} M_{\odot} \text{ yr}^{-1} \text{ Mpc}^{-3}, \quad (94)$$

corresponding to an energy deposition rate into black-hole mass of

$$\dot{u}_{\text{in}}^{(\text{tot})} \sim (5\text{--}10) \times 10^{-34} \text{ W m}^{-3}. \quad (95)$$

Black-hole growth at late times is dominated by supermassive black holes with typical masses in the range $M \sim 10^7\text{--}10^9 M_{\odot}$, for which the Hawking temperature lies in the interval

$$T_{\text{BH}}^{\text{eff}} \sim 10^{-17}\text{--}10^{-15} \text{ K}. \quad (96)$$

Required free-energy throughput. The phenomenological free-energy scale associated with “tile creation” may be estimated from the effective dark-energy density inferred in Λ CDM fits,

$$P_{\text{tile}} \equiv 3H_0\rho_{\Lambda}c^2 \sim (3\text{--}4) \times 10^{-27} \text{ W m}^{-3}. \quad (97)$$

Maintaining a stationary baryon density against dilution contributes a subleading requirement,

$$P_{\text{baryon}} \sim 3H_0\rho_b c^2 \sim \text{few} \times 10^{-28} \text{ W m}^{-3}, \quad (98)$$

so that the total required free-energy throughput is

$$P_{\text{req}} \approx P_{\text{tile}} + P_{\text{baryon}} \sim \text{few} \times 10^{-27} \text{ W m}^{-3}. \quad (99)$$

Implied exterior temperature. Equating the required throughput to the free-energy production rate Eq. (93) yields

$$T_{\text{ext}} \approx P_{\text{req}} \frac{T_{\text{BH}}^{\text{eff}}}{\dot{u}_{\text{in}}^{(\text{tot})}}. \quad (100)$$

Using the observational ranges above gives

$$T_{\text{ext}} \sim 10^{-10}\text{--}10^{-8} \text{ K}, \quad (101)$$

with a characteristic value of order

$$T_{\text{ext}} \sim \text{few} \times 10^{-9} \text{ K} \quad (102)$$

for accretion dominated by $\sim 10^8 M_{\odot}$ black holes.

Interpretation. This nanoKelvin-scale temperature is not a thermal bath temperature of the photon field, but an effective entropy-acceptance temperature governing the free-energy bookkeeping of resolved degrees of freedom. Within the present framework, entropy removal through black-hole growth at observed rates is sufficient to support both baryon creation and the effective growth of the resolved exterior domain without introducing any additional energy reservoir.

13 Emergent Carnot–Carathéodory Geometry and the Horizon Fixed Point

The mesoscopic framework developed in this work assumes a non-Riemannian tangent structure of Carnot–Carathéodory (CC) type, characterized by a horizontal distribution, a degenerate vertical sector, and an associated sub-Laplacian generating large-scale mixing. In this section we argue that the CC tangent geometry is not merely a kinematical ansatz but an *emergent fixed point* selected by the thermodynamic requirements of a horizon-coupled nonequilibrium steady state.

The argument is not one of mathematical uniqueness. Rather, we show that a CC-type sub-Riemannian geometry provides a particularly efficient constitutive response of the exterior spacetime to three coupled constraints: (i) the presence of an observer-dependent horizon enforcing a 2.7 K radiation temperature, (ii) continuous inflow of thermodynamically cold entropy from collapsing matter and black holes, and (iii) the requirement that repopulated baryons have sufficient time to cool, mix, and condense into extremely high-entropy configurations before ultimately exiting the resolved exterior description.

13.1 The horizon as a thermodynamic boundary condition

For any timelike observer, the causal horizon defines an operational boundary across which degrees of freedom become permanently inaccessible. Tracing over those degrees of freedom places the residual exterior algebra of observables in a stationary KMS state [34]. In the open-system picture developed here, this KMS structure is not interpreted as a literal horizon temperature imposed on the radiation field, but as a constraint on the large-scale exterior dynamics: the reduced state must remain compatible with stationary thermal correlations at long wavelengths.

The observed 2.7 K cosmic radiation field is then understood not as the fossil of an initial thermal episode, nor as the direct temperature of the horizon, but as the working temperature of the photon bath that mediates mesoscopic free-energy flow. In this view, the radiation field acts as a dynamical buffer between gravitational collapse (which generates entropy and free energy) and the causal boundary (which absorbs entropy but admits no ballistic transport). The exterior bath temperature emerges from this steady exchange: it is the signature of a quasi-stationary balance between entropy production in the interior and entropy export to the horizon, not a prescribed boundary value.

Standard FRW cosmology treats the comoving horizon as receding and its Gibbons–Hawking temperature as diminishing with time [31]. By contrast, in the mesoscopic framework, the relevant horizon quantity is not the microscopic Gibbons–Hawking temperature but the macroscopic constraint on stationarity: the exterior must remain in a KMS-compatible state while supporting continuous entropy flux. The photon bath temperature is therefore governed by free-energy throughput and radiative relaxation, rather than by the bare horizon

temperature.

The horizon itself is not a physical membrane and carries no independent local degrees of freedom. Its thermodynamic role is encoded entirely in the conditions that viable exterior geometries must satisfy: (i) maintain near-KMS correlations under large-scale transport; (ii) prevent rapid ballistic leakage of photons to the horizon; and (iii) accommodate ongoing entropy export from collapsed structures without destabilizing the cavity. These constraints organize the mesoscopic thermodynamics of the exterior and select the photon bath as the natural free-energy buffer supporting the observed 2.7 K equilibrium.

13.2 Cold entropy, collapse timescales, and geometric response

Black holes occupy a distinguished place in the entropy budget of the exterior sector. Their Hawking temperatures are extremely small [5, 37], $T_{\text{BH}} \ll 1 \text{ K}$, while their absolute entropies are enormous. The formation of a black hole therefore represents a substantial injection of *cold entropy* into the thermodynamic accounting of the exterior.

Crucially, black holes are not formed instantaneously. They are the end states of long baryonic cooling and condensation histories involving galaxy formation, star formation, and successive phases of collapse and accretion. A consistent mesoscopic geometry must therefore satisfy a dual requirement: it must efficiently export the entropy of mature collapsed objects to the horizon at late times, while simultaneously allowing repopulated baryons sufficient time to cool, mix, and assemble into high-entropy configurations at intermediate times.

These requirements strongly constrain the admissible tangent structures. A geometry that transports radiation and matter too efficiently toward the horizon would starve the system of collapsed entropy sources; one that confines matter indefinitely would violate the steady-state entropy balance.

13.3 Why purely Riemannian tangent geometries are disfavored

A purely Riemannian (or Euclidean) tangent geometry does not naturally satisfy these constraints. In such geometries, null geodesics free-stream, photons disperse ballistically, and there is no intrinsic mechanism for large-scale confinement or spectral mixing. Maintaining a stable 2.7 K photon cavity would require fine-tuned boundary conditions, as radiation would continually leak toward the horizon without re-equilibration.

Moreover, attempting to absorb continuous cold-entropy inflow directly into Riemannian curvature degrees of freedom would tend to produce large-scale geometric distortions or instabilities, rather than the observed near-homogeneity of the late-time universe. From a thermodynamic standpoint, Riemannian tangent structures are too rigid to act as efficient steady-state mediators between cold-entropy production, cavity equilibration, and horizon export.

13.4 CC geometry as a thermodynamic fixed point

A Carnot–Carathéodory geometry [33] provides a natural resolution of these constraints.⁵ Horizontally constrained null propagation forces photons into recurrent trajectories on mesoscopic scales, while the associated sub-Laplacian induces strong mixing [38]. As a result, local perturbations in photon and baryon densities are rapidly homogenized, and the exterior remains in approximate KMS equilibrium with the horizon.

At the same time, the degenerate vertical sector supports ultrasoft geometric modes that act as entropy absorbers for the cold-entropy flux generated by collapse. These modes do not represent propagating forces or local curvature dynamics; rather, they provide a channel through which entropy can be irreversibly sequestered without disrupting the local CC constitutive law.

Importantly, the CC geometry itself does *not* drive expansion. The large-scale expansion of the resolved exterior arises from tile bookkeeping and coarse-graining drift, as described in Sec. 12. The role of the CC geometry is instead to ensure that this expansion proceeds in a thermodynamically efficient and observationally consistent manner: photons are confined and mixed on intermediate timescales, baryons cool and condense before exiting the resolved description, and entropy is exported steadily to the horizon.

13.5 Fixed-point interpretation

The apparent circularity of this construction—the geometry is shaped by horizon thermodynamics, while horizon thermodynamics is defined relative to the geometry—is best understood as a fixed-point relation. The CC tangent structure and the horizon KMS state emerge together as a self-consistent solution of the open-system entropy balance.

Schematically, the steady state satisfies

$$\frac{dS_{\text{ext}}}{dt} = \Phi_{\text{prod}} - \Phi_{\text{hor}} = 0, \quad (103)$$

where Φ_{prod} denotes entropy production from structure formation and collapse, and Φ_{hor} denotes entropy export through horizon-coupled and geometric channels. At the fixed point, the exterior photon bath is approximately blackbody with temperature 2.7K, baryons have sufficient time to condense into high-entropy objects, and the CC tangent geometry remains stationary as a constitutive law.

⁵Although the CC tangent structure is formally anisotropic—distinguishing horizontal from vertical directions in the tangent space—this anisotropy is not visible to observers within the mesoscopic exterior. The sub-Riemannian anisotropy operates at the level of constraint structure in phase space, not at the level of macroscopic propagation speeds or metric eigenvalues. After coarse graining, the observable dynamics are statistically isotropic: photon free paths, baryon diffusion, and geometric correlations obey rotational symmetries to high precision. In this sense, CC geometry is functionally isotropic but kinematically constrained: it provides efficient mixing and confinement without generating any directional bias in observable propagation.

In this sense, the Carnot–Carathéodory structure is not imposed but selected. It represents a thermodynamically efficient phase of spacetime geometry for a horizon-coupled exterior universe operating in a nonequilibrium steady state, with expansion governed by coarse-graining and tile creation rather than by local metric dynamics.

13.6 Relaxation of the Control Parameter σ

The parameter σ introduced in the preceding sections is not a dynamical field nor an externally tunable constant. Rather, it is an *emergent infrared relaxation rate* characterizing the long-time decay of geometric correlations into the horizon. In this section we explain how σ is dynamically selected and why the system relaxes [55] toward a unique entropy-maximizing value σ_* .

13.6.1 Definition of σ

Operationally, σ is defined as the slowest nonzero decay rate of large-scale geometric correlations under coarse-graining,

$$\langle \mathcal{O}(t)\mathcal{O}(0) \rangle \sim e^{-\sigma t} \quad (t \rightarrow \infty), \quad (104)$$

where \mathcal{O} denotes long-wavelength geometric observables. Equivalently, σ^{-1} is the characteristic timescale on which directional information, anisotropies, and large-scale memory are irreversibly lost to horizon-coupled degrees of freedom.

Importantly, σ is inferred from the behavior of the geometry; it does not govern that behavior via an equation of motion.

13.6.2 Entropy Export and the Throughput Functional

Entropy transport to the horizon proceeds through geometric correlation decay. At fixed horizon scale and exterior temperature, the entropy export rate may be written schematically as

$$\dot{S}_{\text{export}}(\sigma) = \sigma \mathcal{I}_{\text{geom}}(\sigma), \quad (105)$$

where $\mathcal{I}_{\text{geom}}(\sigma)$ measures the amount of long-lived geometric structure available to be erased. The two factors have opposite dependence on σ :

- Increasing σ accelerates relaxation and increases the transport rate per unit structure.
- Increasing σ also suppresses structure formation by erasing correlations before they can seed collapse, thereby reducing $\mathcal{I}_{\text{geom}}$.

As a result, $\dot{S}_{\text{export}}(\sigma)$ generically possesses a single maximum at an intermediate value σ_* .

14 A Geometric Viewpoint on Luminosity Decay

The purpose of this section is to articulate a purely geometric mechanism by which observed luminosity may decay more rapidly with distance than in standard Friedmann–Robertson–Walker optics, without invoking absorption, scattering, or any explicit loss of energy. The key idea is that, in a mesoscopic Carnot–Carathéodory (CC) geometry, an observer’s angular degrees of freedom need not parameterize the full geometric extent of a propagating wavefront.

14.1 Wavefronts and angular accessibility

In ordinary Riemannian geometry, the null wavefront emitted by a point source at a fixed emission time is a smooth sphere whose area growth is faithfully tracked by angular coordinates at the observer. Angular resolution therefore provides a natural parametrization of the wavefront, and luminosity decay follows directly from the familiar area law.

In a CC geometry, the situation is more subtle. The wavefront remains an isodistance surface, but it may possess intrinsic geometric structure that is not resolved by the observer’s angular coordinates. In this case, the observer’s celestial sphere parameterizes only a *projection* of the true wavefront. Radiative power is conserved on the full wavefront, but the fraction of that power accessible per observed solid angle may decrease with propagation distance.

Crucially, this effect need not arise from rapid angular mixing or local diffusion. Instead, it may be governed by an additional geometric “phase” direction whose evolution is characterized by an exceptionally low frequency. As a result, the loss of angular accessibility accumulates only over very long propagation times, becoming appreciable only on cosmological scales.

14.2 The Heisenberg group as a geometric toy model

The simplest setting in which this mechanism can be visualized explicitly is the $2 + 1$ -dimensional Heisenberg group equipped with its standard Carnot–Carathéodory structure.

In this geometry, admissible curves are constrained to lie in a distinguished two-dimensional horizontal distribution. A defining feature of the space is that horizontal motion necessarily generates an additional geometric degree of freedom: when a horizontal trajectory sweeps out signed area in the horizontal plane, it accumulates displacement in a third (“vertical”) direction. This vertical coordinate records a phase history of the motion rather than a directly observable spatial separation.

Consider a point source at the origin emitting signals uniformly in all horizontal directions. At a fixed propagation time t , the set of points reached by horizontal geodesic arcs forms a Carnot–Carathéodory wavefront. Unlike a Euclidean circle, this wavefront contains structure associated with different amounts of vertical phase accumulation. Distinct geodesic arcs may arrive at

nearly the same horizontal location and with nearly the same horizontal tangent direction, while differing substantially in their accumulated vertical phase.

Now place an observer at some horizontal distance from the source. The observer's celestial "sky" consists of horizontal arrival directions. Near the source, horizontal angle remains a faithful label of the wavefront: different emission directions correspond to different arrival directions, and the observer's angular coordinate distinguishes most of the wavefront's structure.

As the propagation distance increases, the geometry enforces a different trade-off. Reaching larger horizontal distances requires geodesic arcs to accumulate substantial signed area, and hence substantial vertical phase. Small variations among long geodesics increasingly manifest as differences in phase history rather than differences in horizontal direction. Since the observer's angular degrees of freedom do not resolve this phase, many geometrically distinct portions of the wavefront collapse onto the same observed direction.

From the observer's perspective, the angular sky remains a circle of fixed length, but it parameterizes the wavefront with increasing multiplicity. The observer has access to a shrinking fraction of the wavefront's intrinsic geometric measure, even though the wavefront itself continues to grow.

14.3 Distance and effective luminosity

This Heisenberg example captures the essential geometric mechanism. Radiative power is conserved on the full CC wavefront, but the observer's angular coordinates fail to resolve an increasing portion of the wavefront's structure as propagation time grows. Equivalently, the effective transverse area over which conserved power is distributed grows faster than the area accessible to image-forming angular degrees of freedom.

Phenomenologically, this can be expressed by writing the observed flux from a standard candle as

$$F_{\text{obs}}(z) = \frac{L}{4\pi A_{\text{eff}}(z)}, \quad (106)$$

where $A_{\text{eff}}(z)$ denotes the effective geometric area of the CC wavefront relative to the observer's accessible angular parametrization. In standard FRW optics, $A_{\text{eff}}(z)$ reduces to the usual luminosity-distance area. In the CC framework, the geometric claim is simply that

$$A_{\text{eff}}(z) \text{ grows faster with distance than the apparent angular area resolved by the observer.} \quad (107)$$

The Heisenberg group illustrates how this can occur without any local loss mechanism: increasing propagation time shifts geometric information from angular separation into an unresolved phase direction. Because the characteristic frequency associated with this phase evolution is infrared, the effect is negligible at small distances and becomes relevant only over cosmological scales.

14.4 Interpretation

The resulting luminosity decay is therefore geometric in origin. It reflects a mismatch between the intrinsic growth of the wavefront in a CC geometry and the observer’s angular access to that wavefront, rather than any failure of energy conservation. Distance correlates with dimming because increasing propagation time increases the portion of the wavefront lying in geometric directions not resolved by the observer’s angular coordinates.

The Heisenberg example serves as a concrete toy model demonstrating how such an infrared bundle effect can arise purely from geometry, and how it naturally leads to a distance-dependent reduction of observed flux without invoking absorption, scattering, or local angular diffusion.

14.5 Local Phase Inheritance and Coarse-Grained Continuity

The “phase” variable appearing in the Carnot–Carathéodory description is not an internal label or conserved quantum number, but a geometric quantity encoding the accumulated transverse holonomy of horizontal transport. As such, it admits no globally preferred trivialization. Any attempt to assign a single, exterior-wide phase reference would amount to introducing an unphysical background structure and would violate coarse-grained continuity by suppressing the very phase drift implied by the geometry.⁶

For this reason, newly created matter excitations cannot be globally phase-locked. Instead, matter must inherit the phase defined by its *local* CC environment at the spacetime region in which it is created. This inheritance is automatic: physical creation processes occur over finite regions and necessarily sample the ambient modular flow and horizontal frame. No additional postulate is required.

Phase continuity is preserved not by constancy but by smooth variation. The CC phase field varies gradually across the exterior, and locally created matter simply joins this existing structure without introducing discontinuities. There is therefore no preferred phase and no global synchronization condition, in direct analogy with the absence of global simultaneity in general relativity.

Once created, matter exhibits strong phase stiffness due to timelike motion, internal dynamics, and continual interaction, which rapidly re-anchors its phase to the local environment. Nevertheless, this stiffness is not absolute. Over sufficiently long proper times, even matter accumulates transverse holonomy incoherently, leading to slow phase drift on cosmological scales. This drift is parametrically weaker than that experienced by radiation, which propagates along null trajectories and therefore integrates the CC connection coherently over large distances.

The distinction between matter and radiation is thus not one of phase versus no-phase, but of *coherent versus incoherent accumulation*. Matter remains

⁶Note: Throughout this section, by phase we mean CC geometric phase (vertical displacement / holonomy), not wave phase. In the Heisenberg case, this is $e^{is\sigma}$.

locally coherent and dynamically stable while gradually becoming relationally distant from a given observer's algebra. Radiation, by contrast, provides a sensitive probe of large-scale phase structure and reveals this drift observationally through flux diminution rather than local decoherence.

This local inheritance principle ensures that phase drift, horizon formation, and effective charge loss emerge continuously and without introducing hidden sectors or preferred reference structures, preserving the open-system and observer-relative character of the exterior description.

14.6 Single-packet CC phase drift and effective luminosity decay

The discussion above was framed in terms of wavefront accessibility and coarse-grained angular resolution. For a feasibility test, however, it is useful to isolate a simpler geometric picture based on the propagation of a *single localized photon wave packet*. Ensemble and bundle effects can be reintroduced later by superposition; at the present stage they are not essential.

CC phase as a geometric observable. In Carnot–Carathéodory geometries of Heisenberg type, horizontal transport generically accumulates displacement in the central direction. For a horizontal curve with coordinates $(x(t), y(t))$, the associated central coordinate $\phi(t)$ is proportional (up to normalization) to the signed area swept by the horizontal projection,

$$\phi(t) \propto \int_0^t (x \dot{y} - y \dot{x}) dt. \quad (108)$$

Thus the CC phase is not an independent degree of freedom but a geometric holonomy recording the cumulative noncommutativity of horizontal transport.

Long-time scaling and normalization. In the Heisenberg model one can compute the central holonomy explicitly for the canonical constant-curvature horizontal motion, obtaining

$$\phi(t) = \frac{1}{\sigma} (t - \sin(\sigma t)/\sigma) = \frac{t}{\sigma} + O(\sigma^{-1}). \quad (109)$$

Thus ϕ grows linearly in t with slope $1/\sigma$, with only bounded oscillatory corrections. We therefore treat ϕ as an area-type central coordinate; only the ratio ϕ/ϕ_0 entering the response function is dimensionless.

Phase-dependent luminosity response. We assume that the observer's image-forming algebra does not resolve the central (CC) coordinate directly. Instead, the contribution of an arriving photon to the perceived flux is effectively weighted by a *phase-luminosity response curve*

$$\ell(\phi) \in [0, 1], \quad \ell(0) = 1, \quad (110)$$

which encodes how arrivals with CC phase ϕ are registered by the observer. The CC phase ϕ is an area-type geometric quantity (central holonomy), and need not be dimensionless; only the ratio ϕ/ϕ_0 entering the response function is dimensionless. As a conservative and analytically tractable choice, we adopt a Cauchy (Lorentzian) response,

$$\ell(\phi) = \frac{1}{1 + (\phi/\phi_0)^2}, \quad (111)$$

where ϕ_0 sets the effective phase-resolution scale of the observer. Arrivals with $|\phi| \gg \phi_0$ are not sharply excluded, but are strongly suppressed.

Effective luminosity decay. For a single localized wave packet propagating for a time t , the observed flux is reduced according to

$$g(t) = \ell(\phi(t)). \quad (112)$$

Using the asymptotic Heisenberg scaling derived above,

$$\phi(t) = \frac{1}{\sigma}(t - \sin(\sigma t)/\sigma) \simeq \frac{t}{\sigma},$$

the attenuation factor becomes

$$g(t) \simeq \frac{1}{1 + \left(\frac{t}{\sigma \phi_0}\right)^2}. \quad (113)$$

It is therefore convenient to introduce the characteristic onset timescale

$$\tau_0 \equiv \sigma \phi_0, \quad (114)$$

so that $g(t) = (1 + (t/\tau_0)^2)^{-1}$. The corresponding shift in distance modulus is

$$\Delta\mu(t) = 2.5 \log_{10} \left[1 + \left(\frac{t}{\tau_0} \right)^2 \right]. \quad (115)$$

Two qualitative features are immediate. First, the effect is negligible at small lookback times: for $t \ll \tau_0$ one has $\Delta\mu(t) \approx (2.5/\ln 10) (t/\tau_0)^2$, so local distance calibrations are unaffected. Second, for propagation times of order the Hubble time, $t \sim H_0^{-1}$, and for an infrared scale dynamically selected such that $\sigma \sim H_0$, the attenuation becomes order unity when τ_0 itself is of Hubble order. In this regime, the observed luminosity suppression is a natural consequence of CC phase accumulation rather than an indication of photon loss or modified expansion kinematics.

Relation to exponential parametrizations. Over a finite redshift interval, the logarithmic slope of Eq. (113) defines an effective decay rate,

$$-\frac{d}{dt} \ln g(t) = \frac{2t}{\tau_0^2 + t^2}. \quad (116)$$

For t restricted to a narrow range around $t \sim \tau_0$, this quantity varies slowly and may be approximated by a constant. In such limited domains, phenomenological fits of the form $\exp(-\varepsilon t)$ can serve as local surrogates for the underlying phase-selection law, but should not be interpreted as evidence for a fundamental exponential attenuation mechanism.

This single-packet picture isolates a purely geometric mechanism for anomalous luminosity suppression that becomes relevant only on cosmological scales, and does so without invoking photon destruction, scattering, or additional propagating degrees of freedom.

Sanity check: observational scale of the phase-resolution parameter. Using the asymptotic Heisenberg scaling from Eq. (109),

$$\phi(t) = \frac{1}{\sigma} (t - \sin(\sigma t)/\sigma) = \frac{t}{\sigma} + O(\sigma^{-1}),$$

we approximate $\phi(t) \simeq t/\sigma$ for the purpose of a crude observational anchor. The single-packet attenuation then becomes

$$g(t) = \ell(\phi(t)) \simeq \frac{1}{1 + \left(\frac{t}{\sigma \phi_0}\right)^2}. \quad (117)$$

It is convenient to define the onset time scale

$$\tau_0 \equiv \sigma \phi_0, \quad (118)$$

so that $g(t) = (1 + (t/\tau_0)^2)^{-1}$ and

$$\Delta\mu(t) = 2.5 \log_{10} \left[1 + \left(\frac{t}{\tau_0} \right)^2 \right]. \quad (119)$$

Solving for τ_0 gives

$$\tau_0 = \frac{t}{\sqrt{10^{\Delta\mu/2.5} - 1}}. \quad (120)$$

As a visual reference, Type Ia supernova data show an apparent dimming of order $\Delta\mu \simeq 0.2\text{--}0.3$ mag at redshifts $z \simeq 0.4\text{--}0.6$, corresponding to lookback times $t \simeq 4\text{--}6$ Gyr for standard cosmological parameters. Taking $\Delta\mu = 0.25$ mag at $t = 5$ Gyr yields $\tau_0 \simeq 10$ Gyr, i.e. $\tau_0 \simeq 0.7 H_0^{-1}$ for $H_0^{-1} \simeq 14$ Gyr.

Interpreting this in terms of the phase-resolution parameter gives

$$\phi_0 \simeq \frac{\tau_0}{\sigma}. \quad (121)$$

If the infrared scale is dynamically selected such that $\sigma \sim H_0$, this implies

$$\phi_0 \sim (0.5\text{--}0.9) H_0^{-2}, \quad (122)$$

i.e. the required phase-resolution scale is of the natural order set by the Hubble scale (in the units appropriate to the central CC coordinate), with no fine tuning.

14.7 Vertical Mixing, Fat-Tailed Phase Occupation, and the Stability of the Photon Bath

The luminosity-decay mechanism introduced above requires careful interpretation when applied to diffuse radiation fields. A reduction in *recoverable* flux from a localized source does not, by itself, imply a corresponding loss of photons from the exterior cavity. The distinction depends on how radiation is distributed over the Carnot–Carathéodory vertical (central) degree of freedom.

Let $p(\phi, t)$ denote the normalized occupation distribution of photons over the affine central coordinate ϕ ,

$$\int_{-\infty}^{\infty} p(\phi, t) d\phi = 1, \quad (123)$$

and let $\ell(\phi) \in [0, 1]$ denote a phenomenological phase-acceptance function encoding how radiation arriving at vertical displacement ϕ contributes to image-forming observables. The corresponding effective observational efficiency is

$$\eta(t) \equiv \int_{-\infty}^{\infty} p(\phi, t) \ell(\phi) d\phi. \quad (124)$$

For radiation emitted by a localized source, $p(\phi, t)$ is initially narrow. Geometric CC phase drift and bundle spreading cause this distribution to broaden with propagation time, leading to a redshift-dependent reduction in $\eta(t)$. This behavior underlies the effective luminosity decay discussed in Sec. 14.6.

The cosmic microwave background occupies a contrasting regime. Over cosmological timescales, the photon bath has undergone not only angular isotropization but also substantial *vertical mixing*. Within the present framework, this suggests that the CMB occupation distribution $p_{\text{CMB}}(\phi)$ is broad, potentially exhibiting a fat-tailed structure over the affine central direction. When the characteristic width of p_{CMB} significantly exceeds the intrinsic scale ϕ_0 appearing in $\ell(\phi)$, the effective acceptance η_{CMB} becomes weakly sensitive to further vertical spreading and remains close to unity.

In this regime, the CMB experiences little effective photon depletion, even though the same geometric mechanisms strongly suppress the recoverable flux from localized emitters. Any small residual leakage from the resolved observational channel can be compensated by ordinary baryonic emission and rapid equilibration with the photon bath, even at low densities.

This perspective also clarifies the role of photons as a large and resilient free-energy buffer. Because free energy can be redistributed not only angularly

but also into vertical degrees of freedom, the photon bath possesses a large effective state space in which injected free energy may be accommodated while maintaining a near-stationary radiative spectrum when projected onto the exterior observable algebra. From this viewpoint, vertical delocalization enhances the buffering capacity of the radiation field rather than undermining it.

Importantly, this mechanism does not preclude the presence of layered or multimodal vertical populations. Such structures may arise for freshly produced or weakly mixed radiation. The CMB may therefore be understood as a late-time, strongly mixed state of the vertical dynamics, in which the occupation distribution is sufficiently broad that luminosity-decay effects do not translate into appreciable photon loss from the exterior cavity.

14.8 Radiation and detection in the (3, 3) Carnot geometry

The Heisenberg example serves as a pedagogical toy model, but the mesoscopic geometry relevant for the present framework is more naturally modeled by a step-2 Carnot group with horizontal and central dimensions (3, 3). In this case the central fiber is three-dimensional,

$$Z \cong \Lambda^2 V \cong \mathbb{R}^3,$$

and the Carnot–Carathéodory “phase” accumulated by horizontal transport is no longer a scalar but a vector-valued geometric holonomy.

At first sight this appears to introduce a qualitative complication: the central holonomy may be decomposed into a magnitude and a direction,

$$\omega = \|\omega\| \hat{\omega}, \quad \hat{\omega} \in S^2,$$

suggesting an additional sphere of “phase directions” beyond the observer’s ordinary celestial sphere. If taken literally, one might worry that radiation emitted with all possible $\hat{\omega}$ would free-stream and uniformly populate this vertical sphere at reception, erasing any distance-dependent selection effect.

This concern is resolved once the correct observable is identified. In the (3, 3) geometry, the vertical direction $\hat{\omega}$ is not a physical emission angle and does not label distinct rays in spacetime. It is an internal axial label encoding the oriented bivector (area normal) generated by horizontal transport. Free streaming routes photons according to their horizontal directions alone; the vertical direction $\hat{\omega}$ does not affect which spacetime points a ray can reach.

Crucially, the observer’s image-forming algebra is assumed to be rotationally invariant in the vertical sector. Detection does *not* depend on selecting a preferred cap or solid angle on the vertical sphere S^2 . Instead, it depends only on the *magnitude* of the central displacement,

$$\|\omega\|,$$

that is, on how far the arriving ray has drifted away from the locally resolved sector of the vertical fiber. The resolved region is therefore a neighborhood of the origin in $Z \cong \mathbb{R}^3$, not a directional subset of S^2 .

With this identification, the apparent emission–reception asymmetry disappears. Emission may populate $\hat{\omega}$ isotropically without consequence. During propagation, Carnot–Carathéodory transport generates a systematic growth of $\|\omega\|$ with distance, while preserving isotropy in $\hat{\omega}$. At reception, arrivals are weighted according to their radial distance from the origin in the vertical fiber. Luminosity diminution therefore arises from *radial escape in a noncompact central direction*, not from any directional selection on S^2 .

In this sense, the $(3, 3)$ case clarifies rather than complicates the geometric mechanism. The role played by the scalar phase in the Heisenberg model is taken over by the central magnitude $\|\omega\|$, while the additional directional structure of the center remains observationally silent. The luminosity decay mechanism thus survives intact: increasing propagation time shifts geometric information into an unresolved central sector whose extent grows without bound, reducing the fraction of the wavefront accessible to the observer’s angular parametrization without introducing anisotropy or violating energy conservation.

15 Late-Time Cosmology, Chemical Steady State, and the Origin of Quasars

In a horizon-coupled steady-state universe, the observable sector is not a fossil left by a unique high-temperature episode but an open, slowly evolving system in which baryons, entropy, and chemical species are continually exchanged with causal horizons. Once the mesoscopic continuity equations are taken seriously, several assumptions inherited from Λ CDM invert: quasars become *late-time* thermodynamic states rather than early-time anomalies; nucleosynthesis becomes an *ongoing* process governed by stellar evolution and baryon replenishment; and the cosmic helium fraction arises as a *regulated equilibrium quantity*, not a primordial boundary condition. This section introduces these structural consequences and motivates the quantitative helium budget developed in Sec. 16.

15.1 Quasars as Terminal Galactic Attractors

Under standard cosmology, quasars require finely tuned early-time conditions: rapid black-hole growth, intense starbursts, and fast chemical enrichment at high redshift. These requirements are widely acknowledged to be contrived.

In the horizon-coupled universe, the evolutionary arrow reverses. A galaxy that persists for Gyr–Tyr naturally undergoes secular baryon depletion through stellar collapse, metal cooling, neutronization, and horizon-mediated sequestration. Over sufficiently long times, the diffuse baryon reservoir contracts toward the center, while the stellar population processes a significant fraction of its gas into helium and heavier elements. The terminal state is a compact, thermodynamically regulated accretion structure feeding an overgrown SMBH.

The observed properties [63, 35, 26] of quasars— 10^8 – $10^{10} M_\odot$ black holes, compact emitting regions, super-solar metallicities, and rapid variability—then follow naturally as signatures of *old galaxies in their final luminous phase*.

Quasars appear not as youthful anomalies but as the late-time attractors of secular galactic evolution.

15.2 Nucleosynthesis Beyond the Primordial Paradigm

Standard cosmology treats light-element abundances as relics of a brief early nucleosynthesis epoch [68, 51]. The horizon-coupled framework replaces this with a slow, ongoing chemical cycle:

1. **Baryon return:** horizon exchange injects light species—primarily hydrogen, with minimal helium—into the diffuse reservoir.
2. **Stellar processing:** long-lived stellar populations continuously convert hydrogen into helium and produce metals according to IMF-weighted yields.

Because the exterior sector is not closed, its chemical composition reflects the *balance* among these processes rather than an imprinted thermal boundary condition. Light-element abundances become emergent properties of long-term baryon cycling rather than diagnostic fossils of the early universe.

15.3 Preferential Metal Sequestration

A classical objection to stellar-driven helium production is that it would over-produce metals in a closed-box universe. The present framework avoids this by introducing a natural one-way sink for metals.

Metal-rich gas cools rapidly, condenses, and sinks into deep gravitational potentials, where it is preferentially accreted by SMBHs or trapped in dense nuclear regions. Observationally, the gas feeding active nuclei is already highly enriched, and metal-rich cores are ubiquitous in clusters and bulges. Over cosmic timescales, this hydrodynamic sorting removes metals from the exterior sector while leaving helium and hydrogen—much poorer coolants—distributed in the diffuse medium or expelled by AGN outflows.

Thus the exterior metallicity remains low even while helium is continually produced, eliminating the closed-box objection and enabling a chemically consistent steady state.

15.4 Chemical Equilibrium and the Helium Fixed Point

The three ingredients above—ongoing baryon return, continuous stellar processing, and preferential metal sequestration—drive the exterior sector toward a chemical steady state. The crucial point is that the *value* of the helium fraction is determined by stellar microphysics.

Stellar populations return only a fraction [79]

$$y_{\text{He}} \simeq 0.20 - 0.33$$

of the baryonic mass they process as newly synthesized helium. This yield is set by nuclear physics and the IMF, with negligible dependence on environment or cosmic epoch.

In a horizon-coupled universe, nearly all helium in the exterior sector must be produced through hydrogen burning, while helium losses into compact objects and horizon-sequestered modes occur slowly and roughly proportionally to the baryon cycle. A mesoscopic continuity equation then forces the helium mass fraction toward

$$Y_{\text{eq}} \approx \frac{y_{\text{He}}}{1 + \epsilon},$$

where $\epsilon \ll 1$ encodes the slight excess sequestration of helium relative to hydrogen.

For empirically supported y_{He} in the range 0.20–0.33 and typical drain efficiencies $\epsilon \sim 0.1\text{--}0.2$, one finds

$$Y_{\text{eq}} \simeq 0.22\text{--}0.26,$$

in striking agreement with the observed [40, 3] cosmic helium fraction $Y \simeq 0.24$.

Thus the helium abundance is not a remnant of an early thermal episode but the *fixed point* of slow baryon cycling:

The Universe has $\sim 25\%$ helium because stars return $\sim 25\%$ helium, and the horizon-regulated baryon cycle forces the exterior sector to inherit that ratio.

15.5 Summary

These ingredients combine into a unified equilibrium picture:

- **Quasars** are the late-time thermodynamic attractors of galactic evolution.
- **Nucleosynthesis** is continuous rather than primordial, governed by stellar evolution and baryon return.
- **Metals** are efficiently removed into SMBHs, preventing over-enrichment.
- **Helium** is a fixed-point quantity determined by stellar nuclear yields and slow baryon cycling, not by a unique early-time epoch.

This motivates the detailed helium-budget analysis presented next in Sec. 16, where the equilibrium value $Y \simeq 0.24$ emerges quantitatively from the mesoscopic continuity equation.

16 The Cosmic Helium Budget

A central phenomenological success of the horizon-coupled framework is that it naturally explains the near-universal cosmic helium fraction $Y \simeq 0.24$ [40, 3] without invoking a primordial nucleosynthesis epoch. Helium is not a fossil

boundary condition but a dynamically maintained quantity governed by stellar microphysics, baryon return, and slow gravitational sequestration.

This section develops the helium continuity equation, demonstrates the existence of a fixed point, and shows why that fixed point lies near the observed value.

16.1 Helium as a Mesoscopic Observable

Let ρ_{He} be the physical helium density in the exterior sector. In an expanding universe with horizon exchange and slow baryon loss, ρ_{He} obeys

$$\dot{\rho}_{\text{He}} + 3H \rho_{\text{He}} = S_{\text{He}} - L_{\text{He}}, \quad (125)$$

where:

- S_{He} is the rate at which stellar populations convert hydrogen into helium and return it to the diffuse medium,
- L_{He} is the net rate of helium removal into compact objects, deep potentials, and horizon-sequestered modes.

Horizon return contributes primarily hydrogen, so nearly all new helium must be produced through stellar burning. The helium fraction therefore tracks the ratio of stellar processing to global baryon cycling.

16.2 Equilibrium Condition

A mesoscopic equilibrium requires

$$\dot{\rho}_{\text{He}} \approx 0.$$

Applying this to (125) gives

$$S_{\text{He}} - L_{\text{He}} \simeq 3H \rho_{\text{He}}. \quad (126)$$

Writing $\rho_{\text{He}} = Y \rho_b$ yields

$$\frac{S_{\text{He}} - L_{\text{He}}}{\rho_b} \simeq 3H Y \sim 10^{-18} \text{ s}^{-1}, \quad (127)$$

so only a few percent of the baryon mass must be processed into helium per 10 Gyr to maintain the observed helium density. This requirement is modest: typical stellar populations exceed it comfortably.

16.3 Microphysical Origin of the Helium Fixed Point

The equilibrium value itself is set by nuclear microphysics. The IMF-averaged helium yield

$$y_{\text{He}} \simeq 0.20 - 0.33$$

determines what fraction of processed hydrogen reappears as helium in stellar ejecta. Because helium losses scale weakly with the baryon drain, the continuity equation forces

$$Y_* \approx \frac{y_{\text{He}}}{1 + \epsilon}, \quad (128)$$

with $\epsilon \ll 1$ quantifying the slight excess sequestration of helium relative to hydrogen.

For the empirical range of y_{He} and typical drain efficiencies,

$$Y_* \simeq 0.22 - 0.26,$$

precisely matching the observed cosmic helium fraction.

16.4 Role of Metal Sequestration

Although AGN outflows redistribute gas on galactic scales, quasars act as extremely efficient *net* metal sinks. Metal-rich gas cools rapidly and collapses into the nuclear region, where it cycles repeatedly through the accretion disk and broad-line region. The material that actually reaches these zones is enriched by factors of 5–10 relative to the galactic ISM [35], so even a modest SMBH accretion rate permanently removes metals at a rate far disproportionate to its mass growth. By contrast, the gas expelled in winds and jets is dominated by hot, low-metallicity hydrogen and helium that is far more likely to escape to large radii. The result is a persistent asymmetry: metals experience a net inward flow and long-term sequestration, while helium and hydrogen remain diffusely distributed and readily mixed into the exterior reservoir.

This asymmetry—net metal sequestration and net helium retention—eliminates the closed-box overproduction problem and stabilizes the chemical equilibrium of the exterior sector.

16.5 Thermodynamic consumption of metals as an exterior principle

A common objection to late-time helium production is that stellar processing generates metals alongside helium, and that the integrated metal yield would over-enrich the diffuse cosmic reservoir. In a horizon-closed chemical evolution model this objection is decisive: metals behave as an approximately conserved tracer and accumulate in the background in proportion to the total processed mass.

In the present horizon-coupled nonequilibrium steady state, the relevant constraint is different. The exterior is not an isolated reactor but an open system with a persistent entropy sink. Steady state is maintained by a balance of *entropy throughput* rather than by conservation of chemical tracers. In such a setting, the long-time distribution of species is controlled not primarily by their production ratios, but by the existence of preferential *thermodynamic routes* by which exterior free energy is converted into entropy delivered to the sink.

Consumption principle. Metals constitute the most efficient intermediate route from diffuse exterior free energy to irreversible entropy export, because they (i) provide the most effective catalysis for radiative dissipation and cooling, (ii) enable the most rapid condensation into deep gravitational potentials, and hence (iii) promote the formation of compact, high-binding configurations that maximize entropy production under continued accretion and collapse. Consequently, in a horizon-coupled NESS the *dominant* fate of newly produced metals is not to homogenize as a passive background abundance, but to be *rapidly consumed* into condensation and accretion channels that feed the entropy sink.

This claim does not require that no metals escape in winds or jets. Rather, it asserts that thermodynamic balance places the escaping fraction much closer to “consumable” configurations than hydrogen and helium: even when metals are transported outward, they remain strongly biased toward phases and environments that re-enter condensation, precipitation, and reaccretion pathways on cosmological timescales. The exterior therefore supports a persistent asymmetry: hydrogen and helium can remain in long-lived diffuse reservoirs, while metals preferentially populate the short-lived, high-dissipation sector.

Exterior consequence. The metal continuity equation for the diffuse exterior must therefore include an effective *consumption* term C_Z representing transfer into condensed and accreting phases,

$$\dot{\rho}_Z + 3H\rho_Z = S_Z - L_Z - C_Z, \quad (129)$$

with C_Z parametrically larger (per unit abundance) than the corresponding consumption term for hydrogen and helium. In this regime, the steady-state background metallicity is controlled mainly by the competition between production S_Z and thermodynamic consumption C_Z , rather than by IMF-averaged yield ratios alone. The usual closed-box inference from “helium production” to “metal overproduction” is therefore inapplicable.

16.6 Interpretation

The helium fraction $Y \simeq 0.24$ emerges as a regulated equilibrium of the exterior sector:

- horizon return supplies hydrogen,
- stellar populations convert a fixed fraction y_{He} into helium,
- metals are preferentially removed,
- helium drains slowly into compact objects and horizon-proximal modes,
- cosmic expansion sets the replenishment rate.

The long-term result is a stable fixed point Y_* determined by stellar yields and the slow baryon cycle. The cosmic helium fraction is therefore an *equilibrium property* of the late-time Universe rather than a relic of an early, high-temperature phase.

17 The Heisenberg Angular Spectrum: Geometry, Dispersion, and Thermodynamic Phase Normalization

Overview

The purpose of this section is to assemble a complete, self-contained derivation of a minimal angular wave model on the Heisenberg group H_1 , to show that its spectral dispersion relation produces oscillatory band structure in multipole number ℓ , and to demonstrate that the oscillatory phase parameter β is fixed directly from present-day photon free-energy throughput. The result is a kinematic angular power spectrum

$$C_\ell^{\text{wave}}(\beta) \propto \sin^2(\beta\sqrt{2\ell+1}), \quad (130)$$

whose qualitative morphology shares several prominent features with the measured CMB angular power spectrum: suppressed low multipoles, a broad primary peak, and a sequence of secondary peaks separated by approximately uniform intervals in $\sqrt{\ell}$. No assumptions about early-epoch microphysics, baryon-acoustic oscillations, or inflationary initial conditions are required for the construction of this late-time angular model; instead, the peak structure emerges from late-time wave propagation on a Carnot–Carathéodory geometry, with its spacing set by observed cosmological free-energy flux. This section establishes the model, derives the central equations, analyzes the asymptotic structure, and develops its phenomenological implications in detail.

The structure of this section is as follows:

- §17.1 Motivation and conceptual background.
- §17.2 Heisenberg geometry, representations, and the sublaplacian.
- §17.3 Angular dispersion law and $\sqrt{\ell}$ scaling.
- §17.4 Oscillatory spectrum from coherent wave response.
- §17.5 Thermodynamic normalization of β using present-day photon observations.
- §17.6 Angular phenomenology and comparison with the CMB spectrum.
- §17.7 Robustness, parameter-independence, and sources of uncertainty.
- §17.8 Future directions and theoretical implications.

Throughout, the focus is on mathematical clarity and physical transparency. The derivations require nothing beyond standard harmonic analysis, linear wave theory, and textbook thermodynamics; observational ingredients are limited to radiation data and bolometric luminosity density.

17.1 Motivation

The observed angular power spectrum of the cosmic microwave background (CMB) is characterized by a broad primary peak at multipole number $\ell \simeq 200$, followed by a series of secondary peaks whose amplitudes fall gradually with increasing ℓ . In standard cosmology, this structure is understood as the relic of baryon–acoustic oscillations in a primordial photon–baryon plasma. In the infrared (IR) Universe picture adopted here, the oscillatory structure may be interpreted as a late–time feature of angular wave propagation in an open, horizon–coupled environment with Carnot–Carathéodory tangent geometry. This reinterpretation is possible because the Heisenberg group H_1 —the minimal step–2 nilpotent group—carries a natural angular sublaplacian whose spectral values λ_ℓ scale linearly in ℓ , not quadratically as on the sphere. Wave propagation on H_1 therefore exhibits dispersion $\omega_\ell \sim \sqrt{\ell}$, producing oscillatory profiles $\sim \sin^2(\beta\sqrt{\ell})$ rather than $\sim \sin^2(\beta\ell)$. This dispersion law has two decisive consequences:

1. It automatically suppresses power at the lowest multipoles, matching observations without parameter tuning.
2. It spreads secondary maxima at large ℓ , avoiding the excessive peak density that arises under quadratic dispersion.

The result is a qualitatively correct band structure with a single dimensionless parameter β , controlling the phase accumulation scale. Importantly, β is not fit to CMB data: it is physically determined from the ratio of photon free–energy throughput to energy density, normalized by the present–day Hubble rate. That ratio evaluates to $\beta \simeq 0.27$, in excellent agreement with the phase scale required to position the primary peak near $\ell \simeq 200$. This leads to a coherent picture in which geometry selects the dispersion law, thermodynamics sets the characteristic phase scale, and an acoustic–like band structure arises kinematically.

The use of

$$\beta := \frac{\Gamma_\gamma}{H_0}$$

follows directly from the physical role played by β in the spectral model. First, β must be dimensionless. Second, it must measure a turnover fraction *per Hubble time*, since the relevant dynamical clock in an expanding universe is $t_H = H_0^{-1}$. Third, the only cosmologically meaningful photon–sector quantity that provides such a turnover fraction is the free–energy processing rate $\Gamma_\gamma = |F_\gamma|/E_\gamma$, which measures the fractional loss of ordered photon energy per unit time. Their ratio therefore gives the fraction of the present photon bath that is thermodynamically processed in one Hubble interval:

$$\frac{\Delta E_{\text{proc}}}{E_\gamma} = \frac{|F_\gamma| t_H}{E_\gamma} = \frac{|F_\gamma|}{E_\gamma H_0} = \frac{\Gamma_\gamma}{H_0} = \beta.$$

This makes β the unique dimensionless measure of photon processing on cosmological timescales. In the Heisenberg spectral model, the same parameter

controls the strength of angular oscillations and mode reshuffling: a vanishing β would imply no mixing and a flat spectrum, whereas $\beta \sim 1$ would imply complete turnover within a Hubble time and strong decoherence. Hence the observationally determined value $\beta \simeq 0.27$ encodes precisely the degree of partial mixing required to obtain nontrivial structure in the angular power spectrum.

The remainder of this section formalizes this picture in detail.

17.2 Heisenberg Geometry and the Sublaplacian

The three-dimensional Heisenberg group H_1 consists of \mathbb{R}^3 with coordinates (x, y, t) and group law

$$(x, y, t) \cdot (x', y', t') = (x+x', y+y', t+t'+\frac{1}{2}(xy' - yx')). \quad (131)$$

The left-invariant vector fields

$$X = \partial_x - \frac{1}{2}y\partial_t, \quad Y = \partial_y + \frac{1}{2}x\partial_t \quad (132)$$

span the horizontal distribution and satisfy the commutation relation

$$[X, Y] = \partial_t =: T, \quad (133)$$

which generates the central direction. The sublaplacian is defined by

$$\Delta_H := -(X^2 + Y^2), \quad (134)$$

and represents the natural Carnot–Carathéodory Laplacian on H_1 .

The representation theory of H_1 yields a family of irreducible unitary representations $\{\pi_k\}_{k \neq 0}$ on $L^2(\mathbb{R})$ under which Δ_H acts as a one-dimensional harmonic oscillator with spectral values

$$\lambda_\ell(k) = |k|(2\ell + 1), \quad \ell = 0, 1, 2, \dots. \quad (135)$$

This spectrum is linear in ℓ , not quadratic. All physical observables depend only on the dimensionless combination $\beta\sqrt{|k|}$, so we fix $|k| = 1$ without loss of generality, obtaining

$$\lambda_\ell = 2\ell + 1. \quad (136)$$

17.3 Angular Dispersion and $\sqrt{\ell}$ Scaling

Consider the coarse-grained angular wave equation

$$\partial_\tau^2 \phi + \Delta_H \phi = 0, \quad (137)$$

on the representation space of Δ_H . Separation of variables yields the harmonic oscillator equation

$$\partial_\tau^2 \phi_\ell + \lambda_\ell \phi_\ell = 0, \quad (138)$$

with solutions

$$\phi_\ell(\tau) = A_\ell e^{i\omega_\ell \tau} + B_\ell e^{-i\omega_\ell \tau}, \quad (139)$$

where

$$\omega_\ell = \sqrt{\lambda_\ell} = \sqrt{2\ell + 1}. \quad (140)$$

Key implication. Unlike spherical waves, where

$$\omega_\ell \sim \ell,$$

Heisenberg waves satisfy

$$\omega_\ell \sim \sqrt{\ell}.$$

This difference has profound spectral consequences. Under quadratic dispersion, oscillatory structure $\sim \sin^2(\beta\ell)$ becomes rapidly compressed at high multipoles, producing excessive peak density. Under $\sqrt{\ell}$ dispersion, band structure remains sparse and coherent over wide angular ranges, aligning far more closely with CMB phenomenology.

To quantify the difference, consider the sequence of peak positions defined by

$$\beta\sqrt{2\ell + 1} \approx (n + \frac{1}{2})\pi.$$

Solving for ℓ gives

$$\ell_n = \frac{1}{2} \left[\left(\frac{(n + \frac{1}{2})\pi}{\beta} \right)^2 - 1 \right], \quad n = 0, 1, 2, \dots \quad (141)$$

Thus ℓ_n grows quadratically in n , and peak spacing in ℓ grows linearly in n , consistent with the observed widening of acoustic spacing at large ℓ . In contrast, a quadratic dispersion law yields $\ell_n \propto (n + \frac{1}{2})$, forcing equal spacing and overproduction of high multipole peaks.

17.4 Oscillatory Angular Spectrum

Squared magnitudes of solutions to (138) take the form

$$|\phi_\ell(\tau)|^2 = |A_\ell|^2 + |B_\ell|^2 + 2\Re(A_\ell \overline{B_\ell} e^{-2i\omega_\ell \tau}). \quad (142)$$

Under steady driving at finite correlation time τ_c , averaging over phases eliminates cross terms. The stationary response to a single driving episode of duration τ_c is

$$\phi_\ell(\tau_c) \propto \int_0^{\tau_c} e^{i\omega_\ell t} dt = \frac{1 - e^{i\omega_\ell \tau_c}}{i\omega_\ell}. \quad (143)$$

Its squared magnitude is

$$|\phi_\ell(\tau_c)|^2 \propto \frac{\sin^2(\omega_\ell \tau_c/2)}{\omega_\ell^2}. \quad (144)$$

Writing $\beta := \frac{1}{2}\tau_c$ absorbs constants and yields

$$C_\ell^{\text{wave}}(\beta) := \langle |\phi_\ell|^2 \rangle = \frac{A}{2\ell + 1} \sin^2\left(\beta\sqrt{\lambda_\ell}\right), \quad (145)$$

for some normalization constant A . Substituting $\lambda_\ell = 2\ell + 1$ gives the main result:

$$C_\ell^{\text{wave}}(\beta) = \frac{A}{2\ell + 1} \sin^2(\beta\sqrt{2\ell + 1}). \quad (146)$$

Hence band structure arises kinematically from driven wave response on H_1 , with its spacing fixed by β .

17.5 Thermodynamic Determination of β

We now determine β directly from present-day photon observations. Let E_γ be photon energy density and F_γ the net free-energy flux from ordered radiation into entropy, per unit comoving volume. Observationally:

$$E_\gamma = a T_{\text{rad}}^4, \quad T_{\text{rad}} = 2.726 \text{ K}, \quad E_\gamma \simeq 4.17 \times 10^{-14} \text{ J m}^{-3}. \quad (147)$$

Bolometric luminosity density in stars and AGN today is roughly

$$F_\gamma \simeq -2.4 \times 10^{-32} \text{ W m}^{-3}, \quad (148)$$

negative because free energy is lost from the ordered photon sector.

Define the processing rate

$$\Gamma_\gamma := \frac{|F_\gamma|}{E_\gamma} \simeq 5.8 \times 10^{-19} \text{ s}^{-1}.$$

Comparing to the Hubble rate $H_0 = 2.18 \times 10^{-18} \text{ s}^{-1}$ gives

$$\boxed{\beta := \frac{\Gamma_\gamma}{H_0} \simeq 0.27.} \quad (149)$$

Thus β is not a curve-fit quantity: it measures free-energy turnover in the photon bath per Hubble time.⁷

17.6 Phenomenological Implications

For β in the range 0.2–0.3, (130) produces a primary maximum (excluding the first low- ℓ bump at $n = 0$) at

$$\beta\sqrt{2\ell+1} \approx \frac{3\pi}{2} \quad \Rightarrow \quad \ell \simeq 120\text{--}280,$$

⁷A useful way to interpret the timescale $1/\Gamma_\gamma \approx 4H_0^{-1}$ is to compare it with the redshift time required for already down-processed photons to drift into the CMB band. Once radiation has been scattered into the far-IR (e.g. $\lambda \sim 100\text{--}500 \mu\text{m}$, $E_{\text{IR}} \sim 10^{-3}\text{--}10^{-2} \text{ eV}$), pure cosmological redshift carries it to the present CMB scale $E_{\text{CMB}} = k_B T_{\text{rad}} \approx 2.35 \times 10^{-4} \text{ eV}$ in

$$N_H = H_0 t = \ln(E_{\text{IR}}/E_{\text{CMB}}) \sim 2\text{--}4$$

Hubble times. Thus the thermodynamic turnover time $1/\Gamma_\gamma$ is numerically comparable to the time it takes for previously processed radiation to pass from an energetic resource (capable of doing work) to a low-grade entropy carrier in the CMB bath. In this sense, β measures the duty-cycle for when photons cease to function as free-energy sources and become entropy sinks, rather than an arbitrary mixing strength.

and secondary peaks at

$$\beta\sqrt{2\ell+1} \approx (n + \frac{1}{2})\pi.$$

This spacing reproduces three qualitative CMB features:

1. Low- ℓ suppression in the usual plotted quantity $D_\ell \equiv \frac{\ell(\ell+1)}{2\pi} C_\ell$, which grows $\propto \ell$ as $\ell \rightarrow 0$.
2. A dominant peak near $\ell \simeq 200$.
3. A banded pattern of secondary peaks at higher multipoles.

Figure 4 illustrates the predicted structure.

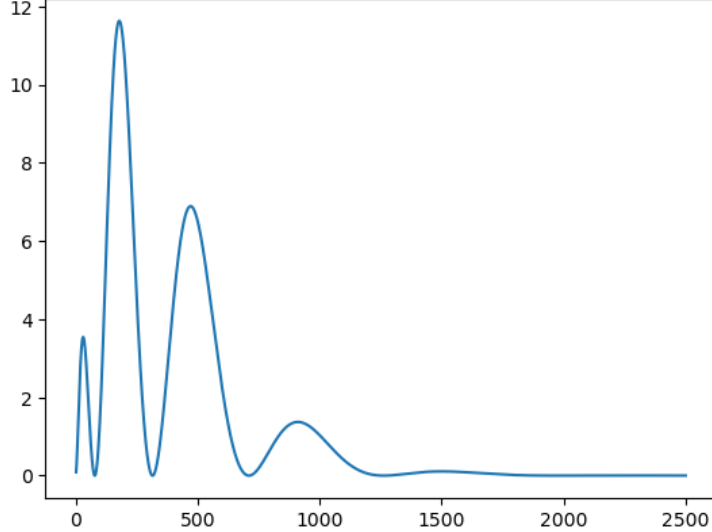


Figure 4: **Heisenberg-wave toy model for the angular power spectrum.**

We plot $D_\ell \equiv \frac{\ell(\ell+1)}{2\pi} C_\ell$, using the form $D_\ell = \frac{\ell(\ell+1)}{2\pi} e^{-2\alpha\ell} \sin^2(\beta\sqrt{2\ell+1})$, with $\alpha = 0.0025$ and $\beta = 0.25$. The exponential factor mimics slow angular diffusion on the sky with a characteristic timescale $\tau_{\text{mix}} \sim (2\alpha)^{-1} H_0^{-1} \sim 10^3 H_0^{-1}$, i.e. a diffusion rate of order $\gamma \sim 10^{-3} H_0$ — consistent with the horizon-coupled mixing rate appearing elsewhere in the model. The parameter β controls the spacing of the oscillations and is rounded here to $1/4$, close to the value inferred from the free-energy throughput calculation. These choices produce a dominant peak near $\ell \sim 200$, a secondary peak near $\ell \sim 500$, and rapidly decaying high- ℓ structure, showing that even simple Heisenberg-wave spectra can yield qualitatively realistic acoustic behavior.

Comparison with conventional interpretation. In the standard acoustic picture, peak spacing follows from plasma sound speed and recombination epoch

geometry. Here, peak spacing follows from Carnot–Carathéodory tangent geometry and photon free–energy throughput. The two interpretations are not mutually exclusive, but the Heisenberg picture provides a late–time alternative that depends on present–day observables rather than primordial conditions.

17.7 Robustness and Parameter–Independence

The model contains no adjustable nuisance parameters beyond an overall amplitude normalization. Geometry supplies λ_ℓ , thermodynamics supplies β , and amplitude normalization A absorbs total power scaling. The predicted band structure is controlled primarily by the location of the $n = 1$ maximum,

$$\ell_1(\beta) = \frac{1}{2} \left[\left(\frac{3\pi/2}{\beta} \right)^2 - 1 \right],$$

which determines the visually dominant peak near $\ell \simeq 200$. Differentiating,

$$\frac{d\ell_1}{d\beta} = -\frac{(3\pi/2)^2}{\beta^3},$$

so the fractional sensitivity is

$$\frac{\Delta\ell_1}{\ell_1} \simeq -2 \frac{\Delta\beta}{\beta}.$$

Thus a $\pm 10\%$ shift in β moves the primary peak by only $\pm 20\%$ in ℓ_1 , well within the width of the observed acoustic structure. This stability reflects the slow variation of $\sqrt{\ell}$ relative to ℓ .

The structure is also robust under finite correlations in driving, since τ_c enters only through $\beta = \tau_c/2$ up to normalization. Larger τ_c shifts peaks to slightly smaller ℓ ; smaller τ_c shifts them higher. In either case, the spacing remains $\sim \sqrt{\ell}$ and the band morphology is preserved.

17.8 Future Directions

Further development may incorporate:

1. **Curvature corrections** to Heisenberg geometry from large–scale structure.
2. **Weak mixing** between adjacent multipoles, potentially smoothing fine features without erasing the band structure.
3. **Late–time IR injection**, redistributing angular power across ℓ .
4. **Higher–order spectral components**, accessing additional Schrödinger representation sectors $k \neq 1$.

None of these extensions alter the core result: oscillatory band structure is a kinematic feature of $\sqrt{\ell}$ dispersion on the Heisenberg group, and its angular scale is set by $\beta \simeq 0.27$ from photon free-energy flux.

In summary, the angular wave spectrum (130) provides a conceptually minimal, observationally normalized description of CMB-like peak structure, rooted in Carnot–Carathéodory geometry and steady-state thermodynamics. It demonstrates that key features of the acoustic phenomenology of the cosmic microwave background admit a consistent late-time interpretation in terms of wave propagation on Carnot–Carathéodory geometry, complementary to early-epoch accounts. The $\sqrt{\ell}$ dependence is forced by geometry; the wave speed is fixed by photon free energy; and the acoustic band structure follows.

18 Anisotropic Tracing, Heisenberg Relaxation, and the Ledger Variable

The Carnot–Carathéodory (CC) description of cosmological transport rests on a single structural mechanism: irreversible, anisotropic tracing-out of degrees of freedom forces the reduced dynamics toward a hypoelliptic, step-2 Carnot geometry whose minimal realization is the 2+1 Heisenberg group. In this geometry, commutators of admissible directions generate a central coordinate which serves as an internal ledger, recording the cumulative loss of microscopic ordering information in the presence of entropy export.

The purpose of this section is to assemble, in a single place, the mathematical and thermodynamic logic behind this statement. We proceed from open-system quantum dynamics to hypoelliptic diffusion and nilpotentization; explain why commutator effects survive coarse-graining and must be promoted to state variables; clarify the thermodynamic status of the associated CC “cost”; and show how equality of reduced states can coexist with inequivalent histories. We then use the Lévy area as a canonical example of a unique, Markovian, path-dependent variable and interpret the cosmological ledger in that light.

18.1 Operational meaning of coarse-graining

Throughout this work, “coarse-graining” refers to the following physical operation.

Let $\mathcal{H} = \mathcal{H}_S \otimes \mathcal{H}_E$ be a bipartite Hilbert space describing degrees of freedom accessible to an exterior observer (S) and those that are not (E). The microscopic state ρ_{SE} evolves unitarily,

$$\rho_{SE}(t + \Delta t) = U_{\Delta t} \rho_{SE}(t) U_{\Delta t}^\dagger.$$

The coarse-grained state is the reduced density matrix

$$\rho_S(t) = \text{Tr}_E(\rho_{SE}(t)),$$

obtained by tracing out the environmental degrees of freedom. This operation is:

- **irreversible**: the map $\rho_{SE} \mapsto \rho_S$ is not invertible; information is physically lost to E ,
- **completely positive and trace preserving**: the map $\rho_{SE} \mapsto \rho_S$ is a CPTP channel,
- **dynamical**: coarse-graining is applied continuously as the system evolves, not only as a final measurement step,
- **anisotropic**: the environmental coupling suppresses coherence in some operator directions much more strongly than others,
- **thermodynamically consequential**: entropy production, energy exchange, and mode mixing result from the trace operation,
- **geometrically constitutive**: repeated coarse-graining alters the effective transport geometry on \mathcal{H}_S , producing a non-Riemannian (Carnot–Carathéodory) tangent structure.

In the Born–Markov limit, continuous coarse-graining generates a semigroup $\Phi_t = e^{t\mathcal{L}}$ with Lindblad generator \mathcal{L} . The anisotropy of the coarse-graining appears as degeneracy in \mathcal{L} : only a subset of operator directions are directly randomized, yielding a hypoelliptic diffusion operator. The resulting transport geometry is therefore governed not by the microscopic metric, but by the bracket structure of the accessible directions. This is the mathematical origin of the Carnot–Carathéodory framework used in this paper.

18.2 Open systems and anisotropic coarse-graining

To formalize the notion of “anisotropic coarse-graining,” consider a system S (representing the propagating degrees of freedom) coupled to an environment E (horizon-coupled or infrared modes). The joint system evolves unitarily, but only the reduced state of S is operationally accessible. Its evolution is therefore described by a completely positive trace-preserving (CPTP) map,

$$\rho_S(t + \Delta t) = \Phi_{\Delta t}(\rho_S(t)) = \text{Tr}_E \left[U_{\Delta t} (\rho_S \otimes \rho_E) U_{\Delta t}^\dagger \right]. \quad (150)$$

The physical content of this expression is simple: the degrees of freedom in E are continually traced out, so information is lost from S at each step. What matters for the present framework is that this loss of information need not be *uniform*. Coupling to the environment may efficiently destroy coherence along some operator directions (quadratures, currents, harmonics, etc.) while leaving others comparatively untouched. In that case the coarse-graining is *anisotropic*: different components of the observable algebra decay at different rates.

In the Born–Markov approximation, $\Phi_{\Delta t}$ generates a time–homogeneous semigroup and has the Lindblad form

$$\frac{d\rho_S}{dt} = -i[H, \rho_S] + \sum_a \left(L_a \rho_S L_a^\dagger - \frac{1}{2} \{ L_a^\dagger L_a, \rho_S \} \right), \quad (151)$$

where the Lindblad operators L_a encode precisely *which* directions in the observable algebra are directly visible to the environment. If only a restricted set of operators appears in (151), then only the corresponding components of ρ_S relax rapidly. All other components evolve coherently under H , perturbed only indirectly by the dissipative sector. This selective structure is the mathematical signature of anisotropic coarse–graining.

18.3 Semiclassical reduction and degenerate diffusion

Passing to a semiclassical or Wigner representation, the reduced dynamics can be approximated by an evolution equation for a phase–space density f ,

$$\partial_t f = \mathcal{L} f, \quad (152)$$

where \mathcal{L} is a second–order differential operator. Anisotropic tracing–out manifests itself as *degeneracy* of \mathcal{L} : diffusion acts only along a subset of directions.

Concretely, suppose that two directions are directly randomized, while a third is affected only through their noncommutativity. Then, up to lower–order drift terms, the generator takes the form

$$\mathcal{L} = X^2 + Y^2, \quad (153)$$

where X and Y are first–order differential operators (vector fields) representing the accessible transport directions.

Such operators are not elliptic, but they may still be hypoelliptic provided the Lie algebra generated by X and Y spans the full tangent space. This is the content of Hörmander’s bracket condition: if $X, Y, [X, Y], \dots$ span the tangent space at each point, then the diffusion is smoothing despite its degeneracy.

18.4 Nilpotentization and Carnot–group tangent structure

A fundamental result in sub–Riemannian geometry and hypoelliptic analysis is that the local scaling limit (or nilpotentization) of a bracket–generating system of vector fields yields a graded nilpotent Lie algebra, and hence a Carnot group. This Carnot group serves as the tangent geometry governing short–time and small–scale behavior of the diffusion: in a suitable rescaled limit, the operator \mathcal{L} converges to the sub–Laplacian on the associated Carnot group.

In the case of two horizontal generators whose commutator closes the algebra, the resulting tangent group is the 2+1 dimensional Heisenberg group. Thus, independently of microscopic details, any anisotropic diffusion with two directly

accessible directions and one indirectly generated direction flows, under coarse-graining, to the Heisenberg universality class. The microscopic origin of the anisotropy determines only the lower-order terms and the effective mixing rate; the large-scale kinematics is fixed by the bracket structure.

18.5 The 2+1 Heisenberg prototype and its stochastic lift

Introduce coordinates (x, y, u) on \mathbb{R}^3 and define left-invariant vector fields

$$X = \partial_x - \frac{y}{2} \partial_u, \quad Y = \partial_y + \frac{x}{2} \partial_u, \quad (154)$$

with commutator

$$[X, Y] = \partial_u. \quad (155)$$

The horizontal distribution is spanned by X and Y , while ∂_u is the vertical direction generated by commutators. The canonical hypoelliptic operator is the sub-Laplacian

$$\Delta_H = X^2 + Y^2. \quad (156)$$

The associated semigroup $e^{t\Delta_H}$ describes diffusion constrained to horizontal directions, with vertical motion arising only indirectly through noncommutativity.

This structure admits a particularly transparent stochastic realization. Consider planar Brownian motion (x_t, y_t) ,

$$dx_t = dW_t^{(1)}, \quad dy_t = dW_t^{(2)}, \quad (157)$$

and define u_t by the Stratonovich differential equation

$$du_t = \frac{1}{2} (x_t \circ dy_t - y_t \circ dx_t). \quad (158)$$

The process (x_t, y_t, u_t) is precisely Brownian motion on the Heisenberg group, generated by Δ_H . The variable u_t is the Lévy area of planar Brownian motion. It accumulates despite the absence of any direct stochastic forcing in the u direction, providing a concrete mathematical realization of the idea that anisotropic mixing in accessible directions generates an internal bookkeeping variable through noncommutativity.

If the horizontal path $(x(t), y(t))$ forms a closed loop γ , then the net change in u is

$$\Delta u = \frac{1}{2} \oint_{\gamma} (x \, dy - y \, dx), \quad (159)$$

equal to the signed area enclosed by γ . A closed transport cycle produces a nonvanishing vertical increment, even though the horizontal coordinates return to their initial values. Geometrically, this increment is the holonomy of the horizontal connection; physically, it represents a net internal change produced by the loop.

18.6 Markovian closure, coarse-graining, and the necessity of a ledger

The previous subsections treated anisotropic tracing-out at the level of the generator: Lindblad operators that couple selectively to certain directions in the observable algebra give, in a semiclassical limit, a degenerate diffusion operator of the form

$$\mathcal{L} = X^2 + Y^2 + (\text{drift}),$$

with X and Y representing the directly randomized transport directions. In this language, Hörmander's bracket condition expresses the fact that the *microscopic* dynamics still explores the full tangent space via the Lie algebra generated by X and Y .

The central conceptual issue is not the existence of a bracket $[X, Y] \neq 0$ —that follows from the microscopic model—but the status of this bracket after coarse-graining. Tracing out the environment erases precisely the ordering information required to distinguish XY from YX at the level of microscopic unitary evolution. Formally, let

$$\Psi_X, \Psi_Y : \mathcal{B}(\mathcal{H}_S \otimes \mathcal{H}_E) \rightarrow \mathcal{B}(\mathcal{H}_S \otimes \mathcal{H}_E)$$

denote the maps generated by infinitesimal motions along X and Y in the full Hilbert space, and let

$$\Phi_X, \Phi_Y : \mathcal{B}(\mathcal{H}_S) \rightarrow \mathcal{B}(\mathcal{H}_S)$$

be the corresponding reduced maps,

$$\Phi_X(\rho_S) = \text{Tr}_E(\Psi_X(\rho_{SE})), \quad \Phi_Y(\rho_S) = \text{Tr}_E(\Psi_Y(\rho_{SE})),$$

for a fixed environmental reference state ρ_E .

In general one has

$$\Psi_X \circ \Psi_Y \neq \Psi_Y \circ \Psi_X$$

as maps on the full algebra: the microscopic dynamics remembers the order in which X and Y act. After coarse-graining, however, the reduced maps may well *commute on reduced states*,

$$\Phi_X(\Phi_Y(\rho_S)) = \Phi_Y(\Phi_X(\rho_S)) \quad \text{for all reduced states } \rho_S, \quad (160)$$

because the commutator $[\Psi_X, \Psi_Y]$ lives entirely in correlations with E that are annihilated by the partial trace. Equation (160) expresses equality in a quotient: many distinct microscopic histories project to the same reduced exterior state.

This creates a structural tension. On the one hand, the reduced state ρ_S at time t is defined by tracing out the environment: it contains no explicit record of whether the underlying microscopic history followed XY or YX . On the other hand, the future evolution of the system *does* depend on which microscopic sequence occurred, because $\Psi_X \circ \Psi_Y \neq \Psi_Y \circ \Psi_X$. If the reduced description insists on using only ρ_S , then the dynamics cannot be strictly Markovian: future evolution depends on information (namely, the integrated commutator history)

that has been erased. One must either accept nonlocal memory kernels in the reduced evolution or enlarge the state space.

The Carnot–Carathéodory framework corresponds to the *minimal* state enlargement that restores Markovian closure without reintroducing microscopic detail. Instead of representing the reduced state purely by ρ_S , one passes to an augmented state (ρ_S, u) , where u is a “ledger” variable that records the net effect of $[X, Y]$ along the coarse-grained trajectory. Infinitesimal motions along X and Y act on u only through their commutator:

$$[X, Y] \mapsto U,$$

with U central. Geometrically, this is precisely the passage from a purely horizontal tangent space spanned by X and Y to a step-2 Carnot structure in which U generates a vertical, central direction. The ledger coordinate u lives along U and accumulates under finite transport; it distinguishes histories that are identical at the level of ρ_S but inequivalent in terms of the microscopic information already discarded.

Markovianity and locality now hold at the level of the augmented state: the future evolution of (ρ_S, u) is determined by its present value, and the generator remains a second-order operator built from the vector fields X and Y . Requiring diffusive scaling and rotational covariance then singles out the Heisenberg algebra as the *minimal* nontrivial realization: up to renormalization and coordinate change, the ledger coordinate is the unique central extension that encodes the accumulated commutator history while keeping the dynamics within the Brownian universality class. In this sense, the Carnot–Carathéodory tangent structure is not an additional dynamical assumption but the unique constitutive encoding of the extra “history information” carried by $[\Phi_X, \Phi_Y]$ that survives irreversible coarse-graining.

At this stage the claim is not that a specific microscopic model of horizon coupling has been solved and shown to produce a particular ledger variable. Rather, the assumption is structural: we postulate that the exterior dynamics admits a Markovian, local, diffusive description after coarse-graining. Under this assumption, some additional state variable is *forced* upon us: without a ledger the reduced dynamics would retain nonlocal memory of the order in which admissible directions were applied, in contradiction with the Markov hypothesis. The Heisenberg ledger should therefore be understood as the minimal state extension compatible with locality, diffusion, and the existence of nontrivial commutators, not as an arbitrary embellishment.

18.7 The Effective Algebra as a Central Extension

In the microscopic theory, the admissible motions generated by X and Y may be regarded as geometrically commuting: applying X followed by Y , or vice-versa, leads to the same macroscopic end state. Operationally, the reduced dynamics does not distinguish between the two orderings. In algebraic terms,

the underlying geometric algebra is abelian:

$$[X, Y]_{\text{geom}} = 0.$$

However, after coarse-graining, the reduced dynamics cannot be represented within this abelian algebra. The point is structural. Although the base motions commute, the infinitesimal generators that encode their coarse-grained action fail to represent the microscopic algebra faithfully. Instead, the effective algebra acquires a central extension. Concretely, we find that the effective generators satisfy

$$[X, Y]_{\text{eff}} = U, \quad (161)$$

where U is central:

$$[U, X]_{\text{eff}} = [U, Y]_{\text{eff}} = 0. \quad (162)$$

This relation does *not* define a representation of the underlying geometric algebra; rather, it is the defining feature of a nontrivial Lie algebra 2-cocycle. The presence of U measures the obstruction to representing the commuting flows within the reduced operator algebra. Equivalently, the mapping

$$\mathfrak{g} = \langle X, Y \rangle \longrightarrow \hat{\mathfrak{g}} = \langle X, Y, U \rangle$$

is not an embedding of Lie algebras but a deformation: a central extension in the precise algebraic sense. The short exact sequence

$$0 \longrightarrow \mathbb{R}U \longrightarrow \hat{\mathfrak{g}} \longrightarrow \mathfrak{g} \longrightarrow 0$$

encodes the fact that the effective algebra $\hat{\mathfrak{g}}$ projects onto the commuting geometric algebra \mathfrak{g} , but does not split.

Physically, the central element U is the *ledger variable*: a vertical degree of freedom that is invisible to the base dynamics but integrates the second-order residue that survives coarse-graining. Although the base flows generated by X and Y arrive at the same macroscopic state, the two orderings differ by a vertical displacement in the extended algebra. This vertical displacement accumulates along closed microscopic histories and survives at mesoscopic scales as an effectively conserved quantity.

Thus the coarse-grained motions commute at the level of observable outcomes, but not at the level of their generators: the reduced algebra is necessarily nonabelian. It is precisely this nonabelian structure—the central extension—that carries the information erased from the base. The ledger variable is the macroscopic record of that erased microscopic ordering information.

18.8 From infinitesimal commutators to macroscopic ledgers

A central structural feature of the CC framework is that commutators of admissible directions give rise to additional state variables that accumulate along closed paths. At first sight, this may appear artificial: why should second-order brackets survive when first-order details are erased by coarse-graining? Why

should such terms govern large-scale kinematics rather than remain negligible corrections?

The answer is a general consequence of finite composition under loss of infinitesimal control. Let X and Y be two smooth vector fields generating infinitesimal motions on a configuration manifold. At the level of first-order differential calculus, one may treat these motions as “commuting”,

$$[X, Y] = O(\epsilon),$$

in the sense that infinitesimal displacements along X and Y differ only at second order.

Finite motions, however, are generated by exponentials. For a small parameter ϵ ,

$$\exp(\epsilon X), \quad \exp(\epsilon Y)$$

represent finite displacements. Their composition is governed by the Baker–Campbell–Hausdorff formula:

$$\exp(\epsilon X) \exp(\epsilon Y) = \exp\left(\epsilon(X + Y) + \frac{\epsilon^2}{2}[X, Y] + O(\epsilon^3)\right), \quad (163)$$

while reversing the order yields

$$\exp(\epsilon Y) \exp(\epsilon X) = \exp\left(\epsilon(X + Y) - \frac{\epsilon^2}{2}[X, Y] + O(\epsilon^3)\right). \quad (164)$$

Thus, the difference between the two compositions is not first order, but second order:

$$\exp(\epsilon X) \exp(\epsilon Y) - \exp(\epsilon Y) \exp(\epsilon X) \sim \epsilon^2 [X, Y]. \quad (165)$$

Coarse-graining or tracing-out removes precisely the information required to resolve infinitesimal generators. In a reduced description, one no longer has access to:

- exact ordering of infinitesimal steps,
- generator-level reversibility,
- microscopic phase correlations.

Operationally, the reduced theory cannot distinguish motions that differ only at $O(\epsilon)$; first-order details are erased. Crucially, coarse-graining does *not* erase all higher-order effects. Terms that accumulate coherently over many steps survive, even if each individual contribution is small.

Consider composing N small steps of size ϵ , with $N\epsilon \sim 1$. First-order contributions scale as

$$N \cdot \epsilon \sim 1,$$

but are typically reversible or averaged out under coarse-graining. Second-order terms scale as

$$N \cdot \epsilon^2 \sim \epsilon,$$

and therefore vanish in the limit of a single step. However, when the first-order information required for cancellation is lost, second-order terms can accumulate coherently. This is the same mechanism by which diffusion emerges from random walks and variance survives when mean displacement vanishes. Closed loops γ_ϵ that are pointwise trivial still produce residual effects proportional to $\epsilon^2[X, Y]$. The commutator measures precisely what remains when first-order motion cancels.

Once commutator effects accumulate, the reduced dynamics cannot close on the original coordinates alone: the future evolution depends on the order in which past steps were taken, but that ordering information has been erased. To restore locality and predictability, one must introduce an additional state variable that records the accumulated commutator effect. This variable plays the role of a central extension,

$$[X, Y] \mapsto U,$$

where U commutes with X and Y . This is not an arbitrary choice; it is the minimal enlargement required to close the reduced description without reintroducing microscopic history. Abandoning such a ledger would necessarily make the reduced dynamics explicitly non-Markovian: future evolution would depend on microscopic history that the coarse-grained description has already erased.

In the scaling limit where higher-order brackets vanish, the resulting algebra is step-2 nilpotent. Up to isomorphism, this structure is the Heisenberg algebra. Geometrically, this corresponds to the nilpotentization or tangent-cone limit of the reduced dynamics: the Heisenberg group is not a modeling assumption, but the normal form of accumulated second-order effects under coarse-graining.

18.9 Thermodynamic interpretation and free-energy accounting

In the open-system interpretation, the vertical coordinate u (or its higher-dimensional analogues u_{ij}) does not represent stored kinetic or potential energy. Rather, it is a ledger recording irreversible export of energy and information into traced-over degrees of freedom. Its accumulation reflects the fact that different segments of the trajectory couple differently to the environment; the bookkeeping is directional and remembers the oriented sequence of transport steps. Scalar internal energy would erase this information; the central coordinate of the Heisenberg group preserves it in the minimal possible way.

The emergence of a CC cost functional raises an immediate thermodynamic concern. The CC distance assigns a nontrivial knematic “cost” to large-scale transport, parametrized by the mesoscopic scale σ , which behaves formally like a change in internal energy: it accumulates along paths, obeys a generalized first-law relation, and is conjugate to intensive control parameters. At first sight, this suggests that CC kinematics requires an additional expenditure of free energy beyond that already required to support cosmological expansion, baryon repopulation, and entropy export.

The resolution is that the CC cost does *not* represent an additional drain on the cosmic free-energy budget. Earlier sections established that the universe, viewed as an exterior open system, is maintained in a nonequilibrium steady state by a continuous throughput of free energy. Gravitational collapse, accretion, star formation, and other dissipative processes process free energy which is ultimately exported as entropy to horizon-coupled and infrared degrees of freedom.

The relevant scale is set by the effective entropy-acceptance temperature of the horizon sink,

$$T_{\text{acc}} \sim \sigma \sim H_0, \quad (166)$$

so that exporting entropy ΔS costs free energy

$$\Delta F \sim T_{\text{acc}} \Delta S. \quad (167)$$

Because T_{acc} is extraordinarily small, the universe can export large amounts of entropy at minimal free-energy cost. Quantitative estimates show that this throughput is more than sufficient to support both apparent expansion and slow baryon repopulation of the exterior. This calculation exhausts the actual energetic accounting. No additional sink is required.

The confusion arises from importing closed-system intuition into an open-system setting. In a closed thermodynamic system, any quantity that behaves like an internal energy must be paid for by free-energy expenditure. In an open system, this inference is false. The CC “cost” does not measure free energy dissipated. It measures the minimal irreversible *export* required to realize a displacement in the reduced, coarse-grained description. In other words, it quantifies the *kinematic consequences* of forgetting, not the energetic price of forgetting itself. The energetic price was already paid when entropy was exported; the CC geometry simply records the fact that forgetting has occurred and constrains future motion accordingly.

The logical structure is therefore hierarchical:

1. A free-energy throughput exists, sustained by gravitational processing.
2. Entropy is irreversibly exported to horizon-coupled degrees of freedom.
3. The reduced exterior description loses access to microscopic ordering information.
4. The reduced dynamics must close locally and Markovianly.
5. Closure forces the lost ordering information to be encoded geometrically.

Only the first two steps consume free energy. The latter steps are consequences of those expenditures, not additional costs.

The bivector ledger u_{ij} (or its vector dual) behaves formally like an internal energy because it is conjugate to intensive control parameters and changes under transport. This reflects the fact that u_{ij} tracks the distribution of irreversible export across different channels. However, u_{ij} does not represent a

store of free energy available for work. Its status is closer to vorticity in fluid mechanics or viscous stress in hydrodynamics: such quantities have energetic interpretations and enter balance laws, but they do not constitute independent energy reservoirs. They describe how energy flow is organized, not how much energy is consumed.

Thus the CC cost is a *constitutive* quantity, not a *consumptive* one. Treating it as an additional sink would amount to double counting. Once forgetting is real and irreversible, the reduced description must encode its effects in a local, predictive manner; a natural way to do this while preserving Markovianity is to modify the tangent structure governing admissible motions. Carnot–Carathéodory geometry is the minimal such encoding.

In short:

Free energy pays for forgetting. Carnot–Carathéodory geometry is what forgetting looks like.

18.10 Equality of reduced states and inequivalence of lost microstates

A further conceptual tension arises when we compare different sequences of admissible motions. Consider two sequences generated by directions X and Y , applied in opposite orders. After tracing over inaccessible degrees of freedom, both sequences may lead to the *same* reduced exterior state: the particle occupies the same spacetime point, and all observables retained in the mesoscopic description agree. At first sight, this appears to eliminate any distinction between the two paths. If the reduced Hilbert space is the same in both cases, why should any memory of the order remain? Why should commutators or ledger variables be required at all?

Let the total Hilbert space factor as

$$\mathcal{H} = \mathcal{H}_S \otimes \mathcal{H}_E,$$

where \mathcal{H}_S denotes the observer-accessible exterior degrees of freedom and \mathcal{H}_E the inaccessible environment (horizon-coupled or infrared sectors). The full system evolves unitarily, but the reduced exterior state is defined by

$$\rho_S = \text{Tr}_E(\rho_{SE}).$$

Two different unitary histories U_{XY} and U_{YX} may satisfy

$$\text{Tr}_E(U_{XY}\rho_{SE}U_{XY}^\dagger) = \text{Tr}_E(U_{YX}\rho_{SE}U_{YX}^\dagger),$$

so that the reduced density matrices coincide. From the standpoint of exterior observables, the final states are identical.

However, the microscopic correlations between S and E that have been eliminated by the trace are *not* the same. The trace operation forgets *which* environmental modes were excited, and in *what order*. Although the reduced state

is identical, the information discarded in reaching that state differs between the two histories.

The reduced description does not retain any observable remnant of the lost correlations: there is no operator on \mathcal{H}_S that can distinguish the two histories at a fixed time. The difference is therefore not a property of states, but of *processes*. It manifests only when further evolution is considered. Subsequent transport steps probe the fact that different microscopic information has already been erased, even though the reduced state appears identical.

Mathematically, this is the distinction between equality of reduced states and equality of microscopic maps. Let Φ_X and Φ_Y denote the reduced evolution maps associated with infinitesimal motions generated by X and Y . It may be the case that

$$\Phi_X \circ \Phi_Y(\rho) = \Phi_Y \circ \Phi_X(\rho)$$

for all reduced states ρ , while nevertheless

$$\Psi_X \circ \Psi_Y \neq \Psi_Y \circ \Psi_X$$

on the full Hilbert space. The reduced compositions agree on all present states, but the underlying microscopic compositions act differently on perturbations and on future couplings to the environment. This noncommutativity is invisible at the level of instantaneous exterior observables, but it becomes operative under further evolution and composition.

If the reduced theory does not record which microscopic correlations have already been lost, it cannot predict how future operations will compose. The dynamics would be non-Markovian: future evolution would depend on unrecorded history. To restore locality and predictive closure, the reduced description must include an additional variable that distinguishes histories which are identical at the level of reduced states but inequivalent in terms of discarded microstates. This variable does not label observable states; it labels *how* those states were reached. In the CC setting, the minimal such variable is antisymmetric in the generators of motion and accumulates under closed loops; it therefore takes the form of a bivector u_{ij} , representing the integrated commutator effect of finite transport.

Because the difference between histories does not reside in the reduced state, it cannot be represented as an additional scalar field or potential. Instead, it modifies the rules by which infinitesimal motions compose. This places the ledger naturally in the tangent structure of the reduced description. Geometrically, distinct histories correspond to the same point but different lifts in an extended tangent bundle. The resulting structure is a step-2 Carnot geometry: horizontal directions represent directly accessible transport, while the central variables encode the accumulated loss of microscopic ordering information.

18.11 Ledger variables, accessibility, and path-dependent observables

A subtle but important refinement concerns the distinction between reduced state and reduced experiment. Let ρ_{SE} denote the full microscopic state and

$$\rho_S = \text{Tr}_E(\rho_{SE})$$

the unconditional reduced density matrix. Coarse-graining ensures that transport histories which differ only at $O(\epsilon^2)$ but return to the same base point produce the same ρ_S . This equality is essential for locality and Markovian closure of the reduced dynamics.

However, physical observations are not determined by ρ_S alone. Any concrete measurement involves an *accessibility structure*: a specification of which modes, directions, or combinations of degrees of freedom are available to the observer. Operationally, this is encoded by a family of observables or projection operators Π acting on the exterior algebra. Observable quantities take the form

$$\langle O \rangle = \text{Tr}(\rho_S \Pi(O)).$$

The ledger variable u does not modify ρ_S as an energetic degree of freedom. Instead, it parametrizes the accessibility structure itself. Transport along admissible directions parallel-transports the observer's accessible subalgebra, and the noncommutativity of finite displacements induces a holonomy in this structure. After traversing a closed horizontal loop γ , the ledger changes by

$$\Delta u = \frac{1}{2} \oint_{\gamma} (x \, dy - y \, dx),$$

and the accessibility map is transformed accordingly,

$$\Pi \longrightarrow \Pi_{\gamma} = U(\Delta u)^{\dagger} \Pi U(\Delta u),$$

for an appropriate representation U of the central direction on the exterior mode algebra.

Thus, two histories that return to the same spacetime point can yield the same reduced density matrix ρ_S but act on observables through different accessibility maps. The reduced *experiment* is path-dependent even though the reduced *state* is not. There is therefore no inconsistency between coarse-graining and path-dependent observables. Coarse-graining erases microscopic ordering information from the state, enforcing $\rho_S^{(XY)} = \rho_S^{(YX)}$, but it does not erase the cumulative record of that loss. The ledger variable encodes precisely this residual information and determines how exterior observables are represented. Augmenting the reduced description from ρ_S to the pair (ρ_S, u) restores local closure and predictive power.

In particular, quantities such as observed luminosity depend on the overlap between the radiation field and the observer's accessible slice of mode space. Holonomy in the accessibility structure therefore leads to systematic luminosity

diminution without invoking absorption, scattering, or additional energy loss: the effect is geometric rather than consumptive. The ledger does not back-react on the microscopic dynamics, nor does it represent stored free energy. It records how irreversible coarse-graining constrains future access to the exterior degrees of freedom. In this sense, CC geometry is not an added dynamical assumption but the constitutive encoding of irreversible information loss. Closed loops return the observer to the same point in spacetime, but not to the same observational slice.

18.12 Uniqueness of the Lévy area and implications for the ledger

The Lévy example provides a canonical toy model of a path-dependent variable required to maintain Markovian closure. It is natural to ask to what extent this construction is unique. Could one introduce a different functional of the planar history—some other nontrivial record of past motion—while preserving Markovian closure and a diffusive scaling limit? Or is the Lévy area, in an appropriate sense, the only viable enlargement of the planar Brownian state space?

It is essential to distinguish two levels of description. The planar projection (x_t, y_t) of Brownian motion is already a Markov process. At this level, no additional variable is required. However, the (x, y) coordinates alone cannot support any nontrivial second-order functional of the past trajectory in a Markovian way. For example, the enclosed area

$$A_t = \frac{1}{2} \int_0^t (x_s dy_s - y_s dx_s) \quad (168)$$

cannot be written as a function of (x_t, y_t) alone, nor as a function of any finite window of recent increments. Retaining such information in a Markovian framework therefore necessitates an enlargement of the state space.

The smallest such enlargement is obtained by adjoining $u_t = A_t$ to (x_t, y_t) , yielding the Heisenberg Brownian motion (x_t, y_t, u_t) generated by the sub-Laplacian

$$\Delta_H = X^2 + Y^2, \quad (169)$$

with X and Y as in (154) (or their local equivalents in a general CC setting). The resulting process is Markovian, locally generated by a second-order differential operator, rotationally covariant, and diffusive under the natural Brownian scaling. No microscopic history is retained; the Lévy area serves exactly to restore local closure without reintroducing nonlocal memory.

The Lévy area may therefore be viewed as the unique nontrivial step-2 augmentation of planar Brownian motion satisfying four independent requirements:

1. **Markovian closure.** The enlarged process must remain Markovian with respect to its own filtration. No hidden history or nonlocal dependence is permitted.

2. **Diffusive scaling.** The enlarged dynamics must remain within the Brownian universality class. Higher-order iterated integrals that diverge, vanish, or rescale anomalously are excluded.
3. **Rotational covariance.** The augmentation must be compatible with the isotropy of planar Brownian motion. This criterion excludes all symmetric, direction-selective, or tensorially mismatched corrections.
4. **Local generation.** The augmented generator must remain a second-order operator built from first-order vector fields. This excludes nonlocal, memory-bearing, or higher-order rough-path structures.

These conditions strongly constrain the possible extensions of (x_t, y_t) . Under diffusive rescaling, any higher-order iterated integral beyond the antisymmetric second level either vanishes or produces a non-Markovian structure. Any scalar or symmetric correction reduces to a function of (x_t, y_t) . Up to deterministic renormalization or trivial coordinate changes, the Lévy area is the only nontrivial invariant that survives. Formally, the Lie algebra of Brownian increments closes at step 2, and the central coordinate provided by the Lévy area is the unique corresponding extension.⁸

This uniqueness result has a direct analogue in the cosmological ledger. The reduced exterior description seeks to preserve the Markov property while retaining certain path-dependent observables (such as accessibility holonomy or luminosity diminution) that do not close on spacetime coordinates alone. The Lévy area provides the canonical example: it is the minimal path-dependent coordinate required to restore Markovian closure. The Heisenberg ledger arises from the same mechanism in the CC setting: it is the unique minimal extension that preserves diffusive scaling, locality, and Markovianity while encoding the cumulative effect of noncommuting transport.

18.13 Emergence of Lévy Area from Directional Coarse Graining

We explain why the planar Lévy area arises *inevitably* once directional coarse graining is formulated at the correct algebraic level. The key observation is that transport-aligned erasure of information cannot be implemented within a commutative algebra. The minimal structure capable of encoding linear motion while retaining an oriented second-order memory is a Clifford algebra. In this setting, the Lévy area appears canonically as the even (second-order) residue of noncommuting infinitesimal motions.

Throughout this section we employ the informal term bubble to denote a finite, co-moving observation region centered at the particle's location. This language is not meant to introduce an additional dynamical degree of freedom, but rather to fix a perspective: observables are defined relative to a moving local

⁸See, for example, Lyons and Qian [45] for the rough-path perspective, or Stroock and Varadhan [67] for Markovian diffusion classification results.

frame, and information is discarded (coarse-grained) in a manner aligned with the instantaneous direction of transport. The “bubble” should be understood as a heuristic stand-in for any finite-resolution observer or horizon-coupled probe whose internal degrees of freedom are precisely those retained. All subsequent constructions are algebraic and probabilistic; no physical assumptions beyond standard planar Brownian motion are required. In particular, the bubble itself carries no dynamics and introduces no additional stochastic variables; it merely fixes the frame relative to which observables are transported and coarse-grained.

Operationally, “coarse graining” means only keeping information observables that an observer retains access to. The bubble merely makes this idea sharp: we keep only those observables that are functions on the interior of the bubble. The planar Lévy area answers the question of “what directional information is forgotten?”

18.13.1 Clifford–valued observables

Let $V \simeq \mathbb{R}^2$ denote the plane equipped with its Euclidean inner product, and let $\text{Cl}(V)$ be the associated real Clifford algebra. Thus $\text{Cl}(V)$ is generated by V subject to the relations

$$vw + wv = 2\langle v, w \rangle 1, \quad v, w \in V.$$

An observable is a $\text{Cl}(V)$ –valued field

$$F : \mathbb{R}^2 \longrightarrow \text{Cl}(V),$$

which we decompose according to the canonical \mathbb{Z}_2 –grading

$$\text{Cl}(V) = \text{Cl}^{\text{even}}(V) \oplus \text{Cl}^{\text{odd}}(V).$$

Accordingly,

$$F(x) = F^{\text{even}}(x) + F^{\text{odd}}(x),$$

where F^{even} takes values in $\text{span}\{1\} \oplus \Lambda^2 V$ and F^{odd} takes values in V .

If desired, the coefficient functions of F may be assumed smooth or holomorphic in a chosen complex coordinate on $\mathbb{R}^2 \simeq \mathbb{C}$. This analytic structure plays no role in the emergence of Lévy area and is entirely auxiliary.

18.13.2 Infinitesimal transport as Clifford multiplication

Transport by a small displacement $a \in V$ acts on observables by left multiplication with the corresponding Clifford element. To each increment $a \in V$ we associate the odd element

$$M(a) := a \in \text{Cl}^{\text{odd}}(V),$$

viewed as an infinitesimal generator of motion. This assignment is linear and rotation-equivariant, and satisfies

$$M(a)^2 = |a|^2 1.$$

At the infinitesimal level, transport updates the observable according to

$$F \longmapsto (1 + M(a)) F, \quad (170)$$

with any accompanying shift of the basepoint treated separately. No normalization or projection is introduced; the Clifford algebra records only the linearized bookkeeping of motion.

18.13.3 Order dependence and second-order structure

For two increments $a, b \in V$, the Clifford product decomposes as

$$M(a)M(b) = \langle a, b \rangle 1 + a \wedge b,$$

where $\langle a, b \rangle$ is the Euclidean inner product and $a \wedge b \in \Lambda^2 V \subset \text{Cl}^{\text{even}}(V)$ is the oriented bivector. Equivalently,

$$\frac{1}{2}\{M(a), M(b)\} = \langle a, b \rangle 1, \quad \frac{1}{2}[M(a), M(b)] = a \wedge b.$$

Thus the symmetric product records rotationally invariant information, while the antisymmetric product produces an oriented second-order element. This decomposition is forced entirely by the Clifford relations and does not depend on any choice of basis.

18.13.4 Discrete evolution and the Lévy area

Let $(B_t)_{t \geq 0}$ be planar Brownian motion, interpreted as the motion of the bubble center. Fix a partition $0 = t_0 < \dots < t_n = t$ and define increments

$$\Delta B_k := B_{t_{k+1}} - B_{t_k} \in V.$$

Transport-aligned evolution along the path is encoded algebraically by the ordered product

$$\prod_{k=0}^{n-1} (1 + M(\Delta B_k)),$$

understood as a step-2 expansion in the Clifford algebra. The antisymmetric second-order contribution arises from commutators of increments:

$$\sum_{k < \ell} \frac{1}{2} [M(\Delta B_\ell), M(\Delta B_k)] = \sum_{k < \ell} \Delta B_k \wedge \Delta B_\ell \in \Lambda^2 V.$$

The scalar coefficient of this bivector is precisely the discrete signed area enclosed by the path. In the continuum limit, this converges to the planar Lévy area

$$A_t = \int_0^t B_s \wedge dB_s,$$

understood as a Stratonovich integral taking values in $\Lambda^2 V$.

18.13.5 Coarse graining as endpoint projection (and centering)

The horizon-coupled coarse graining we have in mind is the operation that forgets all pathwise degrees of freedom not determined by the endpoint. Accordingly, for any square-integrable (possibly $\text{Cl}(V)$ -valued) functional X of the path up to time t we define the endpoint projection

$$\Pi_t(X) := \mathbb{E}[X \mid \sigma(B_t)], \quad (171)$$

i.e. the L^2 -orthogonal projection onto the subspace of $\sigma(B_t)$ -measurable variables.⁹

In applications one is typically interested not in the endpoint-visible part itself, but in the *coarse-graining defect*—the component of X that cannot be read off from B_t . We therefore also introduce the centered functional

$$X^\circ := X - \Pi_t(X), \quad (172)$$

which is characterized by $\mathbb{E}[X^\circ \mid B_t] = 0$.

18.13.6 Odd components and endpoint garbage

Let $V \simeq \mathbb{R}^2$ and $\text{Cl}(V)$ be the associated real Clifford algebra. We write $M(a) := a \in V \subset \text{Cl}^{\text{odd}}(V)$ for the odd Clifford representative of an increment $a \in V$. For a partition $0 = t_0 < \dots < t_n = t$ set $\Delta B_k := B_{t_{k+1}} - B_{t_k}$ and consider the step-2 transport word

$$\mathcal{T}_t^{(n)} := \prod_{k=0}^{n-1} (1 + M(\Delta B_k)). \quad (173)$$

The first-order (odd) term in the expansion of (173) is

$$\sum_{k=0}^{n-1} M(\Delta B_k) = M\left(\sum_{k=0}^{n-1} \Delta B_k\right) = M(B_t),$$

which is *completely determined by the endpoint*. In particular,

$$\Pi_t\left(\sum_{k=0}^{n-1} M(\Delta B_k)\right) = M(B_t), \quad \left(\sum_{k=0}^{n-1} M(\Delta B_k)\right)^\circ = 0. \quad (174)$$

Thus the leading odd contribution is *endpoint garbage*: it contains no coarse-graining defect beyond what is already visible in B_t .

Higher odd contributions in the step-2 truncation are absent by parity. At step > 2 one encounters odd iterated integrals (odd Wiener chaos), and the same principle applies: the endpoint projection Π_t extracts the $\sigma(B_t)$ -measurable component, and the centered remainder X° is the genuine coarse-graining residue.

⁹In the “bubble” model, the Brownian particle is carrying a finite disc, whose internal degrees of freedom are B_t -measurable because they depend on the basepoint. These internal degrees survive coarse graining, and are not “forgotten” under our scheme. Thus whether one includes the internal degrees of freedom of the bubble, it makes no difference to the traceout of directional degrees of freedom.

18.13.7 Even second-order residue and Lévy area

The first nontrivial coarse-graining residue appears at second order. Expanding (173) to second order yields

$$\sum_{0 \leq k < \ell \leq n-1} M(\Delta B_k) M(\Delta B_\ell) \in \text{Cl}^{\text{even}}(V).$$

Using the Clifford relation $ab + ba = 2\langle a, b \rangle 1$ for $a, b \in V$, we have the canonical decomposition

$$M(\Delta B_k) M(\Delta B_\ell) = \langle \Delta B_k, \Delta B_\ell \rangle 1 + \Delta B_k \wedge \Delta B_\ell, \quad \Delta B_k \wedge \Delta B_\ell \in \Lambda^2 V \subset \text{Cl}^{\text{even}}(V).$$

Summing over $k < \ell$ separates a symmetric scalar part from an antisymmetric bivector part:

$$\sum_{k < \ell} \langle \Delta B_k, \Delta B_\ell \rangle 1 + \sum_{k < \ell} \Delta B_k \wedge \Delta B_\ell.$$

The bivector sum is the discrete signed area enclosed by the path. In the continuum limit it converges (in the usual sense) to the Stratonovich Lévy area

$$A_t := \int_0^t B_s \wedge \text{od}B_s \in \Lambda^2 V. \quad (175)$$

Moreover, by symmetry of the Brownian bridge one has

$$\Pi_t(A_t) = \mathbb{E}[A_t \mid B_t] = 0, \quad (176)$$

so the Lévy area is already centered relative to the endpoint data: $A_t^\circ = A_t$. Thus the oriented even component is *pure coarse-graining residue*.

18.13.8 Small-Noise Coarse Graining and Quadratic Response

We now justify restricting to the quadratic term only. The basic idea is that the terms of higher degree in the increment dB constitute low-power “noise” which cannot be effectively measured.

We fix a filtered probability space $(\Omega, \mathcal{F}, (\mathcal{F}_t)_{t \geq 0}, \mathbb{P})$ carrying a planar Brownian motion B_t with white-noise increment dB_t . Let \mathcal{N} be a path functional (taking values in a finite-dimensional algebra, e.g. a Clifford algebra) and define the \mathcal{F}_t -measurable process

$$N_t = \mathcal{N}((dB_s)_{s < t}).$$

We consider the small-noise family obtained by scaling the driver,

$$N_t^\varepsilon := \mathcal{N}((\varepsilon dB_s)_{s < t}), \quad \varepsilon > 0.$$

Assume \mathcal{N} is regular enough for a stochastic Taylor (Dyson/Chen) expansion. Then, on any finite time interval,

$$N_t^\varepsilon = N_t^{(0)} + \varepsilon N_t^{(1)} + \varepsilon^2 N_t^{(2)} + R_t^{(3)}(\varepsilon), \quad (177)$$

with a remainder satisfying $\|R_t^{(3)}(\varepsilon)\|_{L^2} = O(\varepsilon^3)$. Here $N_t^{(k)}$ is the k th-order response, corresponding to the k -fold time-ordered iterated integral of the driving noise.

For the multiplicative (Stratonovich) stochastic exponential, $N_t^{(1)}$ is linear in the endpoint B_t , while $N_t^{(2)}$ contains a scalar (quadratic-variation) part and, in the planar case, an antisymmetric bivector part proportional to the Lévy area.

As above, define the endpoint-centering operator

$$P_t(X) := X^\circ = X - \mathbb{E}[X \mid B_t],$$

the L^2 -orthogonal projection onto the complement of $L^2(\sigma(B_t))$. We define the *coarse-grained observable*

$$\mathcal{C}_t^\varepsilon := P_t(N_t^\varepsilon).$$

Applying P_t to (177) yields

$$\mathcal{C}_t^\varepsilon = P_t(N_t^{(0)}) + \varepsilon P_t(N_t^{(1)}) + \varepsilon^2 P_t(N_t^{(2)}) + P_t(R_t^{(3)}(\varepsilon)). \quad (178)$$

Since P_t is a contraction in L^2 , the remainder remains $O_{L^2}(\varepsilon^3)$.

In the situations of interest, the linear response $N_t^{(1)}$ is $\sigma(B_t)$ -measurable (e.g. $N_t^{(1)} = M(B_t)$ in the Clifford model), hence

$$P_t(N_t^{(1)}) = 0.$$

Moreover, $N_t^{(0)}$ is deterministic, and so $P_t(N_t^{(0)}) = 0$. Consequently,

$$\mathcal{C}_t^\varepsilon = \varepsilon^2 P_t(N_t^{(2)}) + O_{L^2}(\varepsilon^3). \quad (179)$$

18.13.9 Quadratic coarse-grained limit

Dividing by ε^2 and letting $\varepsilon \rightarrow 0$,

$$\varepsilon^{-2} \mathcal{C}_t^\varepsilon \xrightarrow[\varepsilon \rightarrow 0]{L^2} P_t(N_t^{(2)}). \quad (180)$$

Thus the coarse graining “feels” only the quadratic response. In the planar Clifford setting, the centered even component of $N_t^{(2)}$ decomposes into

$$N_t^{(2)} = (\text{scalar renormalization}) + (\text{bivector term}).$$

The scalar renormalization is a quadratic variation term, which is B_t -measurable. Therefore

$$P_t(N_t^{(2)}) = (\text{bivector term}).$$

The bivector term is proportional to the Lévy area $A_t = \int_0^t B_s \wedge \circ dB_s$.

18.13.10 Interpretation

Equation (180) provides the analytic justification for the quadratic coarse graining: after removing the endpoint-measurable martingale component, the leading nontrivial contribution in the small-noise limit is quadratic, with higher chaos suppressed by an additional power of ε and controlled in L^2 . This realizes the coarse-grained observable as the quadratic approximation to the dB -driven flow, with Lévy area as the first noncommutative geometric residue.

18.14 Summary

We can now summarize the structural picture.

- Anisotropic tracing-out of degrees of freedom in an open quantum system produces degenerate (hypoelliptic) reduced dynamics whose scaling limit is governed by a Carnot-group tangent structure. In the minimal nontrivial case, this is the 2+1 Heisenberg group.
- Finite noncommutative effects, captured by commutators of admissible directions, survive coarse-graining because first-order ordering information is erased while second-order contributions accumulate. Promoting these commutators to central state variables is the minimal way to restore local, Markovian closure.
- The resulting ledger variables do not represent additional energy reservoirs. They encode the constitutive consequences of irreversible entropy export. Free energy pays for forgetting once; CC geometry is the kinematic expression of that forgetting.
- Equality of reduced states after different transport histories does not eliminate the need for a ledger. The distinction lies in which microscopic correlations were discarded; this distinction is invisible at the level of states but essential at the level of processes. It is naturally encoded in the tangent structure and in the accessibility of observables.
- The Lévy area provides a canonical and essentially unique example of a Markovian, path-dependent variable that restores closure for planar Brownian motion. The cosmological ledger is its geometric analogue in the CC setting.

In this sense, the Heisenberg group is not an arbitrary geometric choice but the universal relaxation state of anisotropic open-system transport, and the ledger variable is the minimal internal coordinate required for local closure under irreversible loss of microscopic order.

19 A Minimal Reaction–Diffusion Model for the Mesoscopic Scale σ

The preceding sections treat the mesoscopic scale σ as a locally defined control parameter governing the strength of step-2 (Heisenberg/ledger) kinematics in the reduced exterior dynamics. The purpose of this section is to supply a deliberately minimal *dynamical closure* for σ that is compatible with that interpretation. Specifically, the closure is constructed so that σ (i) relaxes toward an isotropic state in quiescent regions, (ii) admits *persistent local excursions* when the reduced dynamics develops sustained directional structure, and (iii) saturates rather than runs away when such excursions become large.

We emphasize at the outset what this toy model is *not*. It is not a microphysical model of star formation, feedback, or detailed baryonic transport. In particular, the role of gas in the present closure is intentionally modest: a fast auxiliary field Σ is included only to encode a locality constraint—reinforcement of σ is effective only where material is present to participate in irreversible processing—and to supply a rapidly adjusting weight (or “availability gate”) for that reinforcement. The qualitative behavior of interest in this section is therefore controlled primarily by the internal σ –dynamics (odd self–reinforcement, superlinear self–limitation, and spatial coherence), not by any sustained “gas pumping” mechanism.

Concretely, we work with a one–dimensional radial surrogate $x \equiv r$ and impose an explicit separation of timescales. The auxiliary field $\Sigma(x, t)$ evolves rapidly and smooths or redistributes on short times, whereas the mesoscopic field $\sigma(x, t)$ evolves slowly through an IMEX reaction–diffusion step. Reinforcement of σ has two components: an *odd self–reinforcement* proportional to σ itself (so that either sign may in principle be sustained), and an additional contribution driven by a time–smoothed local “activity” proxy $\bar{\Omega}$ (compression or divergence of the fast flux), included only to represent the idea that coherent nonequilibrium episodes can refresh directional memory. Large excursions are suppressed by an odd cubic squelch term and by diffusion, yielding finite–amplitude, spatially coherent σ profiles.

Finally, because the kinematic consequences of $\sigma(r)$ are especially sensitive to radial derivatives (through the circular–orbit condition in the step–2 Hamiltonian), we distinguish two notions of σ : the instantaneous field $\sigma(r, t)$, and a short–time average $\bar{\sigma}(r, t)$ used as a numerical proxy for the slow manifold. When we later translate $\bar{\sigma}(r, t)$ into an *effective* circular–speed curve $v_c(r)$ (with or without an additional central potential), this mapping should be read diagnostically. It isolates the profile–selection and gradient–sensitivity implied by the step–2 structure, rather than asserting that the toy Σ –dynamics itself is the dominant agent shaping galactic gas discs.

19.1 Thermodynamic status of the mesoscopic scale σ

The mesoscopic scale σ is neither a conserved quantity nor an extensive thermodynamic variable. It does not represent an orbital frequency, a local expansion rate, or a microscopic interaction scale. Rather, σ is an *intensive control variable* that parametrizes how strongly the reduced (open) dynamics retains directional structure under irreversible coarse-graining. Operationally, it controls the weight of step-2 (Heisenberg/ledger) contributions in the effective equations of motion.

In the absence of sustained nonequilibrium structure, σ relaxes toward zero. The state $\sigma = 0$ corresponds to an isotropic, weakly structured reduced dynamics in which directional memory is rapidly erased by phase mixing, orbit dephasing, scattering, and turbulence. In this regime the step-2 nilpotentization is negligible, and the reduced dynamics is effectively step-1 (commutative) at the coarse-grained level.

Nonzero values of σ arise only when irreversible processing becomes *directionally selective*. This occurs when the reduced state develops persistent directional excitation—misaligned shear, compressive structures, streaming, or other anisotropic patterns that survive coarse-graining for many steps without phase-aligning into a macroscopic circulation. In such situations, trace-out into inaccessible degrees of freedom is biased rather than isotropic, and the effective dynamics acquires a nontrivial step-2 character. The magnitude of σ therefore measures the degree to which directional memory is retained by the reduced system. In particular, large σ reflects the persistence of directional excitation that has not yet settled into an energetically efficient macroscopic order, rather than the presence of a stable coherent flow.

A convenient way to express this condition is in terms of competing timescales. Let t_{mix} denote the characteristic time over which mixing processes erase directional correlations, and let t_{coh} denote the time over which coherent structures maintain those correlations. Sustained excess $\sigma > 0$ requires

$$t_{\text{coh}} \gtrsim t_{\text{mix}},$$

so that anisotropic coarse-graining persists rather than being washed out by rapid decorrelation.

Crucially, reinforcement of σ is *self-referential* but not unbounded. Once σ becomes positive, the reduced dynamics becomes more strongly step-2 dominated: commutator (ledger) effects carry greater weight, and the same directionally-biased forcing becomes more effective at preserving directional memory. Small positive values of σ can therefore reinforce themselves. However, increasing σ also shortens characteristic turnover times, steepens gradients, and opens additional decorrelation channels. Collisionless phase mixing, orbit overlap, shocks, and turbulent cascades become easier to excite as σ grows, reducing t_{mix} and undermining the very directional correlations that sustain anisotropic trace-out.

When decorrelation dominates,

$$t_{\text{mix}} \ll t_{\text{coh}},$$

directional memory is destroyed faster than it can be replenished and σ relaxes back toward zero. Large values of σ are therefore intrinsically self-limiting, not because driving ceases, but because enhanced mixing provides an increasingly efficient relaxation channel. Beyond a finite amplitude, additional nonequilibrium forcing is dissipated primarily through rapid isotropization rather than by sustaining directional structure.

In this sense, σ behaves as a *nonequilibrium order parameter* with a single trivial equilibrium fixed point. It does not label distinct thermodynamic phases or a broken symmetry protected in the thermodynamic limit. Instead, it characterizes a metastable, dynamically maintained mesoscopic state whose amplitude is set by the balance between self-reinforcement of anisotropic coarse-graining and superlinear decorrelation at large excess.

This interpretation explains how large, spatially localized values of σ can arise and persist for long periods without implying a fundamental new scale or a departure from global stationarity. Nonzero σ reflects the temporary dominance of directionally selective irreversible processing in the reduced dynamics, while its eventual decay reflects the restoration of efficient mixing and isotropization.

19.2 What is being modeled, and why a self-limiting feedback is expected

Up to this point, the CC framework has treated the mesoscopic frequency scale σ as a local parameter entering the step-2 nilpotentization of the reduced dynamics, controlling the strength of commutator (ledger) effects. In the present section we promote σ to a slow, spatially varying field

$$\sigma = \sigma(x, t),$$

interpreted as a coarse-grained measure of *directional persistence* in irreversible trace-out. The goal is not to resolve the microphysics of nonequilibrium driving, but to encode the minimal balance structure required of any such mesoscopic control variable.

The central modeling assumption is that σ is a *state variable* of the reduced dynamics rather than a conserved quantity. It can grow or decay depending on how effectively directional correlations are refreshed relative to how quickly they are erased. The simplest generic expectation for such a variable is therefore a competition between two effects:

19.2.1 (a) Self-reinforcement of directional persistence at small amplitude.

When σ is small but positive, the reduced dynamics already privileges step-2 structure: commutator terms contribute nontrivially, and directional memory survives coarse-graining for longer intervals. In this regime, irreversible processing is *biased* rather than isotropic, and the same coherent forcing becomes more effective at sustaining directional correlations. As a result, small positive excursions of σ tend to reinforce themselves.

This reinforcement is not assumed to depend on a fixed external baseline. Instead, it is intrinsic: once anisotropic trace-out is present, it feeds on its own persistence. The feedback is therefore *odd* in σ : either sign may in principle be sustained, corresponding to opposite orientations of the effective step-2 structure.

19.2.2 (b) Accelerated decorrelation and isotropization at large amplitude.

The same departure that enables reinforcement also opens additional relaxation channels. As $|\sigma|$ increases, characteristic turnover and coherence times shorten, gradients steepen, and orbit families overlap more readily. Collisionless phase mixing, shocks, scattering, and turbulent cascades are easier to excite, and directional correlations are destroyed more rapidly. The effective mixing time therefore decreases with increasing $|\sigma|$.

This leads to diminishing returns: beyond a finite amplitude, additional nonequilibrium forcing no longer increases directional persistence, but is instead dissipated primarily through rapid isotropization. Large excursions of σ are thus intrinsically unstable and decay back toward the isotropic state.

These considerations motivate a minimal closure with the following qualitative features:

1. a single trivial fixed point $\sigma = 0$ in the absence of sustained directional structure,
2. linear (odd) self-reinforcement for small $|\sigma|$,
3. superlinear self-limitation at large $|\sigma|$,
4. spatial coupling to enforce coherence over finite domains.

The simplest realization is a reaction-diffusion equation with odd linear gain, odd superlinear squelching, and diffusive coupling.

19.2.3 Role of fast auxiliary fields.

In applications where baryons or other material components respond rapidly to the instantaneous kinematics, it is useful to include a fast auxiliary field $\Sigma(x, t)$. In the present model, Σ does not *drive* σ directly and does not act as a pump. Its role is purely modulatory: reinforcement of σ is effective only where material is present to participate in irreversible processing. Mathematically, this is encoded by a smooth gate function $F(\Sigma) \in [0, 1]$ multiplying the reinforcement terms.

Because Σ evolves on a much shorter timescale than σ , it adjusts rapidly to the instantaneous force balance implied by the current $\sigma(x, t)$. The slow evolution of σ then reflects a coarse-grained average over many such fast rearrangements. This separation of timescales is essential: it ensures that σ captures persistent mesoscopic structure rather than transient fluctuations induced by rapid transport.

19.2.4 Minimality of the closure.

The resulting reaction–diffusion model should be understood as a lowest–order phenomenological closure. It suppresses explicit dependence on the detailed sources of nonequilibrium activity and replaces them with a generic self–reinforcing term and a generic self–limiting term. Any more detailed model consistent with the CC interpretation would reduce to this structure near the isotropic state and would differ only in higher–order corrections or in the specific form of the saturation.

The purpose of the toy model is therefore not quantitative prediction, but to isolate the qualitative consequences of treating σ as a slow, self–reinforcing but self–limiting mesoscopic control variable with spatial coherence.

19.3 A minimal reaction–diffusion closure

We now specify a minimal dynamical closure for the mesoscopic field $\sigma(x, t)$ consistent with the qualitative structure outlined above. The closure is intended to capture only the balance between self–reinforcement of directional persistence, superlinear self–limitation through enhanced decorrelation, and spatial coherence. It is not meant to represent detailed microphysics.

The starting point is a reaction–diffusion equation with a single trivial fixed point $\sigma = 0$:

$$\partial_t \sigma = D_\sigma \nabla^2 \sigma + \varepsilon_{\text{slow}} \left[k_{\text{self}} F(\Sigma) \sigma + \lambda F(\Sigma) G(\bar{\Omega}) \bar{\Omega} - \frac{\sigma}{\tau} - b \sigma^3 \right]. \quad (181)$$

Here D_σ is a mesoscopic diffusivity enforcing spatial coherence, $\varepsilon_{\text{slow}} \ll 1$ enforces a separation of timescales between fast transport and slow mesoscopic relaxation, and the remaining terms encode reinforcement and saturation.

19.3.1 Odd self–reinforcement.

The term $k_{\text{self}} F(\Sigma) \sigma$ represents intrinsic self–reinforcement of directional persistence. It is *odd* in σ , allowing either sign to be sustained, and vanishes where material is absent. Physically, it encodes the statement that once anisotropic trace–out is present, the reduced dynamics becomes more effective at maintaining it.

19.3.2 Activity–driven refresh.

The term proportional to $\bar{\Omega}$ represents episodic reinforcement associated with coherent nonequilibrium activity. Here $\Omega := -\nabla \cdot (\Sigma u)$ is a signed local compression/divergence proxy constructed from the fast transport field, and $\bar{\Omega}$ denotes a short–time exponential average used to suppress high–frequency noise. The factor $G(\bar{\Omega}) \in [0, 1]$ is an even threshold function that suppresses spurious reinforcement from small fluctuations. Importantly, this term does not act as a sustained pump: it refreshes σ only when coherent activity persists over multiple fast timescales.

19.3.3 Linear relaxation and superlinear squelching.

The term $-\sigma/\tau$ represents passive isotropization in the absence of reinforcement, while the odd cubic term $-b\sigma^3$ implements diminishing returns at large amplitude. As $|\sigma|$ grows, decorrelation channels open rapidly and dominate the balance, ensuring that the mesoscopic state saturates at finite amplitude rather than running away.

19.3.4 Spatial coupling.

The diffusion term $D_\sigma \nabla^2 \sigma$ enforces coherence of the mesoscopic state over finite domains. In regions where reinforcement is weak or absent, it causes σ to relax smoothly back toward the isotropic state $\sigma = 0$ rather than fluctuating pointwise.

19.3.5 Gas as a fast auxiliary field.

The auxiliary field $\Sigma(x, t)$ enters only through the smooth gate

$$F(\Sigma) = \frac{\Sigma}{\Sigma + \Sigma_c}, \quad (182)$$

which restricts reinforcement to regions where material is present. The gas itself evolves rapidly according to

$$\partial_t \Sigma = D_{\text{gas}} \nabla^2 \Sigma - \nabla \cdot (\Sigma u), \quad (183)$$

$$u = \chi (-\nabla \sigma)_+, \quad (184)$$

with an outward drift induced by negative σ -gradients. This coupling allows the fast field to respond quickly to the instantaneous mesoscopic geometry while leaving the slow evolution of σ governed by coarse-grained balance rather than by sustained pumping.

19.3.6 Well-mixed limit.

In a spatially homogeneous region with $\Sigma > 0$ and negligible diffusion, (181) reduces to

$$\partial_t \sigma = \varepsilon_{\text{slow}} \left(k_{\text{self}} \sigma - \frac{\sigma}{\tau} - b \sigma^3 \right),$$

which admits a trivial fixed point $\sigma = 0$ and, when $k_{\text{self}} > 1/\tau$, a pair of finite-amplitude stable states

$$\sigma_* = \pm \sqrt{\frac{k_{\text{self}} - 1/\tau}{b}}.$$

These correspond to metastable mesoscopic configurations with sustained directional persistence, bounded by superlinear self-limitation.

19.3.7 Interpretation.

Equation (181) should be read as a statement about *mesoscopic distance from isotropy*. Nonzero σ signals a reduced state in which irreversible processing is directionally biased and step-2 structure dominates the effective kinematics. The closure isolates the minimal dynamical structure required for such a state to exist: intrinsic self-reinforcement, saturation by enhanced mixing, and spatial coherence.

19.4 Radial variation of the mesoscopic scale and kinematic admissibility

We now consider the consequences of allowing the mesoscopic control variable σ to vary radially. Throughout this subsection we work in a one-dimensional surrogate geometry $r \equiv x$, interpret $\sigma(r, t)$ as slowly varying, and use the circular-orbit condition of the step-2 Hamiltonian as a diagnostic mapping from $\sigma(r)$ to an effective tangential velocity profile.

19.4.1 Circular orbits as an admissibility condition.

For stationary circular motion one imposes

$$\dot{r} = -\partial_r H = 0, \quad (185)$$

which determines the admissible angular-momentum branch $L(r)$. The tangential velocity is then

$$v(r) = r \dot{\theta} = r \frac{\partial H}{\partial L} = \frac{L(r)}{r} + r \sigma(r). \quad (186)$$

In the special case $V \equiv 0$ and on the branch where L is constant along the orbit, the circularity condition yields the closed form

$$v(r) = r(\sigma(r) + r\sigma'(r)), \quad (187)$$

which we use here as a diagnostic projection from $\sigma(r)$ to an effective rotation curve.

Equation (187) makes explicit that the kinematics is sensitive not only to the amplitude of σ , but crucially to its radial gradient. Constant σ produces linear growth $v \propto r$, while abrupt spatial variation directly modifies the admissible angular-momentum branch.

19.4.2 Gradient-induced squelching.

Define

$$A(r) := L + r^2 \sigma(r). \quad (188)$$

The radial force balance implicit in (185) contains the term

$$\partial_r H \supset A(r) \sigma'(r). \quad (189)$$

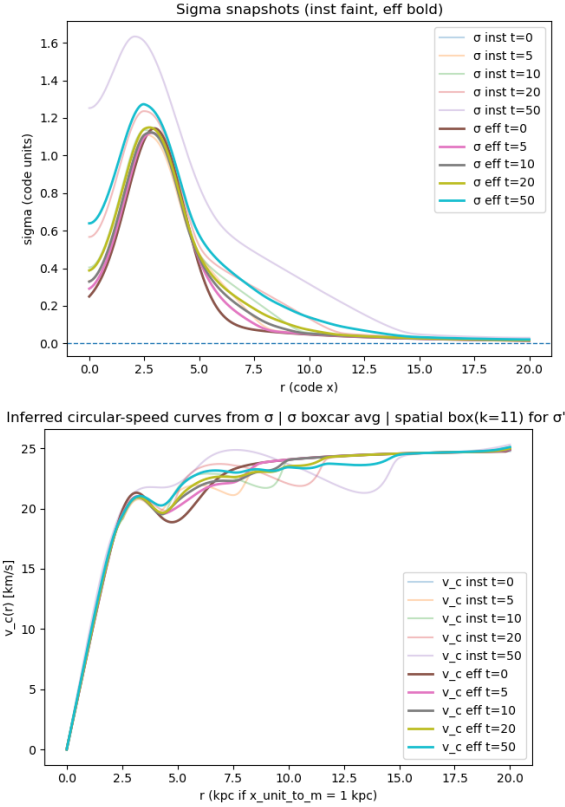


Figure 5: Toy two-field experiment in a one-dimensional radial surrogate. Left: evolution of the temporally averaged mesoscopic field $\bar{\sigma}(r, t)$ under the fast- Σ , slow- σ reaction-diffusion closure. Right: corresponding effective circular-speed profiles $v_c(r, t)$ computed from $\bar{\sigma}(r, t)$ using the step-2 circular-orbit condition. The mapping from σ to v_c is diagnostic and isolates the sensitivity to radial gradients rather than asserting a literal gravitational interpretation.

A large negative gradient $\sigma'(r) < 0$ therefore contributes a strong radial force that must be compensated by a reduction in $A(r)$. Since the tangential velocity satisfies $v(r) = A(r)/r$, steep gradients in $\sigma(r)$ necessarily *squelch* the attainable circular speed, even when $\sigma(r)$ itself is large.

This establishes a structural constraint on admissible mesoscopic profiles: high- σ regions cannot terminate abruptly. Sharp “walls” in $\sigma(r)$ destroy circular support and are dynamically excluded. Only profiles in which $\sigma(r)$ decreases sufficiently slowly can sustain large tangential velocities over extended radial ranges.

19.4.3 Profile selection rather than transport.

In the present model, this squelching mechanism acts as a *profile selector* rather than as a transport driver. The fast field $\Sigma(r, t)$ responds rapidly to the instantaneous kinematic admissibility implied by $\sigma(r)$, but it does not set the mesoscopic profile. Instead, the slow reaction-diffusion dynamics of σ evolves toward configurations whose gradients are kinematically admissible.

Regions in which $\sigma(r)$ develops overly steep gradients are unstable: they fail to support circular motion and are therefore rapidly smoothed, either by diffusion of σ itself or by the suppression of reinforcement in those regions. Over long times, the system preferentially selects smooth, slowly varying $\sigma(r)$ profiles that avoid strong gradient-induced squelching.

19.4.4 Fast response and slow geometry.

Because Σ evolves on a much shorter timescale than σ , any redistribution of material occurs *before* the mesoscopic geometry can respond appreciably. The slow evolution of $\sigma(r, t)$ therefore reflects a coarse-grained average over many fast adjustments of the auxiliary field. Temporal averaging of σ over short windows projects onto this slow manifold and suppresses transient fluctuations induced by rapid rearrangement.

Rotation curves computed from the averaged field $\bar{\sigma}(r, t)$ thus probe the persistent mesoscopic geometry rather than momentary departures from admissibility. In this sense, the mapping from $\sigma(r)$ to $v_c(r)$ should be read as a statement about long-lived kinematic structure, not as a model of instantaneous baryonic motion.

19.4.5 Interpretation.

Figure 5 illustrates three generic consequences of the step-2 kinematics:

1. uniform σ produces linearly rising tangential support,
2. steep radial gradients in $\sigma(r)$ suppress admissible circular speed,
3. sustained high velocities require extended regions of slowly varying $\sigma(r)$.

These features are independent of the detailed evolution of the fast auxiliary field and follow directly from the structure of the reduced Hamiltonian. They motivate treating observed rotation curves as constraints on the *radial admissibility* of mesoscopic profiles rather than as direct tracers of local mass distribution.

In this framework, the dominant dynamical role of the radial coupling is not to pump gas outward, but to exclude mesoscopic configurations whose gradients would destroy circular support. The emergent profiles are therefore selected by a balance between self-reinforcement, superlinear squelching, diffusion, and kinematic admissibility.

19.5 Fast response, slow mesoscopic relaxation, and hysteresis

A central qualitative feature of the closure (181) is the explicit separation of timescales between the auxiliary field Σ and the mesoscopic control variable σ . The gas responds rapidly to the instantaneous kinematic admissibility implied by the current mesoscopic geometry, while σ evolves only through slow, coarse-grained irreversible processes. This ordering of timescales has important dynamical consequences, the most significant of which is hysteresis.

19.5.1 Geometry first, response second.

In the present framework, changes in $\sigma(r)$ precede and constrain the baryonic response rather than being driven by it. When σ enters a high-amplitude configuration, steep radial gradients may temporarily render certain circular orbits inadmissible. The fast field Σ responds immediately to this change in admissibility, redistributing on orbital, sound-crossing, or shock-dissipation timescales. Crucially, this redistribution does not itself set the value of σ ; it merely reflects the instantaneous geometry.

19.5.2 Slow relaxation of the mesoscopic state.

The subsequent evolution of σ is governed by the balance between self-reinforcement, superlinear squelching, and diffusion. Even after the fast field has adjusted and local gradients have softened, the mesoscopic geometry does not immediately relax. Because σ encodes directional persistence in irreversible trace-out, it can decay only through enhanced mixing and isotropization, processes that act on timescales long compared to baryonic redistribution. The mesoscopic state therefore retains memory of past nonequilibrium episodes long after the auxiliary field has reconfigured.

19.5.3 Origin of hysteresis.

This mismatch of timescales implies that entry into and exit from a high- σ state occur under different conditions. To enter such a state, directional persistence must be reinforced strongly enough to overcome rapid baryonic adjustment and

gradient squelching. Once established, however, the same state can persist even after the fast field has redistributed, because the decay of σ is limited by slow isotropization rather than by instantaneous force balance. The system therefore exhibits hysteresis: the threshold for establishing excess σ is higher than the threshold for maintaining it.

19.5.4 No permanent expulsion or catastrophic loss.

Because the fast response of Σ is driven by kinematic admissibility rather than by energetic blowout, redistribution of material does not imply permanent loss. Gas is displaced only insofar as local circular support is temporarily disallowed; when gradients soften and admissibility is restored, material can re-circularize through dissipation and mixing. The outer reservoir acts as a dynamically active buffer rather than as a one-way sink.

19.5.5 Persistence of kinematic structure.

The observable implication is that large-scale kinematic features are controlled primarily by the slow mesoscopic geometry rather than by the instantaneous distribution of baryons. Substantial rearrangement of Σ can occur without large or rapid changes in the effective rotation curve inferred from σ . Conversely, long-lived kinematic states can persist even as the auxiliary field undergoes repeated and rapid adjustment.

19.5.6 Interpretation.

Hysteresis in this framework is therefore not a consequence of delayed feedback or reservoir depletion, but a direct reflection of the slow relaxation of the mesoscopic control variable. The reduced dynamics remembers past episodes of directionally selective irreversible processing even after the fast degrees of freedom have equilibrated locally. This separation between fast response and slow geometric relaxation is a generic feature of the CC interpretation and does not rely on detailed assumptions about star formation, feedback, or accretion.

19.6 Observational diagnostics and falsifiability

The reaction-diffusion closure for the mesoscopic scale σ is not intended as a complete dynamical model of galactic structure. Its purpose is narrower: to identify the kinematic and geometric consequences of allowing a slow, self-reinforcing but self-limiting mesoscopic control variable to vary spatially. The value of the model therefore lies not in detailed predictions of baryonic morphology, but in the constraints it imposes on admissible kinematic profiles. These constraints are directly testable.

19.6.1 Rotation curves as geometric constraints.

In this framework, observed rotation curves do not directly trace local mass density or transport efficiency. Instead, they constrain the *radial admissibility* of the mesoscopic field $\sigma(r)$. Equation (187) shows that the effective circular speed depends not only on the magnitude of σ , but crucially on its radial gradient. Extended regions of approximately flat or slowly rising rotation curves require $\sigma(r)$ profiles that are both nonzero and slowly varying over large radial intervals.

Conversely, sharp features in $\sigma(r)$ would generically suppress circular support through gradient-induced squelching and are therefore excluded by the existence of long-lived circular orbits. Observed smoothness of rotation curves thus constrains not only the amplitude of the mesoscopic scale but also its spatial regularity.

19.6.2 Insensitivity to instantaneous baryonic rearrangement.

Because the auxiliary field Σ responds rapidly to changes in admissibility while σ evolves slowly, the model predicts that effective rotation curves should be relatively insensitive to short-timescale baryonic rearrangement. Events that substantially redistribute gas—such as bars, spiral shocks, or localized feedback episodes—need not produce immediate or dramatic changes in the inferred kinematic support, provided they do not alter the slow mesoscopic geometry.

This distinguishes the present framework from models in which kinematics is tied directly to the instantaneous mass distribution. Observationally, it suggests that galaxies with markedly different gas morphologies may nevertheless share similar rotation curves if their mesoscopic geometry is comparable.

19.6.3 Persistence and memory effects.

A direct consequence of slow mesoscopic relaxation is kinematic memory. Rotation curves inferred from $\bar{\sigma}(r, t)$ can remain stable over times long compared to gas redistribution or star-formation timescales. The model therefore predicts hysteresis: the conditions required to establish a given kinematic state need not coincide with the conditions required to maintain it.

This can be tested by comparing systems undergoing recent or ongoing baryonic disturbances to dynamically quiescent systems with similar kinematic profiles. Persistence of rotation curves in the former case supports the interpretation of σ as a slow geometric control variable rather than as a proxy for instantaneous baryonic forcing.

19.6.4 Radial coherence and profile selection.

Because steep gradients in $\sigma(r)$ suppress admissible circular motion, the model predicts a preference for smooth, extended mesoscopic profiles. Galaxies exhibiting long radial ranges of flat or gently rising rotation curves must therefore correspond to configurations in which the effective mesoscopic geometry varies only weakly with radius. Strongly truncated or sharply featured rotation curves

would signal either breakdown of the step-2 description or the dominance of additional potentials not included in the toy model.

19.6.5 Null predictions and exclusions.

Equally important are the model’s null predictions. Because gas acts only as a fast responder and gate, the framework does *not* predict:

- a one-to-one correspondence between gas surface density and rotation speed,
- systematic outward pumping or permanent evacuation of baryons,
- rapid kinematic response to short-lived feedback events,
- universal coupling between star-formation rate and rotation-curve shape.

Observation of strong, systematic correlations of these types would therefore count against the present interpretation.

19.6.6 Scope of applicability.

Finally, it bears emphasis that the diagnostic mapping from $\sigma(r)$ to $v_c(r)$ isolates only the step-2 contribution to kinematic support. Additional gravitational potentials, pressure support, and relativistic effects can be incorporated additively and may dominate in some regimes. The model is falsified not by the existence of such effects, but by the failure of the admissibility logic itself: if long-lived circular orbits are observed in situations where no smooth $\sigma(r)$ profile can satisfy the kinematic constraints, the mesoscopic interpretation must be rejected.

In this sense, the reaction-diffusion model for σ is falsifiable not by detailed fits, but by its geometric consistency with observed kinematic structure.

20 Baryon acoustic oscillations, redshift and polarization

20.1 What BAO Observations Measure

Baryon acoustic oscillation (BAO) measurements provide one of the most robust and geometrically clean probes of large-scale structure. However, the quantities directly extracted from BAO data are often conflated with model-dependent distance measures. To avoid ambiguity, we begin by stating precisely what is observed, what is inferred, and where physical assumptions enter.

20.1.1 Direct observables

BAO analyses identify a preferred separation scale in the two-point correlation function of galaxies (or related tracers). This feature is observed in two independent directions:

- *Transverse to the line of sight*, as an angular separation

$$\theta_{\text{BAO}}(z), \quad (190)$$

measured at an effective redshift z .

- *Along the line of sight*, as a redshift separation

$$\Delta z_{\text{BAO}}(z). \quad (191)$$

These quantities are directly measurable from survey data. No assumption about cosmological expansion, metric form, or distance–redshift relation is required at this stage. Importantly, BAO observations do *not* directly measure physical or comoving lengths.

20.1.2 Inferred distance measures

To interpret $\theta_{\text{BAO}}(z)$ and $\Delta z_{\text{BAO}}(z)$ as spatial separations, one introduces effective distance measures. Conventionally, these are written as

$$D_M(z) \equiv \text{transverse distance}, \quad (192)$$

$$D_H(z) \equiv \frac{c}{H(z)} \quad (\text{radial distance scale}). \quad (193)$$

Given a choice of redshift–distance mapping, one defines inferred BAO lengths

$$L_{\perp}(z) = D_M(z) \theta_{\text{BAO}}(z), \quad (194)$$

$$L_{\parallel}(z) = D_H(z) \Delta z_{\text{BAO}}(z). \quad (195)$$

These inferred quantities are *not observables*. They depend explicitly on how redshift is related to spatial separation. Different cosmological frameworks correspond to different choices of $D_M(z)$ and $D_H(z)$.

20.1.3 Observational content versus interpretation

The key point is that BAO data constrain the dimensionless combinations

$$\theta_{\text{BAO}}(z), \quad \Delta z_{\text{BAO}}(z), \quad (196)$$

and their statistical consistency across redshift. Any statement about a “standard ruler”—whether comoving or physical—is an interpretive step that depends on the assumed mapping between redshift and distance.

In standard cosmological analyses, the BAO feature is interpreted as a *fixed comoving length* transported by cosmic expansion. In the present work, we will instead ask a more general question:

Under what conditions can the observed BAO feature be interpreted as a *fixed physical separation at the time of emission*, independent of redshift?

Answering this question requires no modification of the observational inputs, only a careful examination of the redshift–distance relation implicit in the interpretation. The remainder of this paper is devoted to formulating those conditions precisely and exhibiting a concrete realization in which they are satisfied.

20.2 Condition for a Constant Physical BAO Ruler

We now state precisely the conditions under which the observed BAO feature may be interpreted as a *fixed physical separation at the time of emission*, independent of redshift. The result is purely kinematical and does not assume any specific cosmological model.

20.2.1 Physical interpretation of BAO observables

Given the observables $\theta_{\text{BAO}}(z)$ and $\Delta z_{\text{BAO}}(z)$ defined in Section 20.1, a physical interpretation requires introducing effective transverse and radial distance measures $D_M(z)$ and $D_H(z)$. These define inferred physical separations

$$L_{\perp}(z) = D_M(z) \theta_{\text{BAO}}(z), \quad (197)$$

$$L_{\parallel}(z) = D_H(z) \Delta z_{\text{BAO}}(z). \quad (198)$$

A necessary condition for a physically meaningful ruler is that the transverse and radial inferences agree,

$$L_{\perp}(z) = L_{\parallel}(z), \quad (199)$$

reflecting the isotropy of the underlying BAO feature.

20.2.2 Constant physical ruler condition

We say that the BAO feature corresponds to a *constant physical ruler* if there exists a length scale L_{BAO} such that

$$L_{\perp}(z) = L_{\parallel}(z) = L_{\text{BAO}} \quad \text{for all observed } z. \quad (200)$$

Equivalently, the redshift dependence of the observables must satisfy

$$D_M(z) \theta_{\text{BAO}}(z) = L_{\text{BAO}}, \quad (201)$$

$$D_H(z) \Delta z_{\text{BAO}}(z) = L_{\text{BAO}}. \quad (202)$$

These relations impose constraints on the admissible redshift–distance mapping, but do not uniquely determine it. In particular, they do not require that $D_M(z)$ or $D_H(z)$ arise from cosmological expansion.

20.2.3 Equivalent formulation

Combining Eqs. (201) and (202), the constant physical ruler condition may be written as

$$\frac{D_M(z)}{D_H(z)} = \frac{\Delta z_{\text{BAO}}(z)}{\theta_{\text{BAO}}(z)}. \quad (203)$$

The right-hand side is entirely observational. Thus, BAO data constrain the *ratio* of transverse to radial distance measures, independently of any assumption about the absolute normalization of distances.

20.2.4 Interpretive freedom

Equation (203) highlights the essential freedom in interpreting BAO observations. Any redshift-distance mapping that satisfies this relation admits an interpretation of the BAO feature as a fixed physical separation. The standard comoving interpretation corresponds to one particular solution, but it is not unique.

The role of the theoretical framework is therefore not to modify the BAO observables, but to supply a physically motivated mapping $z \mapsto (D_M, D_H)$ that satisfies the above condition. In subsequent sections, we will show that this can be achieved without invoking global cosmic expansion, while remaining fully consistent with existing BAO measurements.

20.2.5 A differential consistency relation

The two algebraic conditions (201)–(202) imply a useful *differential* relation between the observables $\theta_{\text{BAO}}(z)$ and $\Delta z_{\text{BAO}}(z)$. This relation is the integrability condition for the existence of a single distance mapping compatible with a constant physical ruler.

Assume the BAO feature corresponds to a fixed physical separation L_{BAO} at emission, so that

$$L_{\text{BAO}} = D_M(z) \theta_{\text{BAO}}(z), \quad L_{\text{BAO}} = D_H(z) \Delta z_{\text{BAO}}(z), \quad (204)$$

where $D_H(z)$ is the radial distance scale converting redshift intervals into radial physical separations.

Define the (model-dependent) radial distance coordinate $r(z)$ by

$$\frac{dr}{dz} = D_H(z). \quad (205)$$

(Equivalently, D_H is the Jacobian of the redshift-distance map.) If we identify $D_M(z) = r(z)$ for the transverse physical distance at emission, then the transverse relation in (204) becomes

$$\frac{1}{\theta_{\text{BAO}}(z)} = \frac{r(z)}{L_{\text{BAO}}}. \quad (206)$$

Differentiating (206) with respect to z gives

$$\frac{d}{dz} \left(\frac{1}{\theta_{\text{BAO}}(z)} \right) = \frac{1}{L_{\text{BAO}}} \frac{dr}{dz} = \frac{D_H(z)}{L_{\text{BAO}}}. \quad (207)$$

Using the radial relation $L_{\text{BAO}} = D_H(z) \Delta z_{\text{BAO}}(z)$ in (207), we obtain the differential consistency condition

$$\boxed{\frac{d}{dz} \left(\frac{1}{\theta_{\text{BAO}}(z)} \right) = \frac{1}{\Delta z_{\text{BAO}}(z)}} \quad (208)$$

20.2.6 Differential condition for a constant comoving BAO ruler

For comparison, we briefly record the differential condition implied by the standard interpretation of the BAO feature as a *constant comoving* separation.

Let $a(z)$ denote the scale factor normalized so that $a(0) = 1$, and let $r(z)$ be the comoving radial coordinate. If the BAO scale corresponds to a fixed comoving length r_{BAO} , then

$$r_{\text{BAO}} = r(z) \theta_{\text{BAO}}(z), \quad r_{\text{BAO}} = \frac{dr}{dz} \Delta z_{\text{BAO}}(z). \quad (209)$$

Proceeding as before, the transverse relation implies

$$\frac{1}{\theta_{\text{BAO}}(z)} = \frac{r(z)}{r_{\text{BAO}}}. \quad (210)$$

Differentiating with respect to z yields

$$\frac{d}{dz} \left(\frac{1}{\theta_{\text{BAO}}(z)} \right) = \frac{1}{r_{\text{BAO}}} \frac{dr}{dz}. \quad (211)$$

Using the radial relation in (209), we obtain

$$\boxed{\frac{d}{dz} \left(\frac{1}{\theta_{\text{BAO}}(z)} \right) = \frac{1}{r_{\text{BAO}}} \frac{r_{\text{BAO}}}{\Delta z_{\text{BAO}}(z)} = \frac{1}{\Delta z_{\text{BAO}}(z)} \frac{dr}{dz}} \quad (212)$$

In a standard expanding cosmology, $dr/dz = c/H(z)$, so the comoving-ruler condition takes the explicit form

$$\frac{d}{dz} \left(\frac{1}{\theta_{\text{BAO}}(z)} \right) = \frac{c}{H(z) \Delta z_{\text{BAO}}(z)}. \quad (213)$$

Contrast with the physical ruler condition. Equations (208) and (213) represent *distinct functional constraints* on the BAO observables. They coincide only if $H(z)$ is constant, which is not the case in standard cosmological models. Thus, the constant physical and constant comoving interpretations are observationally distinguishable in principle.

20.3 Non-uniqueness of the Redshift–Distance Mapping

The consistency condition derived in Section 20.2 constrains the relationship between transverse and radial distance measures, but does not uniquely determine their functional form. In this section we make explicit the limited extent to which BAO observations fix the underlying redshift–distance mapping.

20.3.1 What BAO measurements determine

From Eq. (203), BAO observations constrain the ratio

$$\frac{D_M(z)}{D_H(z)} = \frac{\Delta z_{\text{BAO}}(z)}{\theta_{\text{BAO}}(z)}, \quad (214)$$

which is directly inferred from data. Crucially, this constraint involves only relative scaling between transverse and radial distances. The absolute normalization of either distance measure remains unconstrained by BAO data alone.

As a result, BAO observations do not by themselves fix:

- the functional dependence of distance on redshift,
- the interpretation of redshift as a measure of expansion,
- or the physical mechanism responsible for redshift accumulation.

Additional assumptions are required to promote the inferred distances to a fully specified cosmological geometry.

20.3.2 Standard cosmological interpretation

In the standard FLRW framework, redshift is attributed to cosmic expansion, and the distance measures $D_M(z)$ and $D_H(z)$ are derived from a metric with a time-dependent scale factor. Within this framework, the BAO feature is interpreted as a fixed *comoving* length, and the constancy of $L_{\perp}(z)$ and $L_{\parallel}(z)$ follows by construction.

This interpretation provides a consistent and successful fit to a wide range of cosmological data. However, from the perspective of BAO observations alone, it represents one admissible solution rather than a uniquely selected one.

20.3.3 Generalized kinematical interpretation

The analysis above shows that BAO data are equally compatible with more general redshift–distance mappings, provided they satisfy the consistency condition of Section 20.2. In particular, nothing in the BAO observables requires that redshift be generated by a uniform stretching of spatial distances.

More generally, one may regard redshift as a cumulative kinematical variable associated with photon propagation, encoding the integrated effect of interactions between radiation and large-scale geometric or infrared degrees of freedom. From this viewpoint, the functions $D_M(z)$ and $D_H(z)$ are emergent constructs derived from the redshift mapping, rather than primary geometric inputs.

20.3.4 Implications for physical interpretation

The essential implication is that the interpretation of the BAO feature as a constant physical ruler is not tied to any specific global expansion history. What matters is the existence of a redshift–distance mapping that:

1. respects the observed transverse and radial BAO scalings,
2. preserves isotropy of the inferred physical separation,
3. and maintains consistency across redshift.

In the following section, we will construct an explicit realization of such a mapping, in which redshift arises from a stochastic accumulation process along null trajectories. This construction will satisfy the BAO consistency condition derived above, while differing fundamentally from the standard expansion-based interpretation.

20.4 Redshift as a Stochastic Accumulation Process

We now present an explicit realization of a redshift–distance mapping that satisfies the constant physical BAO condition derived in Section 20.2, without invoking global metric expansion. The construction treats redshift as a cumulative process along null trajectories, rather than as a kinematic consequence of an evolving scale factor.

20.4.1 Ledger coordinate and redshift accumulation

Consider a photon propagating along a null trajectory parameterized by a monotonically increasing *ledger coordinate* ℓ . The ledger coordinate is not directly observable; it encodes the cumulative interaction of the photon with unresolved infrared geometric degrees of freedom along its path.

We define the redshift variable

$$u \equiv \ln(1+z), \quad (215)$$

and model its evolution along the trajectory as an accumulation process

$$\frac{du}{d\ell} = \lambda(\ell), \quad (216)$$

where $\lambda(\ell)$ is a nonnegative *hazard rate*. In general, $\lambda(\ell)$ may vary along the path and may include stochastic contributions; its detailed microphysical origin is not required for the present analysis.

Integrating Eq. (216) yields

$$u(\ell) = u_0 + \int_0^\ell \lambda(\ell') d\ell', \quad (217)$$

which defines a monotonic mapping between the ledger coordinate and the observed redshift.

20.4.2 Distance measures induced by the ledger

Given the mapping $\ell \mapsto z$, effective distance measures may be defined kinematically. For transverse separations, the physical distance at the time of emission is proportional to the ledger separation,

$$D_M(z) \propto \ell(z), \quad (218)$$

up to an overall normalization.

Radial separations are determined by the local sensitivity of redshift to ledger distance. From Eq. (216),

$$D_H(z) \equiv \left(\frac{du}{d\ell} \right)^{-1} = \lambda(\ell(z))^{-1}, \quad (219)$$

again up to normalization.

These definitions supply the redshift–distance mapping required to interpret BAO observables, without reference to metric expansion.

20.4.3 Satisfaction of the BAO consistency condition

Substituting the induced distance measures into the BAO consistency condition (203), we obtain

$$\frac{D_M(z)}{D_H(z)} \propto \ell(z) \lambda(\ell(z)). \quad (220)$$

Thus, the requirement that the BAO feature correspond to a constant physical separation reduces to a constraint on the functional form of the hazard rate $\lambda(\ell)$. In particular, any hazard profile for which the product $\ell \lambda(\ell)$ reproduces the observed ratio $\Delta z_{\text{BAO}}(z)/\theta_{\text{BAO}}(z)$ yields a constant physical BAO ruler.

Importantly, this condition places no restriction on the global interpretation of redshift as expansion. The BAO observables constrain only the accumulated redshift structure along null trajectories.

20.4.4 Interpretive consequences

In this framework, redshift is an emergent, path-dependent quantity rather than a direct measure of global geometric dilation. Distance measures arise as derived constructs from the redshift accumulation process, and the constancy of the BAO scale reflects a balance between transverse and radial ledger sensitivities.

This realization provides a concrete counterexample to the claim that BAO observations uniquely require an expanding metric interpretation. In the next section, we will examine how this construction interfaces with standard observational calibrations and large-scale isotropy.

20.5 Observational Calibration and Consistency

The redshift–distance mapping constructed in Section 20.4 is designed to reproduce the observed BAO scalings while allowing redshift to arise from a non-expansion-based mechanism. In this section we examine its consistency with key observational requirements and clarify the role of calibration.

20.5.1 Transverse–radial consistency and isotropy

BAO measurements provide independent transverse and radial determinations of the preferred separation scale. As emphasized in Section 20.2, consistency requires that these inferences agree,

$$L_{\perp}(z) = L_{\parallel}(z). \quad (221)$$

In the present framework, this condition is enforced by construction through the constraint on the induced distance measures

$$\frac{D_M(z)}{D_H(z)} = \frac{\Delta z_{\text{BAO}}(z)}{\theta_{\text{BAO}}(z)}. \quad (222)$$

As a result, isotropy of the inferred BAO separation is preserved independently of the detailed form of the hazard rate $\lambda(\ell)$, provided it satisfies the observational ratio constraint. The framework therefore reproduces the observed agreement between transverse and radial BAO measurements across redshift.

20.5.2 Normalization and absolute scale

BAO observations constrain relative distances but do not fix the absolute normalization of length scales. In the hazard–ledger construction, this freedom appears as an overall scaling of the ledger coordinate ℓ .

Fixing the absolute physical BAO scale L_{BAO} requires one external normalization condition. This may be supplied by:

- local distance measurements,
- standardizable astrophysical rulers,
- or early-universe calibrations.

The present analysis does not require a specific choice. Its purpose is to demonstrate internal consistency rather than to advocate a particular calibration strategy.

20.5.3 Large–scale isotropy and homogeneity

The construction assumes statistical isotropy of the hazard rate at large scales, ensuring that redshift accumulation is directionally unbiased on average. This condition is sufficient to preserve the observed isotropy of BAO features and of the cosmic microwave background at leading order.

Importantly, isotropy constrains only the angular structure of the hazard field, not its detailed microphysical origin. Small-scale fluctuations in $\lambda(\ell)$ contribute to stochastic scatter but do not spoil the mean BAO scaling relations.

20.5.4 Relation to CMB and early-universe observables

The BAO feature observed at late times is closely related to the acoustic scale imprinted in the cosmic microwave background. Within the present framework, this correspondence arises through the same redshift–distance mapping applied along null trajectories from the surface of last scattering.

A detailed treatment of CMB anisotropies, polarization spectra, and damping effects lies beyond the scope of this section. However, the kinematical structure introduced here is compatible with a fixed physical acoustic scale at emission, provided the hazard accumulation process operates uniformly along photon paths.

20.5.5 Scope and limitations

The purpose of the hazard–ledger construction is not to replace the full phenomenology of standard cosmology, but to demonstrate that BAO observations do not uniquely select an expanding metric interpretation. Additional observational probes are required to distinguish between competing redshift mechanisms.

In particular, questions of structure growth, lensing, and dynamical evolution must be addressed separately. The present results establish only that a constant physical BAO ruler can be realized consistently within a non-expansion-based redshift framework.

20.6 Stochastic Redshift Accumulation on Ledger Space

The construction of Sections 20.2 and 20.4 fixed the *mean* redshift–distance relation kinematically, using BAO observables to determine the functional form of the hazard $\lambda(\ell)$ up to a monotone reparametrization of the ledger coordinate. Those results were purely geometric and made no reference to fluctuations, dispersion, or angular structure.

In this section we supply the missing dynamical layer. We model redshift accumulation along null trajectories as a stochastic process on ledger space whose first cumulant reproduces the BAO–fixed mean mapping, while higher cumulants encode observable dispersive effects. The purpose of this construction is not to introduce additional freedom, but to show that a single stochastic mechanism naturally accounts for both coherent redshift structure and its fluctuations.

20.6.1 Ledger events and Poisson structure

We model redshift accumulation as arising from a sequence of discrete, unresolved interaction events ordered along the ledger coordinate ℓ . These events

represent coarse-grained couplings between photon wave packets and infrared geometric degrees of freedom that are not individually observable.

Let $\{\ell_i\}$ denote the ordered set of ledger locations at which such events occur. Conditional on the hazard density $\lambda(\ell)$ fixed by the BAO consistency condition, we assume that the event locations form an inhomogeneous Poisson process on ledger space. For any infinitesimal interval $[\ell, \ell + d\ell]$, the expected number of events satisfies

$$\mathbb{E}[dN_\ell] = \lambda(\ell) d\ell, \quad (223)$$

where N_ℓ is the associated counting process.

The Poisson assumption encodes two physical statements. First, interaction events are localized and approximately independent after coarse-graining. Second, all large-scale structure enters through the inhomogeneity of the hazard $\lambda(\ell)$ rather than through correlations between individual events.

Each event carries a scalar *mark* Δu_i representing its contribution to the logarithmic redshift variable

$$u(\ell) \equiv \ln(1 + z(\ell)). \quad (224)$$

Redshift accumulation along the trajectory is then described by the jump sum

$$u(\ell) = \sum_{\ell_i \leq \ell} \Delta u_i. \quad (225)$$

The marks $\{\Delta u_i\}$ are drawn independently from a fixed distribution with finite first and second moments. No assumption is made about their microscopic origin; only their statistics enter observable predictions.

20.6.2 Diffusion limit and cumulants

Observables such as BAO and CMB anisotropies probe regimes in which a large number of interaction events occur along each null trajectory. In this high-rate, small-jump limit, the compound Poisson process (225) admits a diffusion approximation governed by its lowest cumulants.

Let the mark distribution satisfy

$$\mathbb{E}[\Delta u] = \bar{\Delta}u, \quad \text{Var}(\Delta u) = \sigma_{\Delta u}^2. \quad (226)$$

Then $u(\ell)$ converges in distribution to a continuous stochastic process satisfying

$$du(\ell) = a(\ell) d\ell + b(\ell) dW_\ell, \quad (227)$$

where W_ℓ is a standard Wiener process on ledger space and

$$a(\ell) = \lambda(\ell) \bar{\Delta}u, \quad b^2(\ell) = \lambda(\ell) \sigma_{\Delta u}^2. \quad (228)$$

Equation (227) should be understood as an effective description of the underlying jump process. Its significance lies in the explicit separation between coherent and dispersive effects encoded in the first and second cumulants.

First cumulant: mean redshift structure. The drift term governs the mean relation between redshift and ledger coordinate,

$$\frac{d}{d\ell} \mathbb{E}[u(\ell)] = \lambda(\ell) \bar{\Delta}u. \quad (229)$$

By construction, this reproduces the BAO–fixed redshift–distance mapping derived in Section 20.4. Localized structure in $\lambda(\ell)$ therefore produces coherent compression or stretching of physical scales when projected into redshift space.

Second cumulant: redshift fluctuations. The variance term controls the growth of redshift fluctuations,

$$\text{Var}[u(\ell)] = \int_0^\ell d\ell' \lambda(\ell') \sigma_{\Delta u}^2. \quad (230)$$

These fluctuations induce stochastic differences between neighboring null trajectories. When projected onto the sky, they act as an effective angular diffusion, suppressing structure on sufficiently small angular scales.

Universality. The diffusion limit depends only on the first two moments of the mark distribution and is therefore universal across a wide class of microscopic models. Higher cumulants generate non–Gaussian corrections, but these are suppressed in the regime relevant for coarse–grained observables.

20.6.3 Scope of the stochastic description

The stochastic redshift process introduced here provides a unified description of coherent redshift structure and its fluctuations. At this stage, only scalar redshift accumulation has been considered. Additional tensorial structure associated with individual interaction events will be introduced in later sections to describe angular distortion and polarization.

In the next section we examine the optical consequences of redshift fluctuations, including angular dephasing and damping of small–scale structure.

20.7 Optical Effects from Redshift Fluctuations

The stochastic redshift process introduced in Section 20.6 implies observable optical consequences beyond the mean redshift–distance relation. These consequences arise directly from the first and second cumulants of the process and require no additional physical assumptions.

In this section we describe how coherent optical compression, angular dephasing, and small–scale damping emerge naturally from the hazard–driven framework.

20.7.1 Optical compression and stretching

The first cumulant of the redshift process controls the mean mapping between physical separation and redshift interval. As shown in Section 20.6.2, the drift term satisfies

$$\frac{d}{d\ell} \mathbb{E}[u(\ell)] = \lambda(\ell) \bar{\Delta}u. \quad (231)$$

Consider a fixed physical separation $\Delta\ell$ transported through the redshift mapping. The corresponding redshift separation is

$$\Delta u \simeq \lambda(\ell) \bar{\Delta}u \Delta\ell, \quad (232)$$

to leading order. Regions of enhanced hazard therefore map a given physical scale into a smaller redshift interval, while regions of suppressed hazard produce stretching.

This effect may be described as *optical compression* or *optical stretching*, depending on the local structure of $\lambda(\ell)$. Because the hazard profile is fixed kinematically by BAO observables, such compression is not an adjustable feature but a necessary consequence of the constant-physical-ruler hypothesis.

20.7.2 Angular dephasing from redshift variance

The second cumulant of the redshift process controls the growth of fluctuations,

$$\text{Var}[u(\ell)] = \int_0^\ell d\ell' \lambda(\ell') \sigma_{\Delta u}^2. \quad (233)$$

Neighboring null trajectories accumulate different redshift realizations due to stochastic variation in the underlying interaction events. These differences induce relative phase shifts and angular deflections when the radiation field is projected onto the observer's sky.

At sufficiently coarse resolution, the cumulative effect is well approximated as an angular diffusion process. Small-scale angular structure is progressively dephased, while large-scale structure remains coherent.

20.7.3 Damping of small-scale angular power

The angular diffusion induced by redshift fluctuations acts as a smoothing operator on the observed radiation field. In harmonic space, this smoothing may be represented by a multiplicative damping envelope applied to angular power spectra,

$$C_\ell \longrightarrow D(\ell) C_\ell, \quad D(\ell) \simeq \exp[-\ell^2 \sigma_\theta^2], \quad (234)$$

where σ_θ is an effective angular width determined by the accumulated redshift variance.

The precise mapping between σ_θ and $\text{Var}[u(\ell)]$ depends on geometric factors and projection details, but the qualitative form of the damping envelope is generic. It reflects the central-limit behavior of many weak, incoherent contributions rather than the presence of a sharp scattering surface.

20.7.4 Unified interpretation

Optical compression, angular dephasing, and small-scale damping are not independent phenomena within the hazard–driven framework. They are different observational manifestations of the same underlying stochastic process:

- the *first cumulant* controls coherent mapping between physical and redshift space;
- the *second cumulant* controls stochastic dephasing and angular diffusion.

No additional interaction channels or epochs are required to generate these effects. They arise inevitably once redshift accumulation is treated as a stochastic process constrained by the BAO–fixed mean hazard.

In the next section we examine how these same stochastic ingredients interact with observability and traceout to produce an apparent late–time window of enhanced polarization and large–scale structure.

20.8 Observability, Ledger Drift, and the Apparent Reionization Window

The stochastic redshift process described in Sections 20.6 and 20.7 operates continuously along null trajectories. Photon–geometry interactions do not turn on or off at special epochs. Nevertheless, observations of the cosmic microwave background exhibit a distinct late–time enhancement of large–scale polarization, commonly interpreted as evidence for a discrete “reionization” event.

In this section we show that such an apparent epoch arises generically from the structure of observability in a theory with internal ledger memory and stochastic traceout. No change in microscopic interaction strength or plasma state is required.

20.8.1 Ledger drift and loss of observability

Between interaction events, a photon propagates freely while unresolved correlations with its geometric environment accumulate in internal degrees of freedom. We refer to this gradual transfer of amplitude from observer–coupled modes into traced–out internal structure as *ledger drift*.

Ledger drift does not destroy photons or suppress interactions. Instead, it reduces the overlap between the photon state and the observer’s measurement basis. Radiation that has propagated for a long ledger interval without a reset therefore becomes progressively less observable, even though it continues to exist dynamically.

In this sense, “darkness” corresponds not to the absence of radiation, but to the absence of radiation that remains coupled to observable degrees of freedom.

20.8.2 Resets as traceout and recoupling

An interaction event that absorbs and re-emits a photon—whether through Thomson scattering or an equivalent coarse-grained process—acts as a local traceout. The accumulated internal ledger is partially erased, and the outgoing photon is re-prepared in a state that is again coupled to the observable sector.

Such events therefore function as *resets* that temporarily restore observability. Only photons that have undergone a sufficiently recent reset can contribute significantly to observed radiation at the detector.

This interpretation does not privilege any specific microscopic interaction. What matters is the existence of processes that locally erase internal memory and recouple radiation to observable modes.

20.8.3 Visibility of the last effective reset

Let interaction events along a null trajectory be modeled as the inhomogeneous Poisson process with hazard $\lambda(\ell)$ introduced previously. The probability density that the *last* reset prior to observation occurs at ledger location ℓ is

$$f_{\text{last}}(\ell) = \lambda(\ell) \exp \left[- \int_{\ell}^{\ell_{\text{obs}}} \lambda(\ell') d\ell' \right] \equiv \lambda(\ell) e^{-\tau(\ell)}, \quad (235)$$

where $\tau(\ell)$ is the accumulated optical depth from ℓ to the observer.

This factor represents the *visibility* of resets at different ledger locations. It is present even when the hazard is stationary and contains no special features.

20.8.4 Convertible ledger memory

A reset produces an observable imprint only if unresolved internal structure is available to be converted at the time of the event. Let $M(\ell)$ denote the amount of *convertible ledger memory* carried by the incoming photon state.

By construction:

- $M(\ell) \rightarrow 0$ immediately after a reset,
- $M(\ell)$ grows during free propagation as unresolved correlations accumulate,
- growth slows or saturates once long-range coherence is exhausted.

No special functional form for $M(\ell)$ is required. Monotone growth from zero with eventual saturation is generic for a coarse-grained memory variable in an open system.

20.8.5 Product structure and the apparent epoch

The expected contribution of resets at ledger location ℓ to any observable that converts internal structure into measured radiation is proportional to the product

$$\mathcal{W}(\ell) \propto \lambda(\ell) e^{-\tau(\ell)} M(\ell), \quad (236)$$

which combines:

- the rate of resets,
- their survival probability to the observer,
- and the amount of convertible internal memory.

Even when the hazard $\lambda(\ell)$ and the underlying microphysics are stationary, the function $\mathcal{W}(\ell)$ generically possesses a single broad maximum at finite look-back. Early resets are suppressed by survival probability, while very late resets occur before sufficient memory has accumulated.

The location of this maximum defines an apparent “epoch” without any underlying phase transition or change in interaction strength.

20.8.6 Origin of the dark ages

At early ledger times, frequent resets prevent the accumulation of internal ledger memory while survival to the observer is strongly suppressed. At very late ledger times, ledger drift removes unreset radiation from the observable channel before it can contribute.

In both regimes, radiation exists and interactions occur continuously, but observable signal is weak. The “dark ages” therefore correspond to a regime of low observability rather than to an absence of radiation or interaction.

The end of the dark ages marks the point at which resets first become efficient at returning radiation to visibility.

20.8.7 Interpretation

Within the hazard–driven framework, reionization is reinterpreted as a consequence of stochastic observability in a system with internal ledger memory. The appearance of a preferred late–time window is generic and does not require a distinct scattering surface, a change in plasma state, or special early–universe conditions.

In the following section we show how this observability window interacts with tensorial distortions of the photon bundle to generate large–scale polarization and the observed structure of EE and TE correlations.

20.9 Observational Status and Falsifiability

The preceding sections reformulate BAO observations in a framework that allows the acoustic feature to be interpreted as a constant physical separation at the time of emission. It is therefore essential to clarify which aspects of the construction are fixed by observation, which are model–dependent, and how the framework may be empirically falsified.

20.9.1 What is fixed by observation

BAO measurements directly constrain the redshift dependence of the angular and radial observables $\theta_{\text{BAO}}(z)$ and $\Delta z_{\text{BAO}}(z)$. Under the assumption of a constant physical BAO ruler, these observables imply:

- a differential consistency relation between transverse and radial BAO measurements;
- a unique redshift–distance Jacobian dr/dz , up to an overall normalization;
- a corresponding hazard profile $\lambda(\ell)$, fixed up to monotone reparametrization of the ledger coordinate.

No assumption about global expansion, early–universe initial conditions, or microscopic interaction mechanisms enters at this stage.

20.9.2 What is model–dependent

The following elements are not fixed by BAO data alone:

- the absolute normalization of the physical BAO scale;
- the microscopic origin of the hazard and its stochastic marks;
- the detailed structure of higher–order cumulants beyond the diffusion limit.

These ingredients must be constrained by additional observables, such as lensing, structure growth, or polarization statistics.

20.9.3 Falsifiability

The constant physical BAO hypothesis is empirically falsifiable. In particular:

- Any statistically significant violation of the differential relation (208) would rule out a constant physical BAO ruler.
- If the inferred transverse and radial distance measures fail to satisfy isotropy at the BAO scale, the framework is excluded.
- If no hazard profile $\lambda(\ell)$ can reproduce the observed BAO ratios while remaining monotone, the construction fails.

Conversely, consistency of BAO observables with these relations supports the existence of a non–expansion–based redshift mapping compatible with current data.

20.9.4 Interpretive scope

The results presented here do not claim to supersede standard cosmology. Rather, they demonstrate that BAO observations alone do not uniquely select an expanding metric interpretation. They instead constrain a class of redshift–distance mappings whose physical realization must be tested using complementary probes.

In this sense, BAO serves not as a direct measurement of expansion, but as an integrability condition on the structure of redshift itself.

20.10 A Resonant Hazard Profile and Emergent Cosmic Noon

The preceding sections developed the hazard–driven framework at a structural level, without committing to any specific functional form for the redshift hazard $\lambda(\ell)$. In particular, the BAO consistency conditions derived in Section 20.2 constrain the *mean* redshift–distance mapping independently of how that mapping is realized microscopically.

In this section we present a simple, explicit choice of hazard profile to illustrate the resulting phenomenology. The purpose is not to introduce additional assumptions, but to demonstrate how several observational features—BAO stability, smooth distance–redshift relations, and an apparent tracer pileup commonly referred to as “cosmic noon”—can arise simultaneously from a single hazard–driven mechanism.

20.10.1 Resonant interaction profile

We consider a phenomenological hazard profile consisting of a nearly scale–free baseline supplemented by a broad resonant enhancement over a finite range of ledger displacement (Fig. 6). Physically, such a profile corresponds to an increased interaction probability when propagating radiation becomes dynamically aligned with infrared geometric modes whose properties are set by horizon–scale physics.

The precise shape of the resonance is not essential. What matters is only that $\lambda(\ell)$ remains smooth, positive, and monotone–integrable, so that the resulting redshift–distance mapping is well-defined and free of singular behavior. This profile therefore represents one member of a broad admissible class rather than a finely tuned choice.

20.10.2 Reconstructed distance–redshift relation

Given the hazard profile, the redshift–distance relation $r(z)$ is reconstructed using the ledger survival formalism described in Section 20.4. Figure 7 shows that the resulting mapping is smooth and monotonic over the entire redshift range, with no singular behavior introduced by the resonant interaction.

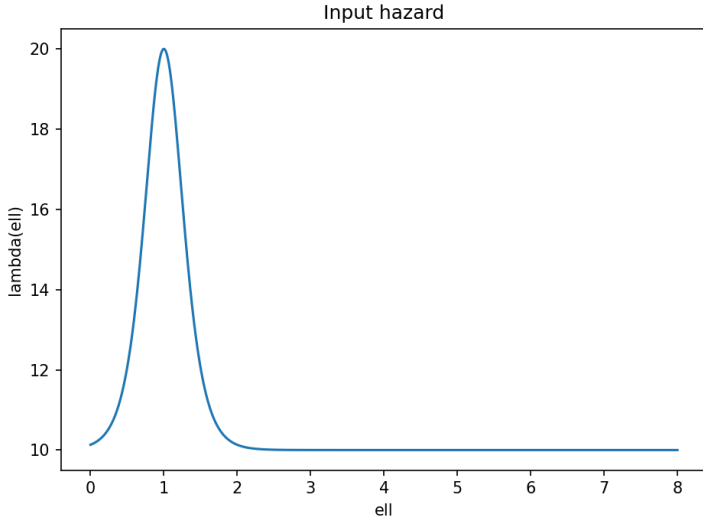


Figure 6: Illustrative redshift hazard $\lambda(\ell)$ as a function of ledger displacement ℓ . A weak baseline interaction is supplemented by a broad resonant enhancement, introducing a preferred ledger scale at which redshifting interactions become temporarily more probable. The ledger coordinate ℓ parametrizes cumulative alignment with horizon-defined infrared geometric modes and is not identified with proper time, affine distance, or a cosmological scale factor. A resonant enhancement necessarily appears once IR geometric modes are sourced predominantly by horizon-adjacent emission, because their interaction probability is a functional of accumulated ledger displacement.

The resonant enhancement produces a nonlinear mapping between emission radius and observed redshift. Regions of enhanced hazard lead to optical compression in redshift space, while the underlying physical distance remains well behaved. This behavior is precisely the optical effect described generically in Section 20.7, now realized in an explicit example.

20.10.3 Emergent BAO behavior

Within this construction, the BAO feature is assumed to correspond to a fixed physical separation at the time of emission. The effective transverse and radial distance measures inferred from the hazard- induced mapping then satisfy the BAO consistency conditions derived in Section 20.2.

For the resonant profile shown here, the inferred BAO scale remains approximately constant in physical units across the redshift range probed by current surveys, while preserving isotropy and Alcock–Paczyński consistency. No additional tuning is required beyond the existence of a smooth hazard profile compatible with the BAO integrability relations.

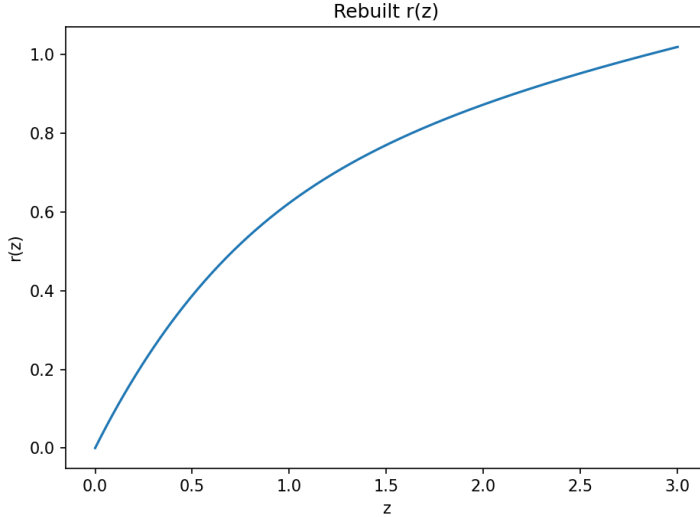


Figure 7: Reconstructed physical emission radius $r(z)$ obtained from the hazard profile in Fig. 6. The distance–redshift relation emerges self–consistently from survival statistics in ledger space rather than being postulated independently. The mapping is smooth, monotonic, and sublinear at large redshift, exhibiting no pathologies or horizons introduced by hand.

20.10.4 Redshift–space pileup and cosmic noon

An immediate consequence of the resonant hazard profile is the appearance of a pronounced enhancement in the Jacobian

$$J(z) = r(z)^2 \frac{dr}{dz}, \quad (237)$$

shown in Fig. 8. This quantity governs the mapping between physical emission volume and observed redshift space. A smooth enhancement in $J(z)$ therefore corresponds to a redshift–space pileup, even when the underlying tracer distribution is uniform.

This effect provides a phenomenological analogue of the observational feature commonly referred to as “cosmic noon.” In the present framework, the enhancement arises purely from optical compression induced by the hazard–driven redshift mapping, rather than from changes in intrinsic luminosity, formation rate, or cosmological expansion dynamics.

20.10.5 Interpretation

Within the hazard–driven framework, the coincidence between BAO stability and the appearance of cosmic noon is not accidental. Both emerge from the

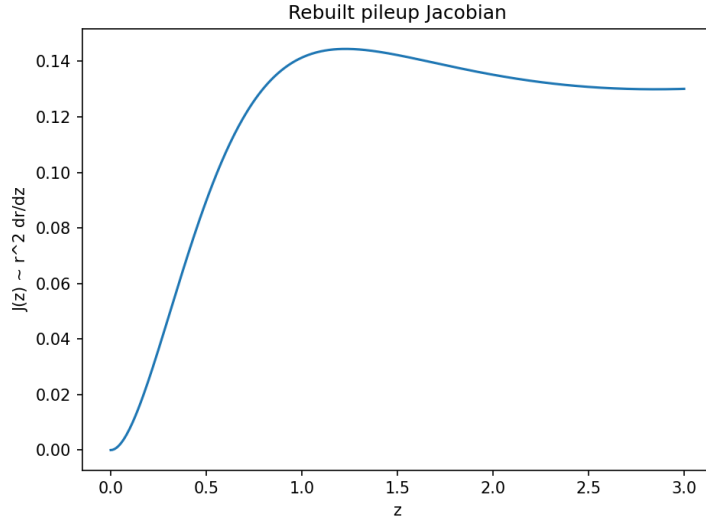


Figure 8: Redshift–space Jacobian $J(z) = r(z)^2 dr/dz$ corresponding to the reconstructed mapping in Fig. 7. The enhancement in $J(z)$ reflects compression of physical emission volume into a narrow redshift interval, producing an apparent pileup in redshift space without any physical overdensity or divergent behavior in the source distribution.

same underlying redshift–distance mapping constrained by BAO integrability and shaped by the cumulative interaction history of radiation with infrared geometric modes.

This example illustrates how apparently distinct observational phenomena can be understood as unified consequences of redshift–space structure, without invoking special epochs, finely tuned source evolution, or expansion as a primitive input.

21 The glass universe

We model the observable universe as an *open thermodynamic subsystem* whose only primitive transportable extensive quantity is heat. In the strictly Jacobsonian view adopted here, there is no fundamental momentum balance, no assumed stress–energy tensor beyond an extensive heat density, and no independent force law. What we call “dynamics” is instead a constitutive closure: a rule for how an open system routes heat in response to entropic affinities, while continually discarding microscopic information to an external sink (the horizon).

A central lesson of planar coarse–graining is that the first nontrivial residue of transport is *even*: it is not a vector drift but an oriented area (a commutator–type history). If directional information is traced out, then a strictly Markovian

macroscopic description cannot close on $\Omega \subset \mathbb{R}^2$ alone; the minimal augmentation is an *internal* coordinate carried by heat packets. We represent this augmentation by a periodic “ledger” coordinate $\alpha \in S^1$, and we resolve the heat density as $Q(x, \alpha, t)$. Observable pseudoscalar structure then arises only through ledger-resolved moments and diagnostics of the routed heat flux, while the rate at which directional history is written and erased is encoded in a slow constitutive pseudoscalar field.

The purpose of this section is to state a continuum model in this spirit and to fix the ontology mirrored by the lattice experiments: (i) conservative transport of mass-like fields on the extended space $\Omega \times S^1$ with Heisenberg horizontal geometry, (ii) Jacobson–Clausius drift driven by the inverse–temperature affinity $\nabla_H \beta$, (iii) open–system loss through a horizon layer (implemented numerically by a smooth sponge), supplemented by geometric push–forward expansion on a fixed observable disk, and (iv) compensating return implemented as *forced replacement* of whatever heat is lost each step, with a local free–power proxy determining *where* replacement lands (allocation), not *how much* is created.

21.1 Ontological postulates

Observable domain and ledger extension. Let $\Omega \subset \mathbb{R}^2$ be a fixed observable disk, interpreted as the interior of a horizon. We extend the resolved state space by an *internal* periodic coordinate $\alpha \in S^1$ (the ledger), yielding the extended domain $\Omega \times S^1$. The ledger coordinate is not a physical direction in space; it labels unresolved even transport residues (area–type history) and provides the minimal augmentation needed for a Markovian coarse description.

Mass–like transported fields. The transported (mass–like) fields are densities on $\Omega \times S^1$, advected conservatively by a velocity $v = (v_x, v_y, v_\alpha)$ and modified only by explicit open–system operations:

- $Q(x, \alpha, t) \geq 0$: heat (energy) density resolved at ledger label α ;
- $S(x, \alpha, t)$: an entropy–moment density transported with Q , defining a specific entropy $\ell(x, \alpha, t) := S/(Q + Q_0)$ with a small regularizer $Q_0 > 0$;
- $B(x, \alpha, t)$: an optional transported ledger–moment density (a passive tracer in the present implementation), from which one may form an intensive $A(x, \alpha, t) := B/(Q + Q_0)$.

No normalization constraint is imposed on the ledger distribution: the primitive extensive object is Q itself, resolved over α .

Constitutive and memory fields. In addition to the transported densities, we introduce internal pseudoscalar fields on $\Omega \times S^1$:

- $\sigma(x, \alpha, t)$: a slow constitutive pseudoscalar controlling the strength of a chiral (skew–Onsager) component in the routing law;

- $m(x, \alpha, t)$: a pseudoscalar memory field that relaxes toward a circulation diagnostic.

Both σ and m reverse sign under parity, while the governing laws are parity-covariant (no sign is preferred).

Thermodynamic affinity and equation of state. We close thermodynamic driving by defining temperature from specific entropy:

$$\ell := \frac{S}{Q + Q_0}, \quad T := T_0 \exp\left(\frac{\ell}{c_T}\right), \quad \beta := \frac{1}{T}, \quad (238)$$

with constants $T_0 > 0$, $c_T > 0$. The inverse temperature β is the primitive entropic affinity that drives transport.

Heisenberg horizontal geometry. Directional trace-out is modeled by Heisenberg horizontal derivatives on $\Omega \times S^1$. With $(x, y) \in \Omega$ and ledger coordinate α , define

$$Xf := \partial_x f - \frac{1}{2}y \partial_\alpha f, \quad Yf := \partial_y f + \frac{1}{2}x \partial_\alpha f, \quad (239)$$

and write $\nabla_H f := (Xf, Yf)$. The associated lifted (central) velocity v_α is the Heisenberg lift of planar motion and is not specified independently (see §21.2).

21.1.1 Diagnostics and openness.

The system is open. Resolved fields are irreversibly damped in a thin horizon layer (a smooth sponge taper), and additional loss occurs when geometric push-forward expansion maps material outside the fixed observable disk. A local “free-power” proxy $p_F(x, t) := \sum_\alpha Q |\nabla_H \beta|^2$ is used to define *allocation weights* for compensating return: it determines where replacement heat is deposited, while the *amount* of replacement is forced to match the explicitly measured loss each step (up to optional additional compensation for pure geometric stretching under expansion).

21.2 Jacobson–Clausius transport on $\Omega \times S^1$

21.2.1 Conservative transport on the extended space.

On the extended domain $\Omega \times S^1$, the transported densities

$$Q(x, \alpha, t) \geq 0, \quad S(x, \alpha, t), \quad B(x, \alpha, t)$$

evolve by conservative advection under a velocity field $v = (v_x, v_y, v_\alpha)$:

$$\partial_t Q + \nabla_x \cdot (Q v_H) + \partial_\alpha (Q v_\alpha) = 0, \quad (240)$$

$$\partial_t S + \nabla_x \cdot (S v_H) + \partial_\alpha (S v_\alpha) = \Sigma_S, \quad (241)$$

$$\partial_t B + \nabla_x \cdot (B v_H) + \partial_\alpha (B v_\alpha) = 0, \quad (242)$$

where $v_H = (v_x, v_y)$ is the spatial velocity and $\Sigma_S \geq 0$ is an (optional) entropy production term defined in §21.3. These equations describe the *closed* (interior) constitutive transport step. Openness (horizon damping, expansion push-forward, sinks, and compensating return) is implemented separately as operator-split updates in §21.4.

21.2.2 Intensive variables and regularization.

The primitive thermodynamic intensive is the specific entropy

$$\ell(x, \alpha, t) := \frac{S(x, \alpha, t)}{Q(x, \alpha, t) + Q_0}, \quad Q_0 > 0, \quad (243)$$

with temperature and inverse temperature given by the EOS (238). When B is used, one may similarly form a ledger intensive

$$A(x, \alpha, t) := \frac{B(x, \alpha, t)}{Q(x, \alpha, t) + Q_0}. \quad (244)$$

The regularizer Q_0 prevents spurious amplification in low-density regions and is negligible in the interior where Q is appreciable.

21.2.3 Heisenberg horizontal affinity.

Transport is driven by the *horizontal* inverse-temperature gradient $\nabla_H \beta$ defined from the Heisenberg operators (239):

$$\nabla_H \beta := (X\beta, Y\beta), \quad X\beta = \partial_x \beta - \frac{1}{2}y \partial_\alpha \beta, \quad Y\beta = \partial_y \beta + \frac{1}{2}x \partial_\alpha \beta.$$

This is the continuum counterpart of using Heisenbergized finite differences in the lattice implementation: admissible entropic affinities are horizontal.

21.2.4 Jacobson–Clausius constitutive velocity.

The spatial routing velocity v_H is taken to be a Jacobson–type Onsager drift plus a chiral skew component controlled by the pseudoscalar σ :

$$v_H = -\kappa(\sigma^2) \nabla_H \beta + \chi \sigma J \nabla_H \beta, \quad J(u, v) = (-v, u), \quad (245)$$

with $\chi \in \mathbb{R}$ a dimensionless chiral strength and $\kappa(\sigma^2) \geq 0$ a parity–even mobility. In the numerical model we use a bounded mobility such as $\kappa(\sigma^2) = \kappa_0 / (1 + \kappa_\beta \sigma^2)$, which suppresses excessive speeds in strongly chiral regions while preserving parity covariance.

21.2.5 Lifted ledger velocity and Heisenberg advection.

The velocity in ledger space is not specified independently. It is fixed by the Heisenberg lift of planar motion:

$$v_\alpha(x, \alpha, t) := -\frac{1}{2}y v_x(x, \alpha, t) + \frac{1}{2}x v_y(x, \alpha, t). \quad (246)$$

Equations (239) and (246) encode the same geometric content: the commutator residue of planar motion is recorded in the central (ledger) coordinate. In particular, there is *no* separate “central force” toward $r = 0$; any apparent central effects arise from the geometry of the observable region (horizon coupling) and from open-system throughput balance, not from an added potential.

21.2.6 Conservative meaning of the constitutive law.

Although (245) is written as a velocity law, it does not introduce a momentum density or an acceleration equation. It is a *constitutive closure* specifying the routing of the conserved densities (Q, S, B) on $\Omega \times S^1$. In the closed interior (horizon and expansion disabled), the mass-like integrals are conserved:

$$\frac{d}{dt} \int_{\Omega \times S^1} Q \, dx \, d\alpha = 0, \quad \frac{d}{dt} \int_{\Omega \times S^1} B \, dx \, d\alpha = 0, \quad (247)$$

while the entropy moment satisfies

$$\frac{d}{dt} \int_{\Omega \times S^1} S \, dx \, d\alpha = \int_{\Omega \times S^1} \Sigma_S \, dx \, d\alpha, \quad (248)$$

up to whatever explicit entropy production Σ_S is included.

21.2.7 A throughput diagnostic used for allocation.

A key diagnostic that reappears in the open-system closure is the local free-power proxy (defined at ledger resolution)

$$p_F(x, \alpha, t) := Q(x, \alpha, t) |\nabla_H \beta(x, \alpha, t)|^2, \quad (249)$$

and its α -sum

$$p_F^{(2)}(x, t) := \int_{S^1} p_F(x, \alpha, t) \, d\alpha \approx \sum_{\alpha} Q |\nabla_H \beta|^2. \quad (250)$$

This quantity is nonnegative, vanishes when entropic gradients vanish, and is parity-even. In the present model it does *not* determine the creation *amount*; instead it provides the *allocation weight* used to decide where compensating return is deposited (after low-pass temporal smoothing).

21.3 Directional memory and constitutive trace-out

The Jacobson–Clausius transport law (245) specifies how heat is routed in response to an entropic affinity, but it contains no intrinsic memory of past transport. To obtain persistent geometric organization without introducing momentum, elasticity, or propagating modes, we introduce a minimal *pseudoscalar trace-out closure* built from diagnostics of the heat flux itself. Memory enters only through slow relaxation channels and feeds back on transport exclusively through the constitutive pseudoscalar σ .

21.3.1 Circulation as the primitive pseudoscalar diagnostic.

The heat flux associated with the constitutive velocity is

$$J(x, \alpha, t) := Q(x, \alpha, t) v_H(x, \alpha, t). \quad (251)$$

In two spatial dimensions, the natural parity–odd diagnostic derived from this flux is its scalar curl. Using the Heisenberg horizontal derivatives (239), we define

$$\omega(x, \alpha, t) := X J_y - Y J_x. \quad (252)$$

Because ω is constructed as a curl, it changes sign under parity and vanishes for purely potential (irrotational) routing. It therefore provides an instantaneous, ledger–resolved diagnostic of *oriented* transport.

Importantly, ω is not treated as an independent dynamical field. It is recomputed diagnostically from the transported flux at each time step.

21.3.2 Relaxed pseudoscalar memory.

Instantaneous circulation is generally too noisy to control constitutive response directly. We therefore introduce a pseudoscalar memory field $m(x, \alpha, t)$ that relaxes toward ω on a finite timescale:

$$\partial_t m = \frac{1}{\tau_m} (\omega - m) + D_m \Delta m, \quad (253)$$

with relaxation time $\tau_m > 0$ and optional diffusion $D_m \geq 0$ on $\Omega \times S^1$. This construction ensures that only *persistent* circulation leaves an imprint in the memory channel: rapidly fluctuating vortical features average away, while long–lived circulation builds a nonzero m .

21.3.3 Constitutive pseudoscalar response.

The pseudoscalar field $\sigma(x, \alpha, t)$ controls the strength of the chiral (skew–Onsager) component in the routing law (245). In the present implementation, σ responds *directly* to the instantaneous circulation diagnostic ω , rather than to the relaxed memory m :

$$\partial_t \sigma = \lambda_\omega \omega - \frac{1}{\tau_\sigma} \sigma + D_\sigma \Delta \sigma, \quad (254)$$

with coupling strength λ_ω , relaxation time $\tau_\sigma \gg \tau_m$, and optional diffusion $D_\sigma \geq 0$.

This choice reflects the operational structure of the model: m serves as a slow diagnostic of sustained circulation, while σ encodes the medium’s constitutive response to current oriented throughput. No independent sign is preferred; both ω and σ are pseudoscalars, and the equations are parity–covariant.

21.3.4 Saturation and bounded response.

Unbounded growth of $|\sigma|$ would lead to excessively strong chiral skew and to numerical or physical pathologies. We therefore impose a constitutive saturation,

$$\sigma \mapsto \sigma_{\text{sat}} \tanh\left(\frac{\sigma}{\sigma_{\text{sat}}}\right), \quad (255)$$

which preserves parity symmetry while enforcing finite response. Together with slow relaxation, this places the constitutive dynamics in a glass-like regime: σ responds to coarse, long-lived circulation but remains insensitive to short-time fluctuations.

21.3.5 Entropy production from entropic throughput.

Directional organization is accompanied by irreversible entropy production. Rather than introducing an independent Shannon entropy for the ledger, we model this production directly through the entropic affinity that drives transport. The simplest local form consistent with the second law and used in the numerical model is

$$\Sigma_S = \mu_S Q |\nabla_H \beta|^2, \quad \mu_S \geq 0, \quad (256)$$

possibly capped to prevent runaway production in extreme gradients. This term is parity-even, vanishes when entropic gradients vanish, and represents the dominant scalar entropy throughput of the open system.

21.3.6 Interpretation.

Equations (252)–(256) implement a minimal and strictly Jacobsonian closure:

- heat is routed down horizontal entropic affinities with an allowed chiral skew;
- instantaneous circulation ω diagnoses oriented routing;
- a slow memory channel m integrates sustained circulation without feeding back directly;
- the constitutive response σ biases future routing while remaining bounded;
- entropy production accompanies throughput but does not itself encode direction.

No force law, momentum balance, or propagating wave mode is introduced. All geometric organization arises from the interaction of conservative transport, slow pseudoscalar response, and irreversible trace-out in an open system.

21.4 Open-system coupling, expansion, and forced return

The constitutive dynamics described in §21.2–§21.3 define a conservative transport system on $\Omega \times S^1$. To obtain sustained structure rather than eventual diffusive decay, the system is treated as *open*: resolved degrees of freedom are irreversibly lost to an external sink, while free energy is returned through a distinct channel. This section specifies the open-system operators used in the numerical model and clarifies their thermodynamic roles.

21.4.1 Horizon as a cold entropy sink

The observable region Ω is coupled to an external environment through a horizon-like boundary. This horizon is modeled as an effectively zero-temperature sink that accepts heat and entropy but does not return directional information.

Operationally, the horizon is implemented as a smooth multiplicative taper (“sponge”) acting in a thin boundary layer near $\partial\Omega$:

$$(Q, S, B, \sigma, m, \omega) \mapsto w(x) (Q, S, B, \sigma, m, \omega), \quad 0 \leq w(x) \leq 1, \quad (257)$$

with $w \equiv 1$ in the interior and $w \equiv 0$ at the horizon. This avoids artificial reflection or gradient discontinuities while enforcing irreversible loss.

Thermodynamically, the horizon removes both scalar entropy and directional structure. No ledger information is stored, and no parity bias is introduced. The horizon therefore defines a one-way channel for entropy export.

In a fully faithful horizon-coupled open-system picture, the trace-out boundary is *observer dependent*: each local packet (or local comoving observer) has its own causal horizon, and the rate at which degrees of freedom are exported depends on that packet’s relative kinematics and on whether information can back-react across the would-be horizon on the timescales of interest. The present lattice model does *not* attempt to track a distinct horizon for each packet. Instead, we adopt an *effective horizon* tied to the chosen observational origin and implement trace-out through a common sponge layer near $\partial\Omega$. This is a controlled idealization: we interpret only the interior region well inside the sponge as “physical,” while the boundary layer functions as a numerical stand-in for irreversible export. Because the goal of this section is qualitative—to exhibit how Jacobson–Clausius routing with σ -coupled Carnot–Carathéodory geometry can self-organize a robust correlation length under expansion and forced throughput—the effective horizon approximation is adequate. In particular, the emergent BAO-like scale is selected by interior transport and return balance, and is insensitive to the detailed microscopic bookkeeping of individual observer horizons at the boundary.

21.4.2 Expansion as a geometric push-forward

Large-scale expansion is treated as a *geometric* operation distinct from local transport. The observable domain Ω is held fixed; expansion acts by stretching material within Ω and discarding what is mapped beyond its boundary.

Over a single expansion step of duration Δt , the push-forward map is

$$x' = c + (1 + H \Delta t) (x - c), \quad (258)$$

where c is the geometric center of Ω . For mass-like fields $U \in \{Q, S, B\}$, the update is

$$U^{\text{after}}(x') = \int U^{\text{before}}(x) \delta(x' - \Phi(x)) dx, \quad (259)$$

realized numerically by conservative splatting. Contributions that land outside Ω are lost irreversibly.

Intensive internal fields (σ, m , and diagnostics derived from them) are transported by Q -weighted averaging under the same map, ensuring that expansion does not artificially create or destroy internal structure.

Expansion is irrotational and therefore does not directly write ledger information or circulation. Its sole dynamical role is to dilute material, export entropy through the horizon, and set a global throughput scale.

21.4.3 Explicit loss accounting

Losses are tracked explicitly and decomposed into distinct channels:

- *Horizon loss*, due to sponge damping at the boundary;
- *Expansion splat loss*, due to mass mapped outside Ω during push-forward;
- *Additional sinks*, such as optional black-hole droplet removal.

The instantaneous heat loss is therefore

$$\Delta Q_{\text{loss}} = \Delta Q_{\text{horizon}} + \Delta Q_{\text{exp}} + \Delta Q_{\text{sink}}, \quad (260)$$

with analogous accounting for entropy and other extensive quantities. This explicit bookkeeping is central to the return mechanism described below.

21.4.4 Forced replacement of lost heat

Free energy extracted from the resolved system is returned to the interior not by reversing trace-out, but by *forced replacement* of lost heat. At each time step, the total amount of injected heat is set equal to the measured loss:

$$\Delta Q_{\text{create}} = \Delta Q_{\text{loss}}, \quad (261)$$

optionally augmented by a separate compensating term when pure geometric stretching under expansion dilutes structure without removing mass. Creation therefore *never* exceeds what has just been lost.

Crucially, the return mechanism fixes the *amount* of creation independently of any local diagnostic. Local diagnostics enter only in determining *where* replacement heat is deposited.

21.4.5 Free–power–weighted allocation

The spatial and ledger distribution of injected heat is determined by a local throughput proxy. At ledger resolution we define

$$p_F(x, \alpha, t) := Q(x, \alpha, t) |\nabla_H \beta(x, \alpha, t)|^2, \quad (262)$$

and its α –sum

$$p_F^{(2)}(x, t) := \int_{S^1} p_F(x, \alpha, t) d\alpha. \quad (263)$$

The quantity $p_F^{(2)}$ is used to build nonnegative allocation weights $W(x)$, possibly softened in low–density regions and raised to a power $\gamma \geq 0$. To avoid instantaneous resonance between loss and injection, the weights are low–pass filtered in time:

$$\partial_t W_{\text{bar}} = \frac{1}{\tau_W} (W - W_{\text{bar}}), \quad (264)$$

and only W_{bar} is used for injection.

Injection events are realized stochastically as localized packets of heat placed in the interior of Ω , with probability density proportional to W_{bar} . The ledger coordinate α of injected packets is sampled from the *ledger–resolved* free–power $p_F(x, \alpha, t)$, so that replacement respects the local orientation structure of throughput.

21.4.6 Entropy content of injected heat

Injected heat carries little or no entropy. In practice, the specific entropy of injected packets is taken to be small or to be a local mixture with the ambient value. This ensures that creation returns *free energy* rather than entropy, consistent with the interpretation of the horizon as a cold sink.

21.4.7 Non–equilibrium steady state

The combination of conservative Jacobson–Clausius transport, irreversible horizon loss, geometric expansion, and forced replacement of losses drives the system toward a non–equilibrium steady state (NESS). In this state, scalar entropy is continually exported, while local transport, directional memory, and constitutive response persist.

No wavelength, oscillatory forcing, or nonlocal kernel is imposed at any stage. Any characteristic separation that appears in correlation diagnostics—including the BAO–like scale observed in numerical experiments—is therefore a self–organized consequence of the balance between transport, memory, expansion, and forced throughput, rather than a built–in feature of the model.

21.5 Interpretation of the BAO–like correlation scale

The numerical experiments described later exhibit a robust bump in the two–point correlation function of the heat density Q , reminiscent of a baryon acoustic

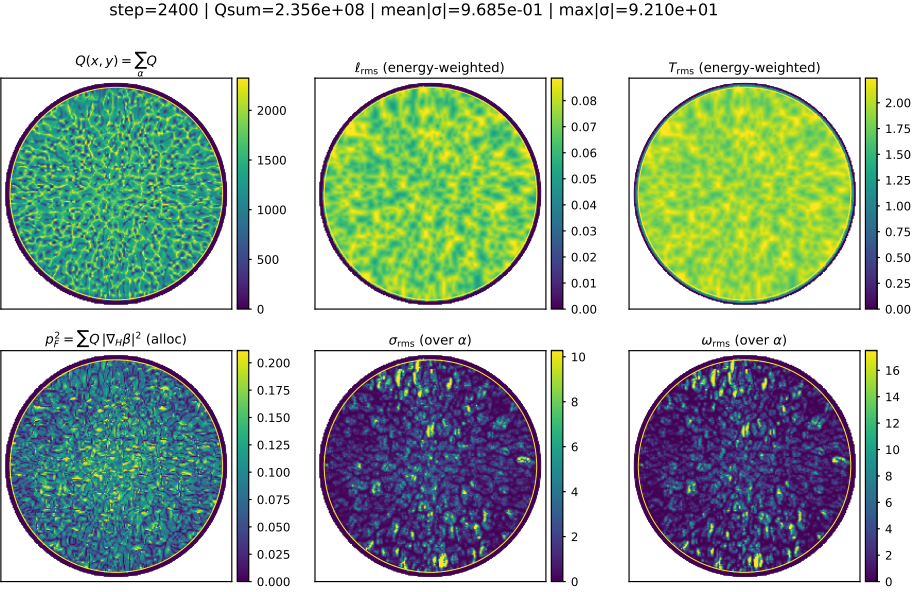


Figure 9: **“Glass” structure in a horizon-coupled Jacobsonian medium.** Representative steady-state frame from the lattice implementation of the Jacobson–Clausius ledger model on a fixed observable disk Ω . Shown are the heat density $Q(x, y) = \sum_{\alpha} Q$, selected ledger-averaged diagnostics of thermodynamic throughput and directional organization ($p_F^{(2)}$, σ_{rms} , ω_{rms}), and the horizon sponge layer near the boundary. The resulting spatial organization is mottled and quasi-frozen, reflecting a non-equilibrium steady state maintained by irreversible horizon loss and forced replacement. In this run, the two-point correlation of Q exhibits a robust primary BAO-like bump that remains locked near $r \simeq 37$ (grid/physical units) over long integration times.

oscillation (BAO) feature. In this subsection we clarify how such a scale arises in the present framework and how it should be interpreted.

21.5.1 No imposed wavelength or oscillatory mode.

At no point does the model introduce an oscillatory kernel, preferred mode, sound speed, or nonlocal interaction analogous to a primordial acoustic horizon. All ingredients are local and constitutive: Jacobson–Clausius routing driven by $\nabla_H \beta$, slow pseudoscalar response through (m, σ) , irreversible horizon loss, geometric expansion, and forced replacement of lost heat. Any characteristic separation that appears must therefore be selected dynamically by the balance of these processes in an open, driven system.

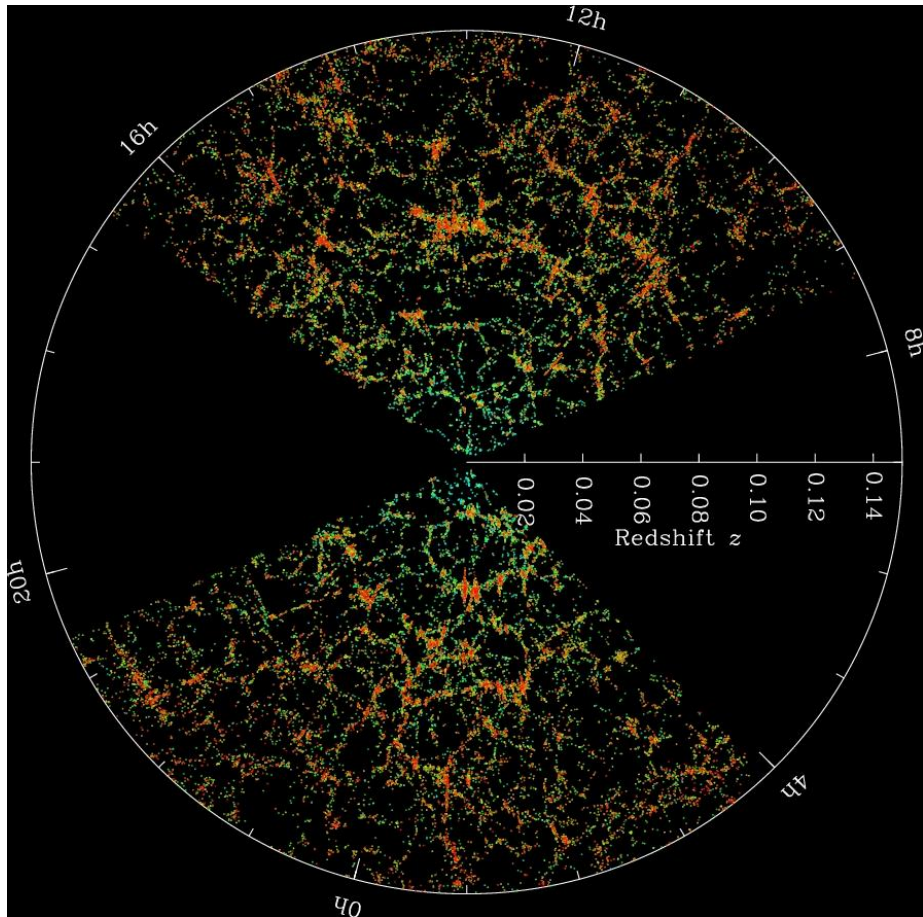


Figure 10: **Observed large-scale structure in the nearby universe.** Galaxy redshift distribution in a thin sky slice from the Sloan Digital Sky Survey [80], shown in polar (“wedge”) coordinates with angular position along the arc and redshift z along the radial direction. Filaments, clusters, and voids form a statistically robust large-scale pattern without a preferred orientation or imposed wavelength. The figure is included for qualitative comparison with the “glass universe” simulations discussed in the text, illustrating that a mottled, non-periodic cosmic web is a generic outcome of sustained structure formation rather than evidence for propagating acoustic modes. Image credit: Sloan Digital Sky Survey (SDSS).

21.5.2 Physical rather than comoving distance.

Expansion is implemented as a geometric push-forward on a *fixed* observable domain Ω . Distances measured on the computational grid after the push-forward therefore correspond directly to *physical* separations. There is no separate comoving coordinate system in which distances are held fixed while the grid expands.

Consequently, a correlation peak that remains stationary in grid units under continued expansion should be interpreted as a constant *physical* length. Any attempt to further rescale such separations by an external scale factor would double-count the expansion already encoded in the push-forward.

21.5.3 Role of forced replacement.

The forced replacement rule

$$\Delta Q_{\text{create}} = \Delta Q_{\text{loss}}$$

plays a crucial role in stabilizing the correlation scale. Because the amount of injected heat is fixed by explicit loss accounting, the system cannot amplify or damp structure arbitrarily. Replacement restores exactly the throughput removed by horizon coupling and expansion, preventing secular decay while avoiding runaway growth.

Importantly, the free-power proxy p_F enters only through allocation: replacement heat is deposited preferentially where entropic throughput is high. This reinforces existing structure without selecting a wavelength by fiat.

21.5.4 Mechanism of scale selection.

The emergent correlation scale reflects a compromise between competing effects:

- Jacobson–Clausius transport smooths heat down horizontal entropic affinities;
- the chiral skew controlled by σ promotes lateral routing and circulation;
- directional memory integrates sustained circulation and biases future transport;
- expansion and horizon loss continuously export material and entropy, setting a global throughput scale;
- forced replacement restores heat preferentially where throughput is already large.

If structure is too fine, it is erased by transport and diffusion. If it is too coarse, expansion and horizon loss dominate before replacement can reinforce it. A characteristic separation emerges when these tendencies balance.

Because this balance is statistical rather than resonant, the resulting bump is broad rather than sharply peaked, consistent with the absence of a true wave mode.

21.5.5 Locking versus drift.

Whether the BAO–like peak remains locked or drifts slowly depends on the separation of timescales. If constitutive response (τ_σ) and memory integration (τ_m) are fast compared to the expansion rate, the system rapidly adapts and the peak remains nearly stationary in physical units. If these timescales are comparable, slow drift may occur as the throughput balance adjusts. Such drift is a genuine dynamical effect, not a coordinate artifact.

21.5.6 Scope of the analogy.

The present mechanism is not a model of acoustic oscillations in a primordial plasma. The analogy to BAO is strictly structural: a statistically robust correlation length emerges in an open cosmological system without being imposed by hand. In this sense, the model demonstrates that a BAO–like feature can arise from thermodynamic transport, horizon coupling, constitutive memory, and forced throughput alone, without invoking propagating sound waves or a primordial clock.

21.5.7 Summary.

Within the Jacobson–Clausius ledger framework:

- the BAO–like bump is an emergent *physical* length, not a comoving one;
- its existence reflects non-equilibrium steady-state balance rather than oscillatory dynamics;
- its stability is tied to forced replacement combined with geometric push-forward expansion.

This interpretation aligns the continuum theory with the numerical implementation and fixes the conceptual meaning of the correlation diagnostics used in what follows.

21.6 Feasibility of galaxy replacement on the BAO scale

A steady-state interpretation of the BAO–like correlation scale requires that galaxies on $\sim 100–150$ Mpc separations can be *replaced* over cosmic time without destroying the correlation itself. In this subsection we show that this requirement is quantitatively modest when evaluated with observed astrophysical rates.

BAO volume and galaxy counts. A characteristic BAO radius of

$$R_{\text{BAO}} \simeq 140 \text{ Mpc}$$

corresponds to a volume

$$V_{\text{BAO}} \simeq \frac{4\pi}{3} R_{\text{BAO}}^3 \approx 1.1 \times 10^7 \text{ Mpc}^3.$$

For a conservative comoving number density of luminous galaxies

$$n_{\text{gal}} \sim 10^{-2} \text{ Mpc}^{-3},$$

this volume contains

$$N_{\text{gal}} \sim 10^5$$

galaxies. This sets the scale for what must be replenished over a Hubble time if the BAO correlation is to persist in a steady state.

Condensation timescale from the mesoscopic scale. In the Heisenberg virial model developed above, a local mesoscopic scale

$$\sigma \sim (1-2) H_0$$

implies a characteristic condensation or restructuring time

$$t_{\text{cond}} \sim \sigma^{-1} \sim 7-14 \text{ Gyr.}$$

This is not a microphysical star-formation time but the timescale on which mesoscopic heat routing and pseudoscalar alignment reorganize matter into long-lived bound structures.

Interpreted conservatively, this allows of order

$$\frac{N_{\text{gal}}}{t_{\text{cond}}} \sim 10^4 \text{ galaxies per Gyr per BAO volume}$$

to be replaced without rapid structural disruption.

Comparison with observed cosmic star-formation rates. The observed cosmic star-formation-rate density peaks at

$$\dot{\rho}_*^{\text{peak}} \sim 0.1-0.2 M_\odot \text{ yr}^{-1} \text{ Mpc}^{-3},$$

and remains above

$$\dot{\rho}_* \sim 10^{-2} M_\odot \text{ yr}^{-1} \text{ Mpc}^{-3}$$

for most of cosmic time. Integrated over a BAO volume, this corresponds to

$$\dot{M}_*^{\text{BAO}} \sim 10^5-10^6 M_\odot \text{ yr}^{-1}.$$

Over 10 Gyr, the cumulative stellar mass formed in a single BAO volume is therefore

$$M_*^{\text{BAO}} \sim 10^{15}-10^{16} M_\odot,$$

comparable to the stellar mass content of $\sim 10^4-10^5$ Milky-Way-scale galaxies.

Thus, *even in standard astrophysical accounting*, the baryonic processing rate within a BAO volume is already sufficient to rebuild the entire galactic population on a Hubble timescale.

Role of baryon repopulation and horizon coupling. In the present framework, this replacement does not rely solely on recycling of existing baryons. Horizon coupling continuously exports entropy and sequesters baryon number into unresolved modes, while compensating return supplies fresh low-entropy heat into the interior. The required baryon repopulation rate is therefore set by the modest replacement rate above, not by the total baryon content of the volume.

Crucially, replacement is *statistical* rather than synchronized: individual galaxies form, age, and dissolve at different times, while the BAO-scale correlation reflects a steady throughput balance rather than the identity of specific objects.

Preservation of a physical BAO scale. Because expansion is implemented as a geometric push-forward and replacement is forced only to compensate explicit loss, the system never undergoes wholesale erasure of structure on the BAO scale. Replacement occurs locally, biased by entropic throughput, and is regulated by the slow constitutive response σ . As a result, galaxy turnover can proceed continuously while the BAO-like correlation length remains locked in *physical* units.

Conclusion. Using conservative observational numbers, we find that:

- the number of galaxies per BAO volume is modest ($\sim 10^5$);
- the mesoscopic condensation timescale naturally permits their replacement over ~ 10 Gyr;
- observed cosmic baryonic processing rates already meet or exceed what is required;
- horizon-coupled baryon repopulation further relaxes any mass-budget constraint.

Galaxy replacement on the BAO scale is therefore not only feasible but *expected* in a steady-state Jacobson–Clausius universe, without smearing out a physical BAO length.

22 Mesoscopic σ Seeding, Amplification, and Relaxation in Hierarchical Structure Formation

The preceding sections treated the mesoscopic relaxation rate σ as an emergent infrared quantity, selected by entropy throughput rather than prescribed by local dynamics. In this section we clarify the *causal order of operations* by which excursions in σ participate in hierarchical structure formation and subsequently relax. The resulting picture is not monotone growth or decay, but

a delayed, sign-changing feedback loop linking early dwarf formation, environmental mesoscopic organization, and late-time isotropization of the intergalactic medium (IGM).

The σ -seeding mechanism developed in this section should be understood as a concrete realization of the dynamical regimes analyzed earlier in the thermodynamic and geometric discussion. As emphasized in Sec. 6.13, elevated σ corresponds to prolonged directional persistence and inefficient angular decorrelation, enabling organized inflow, coherent streaming, and the assembly of shallow gravitational structures, while simultaneously enforcing energetic self-limitation through mass loss and inefficient sequestration. The present section identifies dwarf-scale collapse and early environmental structure as the natural physical loci in which such high- σ excursions are first excited and amplified.

Crucially, the seeding and amplification of σ described here do not require that σ remain permanently elevated. As shown in Sec. 13.6, σ is an emergent infrared relaxation rate that decays only through slow, irreversible coarse-graining of geometric correlations. The same directional coherence that enables early hierarchical assembly ultimately drives σ self-limitation and relaxation once sustained rotation, shear, and deep potentials develop. This section therefore completes the feedback loop implicit in the earlier analysis: local excursions of σ enable structure formation, while global horizon-coupled thermodynamics ensures relaxation toward the infrared fixed point $\sigma^* \sim H_0$.

22.1 Elevated σ as a Mesoscopic Seed

We emphasize at the outset that σ is not generated *by* galaxies. Rather, localized excursions to elevated σ may arise from environmental, geometric, or boundary-driven effects prior to the formation of deep bound structures. Operationally, elevated σ indicates prolonged survival of directional information under coarse-graining, corresponding to reduced angular decorrelation and enhanced step-2 (Heisenberg) kinematics.

In regions where the gravitational potential is shallow, such elevated σ biases collapse toward anisotropic and organized inflow. Because binding energies are small, even modest directional persistence suffices to trigger early collapse on dwarf-galaxy scales. In this sense, elevated σ acts as a *mesoscopic seed*: it does not directly determine the mass scale of collapse, but preferentially selects small, early-forming, directionally organized bound systems.

22.2 Dwarf Galaxies as Environmental σ Amplifiers

Once formed, dwarf galaxies play a dual role. On the one hand, they are highly sensitive probes of the local mesoscopic state, responding strongly to elevated σ through coherent inflow, rotation, and bursty feedback. On the other hand, they act as *environmental amplifiers* of σ .

Because dwarfs reside in shallow potentials, their star formation, feedback, and orbital motions efficiently imprint directional structure on the surrounding IGM. Outflows, wakes, and anisotropic heating extend the region over which

directional correlations persist, effectively exporting mesoscopic organization beyond the immediate halo. As a result, σ becomes an *environmental* property of the surrounding IGM rather than a purely local one.

This amplification stage is crucial: it allows elevated σ to operate coherently on scales larger than individual dwarf halos, preparing the geometric and kinematic conditions necessary for subsequent assembly of more massive systems.

22.3 Coherent Assembly of Larger Galaxies from σ –Seeded Regions

Once σ is elevated over extended regions, gas accretion proceeds in a more organized manner. Directional persistence preserves angular momentum over larger distances, facilitates filamentary inflow, and supports sustained non-isotropic collapse. In this regime, deeper and more massive galaxies assemble from σ –seeded environments, rather than forming independently from an isotropic background.

Importantly, this stage does not require that σ continue to increase. Rather, it requires only that σ remain elevated long enough to organize inflow across multiple dynamical times. The mesoscopic geometry thus acts as an enabling constraint, shaping the admissible modes of assembly without dictating detailed baryonic microphysics.

22.4 Self–Limitation and Relaxation of σ

The same directional coherence that enables organized assembly ultimately triggers the self–limitation of σ . As galaxies grow and develop sustained rotation, shear, and coherent inflow, characteristic velocities rise toward binding–energy limits. At this stage, further directional persistence no longer enhances entropy throughput. Instead, it promotes mass loss, heating, and isotropization through fountains, winds, and inefficient sequestration into deep gravitational sinks.

Because σ encodes irreversible directional memory rather than instantaneous motion, its decay proceeds slowly, governed by enhanced mixing and angular decorrelation. The result is a delayed relaxation of σ toward its infrared optimum σ^* , even after baryonic fields have rapidly adjusted. Mature galaxies therefore act as σ *regulators*: enabled by elevated σ during formation, but driving its decay once coherent structure becomes dynamically excessive.

22.5 Late–Time IGM and Observable Consequences

At late times, the IGM surrounding overdense regions reflects this history of mesoscopic relaxation. Regions that hosted early σ –seeded assembly exhibit reduced directional persistence and enhanced isotropization, corresponding to a slow secular evolution of the gravitational potential. Because σ relaxes through geometric back–reaction rather than local collapse, this evolution is smooth and non–oscillatory.

Photons traversing such regions therefore experience a net positive contribution to the integrated Sachs–Wolfe signal, arising from the gradual relaxation of the mesoscopic geometry rather than from any global transition in the expansion history. Since observational tracers of overdensity are concentrated at low and intermediate redshift, ISW cross-correlations preferentially sample this late-time relaxation regime.

In the present framework, late-time overdense regions are generically sampled during the relaxation phase of the mesoscopic control variable σ . Because σ encodes directional persistence rather than instantaneous motion, its decay corresponds to a gradual reduction in organized kinematic support and a slow shallowing of the effective gravitational potential. Photons traversing such regions therefore experience a net positive integrated Sachs–Wolfe contribution. This mechanism does not rely on a global transition in the expansion history, but arises from the delayed relaxation of mesoscopic geometry following earlier structure formation.

22.6 Summary of the Mesoscopic Feedback Loop

The full causal sequence may be summarized schematically as

elevated σ \longrightarrow early dwarf formation \longrightarrow environmental σ amplification
 \longrightarrow coherent galaxy assembly \longrightarrow σ self-limitation and decay.

This loop is stabilized by the separation of timescales between fast baryonic response and slow mesoscopic relaxation. Rather than driving runaway behavior, σ excursions enable hierarchical structure formation while ensuring that the universe relaxes toward a nonequilibrium steady state with maximal entropy throughput to the horizon.

22.7 Timing of Dwarf Formation and the Persistence of Satellite Populations

A potential concern for the mesoscopic seeding picture is whether the formation of dwarf galaxies can plausibly precede, and influence, the assembly of larger systems. Here we clarify that the relevant ordering is not one of disappearance and replacement, but of early formation followed by long-lived coexistence. When interpreted in this way, the observed timing and persistence of dwarf galaxies are fully consistent with, and in fact support, the σ -seeding scenario.

Observationally, small bound systems with ancient stellar populations are known to exist at very high redshift, while dynamically settled, rotation-supported galaxies are more readily identified at later cosmic times. This observational ordering should not be read as implying a strict evolutionary succession in which dwarf galaxies precede the emergence of larger, organized systems. In the present framework, dwarf galaxies represent a persistent population of long-lived bound systems that coexist with larger galaxies at all epochs. Rotation-supported galaxies are likewise expected to be present early on, though their

dynamical maturity and observational visibility may evolve gradually. At any given time, dwarfs function as reservoirs and seeds that contribute to the ongoing formation and renewal of larger galaxies on cosmic timescales. Their continued presence as satellites of mature galaxies demonstrates that such systems are not generically erased during subsequent assembly, but instead survive as dynamically distinct subsystems within a steady, coexistent population of galactic structures.

In the present framework, this persistence has a natural interpretation. Elevated σ regions preferentially seed early collapse on dwarf scales, where shallow potentials are most sensitive to directional persistence. Once formed, these dwarfs act as environmental amplifiers of σ , imprinting directional structure on the surrounding intergalactic medium through coherent inflow, outflow, and orbital motion. As larger galaxies assemble from these σ -seeded regions, the original dwarfs are incorporated not as raw material to be homogenized, but as pre-existing bound systems that remain identifiable as satellites.

Satellite populations therefore function as a *mesoscopic fossil record* of the earlier high- σ phase. The central galaxy reflects the later stage of the feedback loop, in which sustained coherent flows and deeper potentials drive σ self-limitation and relaxation, while the satellites preserve structural and dynamical memory of the seeding and amplification stages. This naturally explains why satellite dwarfs often exhibit correlated spatial distributions, coherent orbital planes, and star-formation histories that appear decoupled from the present-day dynamics of the host.

Crucially, the timescale separation emphasized throughout this work ensures that σ need not decay before playing its organizing role. Baryonic fields respond rapidly to the instantaneous mesoscopic geometry, while σ itself evolves only through slow, irreversible coarse-graining. As a result, elevated σ can persist long enough to seed dwarfs, be amplified environmentally, and enable coherent assembly of larger systems before relaxing toward its infrared optimum. The observed coexistence of ancient dwarf satellites with dynamically mature galaxies is therefore not incidental, but a direct consequence of mesoscopic self-regulation.

In this sense, the hierarchical appearance of structure reflects not merely a statistical ordering of mass scales, but a causal sequence governed by mesoscopic admissibility. Dwarf galaxies form early because they are the smallest systems capable of exploiting elevated σ , and they persist because the later relaxation of σ acts on the surrounding geometry rather than retroactively erasing bound structure.

22.8 Temperature–Polarization Correlations: Interpretation of EE and TE

The angular polarization of the cosmic microwave background provides an important consistency check on any proposed cosmological framework. In particular, the observed E-mode auto-correlation spectrum (EE) and temperature–E-mode cross-correlation spectrum (TE) are often regarded as sensitive probes of

primordial initial conditions. In the present framework, however, these observables admit a simpler and more structural interpretation. They arise as generic consequences of a stationary, well-mixed radiative field subject to large-scale geometric forcing, rather than as fossils of a specific early-universe epoch.

In this subsection we clarify (i) what the EE and TE observables measure, (ii) why their near-Gaussian statistics are expected in an open, horizon-coupled radiative system, and (iii) how their qualitative features follow naturally from the coexistence of a mesoscopic angular mixing scale σ , a BAO-scale forcing spectrum, and sub-Laplacian angular transport.

22.8.1 Observables and definitions.

The observed CMB temperature field $T(\hat{n})$ and E-mode polarization field $E(\hat{n})$ are expanded in spherical harmonics,

$$T(\hat{n}) = \sum_{\ell m} a_{\ell m}^T Y_{\ell m}(\hat{n}), \quad E(\hat{n}) = \sum_{\ell m} a_{\ell m}^E Y_{\ell m}(\hat{n}), \quad (265)$$

with angular power spectra defined by ensemble averages

$$C_{\ell}^{TT} = \langle |a_{\ell m}^T|^2 \rangle, \quad C_{\ell}^{EE} = \langle |a_{\ell m}^E|^2 \rangle, \quad C_{\ell}^{TE} = \langle a_{\ell m}^T a_{\ell m}^{E*} \rangle. \quad (266)$$

The EE spectrum measures the variance of parity-even (gradient-type) polarization, while the TE spectrum measures the statistical coherence between temperature anisotropies and polarization anisotropies on the same angular scales.

Crucially, neither observable directly measures a matter density field nor a primordial curvature perturbation. They characterize the angular structure of the photon bath as observed on the sky.

22.8.2 Physical origin of E-mode polarization.

Linear polarization of the CMB arises from Thomson scattering of radiation with a quadrupolar angular anisotropy. E-modes therefore measure the presence of directional (specifically, quadrupolar) structure in the radiation field at the time and location of scattering. They do not encode a record of scalar density perturbations directly, but rather of angular anisotropy in the photon distribution function.

From this perspective, the existence of E-modes requires only two ingredients: (i) a mechanism that produces angular anisotropy in the radiation field, and (ii) sufficient coherence of that anisotropy over angular scales large enough to be observed. Both ingredients are generic in the horizon-coupled steady-state framework developed here.

22.8.3 Gaussianity as a generic consequence of angular mixing.

One of the most robust empirical facts about the E-mode field is its near Gaussianity: for fixed ℓ , the coefficients $a_{\ell m}^E$ are well described by Gaussian random

variables with variance C_ℓ^{EE} . In the present framework this property is not surprising and requires no special assumptions about initial conditions.

The photon bath is a stationary, open radiative system undergoing continual injection, scattering, absorption, and redistribution of angular modes. Angular anisotropies are generated additively by many weak, incoherent processes—including gravitational lensing, Doppler shifts, and geometric shear—and are continually mixed by sub-Riemannian angular transport. In such a regime, the central limit theorem applies: the resulting angular mode amplitudes approach Gaussian statistics irrespective of the detailed microphysics of individual events.

The mesoscopic scale σ plays a central role here. As discussed in Sections 11 and 17, σ governs the rate of angular phase mixing induced by the Carnot–Carathéodory geometry. It controls how rapidly directional information decorrelates and sets the effective angular response kernel of the photon bath. Gaussianity of E-modes is therefore a kinematic and thermodynamic consequence of efficient angular mixing in a stationary radiative medium, not a relic of primordial quantum fluctuations.

22.8.4 Separation of forcing and processing scales.

It is important to distinguish between two physically distinct scales that enter the polarization problem. The first is the mesoscopic angular mixing scale σ , which controls how angular anisotropies propagate, mix, and decohere. The second is the characteristic spatial forcing scale associated with large-scale structure, most notably the baryon acoustic oscillation (BAO) scale.

In this framework, the BAO scale determines where matter correlations are strong and therefore where gravitational lensing and large-scale geometric distortions are most effective. These BAO-scale structures act as a source of correlated angular forcing on the photon bath. The role of σ is not to set the location of these correlations in ℓ -space, but to determine how the induced anisotropies are processed once generated. Observed EE power spectra should therefore be understood as BAO-scale forcing filtered through a σ -controlled angular transport kernel.

This division of labor is essential. It prevents the mesoscopic scale σ from being overburdened with structural responsibilities that properly belong to the matter sector, and it aligns naturally with the discussion of BAO observables in Section 20.

22.8.5 Interpretation of the EE spectrum.

With this separation in mind, the qualitative features of the EE spectrum are readily understood. Large-scale matter correlations induce angular anisotropies in the photon field through lensing and path distortion. These anisotropies generate quadrupolar structure at scattering, producing E-mode polarization. The angular coherence and smoothness of the resulting EE spectrum reflect the efficiency of angular mixing governed by σ , while the location of enhanced power reflects the underlying BAO-scale forcing spectrum.

No special tuning is required to obtain a smooth, nearly Gaussian EE spectrum with a characteristic angular scale. Such behavior is the generic outcome of a stationary radiative system subject to broadband large-scale forcing and efficient sub-Laplacian mixing.

22.8.6 Interpretation of the TE cross-correlation.

The TE spectrum measures whether the same spacetime processes that modulate the brightness of the CMB also induce directional anisotropy in a coherent way. A nonzero TE signal therefore indicates shared dynamical origin, not direct causation.

In the present framework, BAO-scale structure and associated geometric distortions influence both the scalar temperature field and the quadrupolar anisotropy responsible for polarization. When these responses are phase-aligned, TE is positive; when they are anti-aligned, TE is negative. The sign and scale dependence of TE therefore reflect the relative phase between scalar brightness modulation and quadrupolar angular forcing, as processed by σ -controlled angular transport.

Importantly, TE does not represent a correlation between present-day matter and a primordial temperature field. It measures the statistical coherence between two responses of the same radiation field to shared spacetime dynamics. This interpretation requires no appeal to distinct growth or decay epochs of gravitational potentials and is fully compatible with a steady-state cosmology.

22.8.7 Summary.

Within a horizon-coupled, mesoscopic cosmological framework, the existence and qualitative properties of EE and TE polarization spectra are natural and expected. E-mode polarization reflects the variance of directional anisotropy in a well-mixed photon bath; its Gaussianity follows from additive forcing and efficient angular mixing. The BAO scale supplies the dominant spatial forcing, while the mesoscopic scale σ governs angular transport and coherence. TE correlations arise when the same large-scale geometric structures modulate both temperature and polarization in a phase-coherent manner. None of these features require primordial fine-tuning or special initial conditions; they are structural consequences of the open, stationary, sub-Riemannian cosmology developed in this work.

23 Ledger Area, Parity, and the Forced Form of the σ Dynamics

Irreversible coarse-graining eliminates almost all directional information carried by a microscopic trajectory. In the planar diffusive setting considered here, this elimination is essentially complete: after truncation of the rough-path lift at step 2, there exists a *single* surviving orientation-sensitive quantity, the Lévy

area. All other directional data—including linear increments, higher iterated integrals, and detailed geometric correlations—either lose invariant meaning or are rendered purely fluctuational.

This structural collapse has immediate consequences. Any persistent memory of orientation or handedness must be mediated through the Lévy-area channel, and no additional pseudoscalar degree of freedom may be introduced without reintroducing discarded microscopic structure. In particular, any constitutive response that survives coarse-graining must be built exclusively from quantities that transform appropriately under orientation reversal and are measurable on the reduced state space.

The purpose of this section is to show that these constraints *force* the form of the slow constitutive dynamics. We introduce a pseudoscalar order parameter σ as a nonlinear memory of directional structure encoded in signed-area production, and we show that its intrinsic evolution is uniquely constrained by parity, locality, and irreversibility. The resulting Landau-type evolution law is not a modeling choice but a consequence of the available invariant structure after coarse-graining.

A central role is played by the pseudoscalar drift J , defined as the predictable component of Lévy-area production at the system level. It is essential to distinguish between J as an *ontic* drift—which may be nonzero and even sign-definite in perfectly coherent or symmetric motions—and the quantities that may enter constitutive response. The order parameter σ does not respond to raw pseudoscalar drift, nor to its sign. Rather, it responds only to the *intensity of unresolved pseudoscalar production*: that part of the signed-area dynamics which remains unpredictable on the macroscopic (Hubble) time scale.

Observer-level coarse-graining is implemented by a filtration \mathcal{O}_t encoding Hubble-scale predictability. Projection onto this filtration separates the system-level drift into resolved and unresolved components. While coherent rotation may generate a large system-level pseudoscalar drift, such motion is typically predictable on macroscopic time scales and therefore contributes to the resolved state rather than to constitutive memory. The admissible constitutive drive is instead a scalar quantity constructed from the observer-unresolved component of the drift, namely the conditional intensity $\mathbb{E}[J_{\text{res}}^2 | \mathcal{O}_t]$. This quantity controls whether the neutral state $\sigma = 0$ is stable or unstable, but does not itself supply a handedness.

Once this distinction is kept explicit, the apparent paradox that coherent rotation produces substantial signed-area drift yet relaxes pseudoscalar memory is resolved. Coherent, Hubble-predictable motion contributes to resolved kinematics, while only unresolved pseudoscalar fluctuations can destabilize the neutral constitutive state. The sign of σ , when amplified, is therefore selected locally and historically rather than imposed by the driving term.

We proceed in stages. We first establish the uniqueness and parity properties of the Lévy area and construct the associated scalar ledger variable. We then derive the forced form of the σ dynamics using Onsager–Machlup theory, showing that unresolved pseudoscalar intensity can only enter multiplicatively, as a control parameter for a symmetry-breaking instability. Only after this system–

level structure is fixed do we address how observer resolution enters through projection, and why coherent macroscopic rotation typically relaxes rather than amplifies pseudoscalar memory.

23.1 Lévy Area as the Unique Surviving Orientation Invariant

Consider a planar stochastic trajectory $B_t = (X_t, Y_t)$ generated by a microscopic dynamics with short-range correlations. Under diffusive coarse-graining, the path is canonically lifted to a rough path and then truncated at step 2. All iterated integrals of order three and higher vanish in the coarse limit, while linear increments lose invariant directional meaning due to isotropization.

The sole nontrivial second-order object that survives this truncation is the antisymmetric area component of the lift, the Lévy area,

$$A_t = \int_0^t (Y_s \circ dX_s - X_s \circ dY_s), \quad (267)$$

where \circ denotes Stratonovich integration. Equivalently, A_t is the signed area enclosed by the trajectory up to time t .

Under orientation reversal in the plane, $(X, Y) \mapsto (X, -Y)$, the Lévy area changes sign:

$$A_t \mapsto -A_t. \quad (268)$$

Thus A_t is a *pseudoscalar*. No other pseudoscalar quantity remains after coarse-graining: all symmetric second-order components are scalars, while all higher-order antisymmetric objects are eliminated by the truncation.

This uniqueness has important structural consequences. Any directional or chiral information that persists under coarse-graining must be encoded entirely through A_t . In particular, there exists exactly one pseudoscalar channel available to the reduced dynamics. Any attempt to introduce additional orientation-sensitive degrees of freedom would necessarily reintroduce discarded microscopic structure and violate the closure of the coarse-grained description.

Accordingly, the Lévy area must be regarded as an *ontic ledger variable*: it is not an optional diagnostic, but a required component of the reduced state that restores Markovianity after irreversible elimination of higher-order path information. All constitutive memory of orientation must ultimately be slaved to this unique channel.

23.2 The Ledger Variable and Parity

The uniqueness of the Lévy-area channel implies that any constitutive memory of orientation must couple to A_t in a parity-consistent manner. We therefore introduce a slow pseudoscalar *memory process* σ_t , carried by each coarse-grained worldline. The variable σ_t is not a kinematic function of the reduced state (X_t, A_t) , but an internal constitutive degree of freedom that evolves autonomously on a slow time scale.

When convenient, we will write $\sigma(t, x, a)$ to denote the conditional expectation

$$\sigma(t, x, a) := \mathbb{E}[\sigma_t | X_t = x, A_t = a],$$

which provides a mesoscopic representation of the memory statistics on the reduced state space. This notation does not imply that σ_t is a function of (X_t, A_t) , nor that it is advected or reconstructed from the reduced kinematics. By construction,

$$\sigma \mapsto -\sigma \quad \text{under orientation reversal,} \quad (269)$$

so σ has the same parity as A .

The role of σ is not to encode microscopic geometry, but to provide a slow, nonlinear memory of sustained *unresolved pseudoscalar activity* in the signed-area channel. It is an intensive field, defined independently of any particular realization of the path, and carries no additional directional information beyond that already present in the Lévy-area channel.

From A_t and σ one may form a scalar accumulation, the *ledger variable* L_t , defined by the differential relation

$$dL_t = \sigma_t \circ dA_t. \quad (270)$$

Here σ_t denotes the worldline-carried pseudoscalar memory process; no functional dependence on (X_t, A_t) is implied. Since both σ and dA are pseudoscalars, their product is invariant under orientation reversal. Thus L_t is a true scalar and represents the unique scalar quantity that can be accumulated from the surviving pseudoscalar channel.

The ledger L_t plays the role of an integrated record of directional memory. Importantly, its existence does not introduce new degrees of freedom: given the reduced state (X_t, A_t) and the constitutive field σ , the evolution of L_t is completely determined. Conversely, no other scalar accumulation sensitive to orientation can be constructed without violating parity or reintroducing eliminated structure.

At this stage, no assumptions have yet been made about the intrinsic dynamics of σ . No assumptions have been made about its sources or its relaxation. Those will be fixed in subsequent subsections by imposing locality, irreversibility, and global symmetry constraints.

23.3 Worldline Memory Versus Mesoscopic Representation of σ

The pseudoscalar memory σ_t is a slow internal degree of freedom carried by each coarse-grained worldline. It is not a function of the reduced state (X_t, A_t) and is not transported, advected, or geometrically sampled along the trajectory. Its evolution represents intrinsic constitutive memory rather than kinematic motion.

Accordingly, σ_t evolves by its own intrinsic dynamics, independent of instantaneous increments of X_t or A_t . In particular, there are no transport, chain-rule,

or Itô correction terms associated with the evolution of σ_t . All such geometric effects are confined to the reduced state variables (X_t, A_t) themselves.

When a mesoscopic field $\sigma(t, x, a)$ is introduced later, it is understood as a statistical descriptor of the ensemble of worldline memories, for example through a conditional expectation $\mathbb{E}[\sigma_t | X_t = x, A_t = a]$. This representation is purely descriptive and does not alter the intrinsic dynamics of the memory process.

This separation is essential. It ensures that σ_t encodes slow constitutive response rather than passive transport, and prevents the reintroduction of discarded microscopic structure through kinematic coupling.

We define the intrinsic time derivative of σ by

$$\dot{\sigma}(t, x, a) \equiv \partial_t \sigma(t, x, a), \quad (271)$$

holding the reduced coordinates (x, a) fixed. This derivative represents the autonomous evolution of the constitutive memory at a given coarse state. It is not a material derivative and does not encode transport along the path.

By contrast, when a mesoscopic representation of the memory is introduced,

$$\sigma(t, x, a) := \mathbb{E}[\sigma_t | X_t = x, A_t = a],$$

it serves only as a statistical descriptor of the ensemble of worldline memories at a given reduced state. Evaluating this conditional expectation along a realization of the reduced process (X_t, A_t) does *not* define the intrinsic evolution of the memory process itself. Any stochastic differential satisfied by $\sigma(t, X_t, A_t)$ arises solely from the motion of the reduced state through (x, a) -space and reflects how the ensemble average is sampled as the system evolves.

Such terms are kinematic in origin. They describe the transport of a fixed statistical field through the reduced state space and would involve chain-rule contributions associated with dX_t and dA_t . They do not correspond to intrinsic memory formation, do not generate constitutive response, and are not retained in the coarse-grained constitutive dynamics. All intrinsic evolution of pseudoscalar memory is instead encoded in the autonomous dynamics of the worldline process σ_t , as specified by its generator.

This distinction is crucial. The purpose of σ is to encode slow constitutive response, not passive advection or geometric transport. Accordingly, the constitutive law governing σ must be expressed entirely in terms of its intrinsic evolution $\partial_t \sigma$.

This separation cleanly decouples fast kinematics from slow memory. The geometry determines how the reduced state moves, while σ responds only to coarse, parity-admissible *control parameters* derived from the reduced dynamics. The form of that response is fixed in the next subsection by imposing irreversibility and Onsager symmetry.

23.4 Onsager Forcing and the Forced Landau Form

Having eliminated microscopic path information and reduced the dynamics to a Markovian system-level state, the constitutive field σ evolves on a slow, coarse-grained time scale. At this level its intrinsic evolution is governed by irreversible

relaxation and is therefore subject to Onsager–Machlup theory. In particular, the intrinsic dynamics of σ must be dissipative and expressible, at leading order, as a gradient flow with respect to an effective scalar functional:

$$\partial_t \sigma = -\Gamma \frac{\partial F}{\partial \sigma}, \quad \Gamma > 0. \quad (272)$$

Here F is not a microscopic free energy, but a coarse–grained generator encoding the leading irreversible response permitted by symmetry and locality.

The functional F may depend on the reduced state and on σ itself, but it must respect the parity structure imposed by coarse–graining. Under orientation reversal, σ changes sign. Consequently, no pseudoscalar quantity may appear linearly in F . In particular, although the reduced dynamics admits a unique pseudoscalar rate associated with signed–area production, its sign cannot act as a constitutive forcing.

The only admissible influence of pseudoscalar dynamics on σ must therefore enter through parity–even scalar quantities constructed from that channel. At leading order, the unique such quantity is the intensity of unresolved pseudoscalar production. We denote by

$$K := \mathbb{E}[J_{\text{res}}^2 | \mathcal{O}_{t-}]$$

the conditional second moment of the observer–unresolved component of the system–level pseudoscalar drift. This scalar controls whether the neutral constitutive state $\sigma = 0$ is stable or unstable, but does not itself supply a handedness.

Parity invariance therefore imposes

$$F(\sigma; K) = F(-\sigma; K), \quad (273)$$

so that F is an even function of σ .

Parity invariance alone does not forbid a term linear in both the order parameter and the pseudoscalar drift, such as σJ_{proj} , since the product of two pseudoscalars is parity–even. However, such a term is inadmissible on constitutive grounds. Any contribution proportional to σJ_{proj} would cause the memory process to track a *predictable* pseudoscalar bias carried by the observer–resolved component of the drift. This would imprint a preferred handedness determined by \mathcal{O}_t –measurable kinematics and thereby violate predictability neutrality.

Constitutive memory is required to be orthogonal to all Hubble–predictable pseudoscalar structure. Accordingly, no term linear in σ and proportional to an \mathcal{O}_t –measurable pseudoscalar may appear in the intrinsic dynamics. The only admissible influence of pseudoscalar activity is therefore through parity–even *scalar* functionals of the observer–unresolved component of the drift, most notably the conditional intensity $\mathbb{E}[J_{\text{res}}^2 | \mathcal{O}_t]$. This restriction excludes linear forcing while allowing instability–controlled symmetry breaking without introducing a global or predictable handedness bias.

Expanding F in powers of σ and retaining the leading terms consistent with stability, locality, and irreversibility yields

$$F(\sigma; K) = \frac{1}{2} (\gamma - \alpha K) \sigma^2 + \frac{\lambda}{4} \sigma^4, \quad \alpha, \gamma, \lambda > 0. \quad (274)$$

Odd powers of σ are forbidden by parity, while higher-order terms are suppressed by additional powers of the slow scale.

The resulting intrinsic evolution equation is

$$\partial_t \sigma = (\alpha K - \gamma) \sigma - \lambda \sigma^3. \quad (275)$$

This is a Landau-type equation with a control parameter K that modulates the stability of the neutral state. When $K < \gamma/\alpha$, the constitutive memory relaxes and $\sigma \rightarrow 0$. When $K > \gamma/\alpha$, the neutral state becomes unstable and σ grows until nonlinear saturation balances the instability. The sign of σ is not imposed by the driving term but selected locally and historically once the instability opens.

This form is not a phenomenological ansatz. It is the unique leading-order dissipative dynamics compatible with Onsager symmetry, parity, and the absence of any admissible linear pseudoscalar forcing. Unresolved pseudoscalar activity can only influence σ by opening or closing a growth channel; it cannot directly bias the order parameter.

Spatial or geometric couplings may be included at higher order. The leading parity-even correction consistent with irreversibility is a quadratic gradient term,

$$F(\sigma; K) = \frac{1}{2} (\gamma - \alpha K) \sigma^2 + \frac{\lambda}{4} \sigma^4 + \frac{\eta}{2} |\nabla \sigma|^2 + \dots, \quad \eta > 0, \quad (276)$$

(or, in the Carnot–Carathéodory setting, $\frac{\eta}{2} |\nabla_{CC} \sigma|^2$). Onsager gradient flow then yields the Ginzburg–Landau form

$$\partial_t \sigma = (\alpha K - \gamma) \sigma - \lambda \sigma^3 + \eta \Delta \sigma + \dots, \quad (277)$$

with Δ replaced by the appropriate sub-Laplacian when anisotropic or constrained mixing is intended. The diffusion term represents the leading mixing correction in the same symmetry-controlled expansion that produces the local nonlinear dynamics.

23.5 Why All Nontrivial Constitutive Control Resides in the Lévy Channel

Equation (275) makes clear that the constitutive field σ is not a generator of geometric structure. It is a symmetry-breaking order parameter whose intrinsic dynamics is dissipative and whose nontrivial behavior arises only through instability. In the absence of admissible control, the intrinsic evolution is purely relaxational: σ decays toward zero and does not retain persistent information.

Spatial or geometric couplings acting on σ serve only to redistribute or mix existing memory within the reduced state space. Such couplings do not generate pseudoscalar structure on their own, but merely renormalize the rate and manner in which σ relaxes when the neutral state is stable.

All nontrivial *constitutive control* therefore enters through the Lévy–area channel. The reduced dynamics admits a unique pseudoscalar rate associated

with signed-area production, encoded in the system-level drift J_{sys} . However, σ does not respond to this drift directly, nor to its sign. Instead, constitutive dynamics is controlled by the intensity of pseudoscalar activity that remains *unresolved* on the observer time scale.

Specifically, the relevant quantity is the scalar

$$K = \mathbb{E}[J_{\text{res}}^2 | \mathcal{O}_t],$$

the conditional second moment of the observer-unresolved component of the pseudoscalar drift. This quantity modulates the stability of the neutral constitutive state. When K is below threshold, $\sigma = 0$ is stable and all memory relaxes. When K exceeds threshold, the neutral state becomes unstable and σ grows until nonlinear saturation balances the instability. The sign of σ is not imposed by the driving term but selected locally and historically once instability opens.

By contrast, the drift J_{sys} itself carries the geometric and kinematic information that survives system-level coarse-graining of the underlying motion. It may be large and sign-definite in perfectly coherent or symmetric flows. Such contributions represent resolved kinematics rather than constitutive memory and do not, by themselves, destabilize σ . Only the observer-unresolved variance of this drift influences constitutive response.

This hierarchy of roles may be summarized as follows:

Quantity	Structural role
A_t	Raw pseudoscalar current (Lévy area)
J_{sys}	System-level pseudoscalar drift
J_{res}	Observer-unresolved pseudoscalar component
$K = \mathbb{E}[J_{\text{res}}^2 \mathcal{O}_t]$	Scalar instability control
σ	Symmetry-breaking constitutive order parameter
L_t	Scalar ledger (integrated record)

Because σ is a parity-odd constitutive memory rather than a kinematic variable, it does not respond to instantaneous or purely fluctuational signed-area production. Nor does it integrate a pseudoscalar flux. Only sustained observer-unresolved pseudoscalar activity can destabilize the neutral state and allow constitutive memory to form.

Equivalently, pseudoscalar structure that is predictable with respect to the observer filtration \mathcal{O}_t contributes to resolved kinematics rather than to constitutive memory. Such contributions do not accumulate in σ . By contrast, irregular, intermittent, or symmetry-breaking circulation generates a substantial unresolved component whose variance controls the onset of constitutive response.

The Landau form (275) therefore does not privilege any specific mechanism of rotation, shear, or circulation. All such mechanisms influence σ only insofar as they contribute to the observer-unresolved pseudoscalar intensity. Once this scalar control parameter is specified, the intrinsic response of σ is fully determined.

This separation of roles is essential. It ensures that constitutive memory is neither arbitrarily introduced nor spuriously amplified by transient geometric effects. All detailed physics enters the theory through the definition and evaluation of the Lévy–area drift and its observer–relative decomposition, which we now make precise.

23.6 The Coarse Pseudoscalar Flux as a Projection Operator

The pseudoscalar rate J appearing in the reduced description is not an additional dynamical variable. It is the system–level projection of the microscopic dynamics onto the unique surviving pseudoscalar channel. This projection may be defined precisely using conditional expectation.

Let (X_t, A_t) denote the reduced Markovian state obtained after system–level coarse–graining, and let \mathcal{F}_t be the filtration it generates. The Lévy area A_t is a real–valued special semimartingale adapted to \mathcal{F}_t , and therefore admits a unique Doob decomposition. In differential form,

$$dA_t = \mathbb{E}[dA_t | \mathcal{F}_t] + \left(dA_t - \mathbb{E}[dA_t | \mathcal{F}_t] \right), \quad (278)$$

where the first term is predictable and the second is a martingale increment.

We define the coarse pseudoscalar flux J by

$$\boxed{\mathbb{E}[dA_t | \mathcal{F}_{t-}] = J_{\text{sys}}(Z_t) dt.} \quad (279)$$

By construction, J is \mathcal{F}_{t-} –adapted, transforms as a pseudoscalar under orientation reversal, and represents the *system–level predictable* component of signed–area production.

All remaining contributions to dA_t are purely fluctuational and average to zero under coarse–graining. No additional pseudoscalar structure survives at the system level. In particular, any two microscopic models that induce the same predictable Lévy–area drift J are indistinguishable to the reduced dynamics.

It is important to emphasize what this definition does *not* imply. The drift J need not vanish in symmetric or coherent motions. For example, rigid rotation or steady shear may produce a sign–definite pseudoscalar drift. At this stage, J is an ontic quantity fixed entirely by the reduced dynamics; no symmetry, neutrality, or observer–resolution constraint has yet been imposed.

Equation (279) therefore isolates the only pseudoscalar current that survives system–level coarse–graining. At this stage, J is a purely kinematic quantity: it characterizes predictable signed–area production in the reduced dynamics but does not, by itself, constitute a source of constitutive memory.

How observer–level coarse graining further decomposes this drift into resolved and unresolved components, and how scalar quantities derived from the unresolved part control constitutive instability, will be addressed in subsequent subsections.

23.7 Continuum Interpretation: Vorticity and Shear

The abstract definition of the pseudoscalar flux J in (279) admits a natural interpretation in continuum settings. Consider a planar diffusion with drift $b(x) \in \mathbb{R}^2$,

$$dX_t = b(X_t) dt + dW_t, \quad (280)$$

and let A_t denote the associated Lévy area. A direct calculation shows that the differential of A_t decomposes as

$$dA_t = X_t \wedge b(X_t) dt + X_t \wedge dW_t, \quad (281)$$

where $x \wedge y := x_1 y_2 - x_2 y_1$. The second term is a martingale increment with zero conditional mean, while the first term is predictable. Accordingly, the system-level pseudoscalar drift is

$$J(x) = x \wedge b(x). \quad (282)$$

For a rigid rotation with angular speed Ω , $b(x) = \Omega(-x_2, x_1)$, one finds

$$J(x) = \Omega |x|^2, \quad (283)$$

which is sign-definite and nonzero throughout the domain. Thus coherent rotation generally produces a nonvanishing pseudoscalar drift J . This is fully consistent with the system-level definition: nothing in the coarse-grained dynamics forbids a persistent signed-area rate.

More generally, J measures the component of the flow that produces systematic signed area relative to the coarse position. It may receive contributions from vorticity, curvature of streamlines, or large-scale geometric asymmetry. However, J is not identical to pointwise vorticity. Pure shear flows, for example, can exhibit substantial local velocity gradients while producing no sustained signed-area drift once averaged over the reduced state. In such cases, the predictable component of dA_t vanishes even though the microscopic deformation is nontrivial.

This distinction is essential. The pseudoscalar flux J is not a local kinematic invariant but a *coarse moment* of the motion. It captures precisely that part of the continuum dynamics which survives projection onto the Lévy-area channel. All other geometric information is eliminated by coarse-graining and cannot enter the constitutive response except through scalar quantities derived from this channel.

At this level, no restriction has been placed on the magnitude or sign of the system-level drift J . In particular, coherent rotation may generate a large and sign-definite pseudoscalar drift without contradiction. However, J itself remains a kinematic quantity. Whether and how pseudoscalar activity influences constitutive memory depends not on the drift directly, but on observer-level decomposition and on scalar quantities constructed from the unresolved component of this drift, introduced in subsequent subsections.

23.8 System–Level Versus Observer–Level Coarse Graining

Up to this point, coarse–graining has been applied at the *system level*. Microscopic path information is irreversibly eliminated until a minimal reduced state is obtained for which the dynamics is Markovian. In the planar diffusive setting, this reduction is forced and unique: the reduced state is (X_t, A_t) , where A_t is the Lévy–area ledger variable. No further path–dependent information may be retained at the system level without destroying closure or reintroducing hidden memory.

System–level coarse graining therefore answers the question: *what variables must the system itself carry in order for the reduced dynamics to be well defined and Markovian?* The answer is fixed by the dynamics and does not depend on observation, resolution, or modeling choice. At this level, the pseudoscalar drift J defined by (279) is an ontic quantity: it is the predictable component of Lévy–area production with respect to the full reduced filtration \mathcal{F}_t .

A logically distinct notion is *observer–level coarse graining*. Here one specifies a sub– σ –algebra

$$\mathcal{O}_t \subseteq \mathcal{F}_t,$$

representing the degrees of freedom that a finite observer is able to resolve. Observer–level coarse graining is implemented by conditional expectation $\mathbb{E}[\cdot | \mathcal{O}_t]$ and reflects epistemic limitation rather than dynamical necessity.

Crucially, enlarging or shrinking \mathcal{O}_t does *not* alter the reduced state (X_t, A_t) or its Markovianity. The system does not acquire new degrees of freedom when the observer resolves more structure. All observer–level coarse graining operates *within* the fixed system–level state and can only redistribute information between predictable and fluctuational components relative to the observer.

This distinction is essential for interpreting the pseudoscalar flux. The quantity J defined at the system level captures the predictable Lévy–area drift with respect to the full reduced dynamics. By contrast, observer–level coarse graining determines which parts of this drift are regarded as *resolved* and which remain *unresolved* from the observer’s perspective. Only the unresolved component can contribute to constitutive control, and only through scalar quantities constructed from it.

Failure to distinguish these two notions leads to apparent paradoxes. In particular, one may be tempted to identify coherent macroscopic rotation with vanishing pseudoscalar drift. This is incorrect at the system level: coherent rotation generally produces a nonzero J . The resolution of this tension lies not in redefining J , but in recognizing that constitutive dynamics is insensitive to the drift itself and depends only on scalar quantities derived from the observer–unresolved component. Observer resolution and global symmetry therefore constrain not the existence of J , but whether unresolved pseudoscalar activity is sufficient to destabilize the neutral constitutive state.

23.9 Resolved Motion, Unresolved Circulation, and the Definition of J

The pseudoscalar drift J defined in (279) is an ontic, system-level quantity: it is the predictable component of Lévy-area production with respect to the full reduced filtration \mathcal{F}_t . As such, J characterizes the kinematic production of signed area in the reduced dynamics, independent of observation or constitutive response.

The constitutive field σ , however, is not driven by raw pseudoscalar drift. Nor does it respond to the sign of J . Constitutive dynamics is sensitive only to those aspects of pseudoscalar activity that remain *unresolved* on the observer time scale, and even then only through parity-even scalar quantities constructed from that unresolved component.

Let $\mathcal{O}_t \subseteq \mathcal{F}_t$ denote a chosen observer σ -algebra, representing the degrees of freedom that a finite observer can resolve. Observer-level coarse graining is implemented by conditional expectation. Decomposing the Lévy-area increment relative to this filtration yields

$$dA_t = \mathbb{E}[dA_t | \mathcal{O}_t] + \left(dA_t - \mathbb{E}[dA_t | \mathcal{O}_t] \right), \quad (284)$$

where the first term is predictable from the observer's retained state and the second is fluctuational from that perspective.

Correspondingly, we define the observer-relative predictable pseudoscalar rate by

$$\mathbb{E}[dA_t | \mathcal{O}_t] = J_{\text{proj}}(t) dt. \quad (285)$$

By construction, J_{proj} is \mathcal{O}_t -measurable and transforms as a pseudoscalar. It coincides with the system-level drift J only when $\mathcal{O}_t = \mathcal{F}_t$.

The difference

$$J_{\text{res}}(t) := J_{\text{sys}}(t) - \mathbb{E}[J_{\text{sys}}(t) | \mathcal{O}_t] \quad (286)$$

represents the observer-unresolved component of pseudoscalar drift. This quantity is orthogonal to $L^2(\mathcal{O}_t)$ and encodes pseudoscalar activity that is unpredictable on the observer time scale.

Crucially, neither J_{proj} nor J_{res} acts as a constitutive forcing by itself. The order parameter σ does not integrate a residual flux, nor does it respond linearly to unresolved circulation. Instead, constitutive control enters only through parity-even scalar quantities constructed from the unresolved component. At leading order, the unique such quantity is the conditional intensity

$$\mathbb{E}[J_{\text{res}}^2 | \mathcal{O}_t],$$

which modulates the stability of the neutral constitutive state.

This distinction resolves apparent tensions. Even in a perfectly coherent flow, the system-level drift J may be large and sign-definite. If that drift is predictable on the observer time scale, then J_{res} is small and the neutral state $\sigma = 0$ remains stable. Conversely, irregular, intermittent, or symmetry-breaking

circulation produces a substantial unresolved component whose variance can destabilize the neutral state and allow constitutive memory to form.

The system-level definition of J is never altered. Observer resolution enters only through projection, determining which aspects of pseudoscalar activity are resolved kinematically and which contribute, through their intensity, to constitutive instability. Once these roles are kept distinct, apparent contradictions between coherent rotation and memory relaxation disappear.

23.10 Coherent Rotation and the Relaxation of σ

We may now resolve the apparent tension between coherent macroscopic rotation and the relaxational behavior of the pseudoscalar order parameter. The resolution rests entirely on the distinction between system-level kinematics and constitutive instability control.

As shown in Subsection 23.7, coherent rotation generally produces a nonvanishing system-level pseudoscalar drift J_{sys} . For example, rigid or differentially rotating flows yield a sign-definite pseudoscalar moment of the velocity field. There is therefore no sense in which coherent rotation suppresses signed-area production at the level of the reduced dynamics.

However, constitutive memory does not respond to pseudoscalar drift itself, nor to its sign. The order parameter σ represents a symmetry-breaking constitutive degree of freedom and cannot acquire a uniform handedness bias. Its intrinsic dynamics is controlled instead by a scalar quantity: the intensity of pseudoscalar activity that remains unresolved on the observer time scale.

In systems dominated by coherent rotation, the induced pseudoscalar drift is largely \mathcal{O}_t -predictable on the Hubble time scale. As a result, the observer-unresolved component J_{res} has small variance, and the scalar control parameter

$$K = \mathbb{E}[J_{\text{res}}^2 \mid \mathcal{O}_t]$$

remains below the instability threshold. The neutral state $\sigma = 0$ is therefore stable, and the intrinsic dynamics of σ is relaxational despite the presence of a large system-level drift.

This behavior is characteristic of dynamically mature systems, such as spiral disks, in which large-scale rotation is coherent, sustained, and resolved. Such systems exhibit substantial signed-area production, but that production is kinematic rather than constitutive and does not generate new directional memory.

By contrast, in systems lacking sustained coherent rotation—for example, small, irregular, or interacting systems—pseudoscalar activity is intermittent, spatially structured, and poorly predicted on macroscopic time scales. In these regimes, the observer-unresolved component J_{res} has substantial variance, so that K exceeds threshold and the neutral state becomes unstable. The order parameter σ is then amplified until nonlinear saturation balances the instability. The sign of σ is selected locally and historically, not imposed by the driving term.

The theory therefore predicts a clear qualitative distinction. Systems with strong, coherent rotational symmetry tend to *relax* pseudoscalar memory, while

systems with broken symmetry or intermittent circulation tend to *amplify* it. This distinction arises not from the magnitude of signed-area production, but from the predictability and symmetry structure of that production.

No contradiction exists between these behaviors. The system-level pseudoscalar drift J_{sys} may be large in both cases. What differs is whether unresolved pseudoscalar activity is sufficient to destabilize the neutral constitutive state and permit memory formation.

23.11 Ontological Status of σ , A , and J

The construction developed above involves three conceptually distinct objects: the Lévy area A_t , the pseudoscalar drift J , and the constitutive field σ . Although they are linked through coarse-graining, they play fundamentally different ontological roles. Keeping these roles distinct is essential for a consistent interpretation of the constitutive dynamics.

23.11.1 The Lévy area A_t .

The variable A_t is an *ontic ledger variable*. Its introduction is forced by system-level coarse-graining: without A_t , the reduced dynamics fails to be Markovian. A_t is part of the system's state, not a diagnostic or observer-dependent quantity. It encodes the irreversible loss of microscopic ordering through the unique surviving pseudoscalar channel. No additional orientation-sensitive state variable may be introduced without reintroducing discarded microscopic structure.

23.11.2 The pseudoscalar drift J .

The quantity J is the predictable component of Lévy-area production. At the system level, it is defined uniquely by the Doob decomposition with respect to the reduced filtration \mathcal{F}_t . As such, J is neither a new degree of freedom nor a constitutive parameter: it is a kinematic rate determined entirely by the reduced dynamics.

When observer-level coarse graining is introduced, J admits a decomposition into resolved and unresolved components via conditional expectation. This refinement does not alter its ontological status. In all cases, J represents a *pseudoscalar rate*, not a memory or state variable. It may be large and sign-definite even in perfectly coherent or symmetric motions, and its existence alone does not imply constitutive response.

23.11.3 The pseudoscalar memory process σ_t .

By contrast, σ_t is a slow pseudoscalar *memory process* carried by each coarse-grained worldline. It is not a kinematic state variable and does not influence the evolution of (X_t, A_t) . Nor is it a function of the reduced state. Instead, σ_t represents an internal constitutive degree of freedom whose dynamics encodes the cumulative effect of unresolved pseudoscalar activity along the worldline.

The process σ_t carries no independent geometric information and does not encode a handedness bias. Its intrinsic evolution is dissipative and controlled by instability rather than by kinematic forcing. All admissible control enters only through parity-even scalar functionals of observer-unresolved pseudoscalar activity.

Mesoscopic representations such as $\sigma(t, x, a)$, when used, refer only to statistical summaries of the ensemble of worldline memories and do not imply that σ_t is a field advected on the reduced state space.

Crucially, σ is not driven by the pseudoscalar drift J itself, nor by its sign. Constitutive control enters only through parity-even scalar quantities constructed from the observer-unresolved component of the drift, most notably the conditional intensity $\mathbb{E}[J_{\text{res}}^2 | \mathcal{O}_t]$. This scalar determines whether the neutral state $\sigma = 0$ is stable or unstable, but does not impose a handedness.

In particular, σ is not a source of global handedness. It represents symmetry-breaking, compensating pseudoscalar memory that emerges only when instability opens. Uniform pseudoscalar offsets correspond to a global handedness bias and are excluded on physical grounds.

23.11.4 Hierarchy of roles.

The relationship between these objects may be summarized schematically as

Object	Ontological role
A_t	Ontic ledger variable (state)
J_{sys}	System-level pseudoscalar drift (kinematic rate)
J_{res}	Observer-unresolved pseudoscalar component
$\mathbb{E}[J_{\text{res}}^2 \mathcal{O}_t]$	Scalar instability control
σ	Constitutive order parameter (symmetry-breaking response)
L_t	Scalar accumulation (record)

System-level coarse graining determines which variables the system must remember in order to evolve. Observer-level coarse graining determines which aspects of pseudoscalar activity are resolved kinematically and which contribute, through their intensity, to constitutive instability. The order parameter σ responds only to this instability control and does not alter the underlying reduced dynamics.

This separation is essential. It prevents both the illicit introduction of hidden memory and the spurious removal of genuine dynamical structure. With the ontology fixed, we may now impose the global symmetry constraint that excludes uniform pseudoscalar bias and derive the neutral, projected form of the σ dynamics.

23.12 Pseudoscalar Neutrality as Predictability Neutrality

The pseudoscalar order parameter σ represents *structured, compensating* directional memory. It does not encode an absolute handedness of the universe,

but rather the emergence of pseudoscalar structure through instability when unresolved circulation is sufficiently intense. Accordingly, pseudoscalar neutrality must be understood not as the vanishing of a flux, but as the exclusion of any *predictable or sign-biased* pseudoscalar component from the constitutive memory.

23.12.1 Why spatial zero-mode neutrality is insufficient.

A natural first attempt at neutrality is to require that σ have zero spatial mean. However, subtracting a global zero mode cannot suppress a large, localized pseudoscalar drift generated inside a galaxy. If J is supported on a region of size R inside a domain of size $L \gg R$, then $P_0 J = O((R/L)^2)$ while $(I - P_0)J \approx J$ on the support. Thus spatial averaging alone cannot explain why dynamically mature spiral disks relax σ despite sustained rotation. Neutrality must therefore be defined in terms of predictability rather than spatial extent.

23.12.2 Predictability defines the neutral channel.

The theory contains a unique macroscopic time scale, the Hubble time $T_H := H^{-1}$. This scale fixes which degrees of freedom are coherently predictable and therefore belong to resolved kinematics rather than constitutive memory. Predictability on this scale is encoded by the observer filtration

$$\mathcal{O}_t := \sigma\left((\mathbf{S}X)(s), (\mathbf{S}A)(s) : s \leq t\right) \subseteq \mathcal{F}_t,$$

where \mathbf{S} is the causal Hubble-scale smoothing operator

$$(\mathbf{S}f)(t) := \int_0^\infty \frac{1}{T_H} e^{-u/T_H} f(t-u) du.$$

This filtration represents all pseudoscalar structure that is resolved by long-time, coherent motion.

23.12.3 System drift and residual pseudoscalar activity.

Let A_t denote the Lévy area and write its Doob–Meyer decomposition with respect to the system filtration \mathcal{F}_t ,

$$A_t = A_0 + \int_0^t J_{\text{sys}}(s) ds + M_t,$$

where $J_{\text{sys}}(t)$ is \mathcal{F}_{t-} -predictable and M_t is a martingale. Observer-level predictability is implemented by conditional expectation. We decompose the drift as

$$J_{\text{res}}(t) := J_{\text{sys}}(t) - \mathbb{E}[J_{\text{sys}}(t) | \mathcal{O}_{t-}]. \quad (287)$$

By construction, $J_{\text{res}} \perp L^2(\mathcal{O}_{t-})$ and represents the unique pseudoscalar component that remains unpredictable on Hubble time scales.

23.12.4 Neutrality as sign blindness.

Constitutive memory cannot respond to the *sign* of J_{res} without introducing a global handedness bias. The admissible constitutive control must therefore be parity-even. The unique scalar quantity constructed from unresolved pseudoscalar activity is its conditional intensity

$$\mathbb{E}[J_{\text{res}}^2(t) \mid \mathcal{O}_{t-}].$$

This quantity measures the strength of unresolved circulation without privileging either handedness.

Accordingly, neutrality is enforced not by requiring vanishing drift, but by requiring that σ respond only to parity-even instability control. The constitutive order parameter itself satisfies

$$\mathbb{E}[\sigma_t \mid \mathcal{O}_t] = 0, \quad (288)$$

ensuring that σ carries no predictable pseudoscalar bias. This condition enforces predictability neutrality of the memory process itself, not of any kinematic field defined on the reduced state space.

23.12.5 Instability-controlled Landau dynamics.

With predictability neutrality enforced, the intrinsic evolution of σ is governed by instability rather than forcing. The admissible Landau form is therefore

$$\dot{\sigma} = (\alpha \mathbb{E}[J_{\text{res}}^2 \mid \mathcal{O}_t] - \gamma) \sigma - \lambda \sigma^3 + (\text{mixing terms}), \quad (289)$$

with $\alpha, \gamma, \lambda > 0$. The neutral state $\sigma = 0$ is stable when unresolved pseudoscalar activity is weak and becomes unstable only when its intensity exceeds a threshold.

23.12.6 Consequence: coherent rotation relaxes σ .

If the system-level pseudoscalar drift is Hubble-predictable, then $J_{\text{res}}(t) = 0$ almost surely and

$$\mathbb{E}[J_{\text{res}}^2 \mid \mathcal{O}_{t-}] = 0.$$

The growth rate is negative and the constitutive dynamics reduces to pure relaxation,

$$\dot{\sigma} = -\gamma \sigma - \lambda \sigma^3.$$

This is the mathematical content of the statement that mature spiral disks relax pseudoscalar memory despite sustained rotation.

By contrast, irregular, interacting, or intermittently circulating systems generate substantial unresolved pseudoscalar activity. In such systems, $\mathbb{E}[J_{\text{res}}^2 \mid \mathcal{O}_{t-}]$ is nonzero and may exceed the stability threshold, triggering spontaneous symmetry breaking and sustained σ .

23.12.7 Why neutrality takes this form.

The condition $\mathbb{E}[\sigma_t \mid \mathcal{O}_t] = 0$ is not an auxiliary assumption but a definition of constitutive memory. The filtration \mathcal{O}_t already contains all pseudoscalar structure that is coherent and predictable on cosmological time scales. Any \mathcal{O}_t -measurable component of σ would therefore duplicate resolved kinematics. Requiring orthogonality ensures that σ encodes only instability-generated, unresolved pseudoscalar structure and nothing else.

23.13 Projected Generator for the Neutral Memory Process

We now formulate the constitutive dynamics in its logically primary form: a Markovian *generator* for the joint reduced state and the slow pseudoscalar memory. Rather than postulating a free-energy functional as an axiom, we treat Landau and Ginzburg–Landau forms as perturbative parameterizations of this generator.

23.13.1 System-level reduced state and pseudoscalar drift.

Let $Z_t := (X_t, A_t)$ denote the system-level reduced Markov state obtained after coarse-graining, with filtration $\mathcal{F}_t := \sigma(Z_s : s \leq t)$. As a real-valued special semimartingale adapted to \mathcal{F}_t , the Lévy area admits the Doob–Meyer decomposition

$$A_t = A_0 + \int_0^t J_{\text{sys}}(Z_s) ds + M_t, \quad (290)$$

where $J_{\text{sys}}(t)$ is \mathcal{F}_{t-} -predictable and M_t is an \mathcal{F}_t -local martingale. The quantity J_{sys} is the system-level pseudoscalar drift generated by the reduced dynamics. No symmetry, neutrality, or constitutive constraint is imposed at this level.

23.13.2 Observer filtration and unresolved pseudoscalar activity.

Fix an observer filtration $\mathcal{O}_t \subseteq \mathcal{F}_t$ representing Hubble-scale predictability. Define the (time-indexed) orthogonal projection on L^2 by

$$P_{\mathcal{O},t-} Z := \mathbb{E}[Z \mid \mathcal{O}_{t-}]. \quad (291)$$

The unresolved pseudoscalar component of the drift is

$$J_{\text{res}}(t) := J_{\text{sys}}(Z_t) - \mathbb{E}[J_{\text{sys}}(Z_t) \mid \mathcal{O}_{t-}], \quad (292)$$

which satisfies $J_{\text{res}} \perp L^2(\mathcal{O}_{t-})$. This quantity carries no admissible sign information but determines the intensity of unresolved pseudoscalar activity.

23.13.3 Neutral pseudoscalar memory as a Markov lift.

Introduce a slow pseudoscalar memory variable σ_t and consider the enlarged Markov state (Z_t, σ_t) . We now impose neutrality

$$\mathbb{E}[\sigma_t | \mathcal{O}_t] = 0 \text{ for all } t. \quad (293)$$

The variable σ_t represents constitutive memory orthogonal to all Hubble-predictable pseudoscalar structure.

23.13.4 Instability-controlled constitutive generator.

The intrinsic dynamics of σ_t is dissipative and parity-odd, but its control parameters must be parity-even. Accordingly, the generator may depend on the unresolved pseudoscalar activity only through the scalar functional

$$\Xi_t := \mathbb{E}[J_{\text{res}}^2(t) | \mathcal{O}_{t-}].$$

Let $N(\sigma)$ be an odd saturating nonlinearity taking values in $(L^2(\mathcal{O}_{t-}))^\perp$ (e.g. $N(\sigma) = -\lambda_3(I - P_{\mathcal{O},t-})\sigma^3 + O(\sigma^5)$). Let $W^{(\sigma)}$ be an \mathcal{F}_t -Brownian motion independent of \mathcal{O}_t (so $\mathbb{E}[dW_t^{(\sigma)} | \mathcal{F}_{t-}] = 0$). The constitutive dynamics is then

$$d\sigma_t = \left[(\alpha \Xi_t - \gamma) \sigma_t + N(\sigma_t) \right] dt + \sqrt{2\Theta} dW_t^{(\sigma)}, \quad (294)$$

with $\alpha, \gamma > 0$ and $\Theta \geq 0$. Since Ξ_t is \mathcal{O}_{t-} -measurable, multiplication by $(\alpha \Xi_t - \gamma)$ preserves $(L^2(\mathcal{O}_{t-}))^\perp$, while N is defined to map into this subspace; moreover $\mathbb{E}[dW_t^{(\sigma)} | \mathcal{O}_{t-}] = 0$. Taking conditional expectation with respect to \mathcal{O}_t , the noise term drops out and the neutrality constraint is preserved: if $\mathbb{E}[\sigma_0 | \mathcal{O}_0] = 0$ and the drift maps neutrality to neutrality (e.g. via the explicit $(I - P_{\mathcal{O},t-})$ in N), then $\mathbb{E}[\sigma_t | \mathcal{O}_t] = 0$ for all t .

23.13.5 Interpretation.

Equation (294) shows that σ_t is not driven by a pseudoscalar flux. Instead, unresolved pseudoscalar activity controls the *linear stability* of the neutral state through Ξ_t . When $\alpha \Xi_t < \gamma$, the neutral state $\sigma = 0$ is stable and memory relaxes. When $\alpha \Xi_t > \gamma$, the neutral state becomes unstable and σ grows until nonlinear saturation balances dissipation.

At this level, the constitutive content of the theory is fully specified by the generator of the enlarged Markov process (Z_t, σ_t) . Landau and Ginzburg-Landau equations arise as low-order representations of this generator, not as independent modeling assumptions.

24 General Relativity as UV Kernel and Emergent IR Geometry

In the present framework, general relativity is not the macroscopic geometry of the universe. It is the microscopic gravitational interaction kernel: the rule

governing how mass–energy generates local transport, curvature, and collapse. The large–scale cosmological geometry is instead emergent, determined by irreversible coarse–graining and horizon coupling. Extensive parameters — temperature, entropy flux, baryon density, Hubble scaling — are not derived from GR but from the mesoscale thermodynamics of the open horizon–coupled exterior.

General relativity supplies the UV interaction kernel; irreversible coarse–graining supplies the IR geometry. Extensive cosmological parameters belong to the latter, not the former.

24.1 Local dynamics versus emergent kinematics

At the microscopic level, the gravitational field is described by a Lorentzian metric $g_{\mu\nu}$ satisfying Einstein’s equations

$$G_{\mu\nu}[g] = 8\pi G T_{\mu\nu}, \quad (295)$$

with $T_{\mu\nu}$ the stress–energy tensor of matter and radiation. These equations govern local curvature, collapse, and transport. They fix the rules by which mass–energy focuses geodesics, generates gravitational waves, and drives black–hole formation. In this sense, GR provides a *microscopic interaction kernel*: it specifies how nearby degrees of freedom interact gravitationally.

The mesoscopic framework developed in this paper addresses a distinct question: given the microscopic kernel (295), what is the effective, large–scale geometry seen by finite observers who continually trace out horizon–coupled and infrared degrees of freedom? The answer is not another Riemannian or Lorentzian metric, but a Carnot–Carathéodory (CC) transport structure induced by irreversible coarse–graining. Hypoelliptic generators, ledger variables, and Heisenberg tangents describe the *kinematics of accessibility* under anisotropic information loss, not the underlying UV field equations.

The distinction is analogous to the passage from Newtonian particle mechanics to Navier–Stokes hydrodynamics. Newton’s laws determine the microscopic collision kernel; viscosity, thermal conductivity, and other transport coefficients belong to the emergent continuum description. They are constrained by, but not explicitly present in, the microscopic equations. In the same way, the CC geometry and associated mesoscopic scales $(\sigma, H, T_{\text{ext}}, \dots)$ are emergent properties of the coarse–grained gravitational ensemble, not quantities that appear directly in (295).

24.2 GR as collision kernel in the open exterior

Operationally, the cosmological exterior is defined as the subsystem of degrees of freedom that remain resolvable by finite observers. Black–hole interiors and horizon–coupled infrared modes are continually traced out; they function as an environment E in the open–system sense discussed above. At each step, the microscopic dynamics of the full system $(S+E)$ is governed by general relativity and local quantum field theory. The role of GR in this picture is to specify:

- the local light cones and causal structure,
- the rules for gravitational collapse and black-hole formation,
- the focusing and shearing of null congruences,
- the coupling between matter, radiation, and curvature.

From the vantage of the reduced exterior description, these ingredients enter through effective Lindblad operators, scattering amplitudes, and transport coefficients. They determine *how* degrees of freedom are transferred to the environment and *which* directions in the observable algebra are strongly coupled to horizon-adjacent modes. In this sense, Einstein gravity is part of the UV micro-physics that feeds into the anisotropic coarse-graining mechanism. It sets the detailed form of the open-system generator, but not the large-scale kinematical law.

Under repeated tracing-out, the reduced dynamics on the exterior degrees of freedom flows toward a hypoelliptic, bracket-generating universality class. The nilpotentization of this class produces a CC tangent structure with Heisenberg prototypes, as in Sec. 18. This emergent geometry encodes how accessible degrees of freedom are transported when microscopic ordering information has been irreversibly lost. GR shapes the collision kernel that drives this loss; the CC structure describes the kinematics of what remains.

24.3 Mesoscopic thermodynamics and emergent cosmological scales

Extensive cosmological parameters — the Hubble scaling H , the effective entropy throughput, the baryon density ρ_b , the cosmic radiation temperature T_{rad} — are, in the present framework, properties of the *mesoscopic* steady state maintained by horizon coupling. They are not derived directly from solutions of (295), but from continuity equations and balance laws on the coarse-grained exterior:

$$\dot{\rho}_b + 3H\rho_b = S_b - L_b, \quad (296)$$

$$\dot{S}_{\text{ext}} = \dot{S}_{\text{prod}} - \dot{S}_{\text{export}}, \quad (297)$$

$$\dot{\rho}_\gamma + 4H\rho_\gamma = (\text{mixing and horizon terms}), \quad (298)$$

where S_b , L_b denote baryon sources and losses, and ρ_γ the photon energy density. These mesoscopic equations close on effective transport coefficients, mixing rates, and horizon-coupling terms that summarize the underlying Einstein–QFT dynamics after coarse-graining.

In particular:

- The observed Hubble scaling H reflects the rate of entropy throughput and horizon coupling in the nonequilibrium steady state, not a fundamental “expansion rate” of a global FRW metric.

- The cosmic blackbody temperature $T_{\text{rad}} \simeq 2.7 \text{ K}$ is the radiative temperature of a stationary photon bath in a CC geometry, maintained by Carnot mixing and horizon exchange, not the cooled remnant of a primordial fireball.
- The cosmic helium fraction and baryon abundance are fixed points of mesoscopic continuity equations governed by stellar microphysics, black-hole processing, and slow sequestration, rather than fossil boundary conditions at a finite “initial time.”

These quantities are constrained by the microscopic kernel — GR and local QFT must permit the required collapse, mixing, and horizon exchange — but their actual values are determined at the IR by the structure of the open, horizon-coupled NESS. They belong to the emergent CC geometry and its thermodynamic closure, not to the UV field equations.

24.4 General covariance and CC constitutive laws

None of this abandons general covariance. The microscopic dynamics remains generally covariant: the Einstein equations and local quantum fields are written without preferred coordinates, and the open-system generator respects this symmetry. What changes is the *constitutive law* relating microscopic fields to observable large-scale kinematics.

In standard cosmology, one typically identifies the macroscopic geometry of the universe with a particular solution of (295), such as an FRW metric with scale factor $a(t)$. Cosmological parameters are then read off directly from $a(t)$ and its derivatives. In the present framework, by contrast, the metric $g_{\mu\nu}$ is part of the UV kernel; the effective large-scale “geometry” is the CC transport structure that emerges after coarse-graining. It is encoded in:

- the admissible horizontal directions (accessible transport),
- the bracket structure (ledger variables and holonomy),
- the mesoscopic scales ($\sigma, H, T_{\text{acc}}, \dots$) determined by entropy throughput and horizon coupling.

General covariance ensures that the microscopic kernel is well posed on any background and that the reduced dynamics can be expressed in covariant form. The CC tangent structure is then a *constitutive* choice: it is the unique minimal extension needed to encode irreversible information loss while preserving Markovian closure under the symmetries and scaling assumptions of the problem. In this sense, GR and CC geometry play complementary roles:

General relativity specifies how mass-energy curves spacetime at the UV. Carnot–Carathéodory geometry specifies how coarse-grained observers move and measure in the IR.

24.5 Einstein Gravity as an Equation of State, and the Mesoscopic Universe as a Bigger Box

Jacobson's derivation of the Einstein field equations from thermodynamic first principles [41] provides a natural conceptual bridge between the open-system interpretation developed in this work and the standard general-relativistic description of spacetime dynamics. His central claim is that the Einstein equation is not a fundamental, microscopic law, but an *equation of state* expressing the thermodynamic response of a coarse-grained geometry to fluxes of energy and entropy across local causal horizons. This perspective aligns closely with the open-system, horizon-coupled viewpoint advanced here.

Jacobson begins by considering an arbitrary spacetime point and the associated local Rindler wedge defined by the past horizon of a uniformly accelerated observer. Across this local horizon, he identifies a flux of boost energy, interpreted as a heat increment δQ . Crucially, the horizon degrees of freedom are taken to carry an entropy S proportional to the cross-sectional area A of the horizon, $\delta S \propto \delta A$. A local Unruh temperature $T = \hbar\kappa/2\pi$ is then associated with the horizon by virtue of the KMS periodicity implied by the local causal structure. By enforcing the Clausius relation

$$\delta Q = T \delta S, \quad (299)$$

for all local Rindler horizons and for all local energy fluxes δQ through those horizons, Jacobson arrives at the Einstein field equations with a cosmological constant:

$$R_{ab} - \frac{1}{2}R g_{ab} + \Lambda g_{ab} = 8\pi G T_{ab}. \quad (300)$$

Because this result follows not from a microscopic action principle but from the equilibrium thermodynamics of coarse-graining, the Einstein equation is interpreted as the macroscopic equilibrium condition governing the geometry of the quantum vacuum. Gravity, in this view, emerges from the statistical behavior of inaccessible (traced-out) degrees of freedom. The gravitational field is not a fundamental interaction but the hydrodynamic limit of horizon thermodynamics.

This interpretation has several direct implications for the present framework. First, if spacetime dynamics are thermodynamic, then they must depend on the relevant state variables and the structure of the coarse-graining boundary. Jacobson's coarse-graining boundary is the local Rindler horizon; the associated state variables are horizon area and local boost energy flux. Second, because the Einstein equation arises as the *lowest-order equilibrium condition* for this system, modifications to the thermodynamic environment—such as nonequilibrium entropy flux, nonlocal coarse-graining rules, or modified reservoir structure—must produce correspondingly modified macroscopic dynamics.

The cosmological setting considered here, which we have termed the *mesoscopic universe*, provides precisely such an extension. Instead of a local Rindler wedge, the relevant thermodynamic boundary for cosmology is the global causal horizon partitioning the accessible exterior universe from a causally inaccessible

reservoir. At late times this horizon defines a natural KMS boundary condition and imposes irreversible entropy flux from radiation, matter, and structure into the causal horizon. In this sense, the observable universe is itself a subsystem—merely a larger “box” than Jacobson’s local wedge—thermodynamically coupled across its boundary to degrees of freedom it cannot access or decode.

Within this enlarged box, the relevant state variables differ from those entering (300). The mesoscopic regime involves, over cosmological timescales, continuous entropy throughput, steady-state baryon repopulation, and persistent radiative free-energy flow into the causal horizon. The horizon acts not only as a geometric boundary but as a dynamic cold reservoir, setting the entropy-acceptance temperature for exterior degrees of freedom and enabling the open-system thermodynamics developed in earlier sections. These additional state variables, absent in local equilibrium, necessarily modify the equation of state that governs large-scale geometry. In the mesoscopic picture, Einstein’s equation remains valid at the local level—where equilibrium holds and curvature responds to local energy fluxes—but must be augmented globally by balance laws encoding entropy production, baryon number continuity, and spectral/angular mixing.

Jacobson’s entropic gravity framework thus serves not as a competing theory, but as a conceptual foundation for the present work. The horizon-induced thermodynamics that he identifies locally are elevated here to a global principle: the large-scale evolution of the universe reflects the thermodynamic response of an open horizon-bounded system rather than a closed one. Just as the equation of state for a fluid depends on the macroscopic variables defining its thermodynamic environment, the equation of state for spacetime must depend on the macroscopic variables defining the mesoscopic, horizon-coupled universe. Einstein’s field equations describe the thermodynamic equilibrium of the quantum vacuum in the short-wavelength limit. The mesoscopic cosmological framework developed here describes the long-wavelength, horizon-coupled thermodynamics of the infrared universe—a bigger box with a richer set of degrees of freedom and correspondingly modified dynamical laws.

24.6 Cosmological interpretation

Recasting GR as a UV interaction kernel and the CC structure as emergent IR geometry has two main interpretive consequences for cosmology.

First, it resolves the apparent tension between the flatness of the late-time tangent geometry and the presence of strong gravitational phenomena. Locally, collapsed objects, gravitational lensing, and wave propagation are governed by Einstein gravity. Globally, the coarse-grained transport of radiation and matter is determined by hypoelliptic mixing in a Heisenberg-type tangent, with ledger variables recording irreversible entropy export. There is no requirement that the macroscopic universe be described by a single smooth FRW metric. Expansion is driven by free-energy throughput associated with the horizon entropy export; the CC tangent structure translates this thermodynamic flow into the observed kinematics, without appealing to a global FRW scale factor.

Second, it clarifies the status of cosmological parameters. Quantities such as H , ρ_b , and T_{ext} are not free inputs fixed by initial conditions in a finite-age spacetime. They are IR outputs of a steady-state balance between microscopic collapse, mesoscopic transport, and horizon coupling. General relativity enters this balance through the UV collision kernel; irreversible coarse-graining and ledger-governed CC transport determine the macroscopic outcome.

In summary, general relativity supplies the UV interaction kernel; irreversible coarse-graining supplies the IR geometry. Extensive cosmological parameters belong to the latter, not the former.

General relativity determines how the system collides; it does not determine how the system organizes.

References

- [1] N. et al. (Planck Collaboration) Aghanim. Planck 2018 results. vi. cosmological parameters. *Astronomy and Astrophysics*, 641:A6, 2020.
- [2] S. K. Andrews, S. P. Driver, A. S. G. Robotham, M. Alpaslan, I. K. Baldry, et al. Galaxy and mass assembly: the evolution of the cosmic spectral energy distribution from $z = 1$ to $z = 0$. *Monthly Notices of the Royal Astronomical Society*, 470(2):1342–1360, 2017.
- [3] Erik Aver, Keith A. Olive, and Evan D. Skillman. The effects of He I $\lambda 10830$ on helium abundance determinations. *Journal of Cosmology and Astroparticle Physics*, 2015(07):011, 2015.
- [4] Jacob Bekenstein and Mordehai Milgrom. Does the missing mass problem signal the breakdown of newtonian gravity? *Astrophysical Journal*, 286:7–14, 1984.
- [5] Jacob D. Bekenstein. Black holes and entropy. *Physical Review D*, 7:2333–2346, 1973.
- [6] Jacob D. Bekenstein. Generalized second law of thermodynamics in black-hole physics. *Physical Review D*, 9(12):3292–3300, 1974.
- [7] André Bellaïche. The tangent space in sub-riemannian geometry. In *Sub-Riemannian Geometry*. Birkhäuser, 1996.
- [8] Eugenio Bianchi and Robert C. Myers. On the architecture of spacetime geometry. *Classical and Quantum Gravity*, 31(21):214002, 2014.
- [9] J. J. Bisognano and E. H. Wichmann. On the duality condition for a hermitian scalar field. *Journal of Mathematical Physics*, 16:985–1007, 1975.
- [10] Joseph J. Bisognano and Egvind H. Wichmann. On the duality condition for a hermitian scalar field. *Journal of Mathematical Physics*, 17(3):303–321, 1976.

- [11] Luca Bombelli, Rabinder K. Koul, Joohan Lee, and Rafael D. Sorkin. Quantum source of entropy for black holes. *Physical Review D*, 34(2):373–383, 1986.
- [12] H.-J. Borchers. On the use of modular groups in quantum field theory. *Annales de l'Institut Henri Poincaré (A) Physique théorique*, 63(4):331–382, 1995.
- [13] Raphael Bousso. The holographic principle, 2002.
- [14] Ola Bratteli and Derek W. Robinson. *Operator Algebras and Quantum Statistical Mechanics 2*. Springer, 1987.
- [15] Heinz-Peter Breuer and Francesco Petruccione. *The Theory of Open Quantum Systems*. Oxford University Press, 2002.
- [16] Herbert B. Callen. *Thermodynamics and an Introduction to Thermostatics*. Wiley, 2 edition, 1985.
- [17] Sean M. Carroll. *Spacetime and Geometry*. Addison-Wesley, 2004.
- [18] E. B. Davies. Markovian master equations. *Communications in Mathematical Physics*, 39:91–110, 1974.
- [19] S. R. de Groot and P. Mazur. *Non-Equilibrium Thermodynamics*. Dover, 1984.
- [20] S. R. De Groot and P. Mazur. *Non-Equilibrium Thermodynamics*. Dover, 1984.
- [21] Scott Dodelson. *Modern Cosmology*. Academic Press, 2003.
- [22] Chas A. Egan and Charles H. Lineweaver. A larger estimate of the entropy of the universe. *The Astrophysical Journal*, 710(2):1825–1834, 2010.
- [23] Massimiliano Esposito and Christian Van den Broeck. Entropy production in open systems. *Physical Review Letters*, 104(9):090601, 2010.
- [24] Massimiliano Esposito and Christian Van den Broeck. Second law and landauer principle far from equilibrium. *Europhysics Letters*, 95:40004, 2011.
- [25] Benoit Famaey and Stacy McGaugh. Modified newtonian dynamics (mond): Observational phenomenology and relativistic extensions. *Living Reviews in Relativity*, 15(10), 2012.
- [26] Xiaohui Fan, Chris L. Carilli, and Brian Keating. Observational constraints on cosmic reionization, 2006.
- [27] D. J. Fixsen. The temperature of the cosmic microwave background. *The Astrophysical Journal*, 707:916–920, 2009.

- [28] D. J. et al. Fixsen. The cosmic microwave background spectrum from the full cobe firas data set. *Astrophysical Journal*, 473:576, 1996.
- [29] Dale J. et al. Fixsen. The cosmic microwave background spectrum from the full cobe firas data set. *The Astrophysical Journal*, 473:576–587, 1996.
- [30] Bernard Gaveau. Principe de moindre action, propagation de la chaleur et estimées sous elliptiques sur certains groupes nilpotents. *Acta Mathematica*, 139:95–153, 1977.
- [31] Gary W. Gibbons and Stephen W. Hawking. Cosmological event horizons, thermodynamics, and particle creation. *Physical Review D*, 15(10):2738–2751, 1977.
- [32] Alister W. Graham. The local supermassive black hole mass density. *Monthly Notices of the Royal Astronomical Society: Letters*, 380(1):L15–L19, 2007.
- [33] Mikhail Gromov. Carnot–carathéodory spaces seen from within. In *Sub-Riemannian Geometry*. Birkhäuser, 1996.
- [34] Rudolf Haag, Nico M. Hugenoltz, and Marinus Winnink. On the equilibrium states in quantum statistical mechanics. *Communications in Mathematical Physics*, 5:215–236, 1967.
- [35] Fred Hamann and Gary Ferland. Elemental abundances in quasistellar objects: Star formation and galactic nuclear evolution at high redshifts. *Annual Review of Astronomy and Astrophysics*, 37:487–531, 1999.
- [36] M. G. Hauser and E. Dwek. The cosmic infrared background: Measurements and implications. *Annual Review of Astronomy and Astrophysics*, 39:249–307, 2001.
- [37] Stephen W. Hawking. Particle creation by black holes. *Communications in Mathematical Physics*, 43:199–220, 1975.
- [38] Lars Hörmander. Hypoelliptic second order differential equations. *Acta Mathematica*, 119:147–171, 1967.
- [39] Werner Israel. Thermo-field dynamics of black holes. *Physics Letters A*, 57(2):107–110, 1976.
- [40] Yuri I. Izotov and Trinh X. Thuan. Systematic effects and a new determination of the primordial helium abundance. *Astrophysical Journal*, 710:L67–L71, 2010.
- [41] Ted Jacobson. Thermodynamics of spacetime: The einstein equation of state. *Physical Review Letters*, 75(7):1260–1263, 1995.
- [42] James Joyce. *Ulysses*. Vintage Books, New York, 1986.

- [43] Joel L. Lebowitz and Herbert Spohn. A gallavotti–cohen-type symmetry in the large deviation functional for stochastic dynamics. *Journal of Statistical Physics*, 95:333–365, 1999.
- [44] Julien Lesgourgues and Sergio Pastor. *Neutrino Cosmology*. Cambridge University Press, 2013.
- [45] Terry Lyons and Zhongmin Qian. *System Control and Rough Paths*. Oxford Mathematical Monographs. Oxford University Press, Oxford, UK, 2002.
- [46] Stacy S. McGaugh, Federico Lelli, and James M. Schombert. The radial acceleration relation in rotationally supported galaxies. *Physical Review Letters*, 117(20):201101, 2016.
- [47] M. Milgrom. A modification of the newtonian dynamics as a possible alternative to the hidden mass hypothesis. *Astrophysical Journal*, 270:365–370, 1983.
- [48] Richard Montgomery. *A Tour of Sub-Riemannian Geometries, Their Geodesics and Applications*. American Mathematical Society, 2002.
- [49] Michael A. Nielsen and Isaac L. Chuang. *Quantum Computation and Quantum Information*. Cambridge University Press, 10th anniversary edition, 2010.
- [50] T. Padmanabhan. Thermodynamical aspects of gravity: New insights. *Reports on Progress in Physics*, 73(4):046901, 2010.
- [51] Bernard E. J. Pagel. *Nucleosynthesis and Chemical Evolution of Galaxies*. Cambridge University Press, 1997.
- [52] P. J. E. Peebles. *Principles of Physical Cosmology*. Princeton University Press, 1993.
- [53] P. J. E. Peebles and B. Ratra. The cosmological constant and dark energy. *Reviews of Modern Physics*, 75:559–606, 2003.
- [54] R. Penrose. Singularities and time-asymmetry. *General Relativity: An Einstein Centenary Survey*, 1979.
- [55] Ilya Prigogine. *Introduction to Thermodynamics of Irreversible Processes*. Interscience, 1967.
- [56] Adam G. et al. Riess. A comprehensive measurement of the local value of the hubble constant, 2022.
- [57] Vera C. Rubin and W. Kent Ford. Rotational properties of 21 sc galaxies with a large range of luminosities and radii. *The Astrophysical Journal*, 238:471–487, 1980.

- [58] George B. Rybicki and Alan P. Lightman. *Radiative Processes in Astrophysics*. Wiley, 1979.
- [59] George B. Rybicki and Alan P. Lightman. *Radiative Processes in Astrophysics*. Wiley, 1979.
- [60] Barbara Ryden. *Introduction to Cosmology*. Cambridge University Press, 2 edition, 2016.
- [61] Francesco Shankar, David H. Weinberg, and Jordi Miralda-Escudé. Self-consistent models of the agn and black hole populations. *The Astrophysical Journal*, 690(1):20–41, 2009.
- [62] Y. Sofue and V. Rubin. Rotation curves of spiral galaxies, 2001.
- [63] Andrzej Sołtan. Masses of quasars. *Monthly Notices of the Royal Astronomical Society*, 200:115–122, 1982.
- [64] James Sorce. An intuitive construction of modular flow. 2023.
- [65] Herbert Spohn. Entropy production for quantum dynamical semigroups. *Journal of Mathematical Physics*, 19:1227–1230, 1978.
- [66] Mark Srednicki. Entropy and area. *Physical Review Letters*, 71(5):666–669, 1993.
- [67] Daniel W. Stroock and S. R. S. Varadhan. *Multidimensional Diffusion Processes*. Classics in Mathematics. Springer, Berlin, Heidelberg, 2006. Reprint of the 1979 edition.
- [68] Beatrice M. Tinsley. Evolution of the stars and gas in galaxies. *Fundamentals of Cosmic Physics*, 5:287–388, 1980.
- [69] William G. Unruh. Notes on black-hole evaporation. *Physical Review D*, 14:870–892, 1976.
- [70] N. Th. Varopoulos, L. Saloff-Coste, and T. Coulhon. Analysis and geometry on groups. *Cambridge Tracts in Mathematics*, 1992.
- [71] Vlatko Vedral. The role of relative entropy in quantum information theory. *Reviews of Modern Physics*, 74:197–234, 2002.
- [72] Robert M. Wald. *General Relativity*. University of Chicago Press, 1984.
- [73] Robert M. Wald. *Quantum Field Theory in Curved Spacetime and Black Hole Thermodynamics*. University of Chicago Press, 1994.
- [74] Robert M. Wald. The thermodynamics of black holes. *Living Reviews in Relativity*, 4(6), 2001.
- [75] S. Weinberg. *Cosmology*. Oxford University Press, 2008.

- [76] Steven Weinberg. *Cosmology*. Oxford University Press, 2008.
- [77] Steven Weinberg. *Cosmology*. Oxford University Press, 2008.
- [78] Edward Witten. Aps medal for exceptional achievement in research: Invited article on entanglement entropy. *Reviews of Modern Physics*, 90:045003, 2018.
- [79] S. E. Woosley and T. A. Weaver. The evolution and explosion of massive stars. ii. explosive hydrodynamics and nucleosynthesis. *Astrophysical Journal Supplement Series*, 101:181–235, 1995.
- [80] Donald G. York, J. Adelman, John E. Anderson, Scott F. Anderson, James Annis, Neta A. Bahcall, J. A. Bakken, Robert Barkhouser, Steven Bastian, et al. The Sloan digital sky survey: Technical summary. *Astronomical Journal*, 120(3):1579–1587, 2000.
- [81] Robert Zwanzig. *Nonequilibrium Statistical Mechanics*. Oxford University Press, 2001.

A Curved model geometries

Context and purpose. The main text models the mesoscopic exterior by a Carnot–Carathéodory (CC) tangent law, whose simplest flat local model is the Heisenberg group (or more generally a step–two Carnot group) equipped with a canonical contact structure and a Hamiltonian geodesic flow. The aim of the present appendix is not to add new cosmological assumptions, but to record the corresponding *curved* homogeneous model geometries that play the same structural role: $SU(2)$ and $SL(2, \mathbb{R})$ are the constant–curvature deformations (positive and negative) of the Heisenberg model, while $Sp(2)$ and $Sp(1, 1)$ are the natural quaternionic analogues relevant to four–dimensional Euclidean and Lorentzian signatures. In each case the construction preserves the same ingredients used in the bulk: a contact (horizontal) distribution, an invariant quadratic (or norm) Hamiltonian, and the resulting second–order dynamics governed by the same step–two bracket structure. These models provide a concrete reference class showing that the CC/Heisenberg tangent law admits geometrically natural global realizations and constant–curvature variants, so that the mesoscopic frequency scale σ should be viewed as an emergent kinematical rate associated with the underlying horizontal/vertical mixing rather than an ad hoc parameter.

A.1 $SU(2)$

We shall work in \mathbb{C}^2 . Let $\epsilon(W \wedge Z)$ be the determinant of the 2×2 matrix with columns $Z, W \in \mathbb{C}^2$. Let $\epsilon(Z) := \epsilon(- \wedge Z)$, so that $W \cdot \epsilon(Z) = \epsilon(W \wedge Z)$. In terms of the standard basis, we have $\epsilon(Z) = [z_2, -z_1]$, i.e.,

$$\epsilon = \begin{bmatrix} 0 & 1 \\ -1 & 0 \end{bmatrix}.$$

We also have

$$\epsilon(\epsilon(Z)) = -Z$$

and

$$\epsilon(Z) \cdot \epsilon(W) = Z \cdot W.$$

Let $Z, P \in \mathbb{C}^2$. Let $\theta = P \cdot dZ + \bar{P} \cdot d\bar{Z}$, and let $d\theta$ define a Poisson bracket. Define $M = \epsilon(P \wedge \bar{Z})$, $\bar{M} = \epsilon(\bar{P} \wedge Z)$, and $H = M\bar{M}$.

Note that $Z \cdot \bar{Z}$ and $P \cdot \bar{P}$ Poisson commute with H . Also, the symplectic gradient of H is tangent to the contact distribution $\theta = i(Z \cdot d\bar{Z} - \bar{Z} \cdot dZ)$ on the 3-dimensional hypersurface $Z \cdot \bar{Z} = 1$.

Let $N = \{M, \bar{M}\} \in i\mathbb{R}$. Then $\dot{N} = \{N, H\} = 0$. We have the Hamilton equations

$$\begin{aligned}\dot{Z} &= \{Z, H\} = \epsilon(\bar{Z})\bar{M} \\ \dot{\bar{Z}} &= \{\bar{Z}, H\} = \epsilon(Z)M.\end{aligned}$$

Taking another derivative on the first of these gives

$$\begin{aligned}\ddot{Z} &= \epsilon(\dot{Z})\bar{M} + \epsilon(\bar{Z})\dot{M} \\ &= \epsilon(\epsilon(Z))M\bar{M} - \epsilon(\bar{Z})\bar{M}N \\ &= -ZM\bar{M} - \dot{Z}N\end{aligned}$$

so that

$$\ddot{Z} + \dot{Z}N + ZM\bar{M} = 0.$$

The characteristic polynomial is $\lambda^2 + \lambda N + M\bar{M}$, with roots λ_1, λ_2 given by

$$\lambda = -\frac{N}{2} \pm \frac{1}{2}\sqrt{N^2 - 4M\bar{M}} \in i\mathbb{R}.$$

We have $N = -(\lambda_1 + \lambda_2)$ and $H = \lambda_1\lambda_2$.

Solutions have the form

$$Z = e^{\lambda_1 t}Z_1 + e^{\lambda_2 t}Z_2.$$

Note that, from $Z \cdot \bar{Z} = 1$, we have $Z_1 \cdot \bar{Z}_2 = 0$, $Z_1 \cdot \bar{Z}_1 + Z_2 \cdot \bar{Z}_2 = 1$.

To find the relation between $Z_1, Z_2, \lambda_1, \lambda_2$, we first deduce a formula for M, \bar{M} in terms of $\lambda_1, \lambda_2, Z_1, Z_2$. We have on one hand

$$\epsilon(Z \wedge \dot{Z}) = \epsilon(Z \wedge \epsilon(\bar{Z}))\bar{M} = -Z \cdot \bar{Z}\bar{M} = -\bar{M}$$

On the other hand,

$$\begin{aligned}\epsilon(Z \wedge \dot{Z}) &= \epsilon((e^{\lambda_1 t}Z_1 + e^{\lambda_2 t}Z_2) \wedge (\lambda_1 e^{\lambda_1 t}Z_1 + \lambda_2 e^{\lambda_2 t}Z_2)) \\ &= (\lambda_2 - \lambda_1)e^{(\lambda_1 + \lambda_2)t}\epsilon(Z_1 \wedge Z_2).\end{aligned}$$

Thus

$$\begin{aligned}\bar{M} &= (\lambda_1 - \lambda_2)\epsilon(Z_1 \wedge Z_2)e^{-Nt} \\ M &= (\lambda_2 - \lambda_1)\epsilon(\bar{Z}_1 \wedge \bar{Z}_2)e^{Nt}.\end{aligned}\tag{301}$$

Next, we have

$$\begin{aligned}\dot{Z} &= \lambda_1 e^{\lambda_1 t} Z_1 + \lambda_2 e^{\lambda_2 t} Z_2 \\ \epsilon(\bar{Z}) \bar{M} &= (e^{-\lambda_1 t} \epsilon(\bar{Z}_1) + e^{-\lambda_2 t} \epsilon(\bar{Z}_2)) (\lambda_1 - \lambda_2) \epsilon(Z_1 \wedge Z_2) e^{-Nt}.\end{aligned}$$

Equating coefficients, we have

$$\begin{aligned}\lambda_1 Z_1 &= (\lambda_1 - \lambda_2) \epsilon(Z_1 \wedge Z_2) \epsilon(\bar{Z}_2) \\ \lambda_2 Z_2 &= (\lambda_1 - \lambda_2) \epsilon(Z_1 \wedge Z_2) \epsilon(\bar{Z}_1).\end{aligned}$$

Note that this can be rewritten in the equivalent form

$$\begin{aligned}\lambda_1 Z_1 &= \bar{M} e^{Nt} \epsilon(\bar{Z}_2) \\ \lambda_2 Z_2 &= \bar{M} e^{Nt} \epsilon(\bar{Z}_1).\end{aligned}\tag{302}$$

Taking the respective inner products with $\epsilon(Z_2)$ and $\epsilon(Z_1)$ gives

$$\begin{aligned}\lambda_1 \epsilon(Z_1 \wedge Z_2) &= (\lambda_1 - \lambda_2) \epsilon(Z_1 \wedge Z_2) Z_2 \cdot \bar{Z}_2 \\ \lambda_2 \epsilon(Z_2 \wedge Z_1) &= (\lambda_1 - \lambda_2) \epsilon(Z_1 \wedge Z_2) Z_1 \cdot \bar{Z}_1.\end{aligned}$$

So we find

$$\begin{aligned}Z_1 \cdot \bar{Z}_1 &= \frac{\lambda_2}{\lambda_2 - \lambda_1} \\ Z_2 \cdot \bar{Z}_2 &= \frac{\lambda_1}{\lambda_1 - \lambda_2}.\end{aligned}$$

(Note that we have the required relation $Z_1 \cdot \bar{Z}_1 + Z_2 \cdot \bar{Z}_2 = 1$.)

We now determine the evolution of the P variable. We have

$$\begin{aligned}\dot{P} &= \{P, H\} = \epsilon(\bar{P}) M \\ \dot{\bar{P}} &= \{\bar{P}, H\} = \epsilon(P) \bar{M}.\end{aligned}$$

$$\begin{aligned}\ddot{P} &= \epsilon(\dot{\bar{P}}) M + \epsilon(\bar{P}) \dot{M} \\ &= \epsilon(\epsilon(P)) M \bar{M} + \epsilon(\bar{P}) M N \\ &= -P M \bar{M} + \dot{P} N.\end{aligned}$$

So we have

$$\ddot{P} - \dot{P} N + P M \bar{M} = 0.$$

The roots are $-\lambda_1 = \bar{\lambda}_1, -\lambda_2 = \bar{\lambda}_2$.

Write $P = e^{-\lambda_1 t} P_1 + e^{-\lambda_2 t} P_2$. Then

$$\begin{aligned}M &= \epsilon(P \wedge \bar{Z}) \\ &= e^{-(\lambda_1 + \lambda_2)t} \epsilon(P_1 \wedge \bar{Z}_2 + P_2 \wedge \bar{Z}_1) + e^{-2\lambda_1 t} \epsilon(P_1 \wedge \bar{Z}_1) + e^{-2\lambda_2 t} \epsilon(P_2 \wedge \bar{Z}_2).\end{aligned}\tag{303}$$

These last two terms must vanish identically, and so $P_1 = A_1 \bar{Z}_1$, $P_2 = A_2 \bar{Z}_2$ for some constants A_1, A_2 to be determined.

We have

$$\begin{aligned}\dot{P} &= \epsilon(\bar{P})M \\ &= e^{\lambda_1 t} \bar{A}_1 \epsilon(Z_1)M + e^{\lambda_2 t} \bar{A}_2 \epsilon(Z_2)M \\ \dot{P} &= -e^{-\lambda_1 t} A_1 \lambda_1 \bar{Z}_1 - e^{-\lambda_2 t} A_2 \lambda_2 \bar{Z}_2.\end{aligned}$$

Equating coefficients, we find

$$\begin{aligned}Me^{-Nt} \bar{A}_1 \epsilon(Z_1) &= -A_2 \lambda_2 \bar{Z}_2 \\ Me^{-Nt} \bar{A}_2 \epsilon(Z_2) &= -A_1 \lambda_1 \bar{Z}_1.\end{aligned}$$

But the terms on the left-hand side can be rewritten using (302) to give

$$\begin{aligned}-\bar{A}_1 \lambda_2 \bar{Z}_2 &= -A_2 \lambda_2 \bar{Z}_2 \\ -\bar{A}_2 \lambda_1 \bar{Z}_1 &= -A_1 \lambda_1 \bar{Z}_1,\end{aligned}$$

i.e., $\bar{A}_1 = A_2$, $\bar{A}_2 = A_1$.

Turning again to (303), we have

$$\begin{aligned}Me^{-Nt} &= \epsilon(P_1 \wedge \bar{Z}_1 + P_2 \wedge \bar{Z}_2) \\ &= (A_2 - A_1) \epsilon(\bar{Z}_1 \wedge \bar{Z}_2)\end{aligned}$$

but by (301), $Me^{-Nt} = (\lambda_2 - \lambda_1) \epsilon(\bar{Z}_1 \wedge \bar{Z}_2)$, so we have $A_2 - A_1 = \lambda_2 - \lambda_1$.

The general solution is thus

$$\begin{aligned}P &= A_1 e^{-\lambda_1 t} \bar{Z}_1 + A_2 e^{-\lambda_2 t} \bar{Z}_2 \\ A_1 &= \frac{\lambda_1 - \lambda_2}{2} + c \\ A_2 &= \frac{\lambda_2 - \lambda_1}{2} + c\end{aligned}$$

where c is real.

A.1.1 Clifford tori

Given a pair of non-zero vectors $Z_1, Z_2 \in \mathbb{C}^2$ such that $Z_1 \cdot \bar{Z}_1 + Z_2 \cdot \bar{Z}_2 = 1$ and $Z_1 \cdot \bar{Z}_2 = 0$, the subset of \mathbb{S}^3 :

$$\{e^{i\theta} Z_1 + e^{i\phi} Z_2 | \theta, \phi \in \mathbb{R}\}$$

is the *Clifford torus* determined by the pair Z_1, Z_2 . A Clifford torus is topologically a torus, and we have shown that each geodesic of $H_{\mathbb{S}^3}$ lies on some Clifford torus. Every Clifford torus is an orbit of a maximal toral subgroup of $U(2)$.

The three-sphere $S^3 \subset \mathbb{C}^2$ is fibred, by the Hopf fibration, over $\mathbb{CP}^1 = S^2$, which results by identifying Z with λZ for $\lambda \in U(1)$. Thus, we can obtain the stereographic projection of the Hopf map by dividing the coordinates of a point of S^3 : $(z, w) \mapsto z/w$. The image of the geodesic $Z = e^{\lambda_1 t} Z_1 + e^{\lambda_2 t} Z_2$ is on a circle of the sphere. The circle is not a great circle unless $N = 0$, a special case to which we now turn.

A.1.2 $N = 0$

The case $N = 0$ is worthy of special consideration. In this case, M is constant and Z satisfies

$$\dot{Z} = -M\bar{M}Z,$$

so the geodesic is a simple harmonic oscillator. In fact, we have $\lambda_1 = -\lambda_2$, and so

$$Z = e^{\lambda_1 t} Z_1 + e^{-\lambda_1 t} Z_2$$

is a great circle of the three-sphere. Under the Hopf map, this projects to a great circle of S^2 . Conversely, any geodesic that projects to a great circle is of this kind.

A.1.3 The Cayley transform

We consider a biholomorphism of the unit ball $B_1(\mathbb{C}^2)$ in \mathbb{C}^2 , defined by $z\bar{z} + w\bar{w} < 1$, onto the Siegel domain

$$\mathcal{S} = \{(Z, W) \in \mathbb{C}^2 \mid i(\bar{W} - W) > 2Z\bar{Z}\}.$$

The mapping $\chi : B_1(\mathbb{C}^2) \rightarrow \mathcal{S}$ is given by the Cayley transform:

$$\chi : (z, w) \mapsto (Z, W) = \left(i \frac{z}{1-w}, i \frac{1+w}{1-w} \right).$$

Note that

$$\chi^{-1} : (Z, W) \mapsto (z, w) = \left(\frac{2Z}{W+i}, \frac{W-i}{W+i} \right).$$

Let $\rho(Z, W) = 2Z\bar{Z} + i(W - \bar{W})$. Then, with $Z = i\frac{z}{1-w}$, $W = i\frac{1+w}{1-w}$, note that

$$\rho(Z, W) = 2 \frac{z\bar{z} + w\bar{w} - 1}{|1-w|^2}$$

which is negative if and only if $(z, w) \in B_1(\mathbb{C}^2)$. The transformation χ has a continuous extension to $\overline{B_1(\mathbb{C}^2)} \setminus \{(0, 1)\}$, and maps bijectively to $\overline{\mathcal{S}}$. The contact one-form $i\theta = (z d\bar{z} - \bar{z} dz) + (w d\bar{w} - \bar{w} dw)$ on the boundary becomes

$$i\theta = 2|w+i|^{-2} (2(Z d\bar{Z} - \bar{Z} dZ) - i(dW + d\bar{W})).$$

With

$$P = p_z \bar{w} - p_w \bar{z},$$

on the boundary (setting $2Z\bar{Z} = I(\bar{W} - W)$):

$$P = \frac{W+i}{\bar{W}-i} \left((\bar{W}+i)(p_Z - ip_W Z) + 2ip_W \bar{Z} \right).$$

Keeping only the terms of lowest homogeneity gives the Gromov tangent space:

$$\begin{aligned} \hat{P} &= p_Z + p_W (2\bar{Z} - iZ) \\ \hat{\bar{P}} &= p_{\bar{Z}} + p_{\bar{W}} (2Z - i\bar{Z}) \\ \{\hat{P}, \hat{\bar{P}}\} &= 2(p_W - p_{\bar{W}}). \end{aligned}$$

Thus we recover the Heisenberg group as the tangent space.

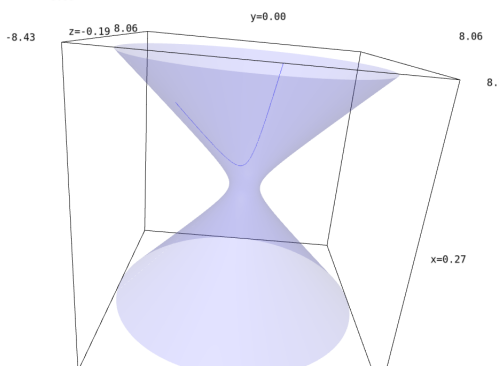


Figure 11: Typical geodesic, projected to the de Sitter space under the Hopf map

A.2 $SL_2(\mathbb{R})$

We consider the spacetime as the three-dimensional Lie group $SL_2(\mathbb{R}) \cong SU(1, 1) \cong Spin(1, 2)$. Regarded as the spin group, this group admits a homogeneous action on the hyperboloid of one sheet in \mathbb{R}^3 (two-dimensional de Sitter space). The corresponding anti-de Sitter space is one sheet of the hyperboloid of two sheets, which is just a model of the hyperbolic plane. As a spacetime, since the group is three-dimensional, this model will have one spatial one one time dimension, plus one small dimension analogous to the h, p_h direction of the Heisenberg model.

We describe the space using a complex model of $SL_2(\mathbb{R})$. For a vector $Z \in \mathbb{C}^2$, $Z = [z_1 \ z_2]$, let

$$Z^\sigma = \begin{bmatrix} \bar{z}_2 \\ \bar{z}_1 \end{bmatrix}.$$

Note that

$$Z^\sigma = S \bar{Z}^T$$

$$\text{where } S = \begin{bmatrix} 0 & 1 \\ 1 & 0 \end{bmatrix}.$$

With ϵ as before, we now have

$$\epsilon(\epsilon(Z^\sigma)^\sigma) = Z.$$

Let $M = \epsilon(P \wedge Z^\sigma)$, $\bar{M} = -\epsilon(P^\sigma \wedge Z)$, $H = M\bar{M}$, $N = \{M, \bar{M}\} \in i\mathbb{R}$. Then $\{N, H\} = \{Z \cdot Z^\sigma, H\} = \{P \cdot P^\sigma, H\} = 0$.

We have $\dot{M} = MN$,

$$\begin{aligned} \dot{Z} &= \epsilon(Z^\sigma)\bar{M} \\ \dot{Z}^\sigma &= -\epsilon(Z)M \\ \ddot{Z} &= \epsilon(\dot{Z}^\sigma)\bar{M} + \epsilon(Z^\sigma)\dot{\bar{M}} \\ &= -\epsilon(\epsilon(Z)M)\bar{M} - \epsilon(Z^\sigma)\bar{M}N \\ &= ZM\bar{M} - \dot{Z}N, \end{aligned}$$

so

$$\ddot{Z} + \dot{Z}N - ZM\bar{M} = 0.$$

The characteristic polynomial is $\lambda^2 + N\lambda - M\bar{M}$, with roots λ_1, λ_2 given by

$$\lambda = -\frac{N}{2} \pm \frac{1}{2}\sqrt{N^2 + 4M\bar{M}}.$$

We have $N = -(\lambda_1 + \lambda_2)$ and $H = -\lambda_1\lambda_2$.

There are three possibilities, depending on the sign of the discriminant:

- $\lambda_1 - \lambda_2 \in \mathbb{R}$: $\lambda_1 = -\bar{\lambda}_2, \lambda_2 = -\bar{\lambda}_1$ (“timelike” case)
- $\lambda_1 - \lambda_2 \in i\mathbb{R}$: $\lambda_1 = -\bar{\lambda}_1, \lambda_2 = -\bar{\lambda}_2$ (“spacelike” case)
- $\lambda_1 = \lambda_2 = -\bar{\lambda}_1 = -\bar{\lambda}_2$ (“null” case)

We shall write

$$Z = e^{\lambda_1 t} Z_1 + e^{\lambda_2 t} Z_2$$

Let $K = Z \cdot Z^\sigma$, which is real, nonzero, and constant.

Note that on the one hand

$$\begin{aligned} \epsilon(Z \wedge \dot{Z}) &= \epsilon(Z \wedge \epsilon(Z^\sigma))\bar{M} \\ &= -Z \cdot Z^\sigma \bar{M} = -K\bar{M}. \end{aligned}$$

On the other hand,

$$\begin{aligned} \epsilon(Z \wedge \dot{Z}) &= \epsilon((e^{\lambda_1 t} Z_1 + e^{\lambda_2 t} Z_2) \wedge (\lambda_1 e^{\lambda_1 t} Z_1 + \lambda_2 e^{\lambda_2 t} Z_2)) \\ &= (\lambda_2 - \lambda_1) e^{(\lambda_1 + \lambda_2)t} \epsilon(Z_1 \wedge Z_2), \end{aligned}$$

so we get

$$\begin{aligned} K\bar{M} &= (\lambda_1 - \lambda_2) \epsilon(Z_1 \wedge Z_2) e^{-Nt} \\ KM &= -(\bar{\lambda}_1 - \bar{\lambda}_2) \epsilon(Z_1^\sigma \wedge Z_2^\sigma) e^{Nt}. \end{aligned} \tag{304}$$

A.2.1 Case $\lambda_1 - \lambda_2 \in \mathbb{R}$

Here $\bar{\lambda}_1 = -\lambda_2$ and $\bar{\lambda}_2 = -\lambda_1$.

We have

$$\begin{aligned} \dot{Z} &= \lambda_1 e^{\lambda_1 t} Z_1 + \lambda_2 e^{\lambda_2 t} Z_2 \\ \epsilon(Z^\sigma) \bar{M} &= (e^{-\lambda_2 t} \epsilon(Z_1^\sigma) + e^{-\lambda_1 t} \epsilon(Z_2^\sigma))(\lambda_1 - \lambda_2) \epsilon(Z_1 \wedge Z_2) e^{-Nt} K^{-1}. \end{aligned}$$

Equating coefficients gives

$$\begin{aligned} \lambda_1 K Z_1 &= \epsilon(Z_1^\sigma)(\lambda_1 - \lambda_2) \epsilon(Z_1 \wedge Z_2) \\ \lambda_2 K Z_2 &= \epsilon(Z_2^\sigma)(\lambda_1 - \lambda_2) \epsilon(Z_1 \wedge Z_2). \end{aligned}$$

Equivalently,

$$\begin{aligned}\lambda_1 Z_1 &= \bar{M} e^{Nt} \epsilon(Z_1^\sigma) \\ \lambda_2 Z_2 &= \bar{M} e^{Nt} \epsilon(Z_2^\sigma) \\ \lambda_2 Z_1^\sigma &= M e^{-Nt} \epsilon(Z_1) \\ \lambda_1 Z_2^\sigma &= M e^{-Nt} \epsilon(Z_2).\end{aligned}\tag{305}$$

Taking the respective inner products with $\epsilon(Z_2)$ and $\epsilon(Z_1)$ gives

$$\begin{aligned}\lambda_1 K \epsilon(Z_1 \wedge Z_2) &= (\lambda_1 - \lambda_2) \epsilon(Z_1 \wedge Z_2) Z_2 \cdot Z_1^\sigma \\ \lambda_2 K \epsilon(Z_2 \wedge Z_1) &= (\lambda_1 - \lambda_2) \epsilon(Z_1 \wedge Z_2) Z_1 \cdot Z_2^\sigma.\end{aligned}$$

So we find

$$\begin{aligned}Z_2 \cdot Z_1^\sigma &= \frac{K \lambda_1}{\lambda_1 - \lambda_2} \\ Z_1 \cdot Z_2^\sigma &= \frac{K \lambda_2}{\lambda_2 - \lambda_1}.\end{aligned}$$

Now for the P variable, we have

$$\begin{aligned}\dot{P} &= \{P, M\} = -\epsilon(P^\sigma) M \\ \dot{P}^\sigma &= \{P^\sigma, M\} = \epsilon(P) \bar{M} \\ \ddot{P} &= -\epsilon(\dot{P}^\sigma) M - \epsilon(P^\sigma) \dot{M} \\ &= -\epsilon(\epsilon(P) \bar{M}) M - \epsilon(P^\sigma) M N \\ &= P M \bar{M} + \dot{P} N.\end{aligned}$$

So

$$\ddot{P} - \dot{P} N - P M \bar{M} = 0.$$

The characteristic polynomial is $\mu^2 - N\mu - M\bar{M}$, with roots $\mu = \frac{N}{2} \pm \frac{1}{2}\sqrt{N^2 + 4M\bar{M}}$, i.e., $\bar{\lambda}_1 = -\lambda_2$ and $\bar{\lambda}_2 = -\lambda_1$.

With $P = e^{-\lambda_1 t} P_1 + e^{-\lambda_2 t} P_2$, we have

$$\begin{aligned}M &= \epsilon(P \wedge Z^\sigma) \\ &= e^{-(\lambda_1 + \lambda_2)t} \epsilon(P_1 \wedge Z_1^\sigma + P_2 \wedge Z_2^\sigma) + e^{-2\lambda_1 t} \epsilon(P_1 \wedge Z_2^\sigma) + e^{-2\lambda_2 t} \epsilon(P_2 \wedge Z_1^\sigma).\end{aligned}\tag{306}$$

The last two terms must vanish identically, so we have $P_1 = A_1 Z_2^\sigma$ and $P_2 = A_2 Z_1^\sigma$ for some constants A_1, A_2 .

Now we have

$$P^\sigma = \bar{A}_1 e^{\lambda_2 t} Z_2 + \bar{A}_2 e^{\lambda_1 t} Z_1$$

and so

$$\begin{aligned}\dot{P} &= -\epsilon(P^\sigma) M \\ &= -(\bar{A}_1 e^{\lambda_2 t} \epsilon(Z_2) + \bar{A}_2 e^{\lambda_1 t} \epsilon(Z_1)) M \\ \dot{P} &= -e^{-\lambda_1 t} A_1 \lambda_1 Z_2^\sigma - e^{-\lambda_2 t} \lambda_2 A_2 Z_1^\sigma.\end{aligned}$$

Equating coefficients,

$$\begin{aligned}-Me^{-Nt}\bar{A}_1\epsilon(Z_2) &= -A_1\lambda_1Z_2^\sigma \\ -Me^{-Nt}\bar{A}_2\epsilon(Z_1) &= -A_2\lambda_2Z_1^\sigma.\end{aligned}$$

Applying (305) to the left-hand sides gives:

$$\begin{aligned}-\bar{A}_1\lambda_1Z_2^\sigma &= -A_1\lambda_1Z_2^\sigma \\ -\bar{A}_2\lambda_2Z_1^\sigma &= -A_2\lambda_2Z_1^\sigma\end{aligned}$$

so that $\bar{A}_1 = A_1$, $\bar{A}_2 = A_2$.

Now, using (306),

$$\begin{aligned}Me^{-Nt} &= \epsilon(P_1 \wedge Z_1^\sigma + P_2 \wedge Z_2^\sigma) \\ &= (A_2 - A_1)\epsilon(Z_1^\sigma \wedge Z_2^\sigma)\end{aligned}$$

But by (304),

$$KMe^{-Nt} = -(\bar{\lambda}_1 - \bar{\lambda}_2)\epsilon(Z_1^\sigma \wedge Z_2^\sigma) = (\lambda_2 - \lambda_1)\epsilon(Z_1^\sigma \wedge Z_2^\sigma).$$

So we have $K(A_2 - A_1) = \lambda_2 - \lambda_1$, and the general solution is

$$\begin{aligned}P &= A_1e^{-\lambda_1 t}Z_2^\sigma + A_2e^{-\lambda_2 t}Z_1^\sigma \\ A_1 &= \frac{\lambda_1 - \lambda_2}{2K} + c \\ A_2 &= \frac{\lambda_2 - \lambda_1}{2K} + c\end{aligned}$$

where c is real.

A.2.2 Case $\lambda_1 - \lambda_2 \in i\mathbb{R}$

Here $\bar{\lambda}_1 = -\lambda_1$ and $\bar{\lambda}_2 = -\lambda_2$.

We have

$$\begin{aligned}\dot{Z} &= \lambda_1 e^{\lambda_1 t}Z_1 + \lambda_2 e^{\lambda_2 t}Z_2 \\ \epsilon(Z^\sigma)\bar{M} &= (e^{-\lambda_1 t}\epsilon(Z_1^\sigma) + e^{-\lambda_2 t}\epsilon(Z_2^\sigma))(\lambda_1 - \lambda_2)\epsilon(Z_1 \wedge Z_2)e^{-Nt}K^{-1}.\end{aligned}$$

Equating coefficients gives

$$\begin{aligned}\lambda_1 K Z_1 &= \epsilon(Z_2^\sigma)(\lambda_1 - \lambda_2)\epsilon(Z_1 \wedge Z_2) \\ \lambda_2 K Z_2 &= \epsilon(Z_1^\sigma)(\lambda_1 - \lambda_2)\epsilon(Z_1 \wedge Z_2).\end{aligned}$$

Equivalently,

$$\begin{aligned}\lambda_1 Z_1 &= \bar{M}e^{Nt}\epsilon(Z_2^\sigma) \\ \lambda_2 Z_2 &= \bar{M}e^{Nt}\epsilon(Z_1^\sigma) \\ \lambda_2 Z_1^\sigma &= M e^{-Nt}\epsilon(Z_2) \\ \lambda_1 Z_2^\sigma &= M e^{-Nt}\epsilon(Z_1).\end{aligned}\tag{307}$$

Taking the respective inner products with $\epsilon(Z_2)$ and $\epsilon(Z_1)$ gives

$$\begin{aligned}\lambda_1 K \epsilon(Z_1 \wedge Z_2) &= (\lambda_1 - \lambda_2) \epsilon(Z_1 \wedge Z_2) Z_2 \cdot Z_2^\sigma \\ \lambda_2 K \epsilon(Z_2 \wedge Z_1) &= (\lambda_1 - \lambda_2) \epsilon(Z_1 \wedge Z_2) Z_1 \cdot Z_1^\sigma.\end{aligned}$$

So we find

$$\begin{aligned}Z_1 \cdot Z_1^\sigma &= \frac{K \lambda_2}{\lambda_1 - \lambda_2} \\ Z_2 \cdot Z_2^\sigma &= \frac{K \lambda_1}{\lambda_2 - \lambda_1}\end{aligned}$$

and (taking the opposite inner products) $Z_1 \cdot Z_2^\sigma = 0$.

Now for the P variable, we have

$$\begin{aligned}\dot{P} &= \{P, M\} = -\epsilon(P^\sigma)M \\ \dot{P}^\sigma &= \{P^\sigma, M\} = \epsilon(P)\bar{M} \\ \ddot{P} &= -\epsilon(\dot{P}^\sigma)M - \epsilon(P^\sigma)\dot{M} \\ &= -\epsilon(\epsilon(P)\bar{M})M - \epsilon(P^\sigma)MN \\ &= PM\bar{M} + \dot{P}N.\end{aligned}$$

So

$$\ddot{P} - \dot{P}N - PM\bar{M} = 0.$$

The characteristic polynomial is $\mu^2 - N\mu - M\bar{M}$, with roots $\mu = \frac{N}{2} \pm \frac{1}{2}\sqrt{N^2 + 4M\bar{M}}$, i.e., $\bar{\lambda}_1 = -\lambda_1$ and $\bar{\lambda}_2 = -\lambda_2$.

With $P = e^{-\lambda_1 t}P_1 + e^{-\lambda_2 t}P_2$, we have

$$\begin{aligned}M &= \epsilon(P \wedge Z^\sigma) \\ &= e^{-(\lambda_1 + \lambda_2)t} \epsilon(P_1 \wedge Z_2^\sigma + P_2 \wedge Z_1^\sigma) + e^{-2\lambda_1 t} \epsilon(P_1 \wedge Z_1^\sigma) + e^{-2\lambda_2 t} \epsilon(P_2 \wedge Z_2^\sigma).\end{aligned}\tag{308}$$

The last two terms must vanish identically, so we have $P_1 = A_1 Z_1^\sigma$ and $P_2 = A_2 Z_2^\sigma$ for some constants A_1, A_2 .

Now we have

$$P^\sigma = \bar{A}_1 e^{\lambda_1 t} Z_1 + \bar{A}_2 e^{\lambda_2 t} Z_2$$

and so

$$\begin{aligned}\dot{P} &= -\epsilon(P^\sigma)M \\ &= -(\bar{A}_2 e^{\lambda_2 t} \epsilon(Z_2) + \bar{A}_1 e^{\lambda_1 t} \epsilon(Z_1))M \\ \dot{P} &= -e^{-\lambda_1 t} A_1 \lambda_1 Z_1^\sigma - e^{-\lambda_2 t} \lambda_2 A_2 Z_2^\sigma.\end{aligned}$$

Equating coefficients,

$$\begin{aligned}-M e^{-Nt} \bar{A}_2 \epsilon(Z_2) &= -A_1 \lambda_1 Z_1^\sigma \\ -M e^{-Nt} \bar{A}_1 \epsilon(Z_1) &= -A_2 \lambda_2 Z_2^\sigma.\end{aligned}$$

Applying (307) to the left-hand sides gives:

$$\begin{aligned}-\bar{A}_2\lambda_1Z_1^\sigma &= -A_1\lambda_1Z_1^\sigma \\ -\bar{A}_1\lambda_2Z_2^\sigma &= -A_2\lambda_2Z_2^\sigma\end{aligned}$$

so that $\bar{A}_2 = A_1, \bar{A}_1 = A_2$.

Now, using (308),

$$\begin{aligned}Me^{-Nt} &= \epsilon(P_1 \wedge Z_1^\sigma + P_2 \wedge Z_2^\sigma) \\ &= (A_2 - A_1)\epsilon(Z_1^\sigma \wedge Z_2^\sigma)\end{aligned}$$

But by (304),

$$KMe^{-Nt} = -(\bar{\lambda}_1 - \bar{\lambda}_2)\epsilon(Z_1^\sigma \wedge Z_2^\sigma) = (\lambda_1 - \lambda_2)\epsilon(Z_1^\sigma \wedge Z_2^\sigma).$$

So we have $K(A_2 - A_1) = \lambda_1 - \lambda_2$, and the general solution is

$$\begin{aligned}P &= A_1e^{-\lambda_1 t}Z_1^\sigma + A_2e^{-\lambda_2 t}Z_2^\sigma \\ A_1 &= \frac{\lambda_2 - \lambda_1}{2K} + c \\ A_2 &= \frac{\lambda_1 - \lambda_2}{2K} + c\end{aligned}$$

where c is real.

In summary, the trajectories in this case are similar to those in the case of $SU(2)$.

A.3 $Sp(2)$

We next consider the structure group $Sp(2) \cong Spin(5)$, which is the Euclidean signature variant of the four-dimensional space-time model. This acts on the 4-sphere in the obvious way, and also on the 7-sphere. Our dynamical manifold will be the 7-sphere, regarded as the unit sphere of \mathbb{H}^2 .

The reduced norm $N(x)$ of an element of a central simple algebra A over k is defined as $N_k(x) = \det_K(x)$, where the determinant is computed in $A \otimes_k K \cong M_n(A)$ where $K|k$ is a splitting field of A . In the case of the real central simple algebra $M_2(\mathbb{H})$, we have $K = \mathbb{C}$. The isomorphism $A \otimes_k K \cong M_n(K)$ is not compatible with the Galois group $G(K|k)$, but is twisted with a cocycle that cancels out when the determinant is taken, so the reduced norm is invariant and hence lies in k .

If $t + xi + yj + zk$ is a quaternionic variable, then we define the associated momentum $p_t - p_xi - p_yj - p_zk$ where p_t, p_x, p_y, p_z are the respective Poisson conjugates of t, x, y, z . For $Z, P \in \mathbb{H}^2$, define $P \oplus Z^*$ to be the matrix in $M_2(\mathbb{H})$ with columns P and Z^* (the quaternionic conjugate of Z^T). Then define the Hamiltonian by

$$H = N(P \oplus Z^*).$$

Then H Poisson commutes with $Z \cdot Z^*, P \cdot P^*$. It is invariant under the group of symmetries $\mathrm{Sp}(2)$. The symplectic gradient of H is tangent to the codimension 3 contact structure $\theta = Z \cdot dZ^* - Z^* \cdot dZ$.

Theorem 1. *The generic geodesic for the Hamiltonian H is given by*

$$Z = e^{\mu_1 u t} Z_1 + e^{\mu_2 u t} Z_2$$

$$P = A_1 e^{-\mu_1 u t} Z_1^* + A_2 e^{-\mu_2 u t} Z_2^*$$

where $u \in \mathrm{im} \mathbb{H}$, $Z_1 u = u Z_1$, $Z_2 u = u Z_2$, $\mu_1, \mu_2 \in \mathbb{R}$, and

$$Z_1 \cdot Z_1^* = \frac{\mu_2}{\mu_2 - \mu_1}, \quad Z_2 \cdot Z_2^* = \frac{\mu_1}{\mu_1 - \mu_2}, \quad Z_1 \cdot Z_2^* = Z_2 \cdot Z_1^* = 0$$

$$A_1 = \frac{\mu_1 - \mu_2}{2} u + c, \quad A_2 = \frac{\mu_2 - \mu_1}{2} u + c$$

where c is a real constant, and μ_1, μ_2, u are conserved along the geodesic.

The limiting geodesics are great circles on S^4 .

Proof. We first count parameters. On the one hand, an initial point on the 7-sphere, and then a vector tangent to the all three contact distributions gets 11 dimensions, minus one dimension because each geodesic is counted overcounted, for a 10 dimensional family of geodesics. On the other hand, there is a 6-parameter family of totally geodesic 2-spheres on the 4-sphere. Each 2-sphere then has a 4-parameter family of geodesics on it for the corresponding copy of $SU(2)$ inside $SP(2)$, again making 10 parameters.

To prove the theorem, we shall show that, for any geodesic Z , there exists an imaginary quaternion u such that $uZ = Zu$.

...

□

A.4 $\mathrm{Sp}(1, 1)$

We come finally to the group $\mathrm{Sp}(1, 1) \cong \mathrm{Spin}(1, 4)$, which is a group of symmetries of the de Sitter spacetime (and a group of isometries of the four-dimensional hyperbolic space). We recall some generalities on this group. Let \mathbb{H} denote the space of quaternions, the degree four division algebra over \mathbb{R} , with conjugation denoted by $z \mapsto \bar{z}$. For a 2×2 matrix $A \in M_2(\mathbb{H})$ with entries in \mathbb{H} , let $A^* = \bar{A}^T$, where the bar denotes entrywise conjugation and the T denotes the transpose. Let

$$S = \begin{bmatrix} 0 & 1 \\ 1 & 0 \end{bmatrix}.$$

Define $A^\sigma = SA^*S^{-1} = SA^*S$.

Definition 1. *The group $\mathrm{Sp}(1, 1)$ is the set of $A \in M_2(\mathbb{H})$ such that $A^\sigma A = I$.*

For $x \in M_2(\mathbb{H})$, define the reduced trace $T_{\mathbb{R}}(x) = T_{\mathbb{H}|\mathbb{R}} \mathrm{tr}(x)$. Also define the \mathbb{R} -bilinear form $k(x, y) = T_{\mathbb{R}}(xy)$. The group $\mathrm{Sp}(1, 1)$ acts on $M_2(\mathbb{H})$ by conjugation: $x \mapsto Ax A^\sigma$, and this leaves the form $k(x, y)$ invariant. The subspace

$\mathbb{X} = \{x \in M_2(\mathbb{H}) \mid x^\sigma = x, k(x, S) = 0\}$ is also invariant under the group. On this subspace, k is a quadratic form of signature $(1, 4)$, and this exhibits the two-to-one spin covering map $\mathrm{Sp}(1, 1) \rightarrow SO_0(1, 4)$.

We take as our phase space again pairs $Z, P \in \mathbb{H}^2$. The kinetic Hamiltonian is

$$H = N([P, Z^\sigma])$$

where $Z^\sigma = Z^*S$. Note that this can be calculated by using a representation of P and Z as 4×2 matrices over \mathbb{C} , and computing a determinant.

Theorem 2. $\{Z \cdot Z^\sigma, H\} = 0$

Proof. A brute force computation. \square

Theorem 3. *The Gromov tangent space associated to the Hamiltonian H is the Poisson algebra generated by*

$$\begin{aligned} P_0 &= r_1 w_1 + r_2 w_2 + r_3 w_3 \\ P_1 &= q_1 + \frac{1}{2}(r_2 w_3 - r_3 w_2) \\ P_2 &= q_2 + \frac{1}{2}(r_3 w_1 - r_1 w_3) \\ P_3 &= q_3 + \frac{1}{2}(r_1 w_2 - r_2 w_1) \end{aligned}$$

where the variables q_i, r_i, w_i satisfy Poisson relations

$$\{w_i, q_j\} = 2\delta_{ij}, \quad \{q_i, q_j\} = \{q_i, r_j\} = \{w_i, w_j\} = \{r_i, r_j\} = 0.$$

In particular, P_0 is central, and P_1, P_2, P_3 generate the six dimensional Poisson algebra of §3.

Proof. The first step of the proof is to express H as a sum of four squares. We do this by taking its hessian in the p , and diagonalizing the resulting symmetric matrix. It is thus shown that

$$H = (Q_0^2 + Q_1^2 + Q_2^2 + Q_3^2)s$$

where

$$\begin{aligned}
s &= 2(z_{00}^2 + z_{01}^2 + z_{02}^2 + z_{03}^2)^{-1} \\
Q_0 &= p_{00}z_{00}^2 + p_{00}z_{01}^2 + p_{00}z_{02}^2 + p_{00}z_{03}^2 - (p_{10}z_{00} + p_{11}z_{01} + p_{12}z_{02} + p_{13}z_{03})z_{10} + \\
&\quad + (p_{11}z_{00} - p_{10}z_{01} + p_{13}z_{02} - p_{12}z_{03})z_{11} + (p_{12}z_{00} - p_{13}z_{01} - p_{10}z_{02} + p_{11}z_{03})z_{12} + \\
&\quad + (p_{13}z_{00} + p_{12}z_{01} - p_{11}z_{02} - p_{10}z_{03})z_{13} \\
Q_1 &= p_{01}z_{00}^2 + p_{01}z_{01}^2 + p_{01}z_{02}^2 + p_{01}z_{03}^2 - (p_{11}z_{00} - p_{10}z_{01} + p_{13}z_{02} - p_{12}z_{03})z_{10} - \\
&\quad - (p_{10}z_{00} + p_{11}z_{01} + p_{12}z_{02} + p_{13}z_{03})z_{11} + (p_{13}z_{00} + p_{12}z_{01} - p_{11}z_{02} - p_{10}z_{03})z_{12} - \\
&\quad - (p_{12}z_{00} - p_{13}z_{01} - p_{10}z_{02} + p_{11}z_{03})z_{13} \\
Q_2 &= p_{02}z_{00}^2 + p_{02}z_{01}^2 + p_{02}z_{02}^2 + p_{02}z_{03}^2 - (p_{12}z_{00} - p_{13}z_{01} - p_{10}z_{02} + p_{11}z_{03})z_{10} - \\
&\quad - (p_{13}z_{00} + p_{12}z_{01} - p_{11}z_{02} - p_{10}z_{03})z_{11} - (p_{10}z_{00} + p_{11}z_{01} + p_{12}z_{02} + p_{13}z_{03})z_{12} + \\
&\quad + (p_{11}z_{00} - p_{10}z_{01} + p_{13}z_{02} - p_{12}z_{03})z_{13} \\
Q_3 &= p_{03}z_{00}^2 + p_{03}z_{01}^2 + p_{03}z_{02}^2 + p_{03}z_{03}^2 - (p_{13}z_{00} + p_{12}z_{01} - p_{11}z_{02} - p_{10}z_{03})z_{10} + \\
&\quad + (p_{12}z_{00} - p_{13}z_{01} - p_{10}z_{02} + p_{11}z_{03})z_{11} - (p_{11}z_{00} - p_{10}z_{01} + p_{13}z_{02} - p_{12}z_{03})z_{12} - \\
&\quad - (p_{10}z_{00} + p_{11}z_{01} + p_{12}z_{02} + p_{13}z_{03})z_{13}.
\end{aligned}$$

We take the tangent space at the point $Z = (1, 1)$. We first find the privileged coordinates of degree 1 and -1 at this point. To do so, we substitute $Z = (1, 1)$ into the equations for Q , giving $q_0 = \sqrt{s}Q_0 = p_{00} - p_{10}$, $q_1 = \sqrt{s}Q_1 = p_{01} - p_{11}$, $q_2 = \sqrt{s}Q_2 = p_{02} - p_{12}$, $q_3 = \sqrt{s}Q_3 = p_{03} - p_{13}$, so these quantities have degree -1 . Next, the pairwise Poisson brackets of the Q_i show that $r_1 = p_{01} + p_{11}$, $r_2 = p_{02} + p_{12}$, $r_3 = p_{03} + p_{13}$ are of degree -2 . We dualize to obtain that $w_1 = z_{01} - z_{11}$, $w_2 = z_{02} - z_{12}$, $w_3 = z_{03} - z_{13}$ are of degree 1. Now applying to $\sqrt{s}Q_i$ the scalings $q_i \mapsto q_i/t$, $r_i \mapsto r_i/t^2$, $w_i \mapsto tw_i$, and keeping terms of order t^{-1} only, establishes the theorem. \square

Corollary 1. *In the diagonalization $H = (Q_0^2 + Q_1^2 + Q_2^2 + Q_3^2)s$, the vector fields generated by $Q_i\sqrt{s}$ generate a 7-dimensional Poisson algebra. In particular, they satisfy Chow's condition on the 7-dimensional space $Z \cdot Z^\sigma = \text{constant}$.*

Proof. The only part of the corollary that is not an immediate consequence of the theorem is the last statement. To show that $Q_i\sqrt{s}$ Poisson commutes with $Z \cdot Z^\sigma$ is again a brute force computation. \square